UNIVERSITY OF OKLAHOMA

GRADUATE COLLEGE

ADVANCING ANNEXIN-DIRECTED ENZYME PRODRUG THERAPY FOR THE

TREATMENT OF SOLID TUMORS

A DISSERTATION

SUBMITTED TO THE GRADUATE FACULTY

in partial fulfillment of the requirements for the

Degree of

DOCTOR OF PHILOSOPHY

By

KATRIN PASSLACK GUILLEN
Norman, Oklahoma
2015

ADVANCING ANNEXIN-DIRECTED ENZYME PRODRUG THERAPY FOR THE
TREATMENT OF SOLID TUMORS

A DISSERTATION APPROVED FOR THE
DEPARTMENT OF BIOMEDICAL ENGINEERING

BY

_____
Dr. Roger Harrison, Chair

_____
Dr. Harold Stalford

_____
Dr. Matthias Nollert

_____
Dr. Rajagopal Ramesh

_____
Dr. Edgar O'Rear

To Gudrun and Matthias, my parents. The caliber of role models you have been, and continue to be, is simply tremendous. Your generous encouragement and heartfelt belief in my ability persevere through moments of frustration have been guiding influences throughout this PhD journey. I am infinitely grateful for the love and support from the both of you.

"A hundred times every day I remind myself that my inner and outer life depend on the labors of other men, living and dead, and that I must exert myself in order to give in the same measure as I have received and am still receiving." Albert Einstein

Acknowledgements

First and foremost my husband, Jon. Graduate school has meant sacrifice for both of us, but you have provided such love and support throughout. I cannot promise that I will never talk your ear off about science again, but I can promise that I will, at the very least, talk about a different protein in the near future.

Dr. Harrison, my advisor, who provided guidance and patience throughout these past four years. Dr. Harrison's optimism and persistence to solve scientific mysteries was essential in guiding these projects to publication.

The undergraduate research students who challenged me to grow as a mentor and renewed my enthusiasm for lab. Antonietta, I would like to thank you for being my first undergraduate guinea pig and setting such a great example for everyone to follow; the authorship that stemmed from your work was well deserved. Beth Huggins, I would like to thank you for your dedication to our late night ventures in radiofrequency land, and bringing a fresh and completely different perspective to the lab; "Instead of asking what I can do to tell the world that I exist, asking who can I lift up to tell the world that they exist?" still sticks with me. Matthew Randolph, I would like to thank you for the sincere interest that you took in absolutely everything cancer related - a year and a half of a constant questions kept me on my toes. I am so glad that lasting friendships grew out of each of these joint ventures in science.

Two OU core facilities and their staff also deserve special mention. Ben Smith at the Samuel Roberts Noble Microscopy Laboratory was instrumental in acquiring our amazing confocal images. Eliza Ruben at the Protein Production Core has gone above and beyond the call of duty as a collaborator and become a good friend along the way.

When we present our work on the βG protein, the audience often marvels at how clean our product is, and that is possible thanks to Eliza and her protein purification powers.

Lastly, I would like to acknowledge my Crossfit family - Kelley, Patrick, Preston, Jamie, EJ, Alex, Brooke, and Uwem. Knowing that I could always go to GZ and see all of you after a rough day in lab has been an emotional lifesaver for me on so, so many occasions. Because when science hands you lemons, Fran with friends is clearly the answer.

Sources of Financial Support

Table of Contents

List of Tables

List of Figures

Abstract

By targeting enzymes to the surface of tumor cells, tumor vasculature, and metastatic lesions, annexin-directed enzyme prodrug therapy aims to create high-dose chemotherapy only in the direct vicinity of the tumor site and therefore mitigate the side effects experienced by healthy tissues. To improve the power and clinical relevance of annexin-directed enzyme prodrug therapy, we aimed to develop and evaluate a new family of fusion proteins centered about the human β-glucuronidase (βG) enzyme. We also intended to provide considerable evidence for the tumor type independence of annexin-directed enzyme prodrug therapy via the evaluation of βG fusion proteins on pancreatic, breast, and colon cancer, as well evaluation of three existing fusion proteins, containing the non-human enzymes L-methioninase, purine nucleoside phosphorylase, and cytosine deaminase on pancreatic and prostate cancer.

When tethered to the tumor cell surface, the enzymes studied are capable of converting relatively harmless prodrugs into potent anti-cancer compounds. For βG we investigated the chemotherapeutic SN-38, which is the preferred first and second line treatment option for colon cancer. In healthy tissue, βG is sequestered within lysosomes, thus posing little risk of prodrug activation by endogenous βG, while allowing for use of the human enzyme, which greatly alleviates any risk of immunogenicity. For the non-human enzymes studied, which carry little risk of endogenous prodrug activation but high risk of immunogenicity, we investigated the toxic compounds methylselenol, 2-flouroadenine, and 5-flourocytosine.

Each enzyme is targeted to the tumor by means of fusion to an annexin A1 or A5 protein, creating a fusion protein. A1 and A5 tightly bind phosphatidylserine, an

xxi

anionic cell membrane phospholipid, which is strictly segregated to the cytoplasmic leaflet in healthy cells but robustly and consistently translocated to the outer leaflet of tumor cells, their metastases, and tumor vasculature. Phosphatidylserine targeting via annexin is an attractive targeting approach that is highly tumor-specific in comparison to normal tissue, yet retains multi cell-type targeting capabilities once within the tumor microenvironment.

Herein, we present substantial evidence that the mechanism of action of annexin-directed enzyme prodrug therapy is realistically tumor type independent. Additionally, we unveil a novel family of fusion proteins, the most notable of which is an A5-16a3 βG mutant fusion. The annexin-βG fusion proteins are the first of their kind as they enable on-site, combination drug therapy covering a variety of chemotherapeutic strategies, which can be tailored to individual patients' genotypes simply based on prodrug selection. Not only do these fully human annexin-βG fusion proteins present a powerful approach for the treatment of metastatic disease, but they also promise to be non-immunogenic and are ready for rapid transition to translational work in solid tumors.

Keywords: annexin, phosphatidylserine, vascular targeting, prodrug, β-glucuronidase, colon cancer, pancreatic cancer, breast cancer, prostate cancer

Chapter 1: Introduction

Motivation

Each day, we further unravel the complexity of the multitude of diseases collectively

termed cancer, and it is becoming increasingly clear that the era of the magic bullet

cure, although quite covetable, is drawing to a close.[1] Growing knowledge of the

intricacies and heterogeneity of tumor progression drive the need for the development

of complex, flexible treatment approaches. It is now clear that our hopes to cure

advanced metastatic disease rest on innovative, multi-target, multi-modal, genotypically

matched, combination treatment strategies.

Specificity in cancer treatment is a fine line. Too much specificity and

metastases go untreated. Not enough specificity, and healthy organs become martyrs of

the treatment itself. Furthermore, selective drugs tend to work only in a subset of

patients. It has thus been proposed that aiming for several targets at once may be a

better strategy for treating complex disease.[1]

Annexin-directed enzyme prodrug therapy is unique in that the targeting

mechanism is simultaneously non-specific and specific. Unlike many other solid tumor

selective approaches, annexin targeting does not discriminate between solid tumors of

different organs, primary tumors verses metastases far removed from the primary tumor

site, or even between tumor cells and tumor vasculature. Hence, annexin has a large

repertoire of solid-tumor associated binding sites, making it relatively non-specific.

In contrast, the annexin target, a phospholipid, is only very rarely accessible in

healthy humans, granting the annexin targeting approach great specificity towards solid

tumors. This phospholipid target becomes accessible in the tumor environment due to

physiological stressors in the absence of endogenous activators, such as when tumor cells experience oxidative stress.[2] Although, the target is expressed on activated platelets in the blood, activated platelets constitute only a very, very small subset of circulating platelets, making non-specific interactions rare and weak.[3] Thus, annexin targeting has the necessary specificity and, therefore, great potential to reduce the awful side effects generally associated with the systemic administration of chemotherapeutics.

Annexin targeting has found initial clinical success in the drug Bavituximab, a chimeric immunoglobin antibody. Upon binding to the phospholipid target, Bavituximab triggers an immune response leading to vascular damage. In a phase II clinical trial, Bavituximab elicited a promising response in combination therapy for advanced stage breast cancer,[4] lending considerable authority to the annexin targeting strategy.

Coupling this remarkably selective but yet non-specific annexin-based targeting approach to enzymes that act as chemotherapeutic-producing factories underlies the work presented herein. By these means, we aim to create chemotherapy treatment directly at the tumor site via annexin-directed enzyme prodrug therapy. Enzyme prodrug therapy not only enables increasing the dose of chemotherapy delivered but also the dose of chemotherapy tolerated systemically, as the drugs created are decidedly localized to the tumor site, in lieu of systemic administration. It has even been suggested that drug concentrations created via enzyme prodrug therapy may be so high that the swift and massive cell death effected could outpace the establishment of acquired drug resistance.[5]

With the work presented herein, we aim to present significant dents to the boundary of existing knowledge in annexin-directed cancer therapeutics. By producing clinically relevant chemotherapeutic concentrations only within the interstitial tumor compartment, we intend to effect better treatment outcomes and ultimately impact patients' lives.

Why breast, prostate, pancreatic, and colon cancer?

Cancer takes not only a human toll, but also presents a substantial financial burden to society. Estimates of the worldwide cost of cancer are as high as $895 billion (US dollars), and cancer has been suggested to carry the highest financial burden of any disease to society.[6] With the global burden of cancer predicted to nearly double by 2030,[7] development of cancer risk control, early diagnostics, and effective treatment options are of great importance for both human health and worldwide economic stability.

In the past, our lab has focused on developing novel targeted treatment strategies for breast cancer, which has one of the highest incidence rates (Figure 1) in females in the US, accounting for 29 % of all new cancer diagnoses and 15 % for cancer deaths, claiming approximately 40,000 lives per year.[8] Worldwide, unlike many other types of cancer, breast cancer does not discriminate between developed and developing countries, as indicated by the overwhelming amount of pink found in Figure 2, and accounts for nearly 460,000 deaths worldwide per year.[7]

Although breast cancer is clearly a deserving target on account of its immense contribution to the global cancer burden, the fusion protein based treatments we develop
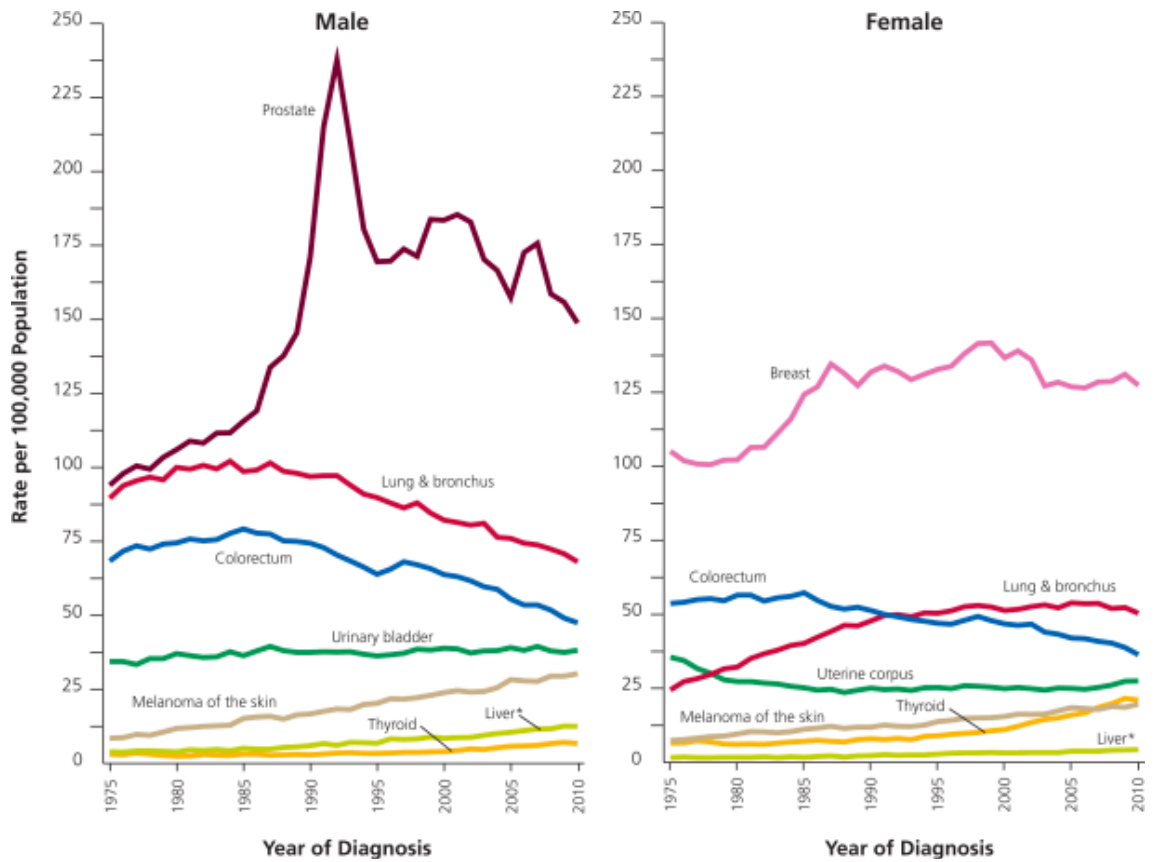
Figure 1: Cancer incidence rates by site for US males and females from 1975 to 2010 [Reproduced from 8]
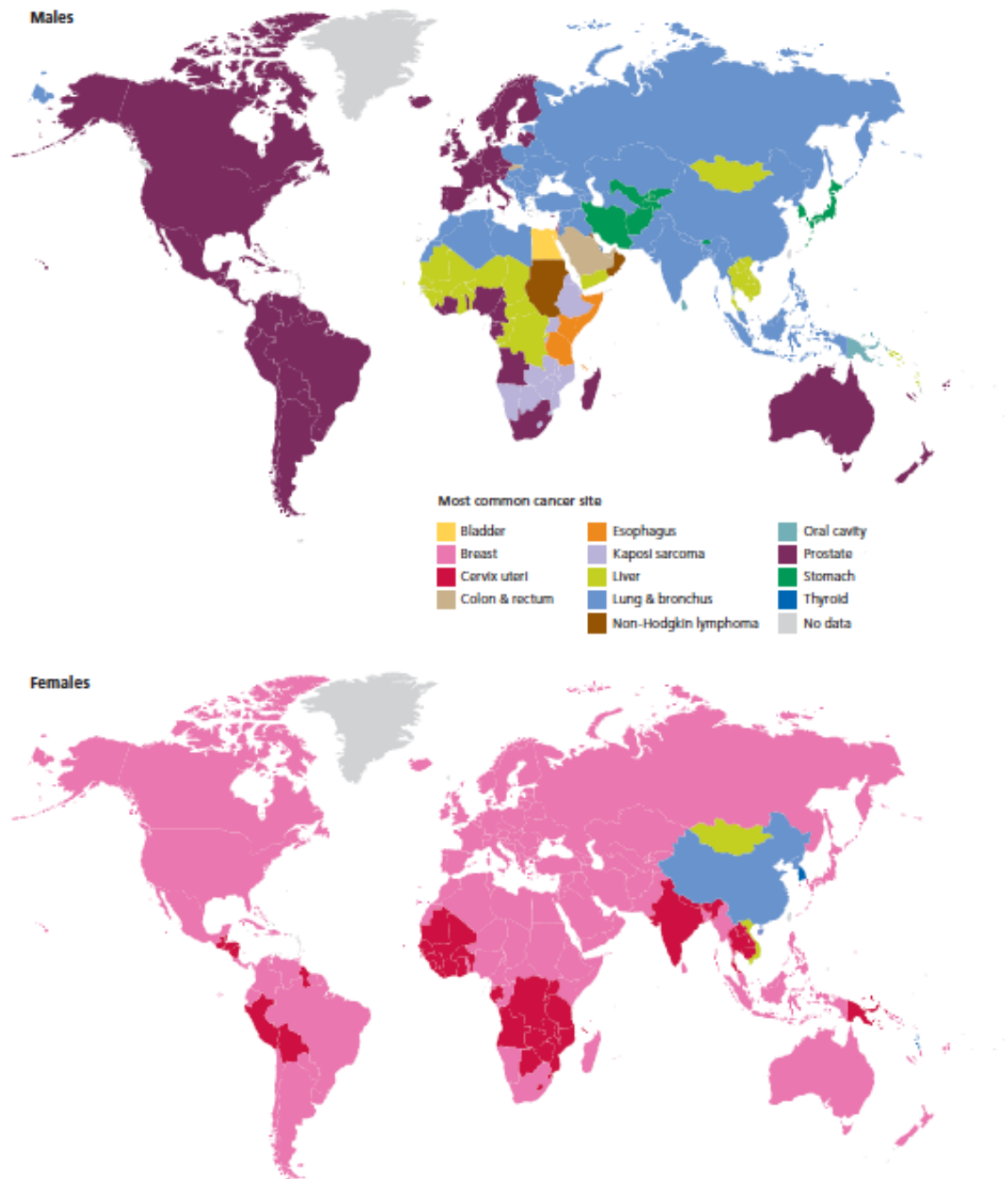
Figure 2: Most common cancer sites for males and females worldwide

are, at least in theory, tumor type independent due to the ubiquitous presence of the target on all solid tumors examined to date. Thus, we were interested in expanding the breadth of applicability of our fusion proteins to other malignancies that also contribute heavily to the global tumor burden.

Prostate cancer emerged as another large contributor to the global cancer burden and no curative treatment for the advanced metastatic form of prostate cancer currently exists. Prostate cancer has the highest incidence rate among US males (Figure 1), accounting for 27 % of new diagnoses, over 230,000 new cases yearly in the US, and 10 % of cancer deaths in the US. [8] Prostate cancer is more localized to developed nations than breast cancer (Figure 2) but still claims over 250,000 lives worldwide, ranking the third and sixth most common cause of cancer death in developed and developing countries, respectively.[7]

Pancreatic cancer also emerged as a potential tumor target due to the large window of opportunity for tumor burden reduction. In the US, pancreatic cancer accounts for 46,000 new cases each year and 40,000 deaths per year.[8] The striking contiguity of these numbers is also maintained worldwide, although with much higher prevalence in developed nations.[7] Possibly most alarming, is that unlike breast, prostate, and colon cancer which have shown steady declines in US death rates since the early 1990s, pancreatic cancer death rates in the US have been steadily on the rise, as shown in Figure 3.[8] If current trends continue, soon the number of deaths caused by pancreatic cancer will be second only to lung cancer.

Colon cancer was the last potential tumor target we investigated. Although colon cancer was originally intended for inclusion in applicability studies, work on
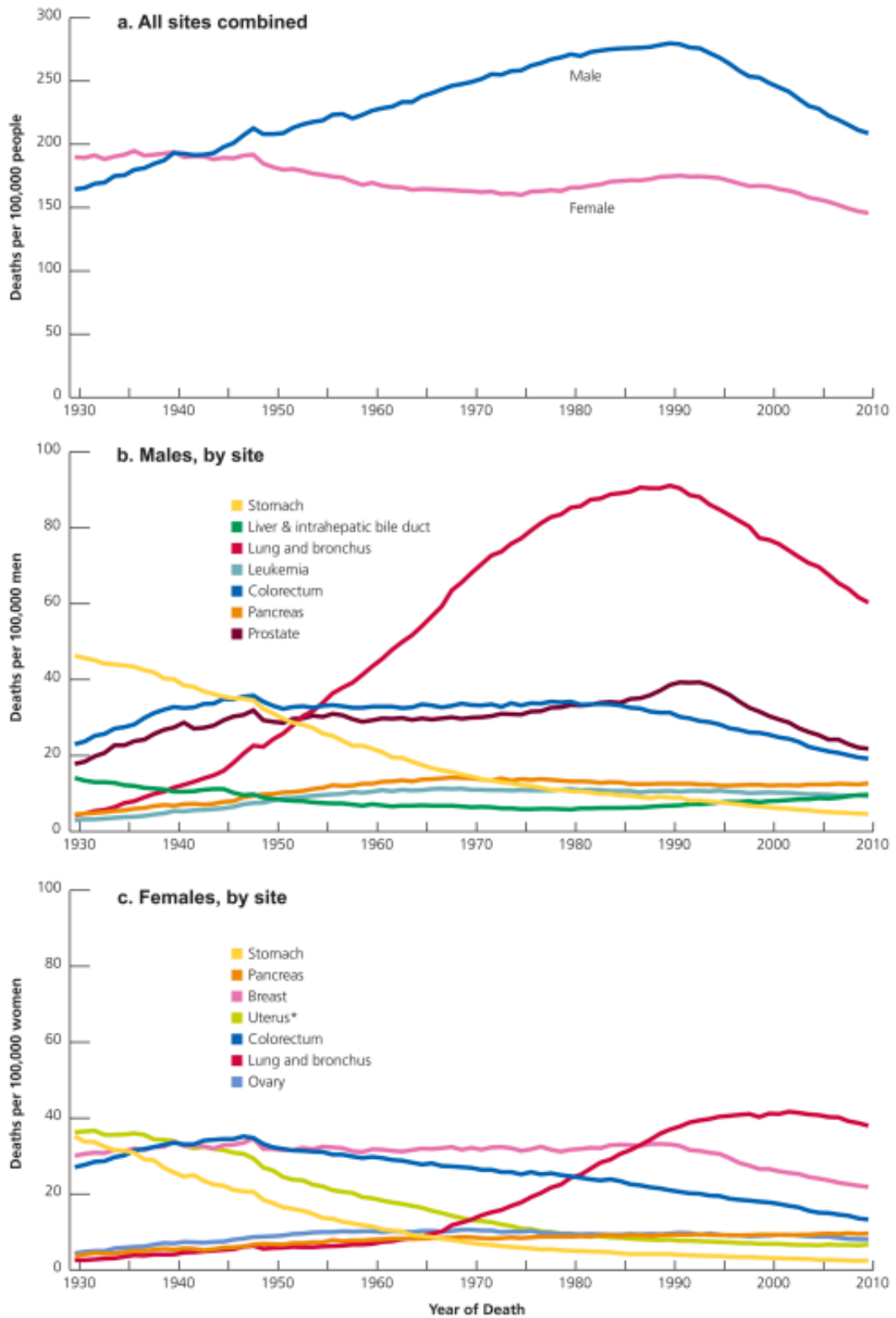
Figure 3: US cancer death rates from 1930 to 2010 for (a) all sites combined (b) males by site and (c) females by site

colorectal cancer did not commence until we developed a novel protein capable of producing a drug with well established efficacy in the clinic for first- and second-line therapy of colorectal cancer.[9] In the US, colorectal cancer ranks third in both new cases and deaths for men and women, causing approx. 50,000 deaths per year.[8] Worldwide, colorectal cancer accounts for over 600,000 deaths per year, and it the 3rd most common cancer in men and women worldwide.[7] Therefore, colon cancer also contributes heavily to the global cancer burden.

The trouble with chemotherapy

Of all cancer patients, 40 % will be cured by radiotherapy and surgery, while the rest will die from metastatic disease.[10] Once metastasized, cancer becomes a systemic disease requiring a systemic treatment approach.[10] However, systemic chemotherapy treatment often fails to achieve a cure. In fact, the overall five-year survival rate increase effected by both curative and adjuvant chemotherapy is just over 2 % in the US and Australia.[11] For the time being, chemotherapy is heavily relied upon as adjuvant treatment post surgery to target micro-metastases, and as palliative care, relieving symptoms of the disease, and improving patient quality of life.[12]

Chemotherapy does, however, harbor curative potential, but for many solid tumors, this potential has simply not yet been achieved.[10] In the 1970's, chemotherapy was deemed effective for select tumors types, but broadening the application of these treatments to other cancer types, especially common epithelial ones, has only afforded marginal benefits thus far.[13] For the tumors types investigated herein, current chemotherapy approaches contribute 1 % of five-year survivors for colon cancer, 1.4 %

for breast cancer, and no observable effect for prostate cancer, with no data available for pancreatic cancer since the 5-year survival rate is devastatingly low.[11] All four of these malignancies have high metastatic potential, making them difficult to treat, with metastatic sites notated by location and frequency of occurrence in Figure 4.

Metastasis is a complex process outlined by the invasion-metastasis cascade, as shown in Figure 5, which is conducted by a cellular program termed the epithelial–mesenchymal transition (EMT). EMT occurs naturally in embryonic development when mesenchymal cells, loosely associating and lacking polarity, are generated from epithelial or endothelial cells, which have distinct apical-basal orientations and functions. When the EMT program is executed in the tumor environment, tumor cells gain the ability to invade the surrounding stroma and forage for access to transport modalities, primarily blood and lymph. By intravasation, tumor cells enter the lumen of transport vessels, where, depending on survival and extraction from the vessel into the surrounding tissues (extravasation), they travel to foreign sites and initiate growth of a metastatic site, requiring a reverse EMT wherein mesenchymal cells transition to epithelial cells.[14] Clearly, the journey from primary tumor cell to macroscopic metastasis is a harrowing one, yet this phenomenon occurs consistently in advanced malignant tumors.

Deterrents of chemotherapeutic efficacy include systemic toxicity limiting the dosage tolerated, a lack of specificity, rapid drug metabolism, and both intrinsic and acquired resistance mechanisms.[15] Intrinsic barriers include physical transport barriers such as the dense capsule in which pancreatic cancer often surrounds itself,[16] and classical drug resistance, such as multi-drug exporters.[15] Contrastingly, acquired
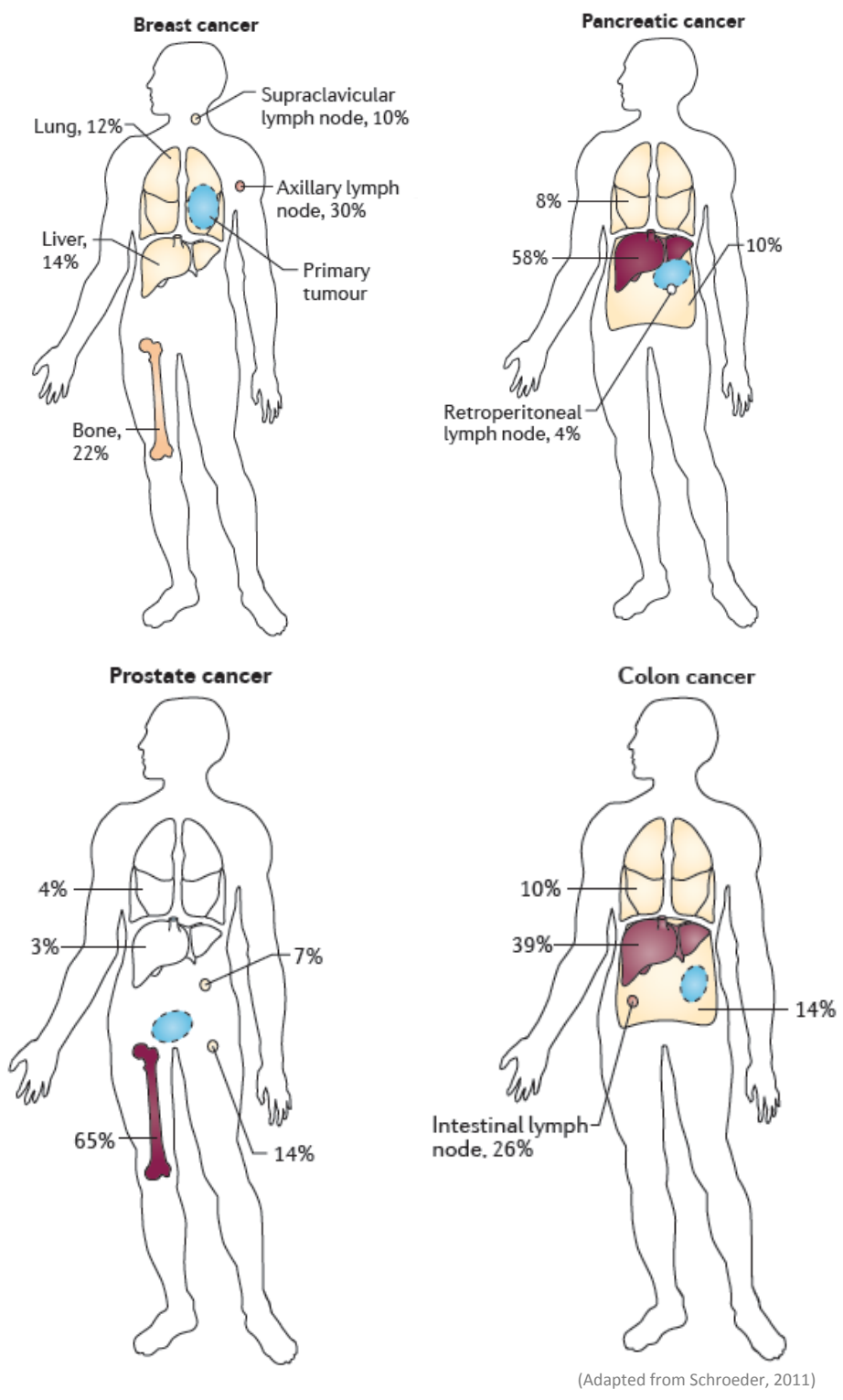
Figure 4: Common metastatic sites for breast, pancreatic, prostate, and colon cancer [Adapted from 17]
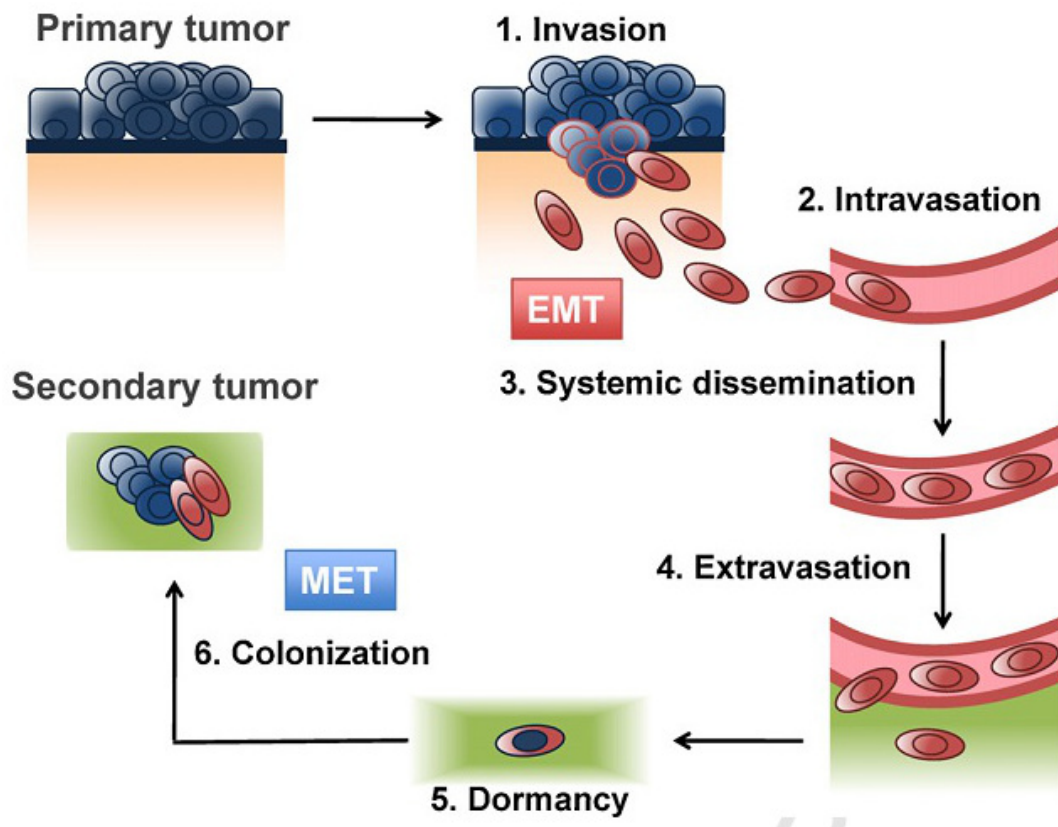
Figure 5: The metastatic cascade Reproduced from 14

The first step in the metastatic cascade is an epithelial/endothelial to mesenchymal transition (EMT), which allows the tumor cells to invade the surrounding tissues. In carcinomas, this requires that the tumor cells break though the basement membrane, as shown. From here, the tumor cells must find access to a blood vessel lumen, via a process called intravasation. Upon surviving the trip to a new location, tumor cells must exist the blood stream, through a process termed extravasation. To form a metastasis, some of the tumor cells must become mesenchymal cells again, via the reverse of EMT, labeled MET.

multidrug resistance is very unpredictable. It arises from genetic mutations and epigenetic changes that occur in downstream events regulating cell cycle, cell survival, adhesion, invasiveness, and angiogenesis if catastrophic death is not achieved following initial chemotherapeutic attack.[15] Lastly, chemotherapy must be 100% effective to prevent relapse. As shown in Figure 6, tumors consist of a heterogeneous cell population, which can change randomly if left untreated. Treating with chemotherapy selectively kills off quickly proliferating phenotypes. However, cells with slow proliferating phenotypes, possibly cancer stem cells, are left free to mutate into aggressively proliferating cell types later on and thus drive tumor progression forward.[18]
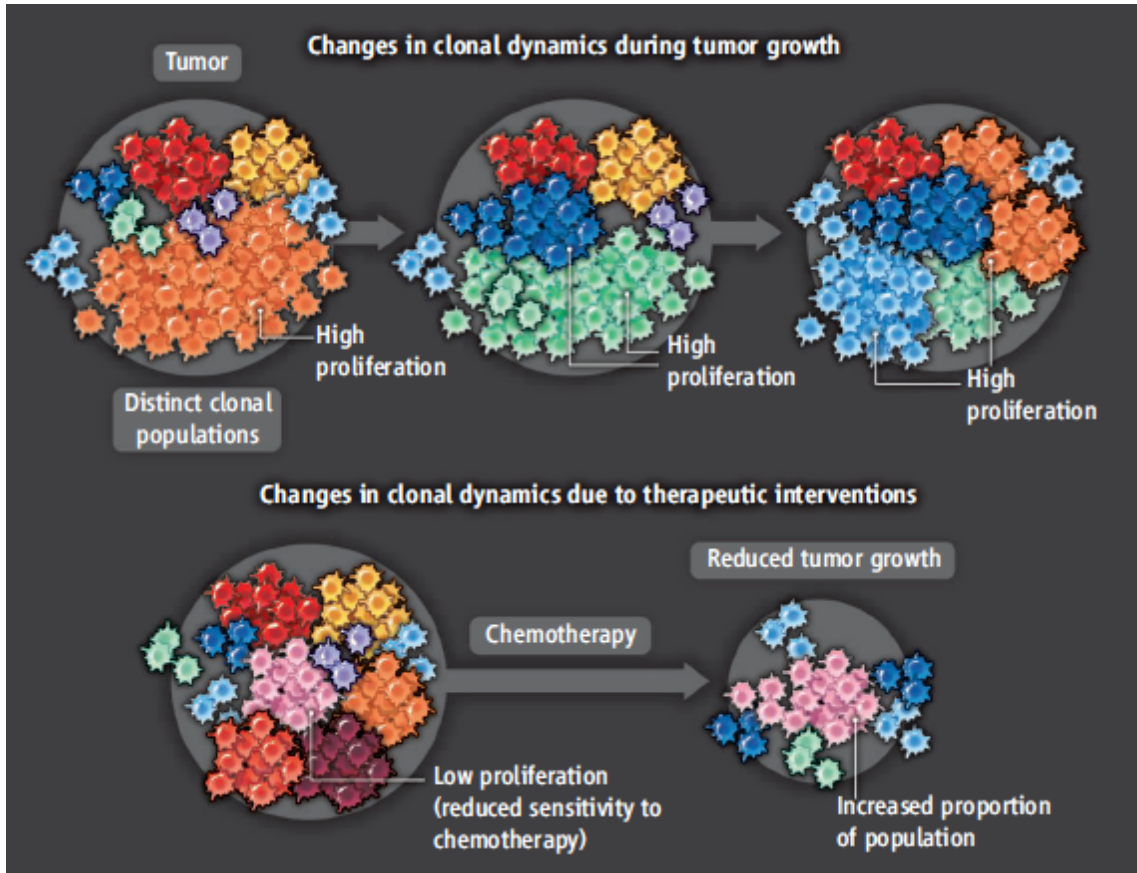
Figure 6: Effect of chemotherapy on the tumor cell population

A tumor consists of a heterogeneous population of clonal cells, some of which proliferate rapidly, while others do not. The distribution of these clones within the population can shift, somewhat randomly, as the tumor grows. Since, chemotherapy selectively targets clones with high proliferation activity, treatment changes the clonal landscape, and shifts the balance towards cells with low proliferation activity, which is the key achievement of palliative care. However, some of the low proliferating cells may act as cancer stem cells, and later mutate into cells with high proliferation activity, causing tumor regrowth.

Enzyme Prodrug Therapy

Basic mechanism of action

Enzymes convert substrates into products, as shown in Figure 7. In enzyme prodrug therapy, the substrate is a relatively harmless substance, a prodrug, whereas the product is a cancer fighting chemotherapeutic drug. With carefully designed systems, we can even synthesize multiple products via the same enzyme, likely improving the clinical applicability of the system. Enzyme selection is crucial to the success of enzyme prodrug therapy, as minimal substrate conversion should occur within healthy tissues by natively present enzymes.

Importantly, the enzyme must be placed within the tumor microenvironment to create enzyme prodrug therapy (EPT), or else substrate conversion will occur systemically and void the entire principle of the therapeutic approach. Several different strategies exist to localize these enzymes to tumors, as discussed in *Types of EPT* in the following section.
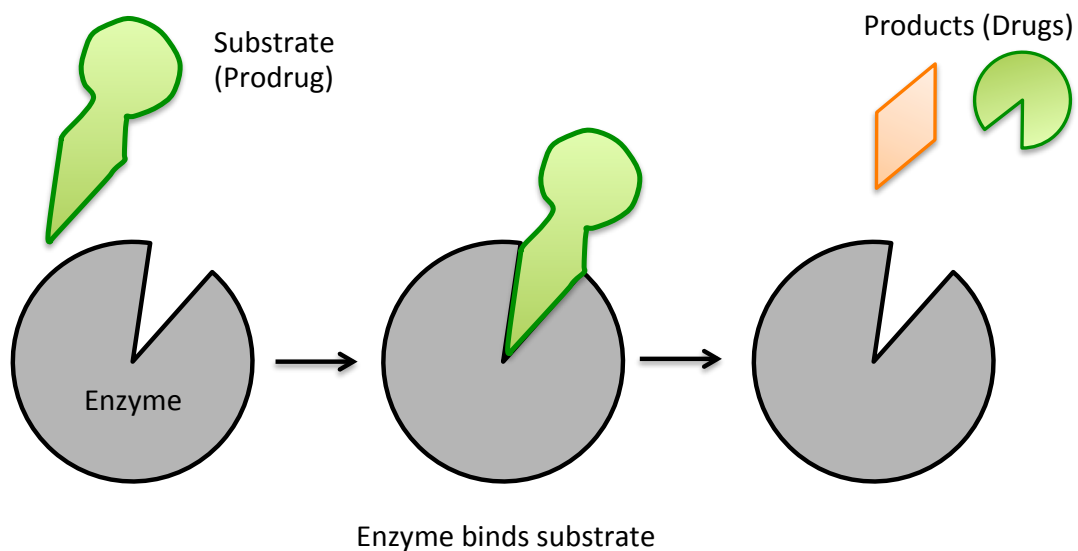
Figure 7: Mechanism of utilizing enzymes to create drugs

Popular types of enzyme-prodrug therapy, and how they localize to the tumor site, are depicted in Figure 8 and briefly explained below. The annexin-directed EPT presented herein most closely resembles ADEPT, but is less selective and can likely overcome the distribution limitations commonly seen in ADEPT.

ADEPT – Antibody directed EPT: To enact ADEPT, an antibody is used to localize and tether the enzyme of interest to the cancer site. The antibody is chosen to bind to a tumor-associated antigen, not commonly expressed on healthy tissues but highly overexpressed on tumor cells. The only target that has been clinically tested is carcinoembryonic antigen (CEA), but numerous others such as c-erbB2-P185 in breast cancer and the A33 antigen, existent on 95% of colon cancers, are also being pursued.[19] In ADEPT, the antibody/enzyme conjugate must cross the vascular wall to reach the tumor cells, which can create a non-ideal heterogeneous distribution of antibody throughout the tumor following intravenous injections.[20]

GDEPT – Gene directed EPT: Also known as suicide gene therapy, GDEPT is enacted by transferring a gene, most commonly through liposomal gene delivery, into a cancer cell that encodes for the enzyme of choice. Once the cancer cell produces the enzyme, the enzyme can then convert any prodrugs present inside the cell. Certain GDEPT approaches include a secretion and tether signal such that the enzyme is can convert prodrugs extracellularly. Vector delivery is a challenge for these systems and limited by the inability to transfect a large number of cells efficiently, currently making GDEPT technology suitable only for local administration and generally unsafe for clinical use.[21,22]
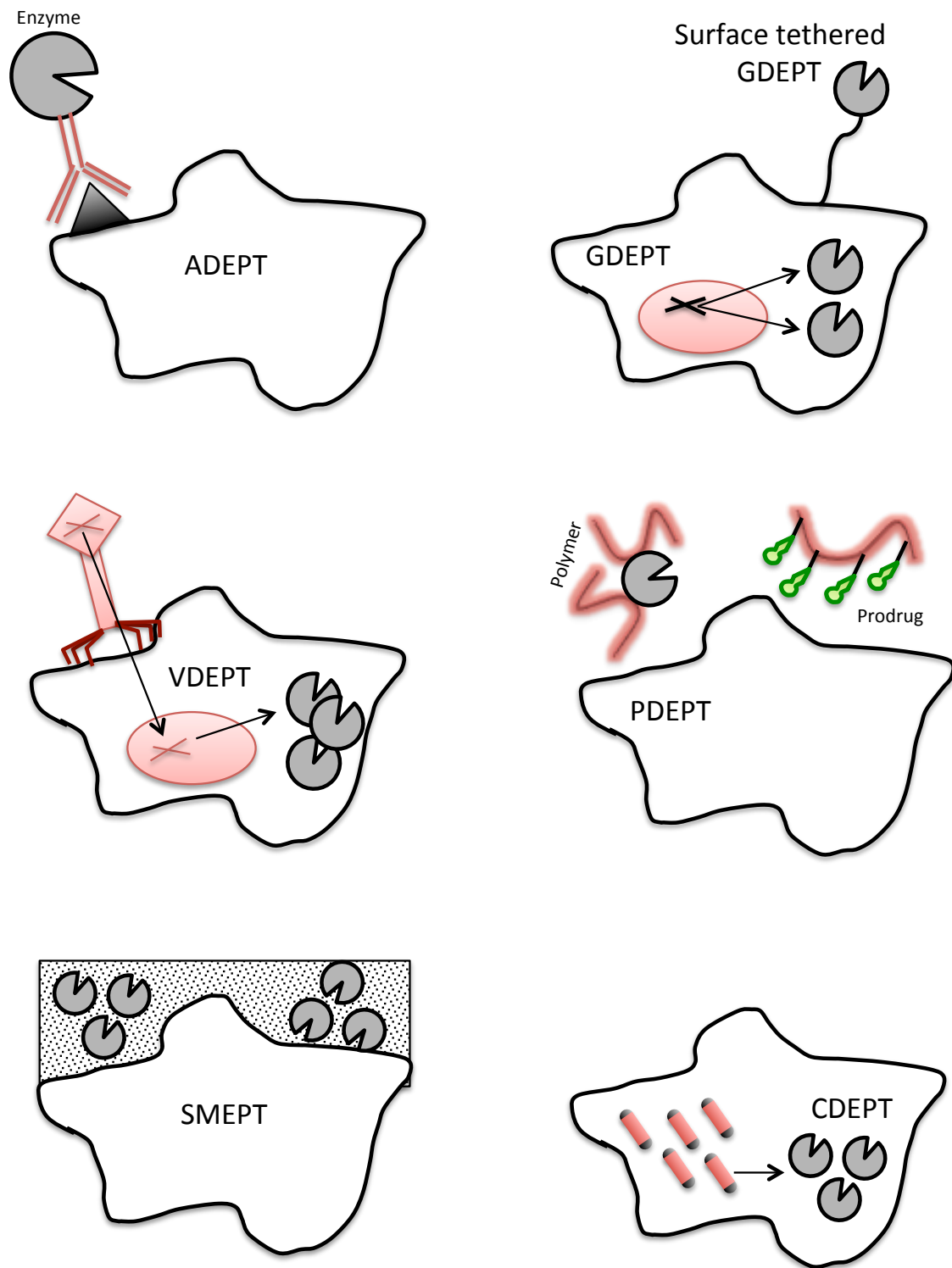
Figure 8: Overview of common EPT approaches

VDEPT – Virus directed EPT: Much like GDEPT, VDEPT relies on inserting a gene encoding for the enzyme of interest into the cancer cell, only that VDEPT uses a virus to deliver the DNA. VDEPT has the potential to cause severe immune responses, is limited by the size and quantity of the plasmid DNA harbored by the virus, and future success hinges upon the development of safe and effective viral vectors.[23,24]

PDEPT – Polymer directed EPT: PDEPT utilizes a combination of a polymer/prodrug conjugate and a polymer/enzyme conjugate, which may or may not be actively targeted. The addition of polymers to the prodrug and the enzyme prolongs circulation time, increases passive uptake in tumors due to increased size, especially for the relatively small prodrug, and reduce immunogenicity of the conjugate. The treatment modality for PDEPT is reversed, in that the polymeric prodrug is administered first, as it has a rapid blood clearance rate, followed by the polymeric enzyme which has a long circulating half-life.[25]

SMEPT - Substrate mediated EPT: In this approach a porous substrate, such as a hydrogel, is infused with the enzyme of interest. This substrate is then implanted near the tumor, such that any prodrugs converted within the substrate can diffuse out to enact their effects.[26] This is a very new approach, and although invasive, shows promise.

CDEPT – Clostridia directed EPT: This approach uses recombinant anaerobic clostridial bacterial spores to essentially colonize tumor cells and express the desired enzyme within the tumor cell. This is only effective if the prodrug readily diffuses across the cell membrane. This method is especially well suited for the nitroreductase system where the enzyme must be situated intracellularly to be active.[27] However,

bacterial therapeutics cannot currently or foreseeably be safely administered in the clinic.[28]

Considerations for successful enzyme prodrug therapy

There are several considerations for successful enzyme selection, which should be given priority vs. selection of the drug/prodrug, as prodrugs can be designed to fit the enzyme, but the opposite carries considerably more difficuly.[29] These considerations are:

(i)   The enzyme should be active at a physiological pH and display rapid and efficient prodrug activation (high k_{cat} and low K_m) at low concentrations of the substrate.[29]

(ii)   Natively present enzymes should not be able to convert the prodrugs into drugs, either due to a different reaction pathway[29] or due to compartmentalization of the enzyme such that interaction with the substrate is unlikely to occur.

(iii)   The enzyme itself should not be cytotoxic.[29]

(iv)   The enzyme selected should non-immunogenic (i.e. human)[29] or have a foreseeable pathway of immunogenicity reduction such as humanization via site-specific mutagenesis, PEGylation, or exon shuffling to address the immunogenicity associated with the use of with therapeutic proteins in clinic.[30]

There are also several considerations for successful drug/prodrug selection:

(i)   The therapeutic index, the ratio of prodrug cytotoxicity to drug cytotoxicity, should be at least 100,[29] although in the work presented herein we propose that a therapeutic index exceeding 1000 is a better, albeit more ambitious, target.

(ii)   The drug created should be lipophilic as to diffuse freely into the cells, where it enacts its killing effects. Even better, if the prodrug is hydrophilic it cannot cross cell membranes, thereby mitigating its systemic toxicity.[29,31]

(iii)   The active metabolites of the drug should be cell cycle independent. The most common oversight on this consideration are the drugs that inhibit DNA replication as these will only kill cells that are in the S phase of growth.[29]

(iv)   The drug created should have a half-life long enough to be transported into surrounding cells and thereby create a bystander effect, but not long enough to infiltrate into systemic circulation in any appreciable quantity.[29]

(v)   In order to be most potent, the drug should be efficacious on a variety of tumor cell populations.[31]

Annexin-Directed Enzyme Prodrug Therapy

Mechanism of action

Annexin-directed enzyme prodrug therapy is a two-step approach, as shown in Figure 9. First the enzyme is localized to the tumor, and then the enzyme is allowed to convert prodrugs into anti-cancer drugs while remaining localized to the tumor. Annexin-directed enzyme prodrug therapy is feasible due to the creation of fusion proteins (FPs), each consisting of an enzyme and an annexin targeting protein, which have been joined together with a short but flexible amino acid linker. The linker serves to create separation between the proteins so each protein can retain its functionality.

FPs are carried to the tumor via the bloodstream, where they bind to a phospholipid target on the endothelial cells that line the blood vessels within the tumor, via the annexin targeting protein. Our fusion proteins are also capable of localizing to tumor cells directly, because tumor endothelium contains gaps, formed during frantic growth, allowing the fusion protein to enter the tumor itself and bind directly to tumor cells. In contrast, the proposed fusion protein will not bind to healthy cells or healthy blood vessel cells, as these do not express the phospholipid target and form tight junctions without gaps, which will not allow the fusion protein to cross into healthy tissues.[2,32,33]

Once tethered to the tumor/tumor vasculature via annexin-phospholipid bonds, the enzyme then converts systemically administered drug precursors, prodrugs, into chemotherapeutics within the tumor microenvironment. Prodrugs are well tolerated systemically as they are generally hydrophilic and therefore unable to cross the cell membrane. Once converted, the resulting drugs are usually hydrophobic and can
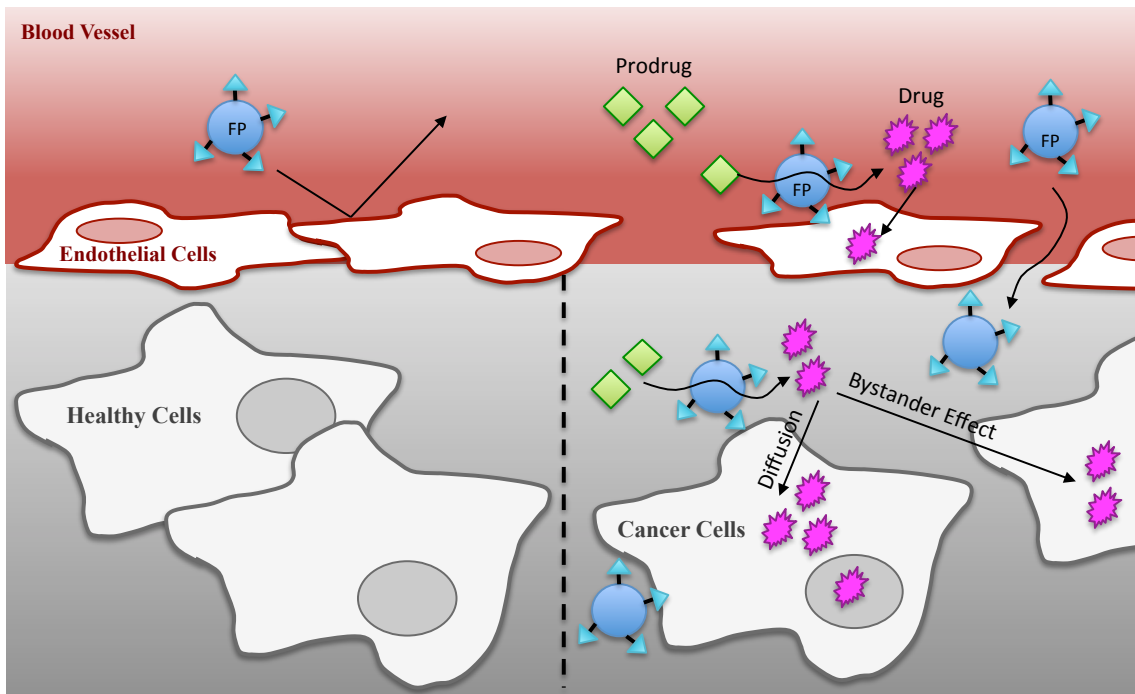
Figure 9: Schematic representation of enzyme prodrug therapy

First, the annexin targeting portion (▲) of the fusion protein (FP) binds to the cancer cells and the blood vessel cells surrounding the tumor. Second, after any unbound FP is allowed to clear from the bloodstream, a prodrug (◆) is injected into the bloodstream, which upon interaction with the enzyme portion (●) of the bound FP is converted into a powerful anticancer drug (✳) that is free to move across the cell membrane to enact its killing effects. Drugs are also free to move between cells (bystander effect), and therefore even cells that do not have FP bound to them can be affected by treatment.

therefore readily diffuse into the tumor cells themselves to enact their killing effects. Drugs can also diffuse into cells that do not have any FP bound, creating a bystander effect. This mechanism also readily transfers to an *in vivo* administration scheme, as presented in Figure 10.
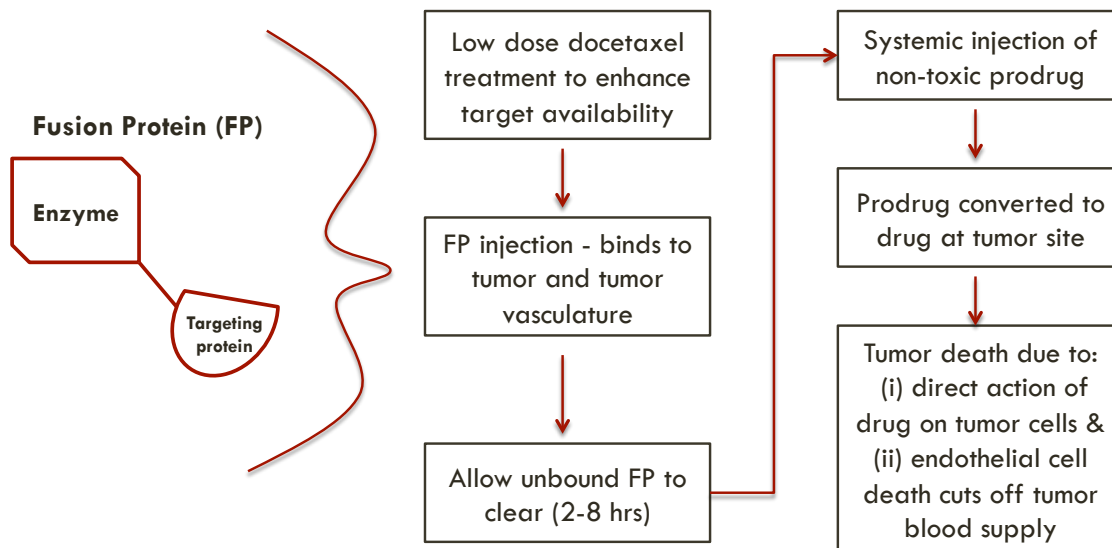
Figure 10: *In vivo* **administration scheme for annexin-directed EPT**

In a clinical setting, annexin-directed EPT therapy can readily be delivered but must be timed carefully. First the tumor can be primed with drugs, such as docetaxel which increases the tumors capacity to interface with the fusion proteins.[34] Alternatively, the tumor microenvironment can be primed for optimum treatment response using drugs, such as Taxol, which decreases the tumor interstitial fluid pressure.[35] An intravenous or intraperitoneal injection then delivers the fusion protein to the primed tumor, where the fusion protein binds to the tumor vasculature and the tumor. After any unbound tumor is allowed to clear from the bloodstream, systemic administration of the prodrug follows. Conversion of prodrugs by tethered enzymes produces drugs in the tumor environment. The optimal dosing schedule will vary for each EPT system as fusion protein clearance rates and prodrug/drug half-lives vary between systems.

Phosphatidylserine (PS) is an anionic plasma membrane phospholipid, contributing approximately 8-15% of membrane phospholipid content.[36] PS is found exclusively on the inner membrane leaflet under normal conditions. The cell actively maintains this asymmetry via the ATP-dependent aminophospholipid translocase membrane transport protein. Any changes in PS distribution are due to the loss of ATP transporter function or the activation of calcium dependent scramblase, which randomizes membrane lipid distribution, as shown in Figure 11.[2,37]

PS exposure on the outer leaflet is most commonly regarded as an early sign of apoptosis. Under normal conditions, the exposure of PS is a "find me" signal that hails nearby macrophages to eat the cell and acts to quell immune response by suppressing inflammation and antigen presentation. In healthy cells, calcium elevation, ATP depletion, oxidative stress, vesicle fusion to the inner membrane, necrosis, and apoptosis can all incite PS exposure.[37] PS exposure has also been found in sickle-cell anemia, thalassemia, uremia, diabetes, malaria, certain viral infections such as influenza, and cystic fibrosis.[36] PS exposure can, however, also occur on viable, non-pathologic, non-apoptotic cells, such as neoplastic cells.

Primary cancer cells, their metastases, tumor vasculature, and cultured tumor cells all explicitly and significantly express PS without cell damage or external activators present, and, importantly, this is not an artifact caused by culturing cells.[38] Thus, PS exposure presents a promising common marker for malignant cells. PS exposure may be caused by tumor microenvironment stressors such as hypoxia, acidity, thrombin, and/or inflammatory cytokines, but once removed from the tumor
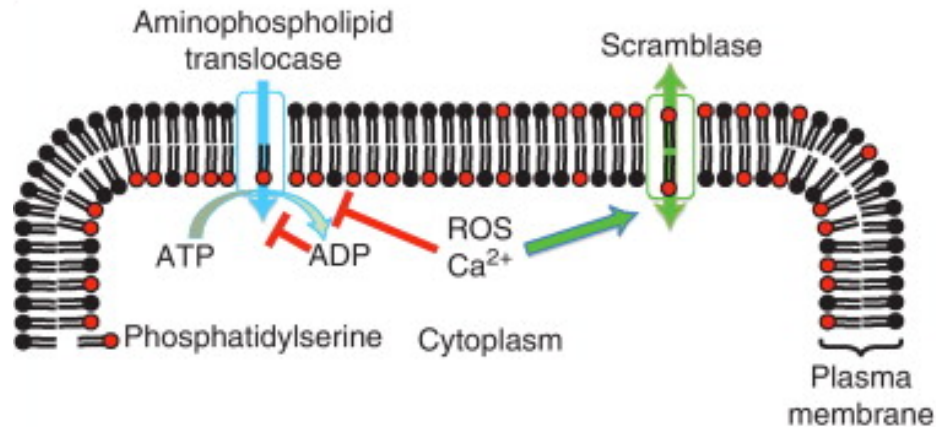
Figure 11: PS exposure mechanism [Reproduced from 37]

Aminophosphlipid translocase works to keep PS on the cytoplasmic side of the membrane. However, if either the translocase ceases to function properly or Ca^{2+} activates scramblase, then PS asymmetry is lost.

microenvironment and into lab-bench, cell-culture conditions, cancer cells continue to express PS.[2] It has been demonstrated that this phenomenon is neither an experimental artifact or of apoptotic origin, suggesting that PS is the "underestimated Achilles heal of cancer".[38] Non-confluent endothelial cells, i.e. not allowing the cells to come in contact with one another to form tight junctions, also natively express PS without endogenous activators present in culture, and can therefore serve as mimics of tumor vasculature.[39] Annexin-directed EPT thus actively targets both tumor cells as well as tumor vasculature, as shown in Figure 12, while also actively targeting metastases.

Why aren't these cancer cells eaten up by macrophages, when they are clearly signaling for phagocytosis? Most human cancer cells overexpress a "don't eat me" signal, CD47, so much so that CD47 expression titers have been correlated with tumorigenicity in mouse models. If CD47 is silenced, phagocytosis ensues. Thus,
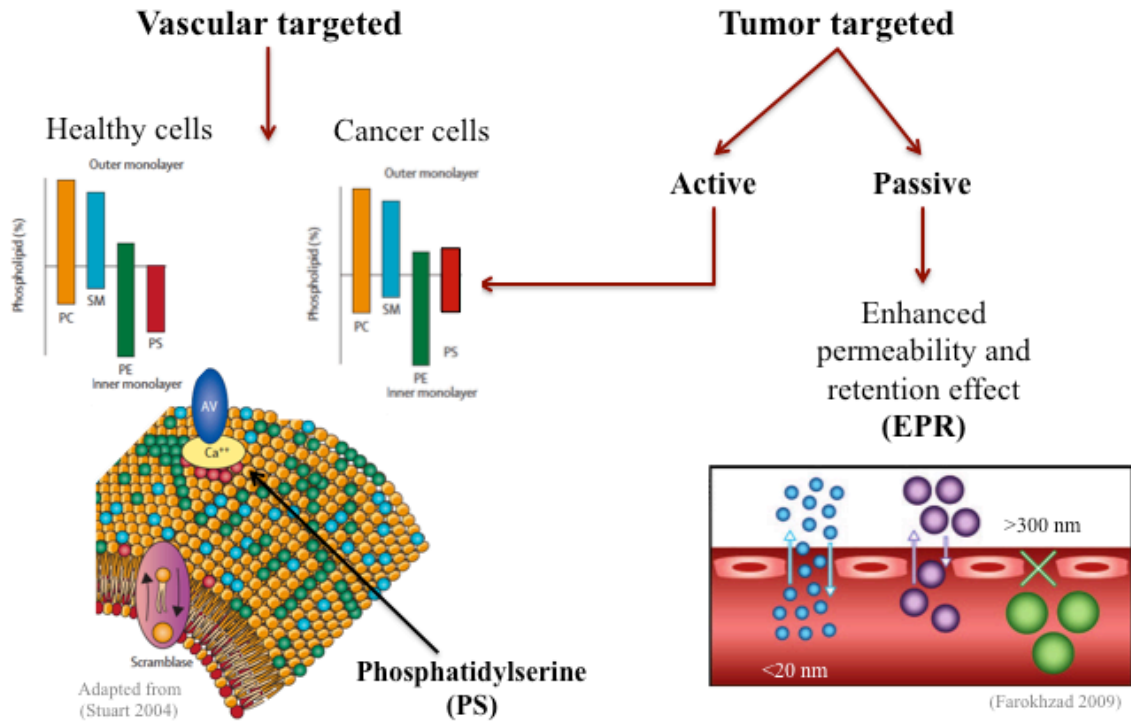
Figure 12: Annexin-directed EPT targeting approach [Adapted from 40,41]

Fusion proteins are actively targeted to the tumor and tumor vasculature via annexin A5, which binds to PS, an anionic phospholipid, shown in red, in a calcium dependent manner. PS is found almost exclusively on the inner membrane monolayer in healthy cells but is exposed on the outer membrane monolayer in malignant cells, their metastases, and the tumor vasculature across all cell lines investigated to date. Fusion proteins are also passively targeted to the tumor via the enhanced permeability and retention (EPR) effect, which enables macromolecules to enter the tumor and entraps them therein, solely based on their size. The EPR effect exists for macromolecules between 20 and 300 nm in diameter, which includes some of the fusion proteins investigated.

malignant cells can overwrite the downstream effects of PS externalization, escaping cell death and possibly even utilizing PS exposure to help subdue immune response.[36,37]

Active targeting: Annexins, the effector proteins

The annexin A protein family consists of 12 proteins, A1-A13, with A12 unassigned. Annexins are Ca^{2+} dependent acidic phospholipid binding proteins that display a differential binding preference: phosphatidic acid > phosphatidylserine > phosphatidylinositol, with some binding noted to neutral phosphatidylethanolamine, but none that has been observed for phosphatidylcholine or sphingomyelin.[42]

Although only 45-55% of amino acid identity is preserved within the annexin A family, the core region is highly conserved with respect to secondary and tertiary structure. The core region consists of four α-helix repeats (70 amino acids each), which coil to form a right-handed super-helix. The core region binds to bind Ca^{2+} and membrane phospholipids on its convex side, as shown in Figure 13.[43–45]

The N-terminal head, however, is less conserved and structurally separated from the core region. When Ca^{2+} is absent, the N-terminal domain is buried within the core region, but once Ca^{2+} is present, the N-terminal is exposed such that it may bind to cytosolic ligands, as shown in Figure 13a.[45] Not surprisingly, the specific biologic activity of each annexin is mediated by the N-terminal domain. For example, annexin A1 is known to interact with epithelial growth factor receptor, formyl peptide receptor, selectin, and integrin A4, whereas annexin A5 is known to interact with collagen type 2, vascular endothelial growth factor receptor 2, integrin B5, protein kinase C, cellular

26
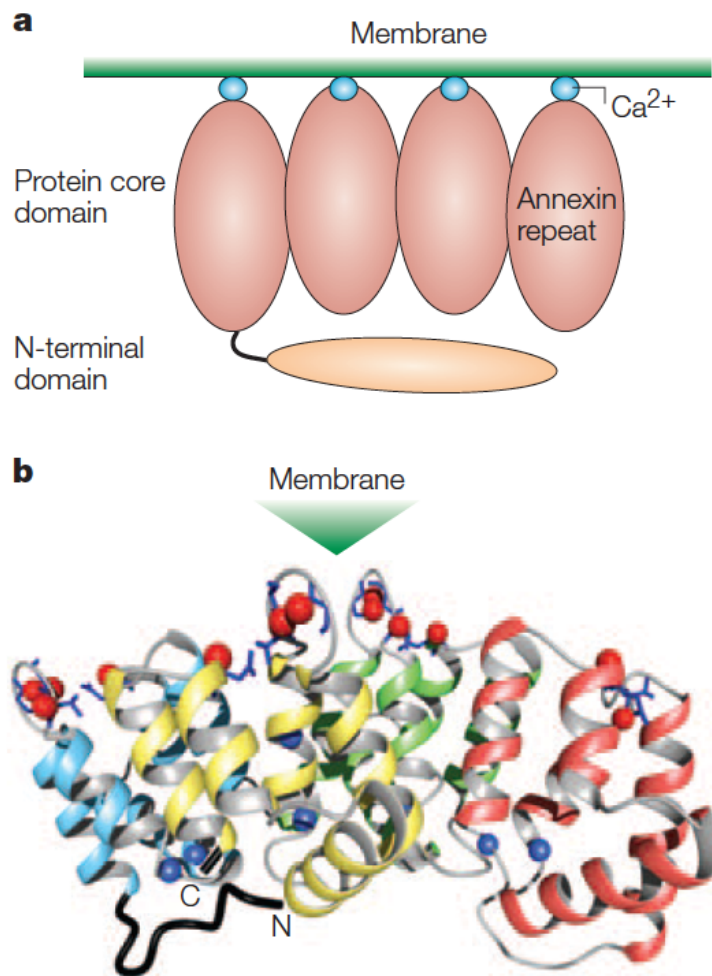
Figure 13: (a) Cartoon annexin binding to membrane (b) conserved annexin core structure binding to membrane

(a) Each annexin core repeat is shown binding to Ca^{2+} and to the phospholipid membrane, with the N-terminal domain free to interact with cytosolic ligands. (b) The crystal structure of the annexin core binds to the membrane and Ca^{2+} on its convex side with the N-terminal region extending from the concave side of the protein disk.

modulator of immune recognition, G-actin, helicase, and DNA (cytosine-5-) methyltransferase 1.[43]

Annexins are typically cytosolic proteins, but for annexin-directed EPT we utilize A1 and A5 extracellularly for their phospholipid binding properties. However, if the fused protein is constructed such that annexin is fused on the C-terminal, upon binding the N-terminal is left free to interact with any ligands present, which could prove therapeutically beneficial.

Annexin A1

Annexin A1 (A1) is one of the largest annexins at 38.7 kDa. A1 does not display a preference for lipid binding other than towards acidic phospholipids[46] and has been shown to bind specifically to PS in a monomeric fashion via scanning probe microscopy.[47] A1 binds to PS with a slightly lower affinity than A5, with a dissociation constant of 39 nM for membrane mimetic artificial lipid layers in the presence of 1 mM Ca^{2+},[48] with no published dissociation constants for cells in culture to date. Due to structural differences in calcium binding domains, A1 requires a lower threshold Ca^{2+} concentration for binding to PS than A5.[49] Although A1 is usually studied as an endogenous ligand, exogenously introduced A1 has been shown to bind to cells expressing PS.[50]

A1 is one of three annexins found both extracellularly and intracellularly (A1, A2, and A5).[51] Upon induced cell death *in vitro* for human primary smooth muscle cells, a distinct ring-like structure of A1 appears by 3 hours post apoptosis induction and the effect increases 6 hours post apoptosis induction.[52] Once externalized, A1 acts

28

as a bridging protein for PS to promote phagocytic uptake[52,53] and contributes to anti-inflammatory signaling,[54,55] possibly even acting as a tumor suppressor by inhibiting proliferation.[56]

Polymerization and subsequent endocytosis, as seen with A5, does not occur with A1 upon binding to PS. Instead, A1 creates a halo-like effect surrounding the cell, as shown in Figure 14a for Jurkat cells.[50] The endocytotic vesicle formation seen with A5 is not present for A1, and, therefore, A1 targeted enzymes may internalize less than their A5 counterparts, leaving more of the fusion protein anchored to the exterior cell surface, and, therefore, free to convert extracellular prodrugs into drugs.

Increasing the amount of A1 bound to PS in a neoplastic environment may promote recognition of the PS apoptotic signal expressed but not recognized in most solid tumors. However, A1 displays diverse upregulation or downregulation in certain cancers without any clear pattern (pancreatic ↑, prostate↓, and breast ↑↓).[56] A1 has also been found to be selectively expressed on the blood exposed surface of tumor blood vessels.[57,58] Recently, low levels of A1 in prostate cancer have led to the investigation of the re-expression of A1, which reduced tumor viability and inhibited proliferation.[59] This may indicate that A1 expression may have a tumor suppressor effect, a potential added benefit to utilizing A1 to target fusion proteins to malignant sites.

(a)

	AnxA5-Alexa568	AnxA1-Alexa568
Jurkats	A	B
HeLa	D	E
AnxA5	+	−
AnxA1	−	+

(b)

- ● PtdSer
- ✕ F-actin
- — Annexin A5
- ⊱ Trimer of Annexin A5
- ■ ■ ■ Microtubules
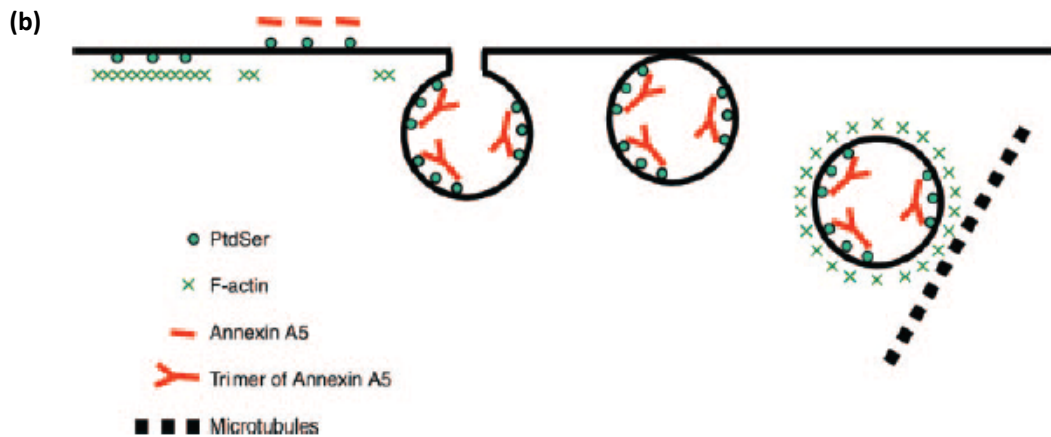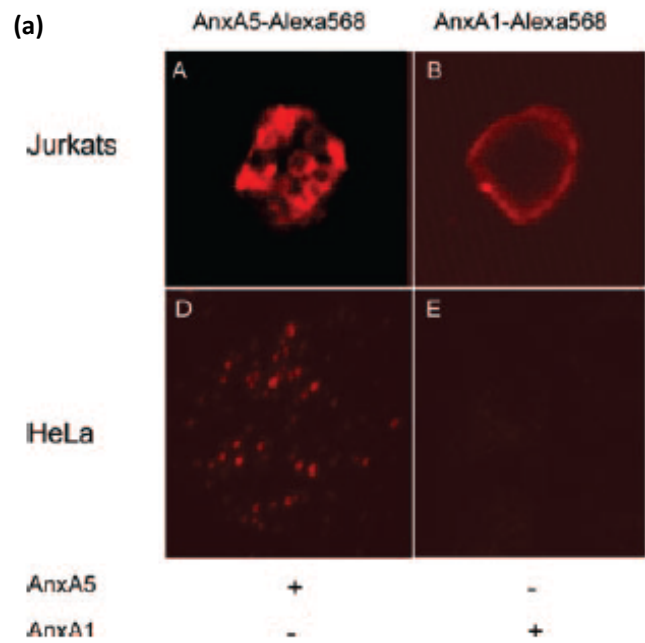
(Adapted from Kenis, 2004)

Figure 14: A5 internalization proposed mechanism [Reproduced from 50]

(a) Fluorescent A5 (AnxA5) and A1 (AnxA1) express distinct localization tendencies post binding to PS on the cell surface, with A5 internalizing into the cell and A1 forming a halo surrounding the cell. (b) Proposed trimerization mechanism that induces endocytotic uptake of A5 post binding. PS is abbreviated as PtdSer in the legend.

Annexin A5

Annexin A5 (A5 or AV), one of the smaller annexin proteins at 35.7 kDa, is one of three annexins found both intracellularly and extracellulary.[51] A5 binds selectively to membrane PS, with reported dissociation constants ranging from 2.7 to 15.5 nM.[60,61] The ionized Ca^{2+} concentration in circulation (approximately 1000 μmol/L) promotes quick binding of A5 to exposed PS residues.[62] Upon binding to Ca^{2+}/phospholipids, A5 becomes remarkably more thermodynamically stable.[63]

Extracellular A5 has been implicated primarily as an anti-coagulation protein. Upon activation, platelets express PS and subsequently become surrounded by A5. Binding of A5 to these PS sites could block accessibility of the cell surface for coagulation agents, thereby blocking their effects.[61,63,64] In wound healing, A5 has been shown to promote membrane resealing, by binding to the edges of the membrane tear, forming a 2D matrix, and thus preventing wound expansion.[65] In apoptotic cells, the role of A5 binding to surface PS residues is still debated.   A5 has been shown to inhibit phagocytosis of apoptotic and necrotic cells, while also mitigating any immune response, but has also been shown to accelerate cell death in cardiomyocytes, suggesting that the role of extracellular A5 in apoptosis is both cell and trigger type dependent.[62] Lastly, A5 may also play a role in regulating immune response, as it has been shown that upon binding to T cells, A5 delays programmed cell death by blocking the release of $CD4^+$.[63]

Evidence exists that A5 may internalize upon binding to PS, as shown for Jurkat and HeLa cells in Figure 14a. Upon binding to cell surface expressed PS phospholipids, A5 polymerizes, forming trimers that dent the cell membrane and initiate endocytosis,

as shown in Figure 14b.[50] It is unclear if this import mechanism is preserved once A5 is integrated into fusion proteins, as the size, molecular weight, and A5 spatial orientation are significantly altered via fusion. Once fused, steric hindrance may inhibit trimer formation, thus voiding the A5-mediated endocytosis pathway.

Active targeting: Vascular

Due to diffusion limitations, tumor volume cannot surpass 1-2 mm^3 without the support of microvasculature for nutrients and oxygen.[66] Following this avascular growth phase, almost all solid tumors, including breast, prostate, pancreatic, and colon malignancies, require a second, angiogenesis-dependent, vascular growth phase in order to become maligant.[67,68] Moreover, tumors rely on vascularization to the extent where vascular density becomes an important prognostic indicator for breast,[69,70] prostate,[71,72] pancreatic,[73] and colon cancer.[74]

Vascular networks in tumors only poorly resemble vasculature in healthy tissue. Tumor vasculature lacks definition, structure, and regularity, with an overabundance of phospholipids, such as PS, and other negatively charged functional groups.[35] Since PS is also exposed robustly and consistency on the tumor vasculature,[2] our fusion proteins actively target the tumor vasculature, as indicated in Figure 12.

Vascular targeting is a very appealing solid tumor targeting strategy. Firstly, tumor endothelial cells present easily accessible targets for systemically administered macromolecules. Secondly, relatively minor vascular damage can amplify into macro-regional tumor infarction, since a single vascular endothelial cell supports the survival of approximately 1000 tumor cells via oxygen, nutrients, and the route for metastatic

spread. Thus, endothelial cell death is magnified downstream. Another feature

contributing to the attractiveness of vascular targeting is that tumor endothelial cells are

genetically more stable than tumors cells and have lower rate of acquisition to treatment

resistance. Lastly, vascular targeting theoretically enables the targeting strategy to be

tumor type independent.[31,75]

Passive targeting: The EPR effect

Our fusion proteins are not only actively targeted to phosphatidylserine on malignant

lesions and vasculature via annexin, but also passively targeted to the tumor

microenvironment by means of the enhanced permeability and retention effect (EPR),

as shown in Figure 12.

The endothelial cells throughout most of the body are either continuous, forming

tight junctions that closely regulate transport as shown for the healthy cells in Figure 9,

or fenestrated for the secretion or excretion of biological fluids. However, in tumors the

endothelium is discontinuous with gaps on the order of 0.4 to 0.6 microns, also shown

in Figure 9, which is significantly larger then the gaps found in the discontinuous

endothelium found in healthy liver, spleen, and bone marrow.[35] These large pores

enable the enhanced permeability and retention effect (EPR).

The EPR effect essentially enables large macromolecules to enter the tumor and

then become entrapped therein, leading to increased accumulation of these

macromolecules within the tumor based on size alone, as shown in Figure 15. Besides

leaky vasculature, other tumor physiology characteristics also contribute to the EPR

Figure 15: Visualization of the EPR effect ^{Reproduced from 17}

The enhanced permeability and retention effect (EPR) consists of two stages. First macromolecules are able to exit tumor blood vessels through leaky junctions and enter the tumor microenvironment. Once in the tumor microenvironment, a number of factors help to entrap the macromolecule within the tumor, such as a lack of lymphatic drainage. The EPR effect is entirely based on size, and is present only for particles 20-300 nm in diameter, with a peak effect seen for a diameter of 100 nm. This effect is more pronounced in primary tumors than in metastases, due to underdeveloped vasculature in micrometastases.

effect: (i) A lack of lymphatic drainage, which closes off one of the clearance routes for therapeutics from the tumor. (ii) A lack of the smooth muscle surrounding the endothelium, which normally controls vasodilation, encourages a higher blood flow

34

volume through tumor capillaries than through healthy capillaries. (iii) Lastly, the increased capillary density in tumors, allows for macromolecular drugs to diffuse through tumors at relatively high rates (1 mm/h), thus allowing the macromolecule to readily diffuse the 20-30 microns adjacent the tumor vasculature which can support growing tumor cells.

The EPR effect is applicable only to large molecules greater than 20 nm in diameter, is maximized around 100 nm diameter particle size, and ceases to exist above a 300 nm particle size, as depicted in Figure 12. Active targeting for particles below 50 nm in size has been shown to improve EPR effect medicated tumor accumulation.[35] Our larger fusion proteins fall within the lower end of this size range, the largest of which (hA1/5-β-glucuronidase) measures approximately 30 nm in diameter and the smallest of which (A5-cytosine deaminase) measures approximately 15 nm (measurements taken on 3D renderings of fusion proteins in Mac PyMol 1.2, educational version). The fusion proteins discussed herein are all also actively targeted to the tumor, serving to anchor them to tumor cells once in the tumor microenvironment and, thereby, enhancing the EPR effect.

In spite of the EPR effect, there exist a host of biological barriers that counteract the intratumoral transport of macromolecules. For example, the tumor vasculature is filled with loops and trifurcations with an at best debatable average vessel density, blood vessel leakiness in tumors also varies widely, and tumor interstitial pressure is generally high, favoring diffusion of macromolecules out of the tumor.[35] Indeed, studies have shown a non-ideal, heterogeneous distribution of antibody throughout the tumor following intravenous injections.[20] However, some of the best tumor

distributions of macromolecules have been achieved by targeting antibodies to extracellular annexin A1 natively bound to surface-exposed PS on tumor cells.[76] This suggests that the annexin-based targeting approach has the potential to overcome traditional distribution limitations.

Meet the fusion proteins

The work presented herein will discuss five different fusion proteins, or FPs. Each consists of an enzyme core linked to annexin targeting proteins, which theoretically surround the enzyme core in a halo-like fashion. All FPs are targeted via annexin A5, with only one targeted via annexin A1. Genetic linkage is accomplished via a serine-glycine linker, which is flexible. For the human fusion proteins, this linker has been engineered to be non-immunogenic. Linkers are slightly shorter in non-human constructs, but in both cases serve to create spatial separation between the enzyme and the annexin, allowing each to maintain its functionality.

Three of the FPs contain non-human enzymes, which are: (i) L-methioninase (MT) from *Pseudomonas putida*, (ii) purine nucleoside phosphorylase from *Escherichia coli*, and (iii) cytosine deaminase (CD) from yeast. The other two FPs both contain the human enzyme β-glucuronidase (βG). Cartoon diagrams of all fusion proteins are presented in Figure 16, showing multimeric structures. Three of the fusion proteins are tetramers, and of the remaining two, one is a dimer and the other a hexamer. Molecular weights are also indicated in Figure 16 and cover a wide range from 106 to 461 kDa, creating a unique EPR effect profile for each fusion protein.
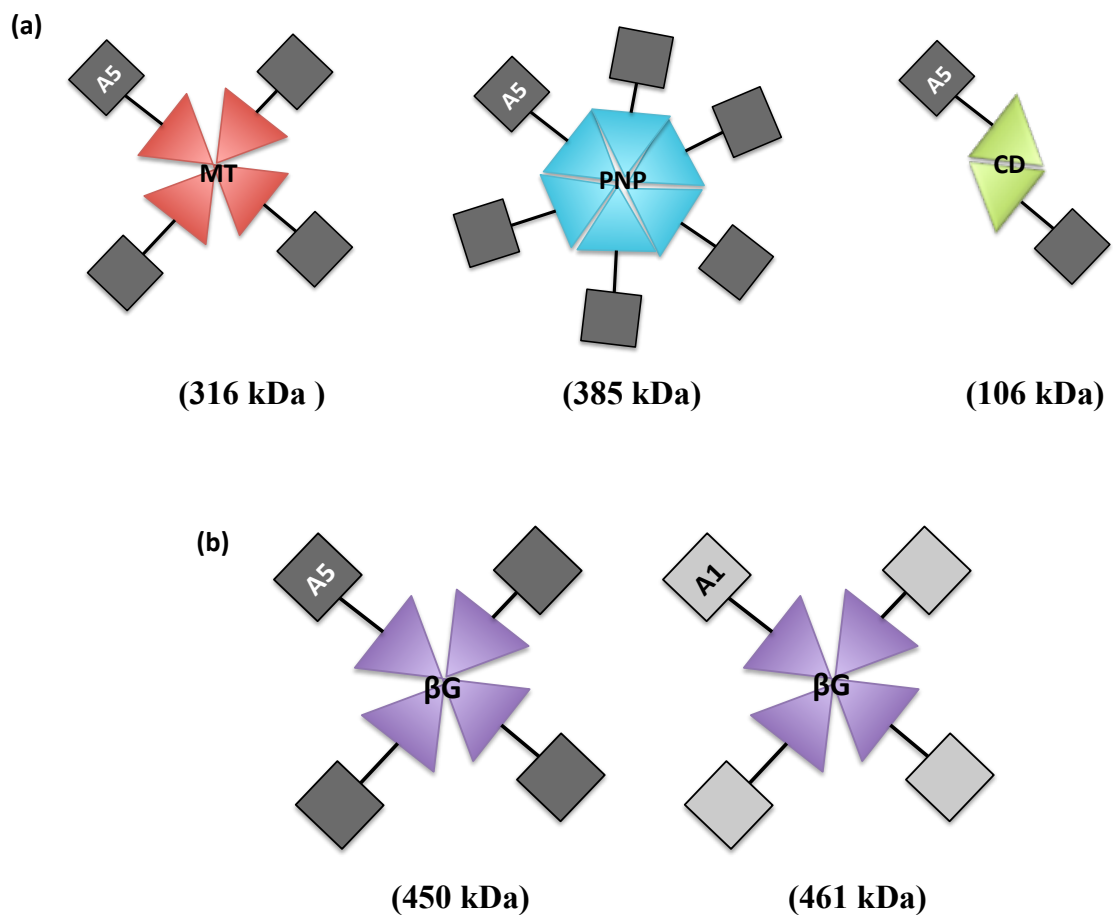
Figure 16: Cartoon fusion protein diagrams

(a) Diagrams of the non-human enzymes studied in fusion with AV. MT-AV is a tetramer, PNP-AV is a hexamer, and CD-AV is a dimer. All are relatively varied in molecular weight as indicated below each fusion protein. (b) Diagrams of the human enzymes studied shown in fusion with A1 and A5. Both are tetramers, with molecular weights indicated.

Each enzyme can convert unique prodrugs into anti-cancer compounds, as shown in Table 1, with prodrugs investigated herein highlighted. The mechanism of cell death induced by these drugs varies and is also specified in Table 1.

Table 1: (a) Non-human and (b) human enzymes utilized in fusion proteins, their prodrug substrates, products created, and product effect on cells

Note: Gray highlights indicate prodrugs studied.

(a) Enzyme	Prodrug	Drug	Mechanism of Action
MT	L-selenomethionine[77]	methylselenol → α-ketobutyrate and ammonia	Oxidation of thiols & generation of superoxides
	methionine[78]	methanethiol	Depletes methionine, an essential amino acid
PNP	fludarabine[79,80]	2-fluoroadenine	Misincorporates into DNA/RNA & inhibits ribonucleotide reductase, DNA ligase and primase
	6-methylpurine deoxyribose[81,82]	6-methylpurine	Misincorporates into DNA/RNA
CD	5-fluorocytosine[83]	5-fluorouracil	Misincorporates into DNA/RNA & inhibits thymidylate synthetase

(b) Enzyme	Prodrug	Drug	Mechanism of Action
βG	SN-38G[84,85]	SN-38	Topoisomerase 1 inhibitor
	HMR 1826[86] Dox-GA3[87]	Doxorubicin	DNA binding, topoisomerase II inhibitor, cytochrome P450 inhibitor
	pHAM glucuronide[88]	p-hydroxyaniline mustard (pHAM)	Crosslinks DNA via alkylation
	seco-CBI-DMAI-glucuronide[89]	seco-duocarmycin SA analog	Alkylation via minor DNA groove binding
	SAHA β-*O*-glucuronide[90]	suberoylanilide hydroxamic acid (SAHA)	Inhibits histone deacetylase (HDAC)

Most of the drugs generated by the human enzyme βG have garnered either FDA approval or at least evidence of efficacy in clinical trials. A precursor of SN-38, irinotecan (CPT-11), which is endogenously converted to SN-38, is the preferred first and second line treatment for colorectal cancer, effectively replacing fluoropyrimidines with topoisomerase inhibiton.[9,91] Additionally, A PEGylated form of SN-38 has shown efficacy in phase II trials for metastatic breast cancer.[92] Suberoylanilide hydroxamic acid (SAHA) has shown activity in patients with solid tumors in a phase I trial, including positive effects for prostate, breast, and colon cancer patients.[93] Doxorubicin is a common anthracycline utilized in combination chemotherapy treatments for metastatic breast cancer.[94] P-hydroxyaniline mustard cannot directly be administered systemically, but analogs have found success in a clinical setting, including for solid tumors;[95] Most notable of the aromatic nitrogen mustard analogs is cyclophosphamide, which is a common first line treatment for breast cancer.[96] The natural cytostatic antibiotic duocarmycin SA is one of the most potent known anti-cancer compounds, but cannot be administered systemically due to severe myelotoxicity, the suppression of bone marrow function.[97] The systemic toxicity of duocarmycin SA can likely be controlled with an EPT approach, possibly allowing this powerful drug to enter the clinical setting. Since the same enzyme can produce all of these drugs, combination therapies of these drugs can be administered within the confines of the βG platform.

It has been proposed that the future success of the clinical treatment of solid tumors will depend on the combination of chemotherapy with immunotherapy. Over the past decade, the immune system, both adaptive and innate, has been increasingly

implicated in crucially contributing to chemotherapeutic antitumor effects. Since chemotherapy is highly selective for rapidly proliferating cells, the immune system must be called upon to destroy tumor stem cells. βG-generated chemotherapeutic drugs target three of the known pathways in which cell stress can lead to cell death via cytotoxic effector cells, for example, natural killer cells and cytotoxic T-lymphocytes, as shown in Figure 17.[98] Interestingly, doxorubicin, unlike other cytostatic agents, has also been shown to elicit immunogenic cell death and shows promise for combination with IL-12.[98] Thus, not only can the βG platform produce multiple drugs at the tumor site, but βG-generated drugs are also prime candidates for immune-modulated effector cell death.

For the non-human enzymes, the clinical efficacy of drugs generated with respect to the cancer types investigated herein is limited in comparison to the βG-generated drugs. Two of the three non-human enzymes produce nucleotide analogs (PNP and CD). The pyrimidine analog 5-fluorouracil is used to manage solid tumors, including breast, colorectal, and pancreatic, and is FDA approved for use within the first line combination treatments FOLFOX and FOLFIRI for colon cancer.[99] 5-fluorouracil has also been implicated in the expression of heat shock proteins, which promote tumor cell antigen uptake by dendritic cells, and sensitizes cells to death by cytotoxic T lymphocytes.[98] The purine analog fludarabine, which is endogenously converted to 2-fluoroadenine, has completed several clinical trials but has been shown to be most effective for indolent leukemias, with myelotoxicity limiting its use in solid tumors.[79,100,101] Perhaps the most unique mechanism of killing presented within this
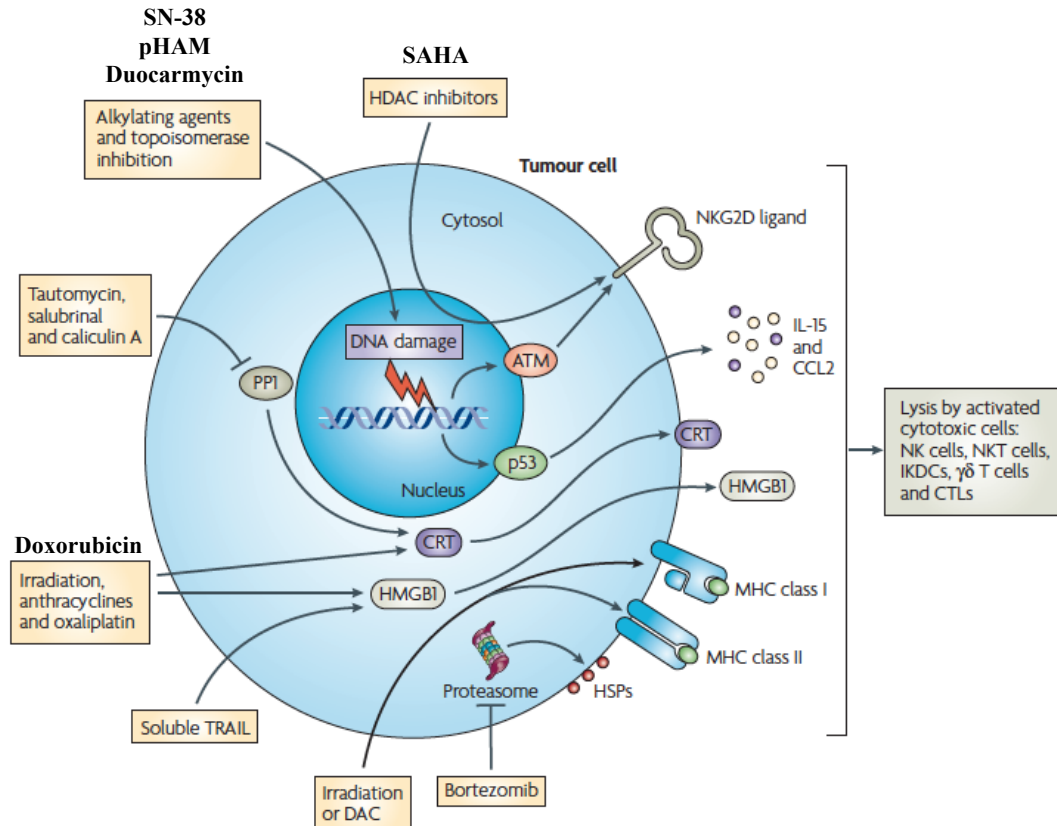
Figure 17: Pathways of βG generated drug induced cell stress provoking effector cell killing [Adapted from 98]

SAHA, an HDAC inhibitor aids the expression of cell surface expressed NKG2D (natural killed group 2, member D) ligands, display of which serves to elicit an innate immune response. Doxorubicin, an anthracycline, causes the release of HMGB1 (high-mobility group box 1 protein), which is essential for dendritic cell (DC) cross presentation of tumor antigens, which promotes cytotoxic T lymphocyte (CTL) tumor cell lysis. DNA damaging agents generated by βG, SN-38, pHAM, and duocarmycin also promote NKG2D ligand display via the ATM (ataxia-telangiectasia mutated) protein kinase, as well as restoring p53 function, which induces CCL2 and IL-15, which in turn help to recruit and activate innate immune cells.[98]

work, reactive oxygen species generated by the decay of methylselenol, has no clinical data as the half-life of the drug is on the time scale of seconds.

Project Aims

Applicability studies to prostate and pancreatic cancer

Annexin tumor targeting is theoretically tumor type independent. However, this cannot

be assumed to be true, as different malignant cell lines have highly varied PS expression

signatures. Even within the same malignancy, PS expression signatures can vary.

Previous work had focused exclusively on breast cancer, and therefore the aim of these

projects was to expand the applicability of existing fusion proteins with the non-human

enzymes MT, PNP, and CD to other high-burden solid tumors that might benefit from

annexin-directed EPT approaches. Chapter 2 aims to explore the effect of MT-AV,

PNP-AV, and CD-AV fusion proteins on prostate cancer, as well as to establish that

increased fusion protein binding is achievable and measureable with the addition of a

cell priming drug, docetaxel. Chapter 3 seeks to further expand tumor type

independence by investigating the effect of all non-human fusion proteins on pancreatic

cancer cell lines combined with docetaxel treatment. Together, these two chapters aim

to provide considerable evidence for the tumor type independence of annexin-directed

enzyme prodrug therapy.

Development and evaluation of β-glucuronidase

Having expended considerable effort towards establishing the tumor type independence

of targeting and efficacy for existing annexin-directed EPT systems, we evaluated the

clinical relevance of these existing systems with respect to the drugs generated and

immunogenicity of the fusion proteins. We decided that a novel approach would be

required to improve these metrics and aimed to develop a fusion protein that could

generate a therapeutic index (ratio of the toxicity of the prodrug to the toxicity of the drug) above 1000, produce FDA approved drugs, and have a significantly lower predicted immunogenicity than our previous non-human fusion proteins.

This search led to the development of a novel EPT system with the human enzyme β-glucuronidase (βG). βG was chosen as it has the potential to be vastly more powerful than previous systems, as it boasts a substantial list of FDA approved chemotherapeutic prodrugs/drugs along with designer super prodrugs capable of generating therapeutic indices approaching one million.[102] Since βG has many prodrugs in its arsenal, it is capable of generating multiple drug species, i.e. combination treatment, at the tumor site. Currently, it is difficult to combine chemotherapeutic approaches due to the buildup of side effects that occur with each additional drug. However, annexin-directed EPT generates these drugs in the direct vicinity of the tumor and therefore this build up of side effects will be markedly reduced, possibly not present at all. The βG enzyme is also a very attractive option with respect to immunogenicity. βG is natively present in both prokaryotic and eukaryotic life forms; However, βG is stringently sequestered to lysosomes inside of cells, therefore posing little risk of prodrug interaction with native βG and allowing utilization of the human βG enzyme, which virtually eliminates the risk of an adverse immune response to βG EPT.

Chapter 4 aims to develop a new annexin-directed enzyme prodrug therapy employing βG, which aims to increase the efficacy and clinical relevance of annexin-directed EPT. To aid translational work, Chapter 4 also aims to develop a scalable, high-yield production method for βG fusion proteins. Specifically, Chapter 4 presents

the design, production, purification, and multi-cell line *in vitro* efficacy investigation of annexin-βG fusion proteins.

Chapter 2: Applicability of Existing Fusion Proteins to Prostate Cancer

The following work was published as "Targeted Enzyme Prodrug Therapy for

Metastatic Prostate Cancer – A Comparative Study of L-methioninase, Purine

Nucleoside Phosphorylase, and Cytosine Deaminase" in the *Journal of Biomedical*

Science, in July of 2014. The authors are: Katrin P. Guillen, Carla Kurkjian, and Roger

G. Harrison.

Abstract

Background: Enzyme prodrug therapy shows promise for the treatment of solid

tumors, but current approaches lack effective/safe delivery strategies. To address this,

we previously developed three enzyme-containing fusion proteins targeted via annexin

V to phosphatidylserine exposed on the tumor vasculature and tumor cells, using the

enzymes L-methioninase, purine nucleoside phosphorylase, or cytosine deaminase. In

enzyme prodrug therapy, the fusion protein is allowed to bind to the tumor before a

nontoxic drug precursor, a prodrug, is introduced. Upon interaction of the prodrug with

the bound enzyme, an anticancer compound is formed, but only in the direct vicinity of

the tumor, thereby mitigating the risk of side effects while creating high intratumoral

drug concentrations. The applicability of these enzyme prodrug systems to treating

prostate cancer has remained unexplored. Additionally, target availability may increase

with the addition of low dose docetaxel treatment to the enzyme prodrug treatment, but

this effect has not been previously investigated. To this end, we examined the binding

strength and the cytotoxic efficacy (with and without docetaxel treatment) of these

enzyme prodrug systems on the human prostate cancer cell line PC-3.

Results: All three fusion proteins exhibited strong binding; dissociation constants were 0.572 nM for L-methioninase-annexin V (MT-AV), 0.406 nM for purine nucleoside phosphorylase-annexin V (PNP-AV), and 0.061 nM for cytosine deaminase-annexin V (CD-AV). MT-AV produced up to 99% cell death ($p < 0.001$) with limited cytotoxicity of the prodrug alone. PNP-AV with docetaxel created up to 78% cell death ($p < 0.001$) with no cytotoxicity of the prodrug alone. CD-AV with docetaxel displayed up to 60% cell death ($p < 0.001$) with no cytotoxicity of the prodrug alone. Docetaxel treatment created significant increases in cytotoxicity for PNP-AV and CD-AV.

Conclusions: Strong binding of fusion proteins to PC-3 cancer cells and effective cell killing suggest that the enzyme prodrug systems with MT-AV and PNP-AV may be effective treatment options. Additionally, low-dose docetaxel treatment was found to increase the cytotoxic effect of the annexin V-targeted therapeutics for the PNP-AV and CD-AV systems.

Keywords: enzyme prodrug therapy, vascular-targeted, docetaxel, annexin V, prostate cancer

Background

Prostate cancer (PC) is the most common non-skin malignancy and the second leading cause of cancer-related death in American men [103], yet remains essentially incurable. Since the introduction of PSA specific screening, the lethality of prostate cancer stems not from a lack of early detection but more commonly from the failure of loco-regional therapies creating a need for improved systemic therapies [104]. Currently, most single-agent anticancer drugs face challenges due to increased multidrug resistance [105], pharmacokinetic limitations [106,107], and restricted clinical dosage or frequency of administration due to cytotoxicity in non-cancerous tissues [108–110].

Antibody-directed enzyme prodrug therapy (ADEPT), gene-directed enzyme prodrug therapy (GDEPT), and viral-directed enzyme prodrug therapy (VDEPT) have been investigated as means to utilize enzymes to convert relatively non-toxic prodrugs into clinically relevant concentrations of cytotoxic drugs directly at tumor sites. However, all three of these approaches have significant limitations [20,23,24]. To improve upon the clinical applicability, efficacy, and safety of enzyme prodrug therapy, we previously developed three fusion proteins (FPs), each targeted to primary tumors, their metastases, and the tumor vasculature. This dual targeting strategy allows for two distinct mechanisms of killing: (i) via the direct action of the cytotoxic drug on the tumor cells and (ii) by killing tumor vasculature endothelial cells and thereby effectively cutting off the tumor blood supply. Vascular targeting makes these FPs an attractive option because endothelial cells are relatively genetically-stable, easily-accessible targets that enable therapeutic effect amplification through tumor infarction, as well as tumor-type independent targeting [31]. PC is especially well suited to this dual

targeting strategy as prostate carcinomas have been shown to have approximately twice the vascular density of healthy prostate tissue [111] and microvessel density serves as a predictor of cancer-specific survival [71]. To date, the efficacy of these targeted enzyme prodrug systems on PC has remained unexplored.

Human annexin V (AV) is used to target each FP. AV has a strong affinity to the anionic phospholipid phosphatidylserine (PS), normally tightly segregated to the inner leaflet in eukaryotic plasma membranes [112], but robustly and consistently expressed on the outer leaflet in a wide range of cancer cell lines, their metastases [38,113], and the luminal side of tumor endothelium [2,32]. To maximize FP binding to tumor cells, we investigated treatment with docetaxel, a tubulin/microtubule targeting chemotherapeutic agent [114], which is becoming increasingly important in combination therapies for metastatic, hormone-refractory PC [115]. Therapeutic docetaxel dosage is limited by drug toxicity [109] but a single subtoxic dose has been shown to increase PS exposure on tumor endothelium by ~70% without causing apoptosis or changing PS exposure on normal endothelium [34]. This large increase in AV binding sites has the potential to increase the cytotoxic power of our enzyme prodrug systems.

We previously developed three AV-targeted FPs, each containing a non-human enzyme [39,116,117]. The enzymes utilized are:

(i)   L-methioninase (MT), which converts L-selenomethionine (SeMet) to toxic methylselenol, α-ketobutyrate, and ammonia [77]. MT also converts the amino acid methionine to methanethiol, which provides a second point of attack since most cancer cells exhibit increased

methionine-dependence [118,119]. PC cell lines have shown sensitivity to non-targeted MT/SeMet treatment *in vitro* [120].

(ii)   Purine nucleoside phosphorylase (PNP), which converts fludarabine (FD) into highly cytotoxic 2-fluoroadenine (2-FA) that incorporates into DNA/RNA, thereby effectively killing both dividing and nondividing cells [80]. PNP exhibits a powerful bystander effect [121,122], and PC cells have shown sensitivity to PNP/FD GDEPT treatment [123–125].

(iii)   Cytosine deaminase (CD), which converts the nucleoside analog 5-fluorocytosine (5-FC) to the more toxic pyrimidine analog 5-fluorouracil (5-FU), metabolites of which misincorporate into DNA/RNA and inhibit the nucleotide synthesis enzyme thymidylate synthetase [83]. PC cell lines have shown sensitivity to 5-FU and GDEPT CD/5-FC treatment [22].

To address the vascular targeting capabilities of these enzyme prodrug systems, we have previously shown that all three FPs bind tightly to PS expressing human abdominal aorta endothelial cells (HAAE-1) *in vitro*, with dissociation constants ranging from 0.5-1.5 nM [39,116,117]. Cytotoxic efficacy of our FP systems on HAAE-1 cells has also been demonstrated previously *in vitro,* with cell killing ranging from 5-100% [39,116,117]. We have validated these *in vitro* methods for determining vascular targeting/cytotoxic efficacy via the successful transition of the MT-AV/SeMet system *in vivo* for mice with implanted MDA-MB-231 breast tumors [126].

In the present study, we characterize the binding and evaluate the *in vitro* anticancer efficacy of three enzyme prodrug systems on human prostate carcinoma cells in the presence and absence of low-dose docetaxel treatment.

Methods

Expression and purification of fusion proteins

All FPs were expressed and purified as described previously [116,39,117]. Briefly, polymerase chain reaction (PCR) was used amplify genes encoding each enzyme, a six residue flexible linker, annexin V, and an N- or C- terminal His_6 tag, and an engineered HRV 3C protease cleavage site. Plasmids containing each FP were created via transformation of NovaBlue competent cells and then expressed in *E.coli* BL21 (DE3) cells. Recombinant FPs were produced and purified according to the procedure of Zang *et al.* [127] using immobilized metal (Ni^{2+}) affinity chromatography. The His_6 tag was removed during purification by cleavage with HRV-3C protease (Merck, Darmstadt, Germany). FPs were lyophilized and stored at -80 °C.

Cell culture

The human prostate adenocarcinoma cell line, PC-3, was obtained from the American Type Culture Collection (ATTC, Manassas, VA, USA) and cultured in F-12K medium (ATTC) supplemented with 10% fetal bovine serum, 100 U/ml penicillin, and 100 μg/ml streptomycin (all from Atlanta Biologics, Flowery Branch, GA, USA) at 37 °C in a 5% CO_2 atmosphere. Cells were passaged at 70-80% confluence, 2-3 times per week, <12 times during the course of experiments.

In vitro binding assays

Cells were grown in T-75 flasks to 70-80% confluence, plated at 50k cells/well in 24-well cell culture plates, and allowed to grow to 90% confluence. Dissociation constants were determined as described previously [116,39,117]. Briefly, cells were fixed with 0.25% glutaraldehyde in PBS, then quenched with 50 nM NH_4Cl in PBS. After a 1 h of incubation with 0.5% BSA in PBS, cells were washed, and varying concentrations (0-20 nM) of SureLINK biotin (KPL, Gaithersburg, MD, USA) labeled FPs were added and allowed to bind at 37°C for 2 h. Cells were washed with PBS containing 0.5% BSA and treated with streptavidin-horseradish peroxidase (2 μg/ml, KPL) for 1 h at room temperature. Cells were washed, and HRP was quantified via chromogenic substrate *o*-phenylenediamine (0.4 mg/ml) in 0.05 mM phosphate–citrate buffer (pH 5.0) containing 0.012% hydrogen peroxide. Since Ca^{2+} is essential for AV binding to PS, the above procedure was conducted in the presence of 2 mM Ca^{2+} (total binding) and in the absence of Ca^{2+} with 5 mM EDTA to chelate any residual Ca^{2+} (non-specific binding). All experiments contained a blank subjected to the same procedure but with 0 nM FP.

In vitro enzyme prodrug cytotoxic efficacy

Studies were carried out over a 6-day (MT-AV, PNP-AV) or 9-day (CD-AV) treatment cycle. Cells were plated as described previously, but only allowed to reach 50-60% confluence. Prior to the first viability assay, selected wells were pre-treated with 50 pM docetaxel (Biotang, Waltham, MA, USA). All medium was enhanced with 2 mM Ca^{2+} since annexin V binding is calcium-dependent. Medium for MT-AV cytotoxicity

studies was also supplemented with 0.02 mM pyridoxal phosphate (co-factor). Cells were treated with a saturating concentration of FP (100 nM) every 3 days for 2 h at 37 °C in accordance with previous binding stability studies [39,116,117]. Each day medium was replaced with medium containing varying concentrations of prodrug (L-SeMet and 5-FC from Fisher Scientific, Waltham, MA, USA and FD from VWR, Radnor, PA, USA) or drug analog (2-FA from Fisher Scientific and 5-FU from Sigma-Aldrich, St. Louis, MO, USA) with or without 50 pM docetaxel. This docetaxel concentration was chosen since it falls in the range of reported values of concentrations that gave PS exposure without cytotoxic effects. An Alamar Blue (Invitrogen, Grand Island, NY, USA) assay was preformed every 2-3 days to measure cell viability [128]. Cells were incubated with 10% Alamar Blue in fresh media for 4 h incubation at 37 °C. From each well, 250 μl was transferred to an opaque 96-well plate, and fluorescence (530/590 nm) was read on a microtiter plate reader. Cells were washed twice after each Alamar Blue assay and three times after each FP incubation before prodrug/drug treatments were added.

Data analysis

All treatments were run in triplicate. Dissociation constants were obtained using Prism 5 software (GraphPad, La Jolla, CA, USA). Statistical significance was determined with Prism 5 via a one-way ANOVA employing the Tukey-Kramer multiple comparisons test.

Results

Binding strength

The ability of each FP to bind to PS on the PC-3 cell surface was determined by measuring the total binding and non-specific binding and subtracting to obtain specific binding, with typical results shown in Figure 18 for MT-AV. The dissociation constant (K_d) was calculated utilizing a one-site, non-competitive binding model, and K_d values are presented in Table 2.

Enzyme prodrug cytotoxic efficacy

We evaluated the cytotoxic effect of each enzyme prodrug therapy on PC-3 cells by comparing the cell viability on days 2, 4, and 6 (MT-AV and PNP-AV) or days 3, 6, and 9 (CD-AV) to day 0 on a per well basis, and results are presented as percent viability compared to day 0. Statistical significance was established by comparing cells treated with varying concentrations of prodrug (or drug analog, if available) to their corresponding control groups treated with 0 µM drug/prodrug on the same day (#, $p < 0.05$; *, $p < 0.01$; and **, $p < 0.001$). Additionally, cells treated with 50 pm docetaxel were compared to cells not treated with docetaxel at the same concentrations of prodrug/drug on the same day (^, $p < 0.05$; +, $p < 0.01$; and ++, $p < 0.001$).

The cytotoxic effect of SeMet conversion by MT-AV was evaluated over 6 days with SeMet concentrations ranging from 0 to 1000 µM with 50 pM docetaxel (data not shown) and without docetaxel (Figure 19). MT-AV/SeMet treatment caused significant cytotoxicity starting at 250 µM SeMet, resulting in 64% viability by day 2 and 14% viability by day 6, with no growth inhibition for SeMet alone. At SeMet concentrations
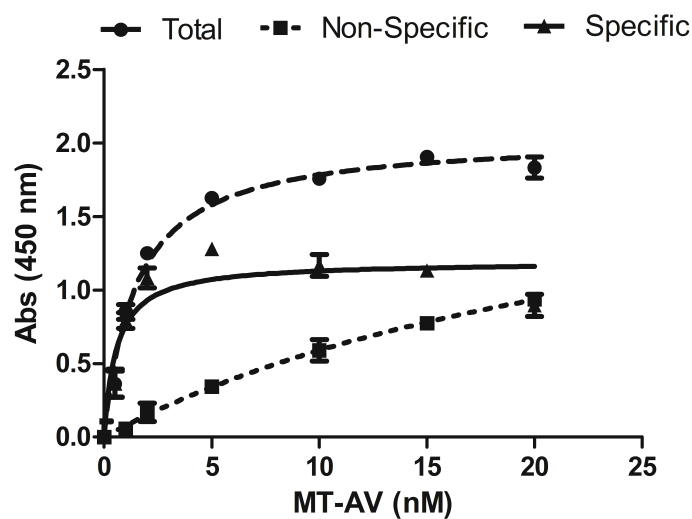
Figure 18: Binding strength of MT-AV to PC-3 cell surface PS

PC-3 cells were incubated with increasing concentrations of biotin labeled MT-AV with total binding ($\bullet$) measured in the presence of 2 mM Ca^{2+} and non-specific binding ($\blacksquare$) measured in the absence of Ca^{2+} with 5 mM EDTA to chelate any residual Ca^{2+}. Specific binding ($\blacktriangle$) was obtained by subtracting non-specific from total binding. Data presented as mean ± SE (n = 3).

Table 2: Dissociation constant (K_d) of each fusion protein binding to PC-3 cells

Fusion Protein	K_d ± SE (nM)
MT-AV	0.572 ± 0.281
PNP-AV	0.406 ± 0.108
CD-AV	0.061 ± 0.026
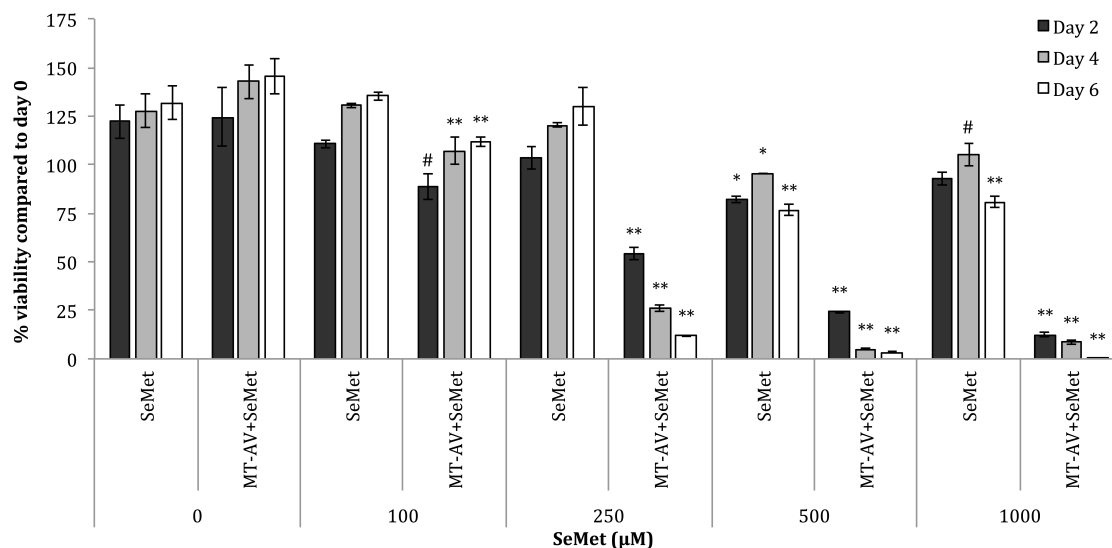
Figure 19: Effect of SeMet conversion by MT-AV on PC-3 cell viability

Cells treated with varying concentrations of SeMet were compared their corresponding control groups treated with 0 nM concentrations on the same day, and significant differences are denoted by # ($p < 0.05$), * ($p < 0.01$), and ** ($p < 0.001$). Data presented as mean ± SE (n = 3).

above 250 μM, MT-AV/SeMet killing velocity increased and near complete killing was achieved by day 6, with only slight growth inhibitory effects of SeMet alone. The addition of docetaxel treatment created no significant additional decreases in cell viability.

The cytotoxic effect of 2-FA converted from FD by PNP-AV in the presence (Figure 20(a)) and absence (Figure 21) of docetaxel treatment was determined over 6 days with FD or 2-FA concentrations ranging from 0 to 10 μM. PNP-AV in combination with 5 μM FD was the lowest concentration of prodrug that showed significant cytotoxic effects, reaching 37% viability by day 6 with docetaxel treatment

56
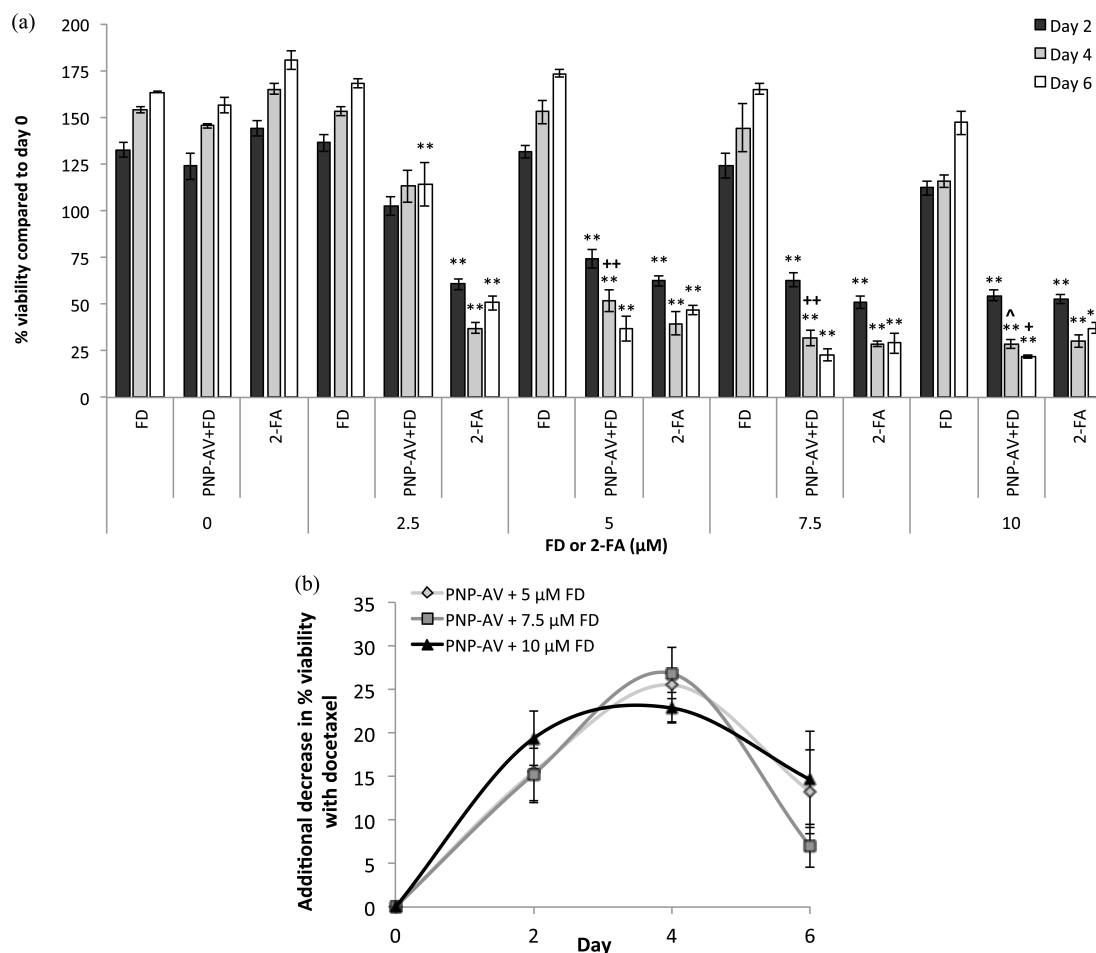
Figure 20: Effect of FD conversion by PNP-AV with 50 pM docetaxel on PC-3 cell viability

(a) Cells treated with varying concentrations of FD or 2-FA were compared to their corresponding control groups treated with 0 nM concentrations on the same day, and significant differences are denoted by # ($p < 0.05$), * ($p < 0.01$), and ** ($p << 0.001$). Cells treated with 50 pm docetaxel (shown) were compared to cells not treated with docetaxel (Figure 21) at the same concentrations of FD or 2-FA on the same day, and significant differences are denoted by ^ ($p < 0.05$), + ($p < 0.01$), and ++ ($p < 0.001$). Data presented as mean ± SE (n = 3). **(b)** Additional decreases in cell viability afforded by the addition of 50 pM docetaxel to the PNP-AV system efficacy, shown for prodrug

titers for which docetaxel treatment influenced treatment outcome. Results shown as non-docetaxel treated % viability minus docetaxel treated % viability to obtain a measure of additional cell killing with docetaxel treatment that alone has no significant effect on cell growth. Data presented as mean ± SE (n = 6).
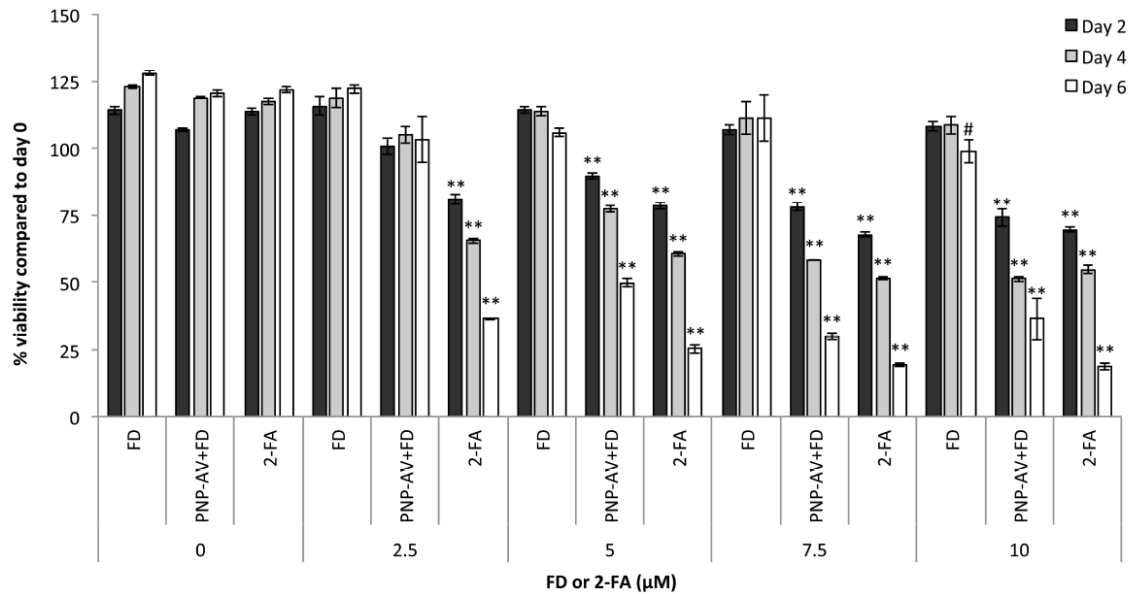
Figure 21: Effect of FD conversion by PNP-AV on PC-3 cell viability

Cells treated with varying concentrations of FD or 2-FA were compared their corresponding control groups treated with 0 nM concentrations on the same day, and significant differences are denoted by # ($p < 0.05$), * ($p < 0.01$), and ** ($p \ll 0.001$). Data presented as mean ± SE (n = 3).

and 50% viability without docetaxel treatment. Cytotoxicity effects increased with increasing FD concentration up to 10 μM, reaching 22% viability by day 6 with docetaxel treatment and 37% viability without docetaxel treatment. Treatment with PNP-AV/FD was statistically indistinguishable from 2-FA treatment alone at concentrations ≥ 5 μM for docetaxel treated cells, but for non-docetaxel treated cells this treatment similarity did not occur until concentrations above 10 μM (Figure 21). FD treatment alone did not show any cytotoxic effects at concentrations ≤ 10 μM. Treatment only with docetaxel did not affect PC-3 cells, but the addition of docetaxel significantly enhanced PNP-AV/FD cytotoxic efficacy at 5 μM FD concentrations and

above as indicated (^, +, ++) in Figure 20(a). Additional decreases in % cell viability that occurred with docetaxel treatment are presented in Figure 20(b) for FD concentrations of 5, 7.5, and 10 μM. On day 2, additional decreases in % cell viability ranged from 15-19%. The highest additional cytotoxicity occurred on day 4 (22-27%), and the effect diminished by day 6.

The cytotoxic effect of 5-FU converted from 5-FC by CD-AV with (Figure 22(a)) and without (Figure 23) docetaxel treatment was evaluated over 9 days with concentrations of 5-FC/5-FU ranging from 0 to 5000 μM. CD-AV/5-FC treatment caused significant cytotoxicity at all concentrations above 500 μM but was most effective at 5000 μM 5-FC resulting in 40% viability by day 9 with docetaxel treatment and 44% without docetaxel treatment. No significant increases in cytotoxicity occurred past 5000 μM CD-AV/5-FC or 5-FU treatment (data not shown). 5-FC treatment alone exhibited no cytotoxic effect for both docetaxel and non-docetaxel treated cells. Treatment with the drug analog 5-FU showed significantly more cytotoxic effects than treatment with CD-AV/5-FC from day 6 onwards and resulted in ~6% viability for both docetaxel and non/docetaxel groups. Treatment only with docetaxel had no effect on PC-3 cells, but the addition of docetaxel significantly affected the killing efficacy of the CD-AV/5-FC system as indicated in Figure 22(a) (^, +). The additional decreases in % viability as a result of docetaxel addition are presented in Figure 22(b). Docetaxel affected CD-AV/5-FC efficacy in an inverse dose dependent manner, with respect to the prodrug, as the largest additional decreases in % viability consistently occurred at 1000 μM 5-FC and the smallest additional decreases were consistently seen at 5000 μM 5-FC. As for PNP-AV/FD, the impact of docetaxel was greatest in the middle of the

study reaching an additional decrease in % viability of 26% on Day 6 for 1000 μM 5-FC.
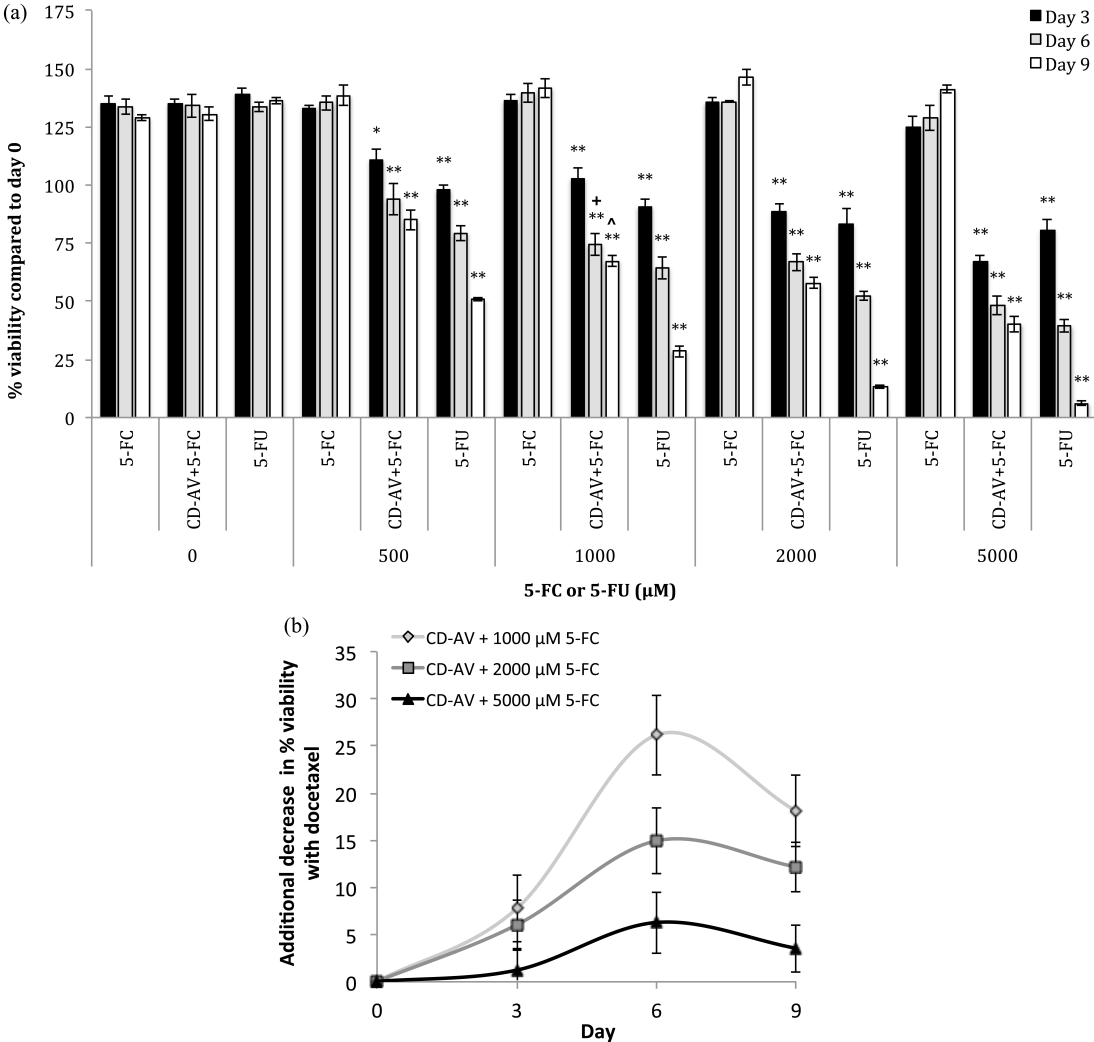
Figure 22: Effect of CD-AV conversion of 5-FC with 50 pM docetaxel treatment on PC-3 cell viability

(a) Cells treated with varying concentrations of 5-FC or 5-FU were compared their corresponding control groups treated with 0 nM concentrations on the same day, and significant differences are denoted by # ($p < 0.05$), * ($p < 0.01$), and ** ($p < 0.001$). Cells

treated with 50 pm docetaxel were compared to cells not treated with docetaxel (Figure

23) at the same concentrations of 5-FC or 5-FU on the same day and significant

differences are denoted by ^ ($p < 0.05$) or + ($p < 0.01$). Data presented as mean ± SE (n

= 3). **(b)** Additional decreases in cell viability by the addition of 50 pM docetaxel,

which alone has no effect on cell viability, for prodrug concentrations where docetaxel

additional affected treatment outcomes. Results shown as non-docetaxel treated %

viability minus docetaxel treated % viability to obtain a measure of additional cell killing

with docetaxel treatment that alone has no significant effect on cell growth. Data

presented as mean ± SE (n = 6).
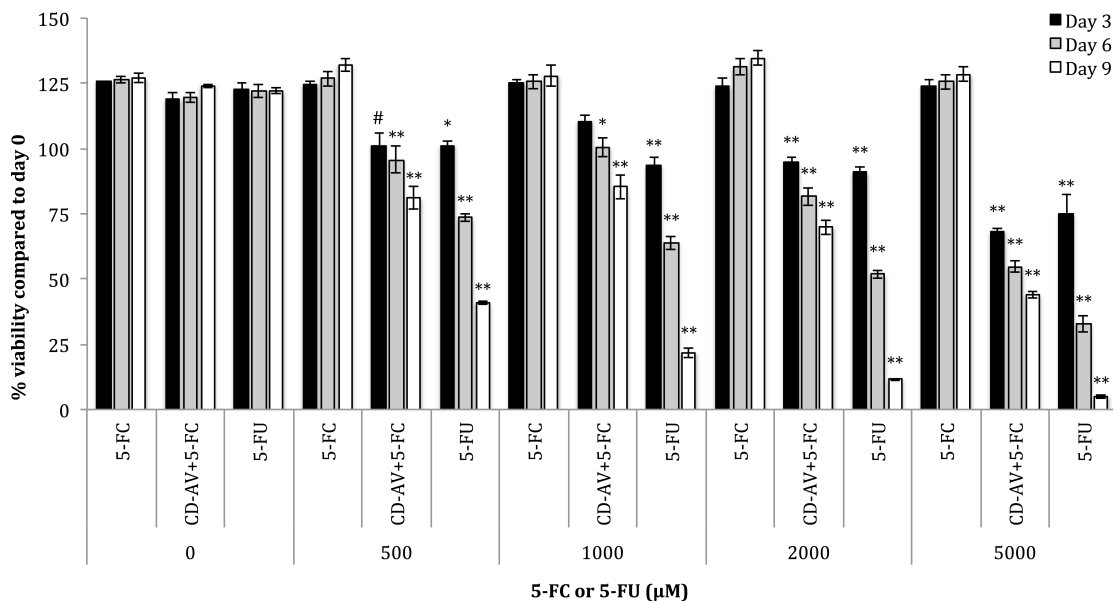
Figure 23: Effect of 5-FC conversion by CD-AV on PC-3 cell viability

Cells treated with varying concentrations of 5-FC or 5-FU were compared their corresponding control groups treated with 0 nM concentrations on the same day, and significant differences are denoted by # ($p < 0.05$), * ($p < 0.01$), and ** ($p < 0.001$). Data presented as mean ± SE (n = 3).

Discussion

The MT-AV/SeMet enzyme prodrug system emerged as a promising treatment option as it displayed significant cytotoxicity *in vitro* at feasible *in vivo* SeMet treatment concentrations. The median lethal dose (LD_{50}) of SeMet *in vivo* for female nude mice is 12.5 mg/kg [129,130], which translates to ~1100 μM *in vitro*. A high degree of prostate cancer cell killing was achieved with SeMet concentrations as low as 250 μM with minimal cytotoxicity of SeMet alone, suggesting a feasible window of opportunity for *in vivo* treatment translation.

PNP-AV also emerged as a feasible option for treating PC as it displayed high killing velocity and killing efficacy, both of which are important for clinical translation. PNP-AV also showed the most robust increase in cell killing efficacy in the presence of docetaxel. PNP-AV/FD (with docetaxel) created up to 78% cytotoxicity over 6 days at an FD concentration of 10 μM *in vitro*, which translates to less than 0.1% of the LD_{50} (~1200 mg/kg) for FD in female nude mice, indicating that this therapy could be administered with minimal harm to healthy tissues.

CD-AV/5-FC treatment was not as effective or as rapid as MT-AV/SeMet or PNP-AV/FD treatment, and we therefore conclude that CD-AV/5-FC would most likely not be effective *in vivo*. Additionally, the prodrug concentration necessary to elicit a cytotoxic effect was significantly higher than for the MT-AV and PNP-AV systems, although even at the highest level of prodrug, there was no effect of the prodrug by itself.

All three FPs exhibited relatively strong binding to PS on PC-3 cells with dissociation constants less than previously reported dissociation constants for AV alone to PS (2.7–15.5 nM) [60,61]. The multimeric structure of each FP likely allows for multiple AV to PS bonds per FP, and we believe this contributes to the observed strong binding of FPs to PS.

Subtoxic docetaxel treatment significantly but selectively increased the cytotoxic efficacy of our enzyme prodrug systems, suggesting that at least two of our FP/prodrug combinations are sensitive to the extent of PS outer leaflet exposure. Tumor xenografts in murine models expose ~ 35% of PS on the external leaflet [32] (with $> 10^6$ PS molecules per cell [34]), but docetaxel treatment can increase PS expose and

thereby the number of potential FP binging sites by up to 70% [34], effectively doubling the FP targets and thereby creating quicker and more powerful treatment. The additional decrease in cell viability caused by introducing docetaxel into the PNP-AV and CD-AV enzyme prodrug treatments is seen in Figure 20(b) and Figure 22(b), respectively.   The maximum effect was present at the midpoint of each study, i.e. at day 4 in the PNP-AV system and at day 6 in the CD-AV system. We suggest that the peak in this effect is a result of increased initial prodrug to drug turnover enabled by the increased presence of bound FPs due to the additional availability of PS binding sites. Therefore, the addition of docetaxel causes the enzyme prodrug treatment to speed up initially; and later, as the number of viable cells dwindles, the effect becomes relatively less noticeable.

We employed subtoxic treatment levels of docetaxel, as we were interested in the PS exposure effects of docetaxel and not its cytotoxic capabilities. Not only did docetaxel treatment alone have no growth inhibitory or cytotoxic effects, but the addition of docetaxel treatment did not alter the cytotoxic efficacy of the drug analogs, 2-FA and 5-FU. This indicates there was no synergism present between the drugs generated by our enzyme prodrug therapies and docetaxel. Therefore, it is probable that the increased cytotoxic effect afforded by docetaxel treatment was in fact due to an increase in PS exposure providing an increase in available binding sites for our FPs.

Unexpectedly, docetaxel treatment did not increase MT-AV cytotoxicity on PC-3 cells. We propose that this effect did not occur because the killing efficacy of the MT-AV system may already be saturated at feasible SeMet concentrations without docetaxel. Saturation could arise if the amount of MT-AV able to bind without

docetaxel treatment is sufficient to convert the available SeMet, as any additional MT-AV binding would increase the initial SeMet turnover rate but would not ultimately affect the quantity of reactive oxygen species the cells are exposed to.

Further validation of the MT-AV and PNP-AV systems will consist of *in vivo* work in murine xenograft models. The immunogenicity of the FP systems can be addressed via functionalization of human homologs [131,132] or via PEGylation [133].

Conclusions

In conclusion, we have substantiated the feasibility of two, novel, non-invasive treatments for prostate cancer and its metastasis with minimal threat to healthy tissues. We were able to achieve both tight binding, with dissociation constants in the low nanomolar range, and excellent cytotoxic efficacy for the MT-AV and PNP-AV enzyme prodrug systems. Additionally we have shown the utility of subtoxic docetaxel treatment for increasing the cytotoxic potential of annexin V-targeted enzyme prodrug systems.

Abbreviations

FP, fusion protein; AV, annexin V; MT, L-methioninase; PNP, purine nucleoside phosphorylase; CD, cytosine deaminase; PC, prostate cancer, ADPET, antibody-directed enzyme prodrug therapy; GDEPT, gene-directed enzyme prodrug therapy; VDEPT, viral-directed enzyme prodrug therapy; PS, phosphatidylserine; FD, fludarabine; 5-FC, 5-fluorocytosine; SeMet, L-selenomethionine; HAAE-1, human abdominal aorta endothelial cells; K_d, dissociation constant; LD_{50}, median lethal dose.

Competing Interests

The only potential competing interest we declare is an application for a U.S. patent on this targeted enzyme prodrug therapy system.

Authors Contributions

KPG, CK, and RGH designed the experiments. KPG conducted experiments and analyzed the data. KPG and RGH wrote the manuscript. All authors read and approved the final manuscript.

Additional Figures

Binding Strength Curves

Curves not selected as the published "sample curve" are presented in Figure 24.
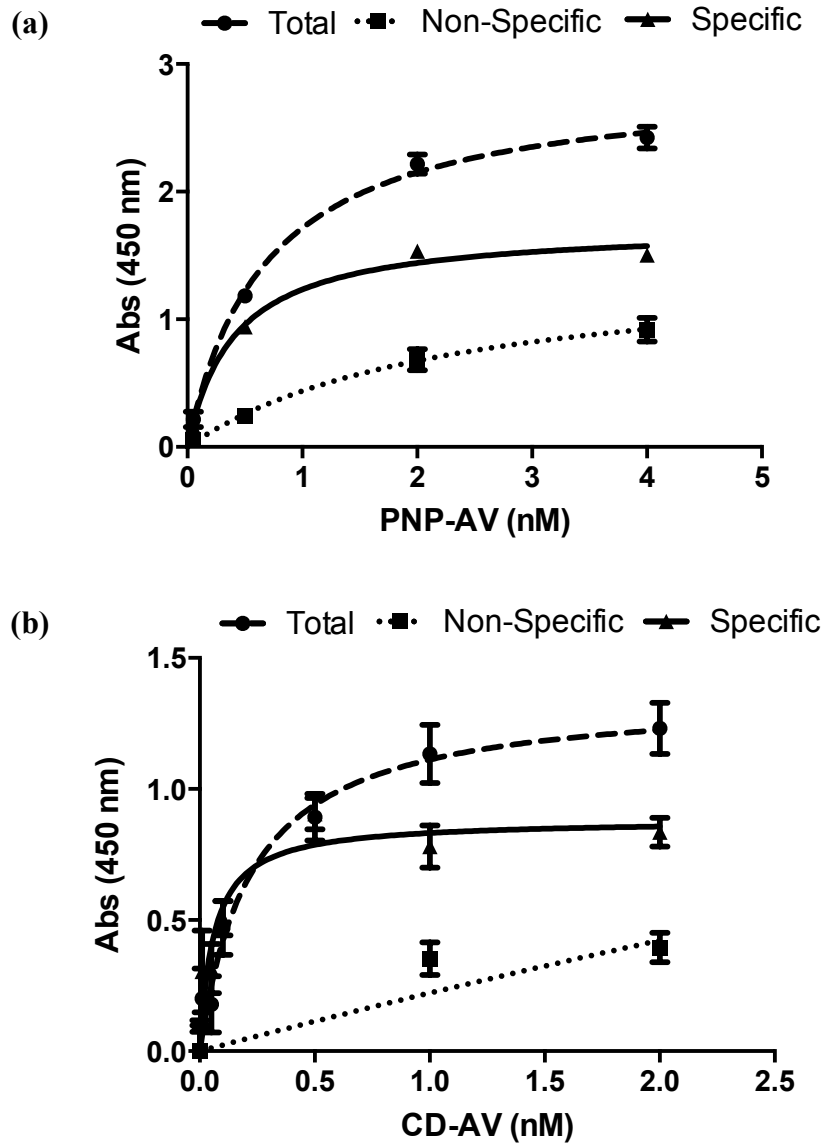
Figure 24: Binding strength of PNP-AV and CD-AV to PC-3 cell surface PS

PC-3 cells were incubated with increasing concentrations of (a) biotin labeled PNP-AV and (b) biotin labeled CD-AV, with total binding (●) measured in the presence of 2 mM Ca^{2+} and non-specific binding (■) measured in the absence of Ca^{2+} with 5 mM EDTA to chelate any residual Ca^{2+}. Specific binding (▲) was obtained by subtracting non-specific from total binding. Data presented as mean ± SE (n = 3).

Additional Data: Docetaxel Modulated Binding

Introduction

Although docetaxel is used in the clinic as an anti-mitotic chemotherapeutic agent, for the purposes of the *in vitro* data in this chapter we were solely interested in its ability to induce PS exposure on the external cell surface, at concentrations so low they are unable to effect any cytotoxicity. However, more PS exposure does not necessarily imply more FP binding. It has been suggested that externalization of PS in viable cells is localized to lipid rafts, clusters of lipids serving to compartmentalize cellular processes via the establishment of microdomains, and that in fact lipid rafts are likely necessary for the maintenance of PS externalization.[134] If the PS externalization effect induced by docetaxel reinforces the clusters of PS already present on PC-3 cells, then it cannot be expected that for each additional PS molecule exposed an additional FP is able to bind. Instead, the possible increase in FP binding due to docetaxel induced PS exposure is very complex as it is influenced by PS distribution and the number of PS bonds per FP (avidity), which varies as all three FPs have different quaternary structures. To this end, we utilized colorimetric and flow cytometric methods to measure FP binding in the presence and absence of low-dose docetaxel.

Methods

Binding strength was determined colorimetrically with *o*-phenylenediamine as previously described. Saturating concentrations of each FP (1-2 nM CD-AV, 4 nM PNP-AV, and 10 nM MT-AV) were investigated, with or without 50 pM docetaxel treatment 24 h prior to cell fixing with glutaraldehyde. Data was collected in the

presence of Ca^{2+} and in the absence of Ca^{2+} (with EDTA), and subtracted to obtain measures of specific binding.

For flow cytometry analysis, all FPs were labeled with FITC (Thermo Scientific, Waltham, MA, USA) according to the manufacturer's protocol. Cells were plated, allowed to adhere, and selected wells were then treated with 50 pM docetaxel 24 h prior to FP binding. Following docetaxel exposure or medium control, cells were incubated with varying saturating concentrations of FITC-labeled FPs at 37 °C for 2 h in medium augmented with 2 mM Ca^{2+}. After a thorough wash, cells were trypsinized, transferred to 1.5 ml microcentrifuge tubes, and centrifuged at 100 x g for 5 min. Cells were resuspended in FACS buffer (PBS containing 0.5% BSA and 2 mM Ca^{2+} or 5 mM EDTA) and stored on ice. A BD Biosciences Accuri C6 (Franklin Lakes, New Jersey, USA), with excitation at 488 nm and a 533/30 band pass filter, was used to capture 5,000 gated events per sample. Data was collected and analyzed with BD C6 Accuri software. All experiments were conducted in triplicate. Statistical significance was determined with GraphPad Prism 5 via a Students' t-test.

Results

Saturating concentrations of each FP binding to PC-3 cells exhibited differences in absorbance as a measure of specific binding, as shown in Figure 25a. CD-AV showed a 30% increase in specific binding with docetaxel treatment ($p = 0.1242$) and PNP-AV showed a 22% increase in specific binding ($p = 0.1077$) with docetaxel treatment. MT AV did not exhibit any increased binding with docetaxel treatment.
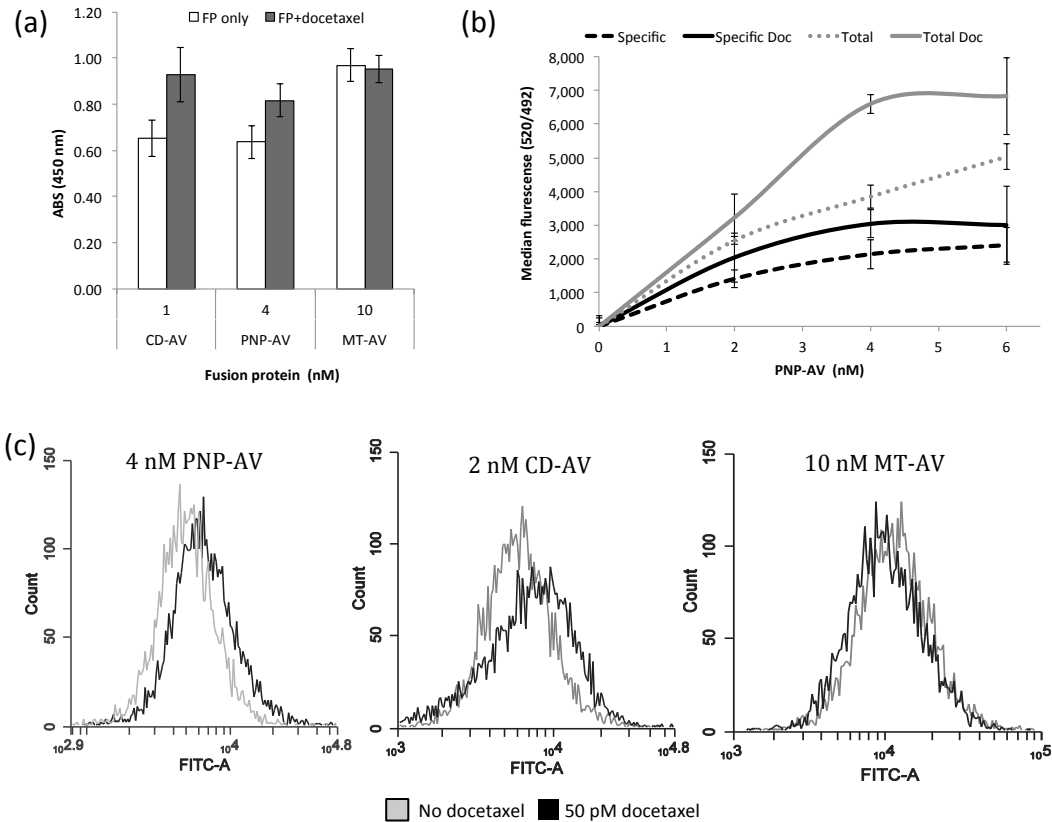
Figure 25: Binding of FPs to PC-3 cells with witout docetaxel

(a) Differences in absorbance (total minus non-specific) were obtained for saturating concentrations of each FP (4 nM PNP-AV, 1 nM CD-AV, 10 nM MT-AV) via binding strength analysis. FP only groups were compared to FP-docetaxel groups match for each FP. Data presented as mean ± SE (n = 3). **(b)** Median florescence values for PNP-AV-FITC (0-6 nM) binding to PC-3 cells, obtained via flow cytometry analysis. Specific binding was compared to specific binding with docetaxel ("Specific Doc") and total binding was compared to total binding with docetaxel ("Total Doc"). Data presented as median/5000 events (n = 3). **(c)** Representative florescence histogram shifts for 4 nM PNP-AV-FITC, 2 nM CD-AV-FITC, and 10 nM MT-AV-FITC. Data presented as counts for 5000 events/sample (n = 1).

72

Flow cytometry was employed to further validate the binding results obtained. Representative binding curves for median PNP-AV-FITC (0-6 nM) fluorescence are shown in Figure 25b for specific and total binding with and without docetaxel. Differences in specific binding were most apparent at lower PNP-AV-FITC concentrations with a 45% increase at 2 nM PNP-AV-FITC and a 42% increase at 4 nM PNP-AV-FITC. Observed differences in binding diminished with increasing PNP-AV-FITC concentrations, decreasing to a 25% increase by 6 nM and further dwindling thereafter (data not shown). Histogram flow cytometry plots of individual samples for all three fusion proteins are shown in Figure 25c, where PNP-AV and CD-AV showed upward shifts in florescence/cell, as opposed to MT-AV, which did not display a shift towards higher florescence/cell.

Discussion

Both CD-AV and PNP-AV showed increases in binding with the addition of docetaxel, whereas MT-AV did not in either method utilized to assess changes in binding with the addition of docetaxel. We propose that this result supports the finding that the addition of docetaxel did not affect the outcome of the MT-AV cytotoxicity studies. Assuming all of the cells treated with docetaxel experience a relatively equal number in additional PS translocations to the outer surface upon treatment, we propose that MT-AV did not show any increased in binding due to the complex, interacting factors of size, metameric structure, and spatial distribution of additional PS exposure. We currently know too little about how each of these factors influences binding to present any definitive conclusions.

Additional Data: Flow Cytometric Analysis of Internal vs. External FP Binding

Introduction

Effective EPT necessitates that the fusion protein be bound and remain bound to the external cell membrane, as once the protein is internalized it is likely degraded. Annexin V (AV or A5) alone can form a 2-dimensional protein network via polymerization, that then bends the membrane and induces endocytotic vesicle formation.[50] This pinocytosis has been shown to occur in both apoptotic cells expressing phosphatidylserine and in non-apoptotic cancer cells that natively express phosphatidylserine.[50] Polymerization, which leads to trimer formation, is essential for the initiation of this internalization pathway, as a similar protein, annexin I (AI or A1), does not polymerize and subsequently shows no evidence of internalization.[50]

It remains unclear if the AVs in fusion proteins retain the capability to polymerize and whether these are subsequently internalized, since the size, structure, and spatial orientation of AV changes drastically once in fusion. It is also feasible that even if polymerization cannot occur in AV fusions, the much larger structure of AV fusion (i.e. AV alone is 36 kDa, whereas MT-AV is 340 kDa) may lead to macro-endocytosis even without the initiation of the AV-mediated import mechanism. To investigate, we utilize external fluorescence quenching during flow cytometric analysis of bound fusion proteins to PC-3 cells.

Methods

PC-3 cells were plated at 50 k/well under standard growth conditions (37°C and 5% CO_2) and allowed to adhere overnight. Medium was removed and replaced with 300 μl

of medium containing 2 mM Ca^{2+} and either 20 or 100 nM of FITC labeled MT-AV and allowed to incubate for 2 h at 37°C, 5% CO_2. Cells were then washed twice with PBS, lifted with trypsin (200 μl/well, 4 minutes, 37°C), quenched with 500 μl of Ca^{2+} containing medium, transferred to microcentrifug tubes, and centrifuged for 5 min at 100 x g. Medium was aspirated and replaced with 300 μl of FACS buffer (1x DPBS, 0.5% BSA, 2 mM Ca^{2+}) with (internal) or without (total) 1.2 mg/ml Trypan Blue. Including Trypan Blue in FACS assays is a standard method for excluding external fluorescence from the total fluorescence measured.[135] Data was collected on a BD Accuri C6 as mean fluorescence per 5,000 gated events. To obtain measures of external fluorescence, internal fluorescence measured in the presence of Trypan Blue was subtracted from total fluorescence, measured in the absence of Trypan Blue.

Results

At 20 nM concentrations of MT-AV-FITC, 91% of the observed FLU was internal to the cells, while 9% was external, as shown in Figure 26. At 100 nM concentration of MT-AV-FITC, only 30% of the observed FLU was internal, and 70% was external.

Discussion

We have previously assumed that AV trimerization would be unlikely, if not unable, to occur in FPs due to the multimeric structure of FPs. However, due to the presence of large amounts of internal fluorescence at a 20 nM MT-AV-FITC concentration, it appears as though internalization might be occurring upon FP binding to phosphatidylserine expressed on the cell surface. However, it remains unclear if this is
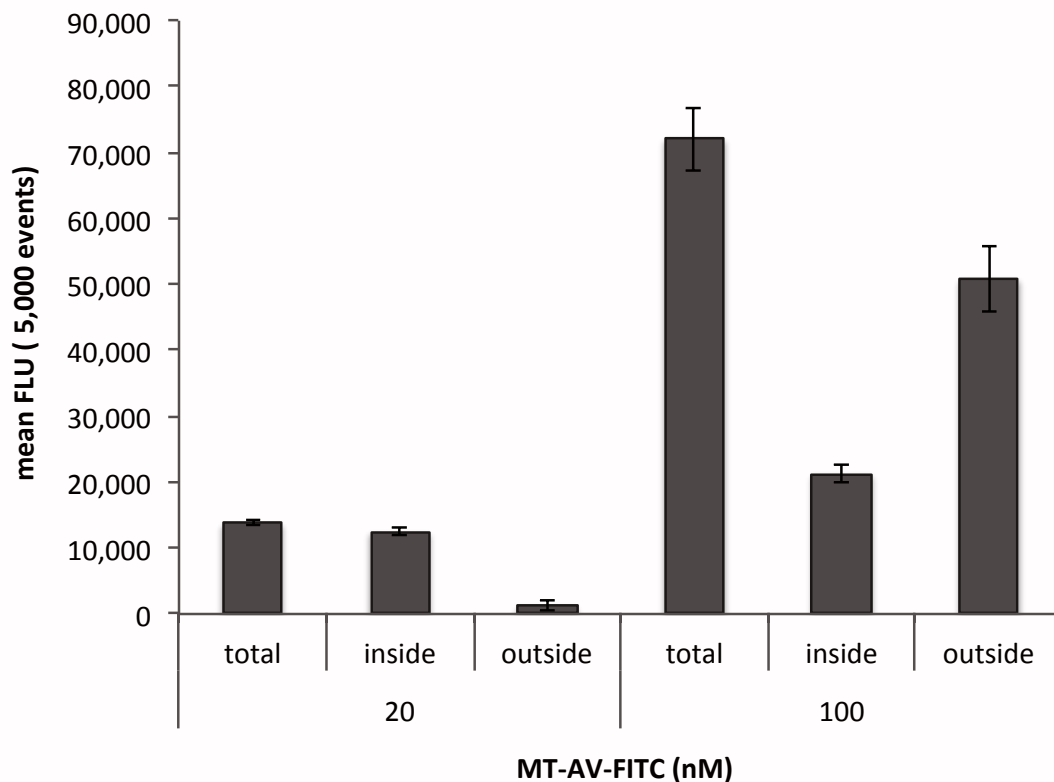
Figure 26: Internal vs. external binding of MT-AV to PC-3 cells

Binding for FITC labeled MT-AV to PC-3 cells at 20 nM MT-AV-FITC (saturating) and 100 nM MT-AV-FITC (supersaturating). Internal fluorescence was measured by quenching with Trypan Blue, and external fluorescence was then obtained by subtracting internal FLU from total FLU. Data presented as mean FLU/5000 events ± SE (n = 3).

due to trimerization or macropinocytosis. We propose that since internalization was substantially less at 100 nM MT-AV-FITC concentrations, the import mechanism is overloaded at higher concentrations, causing external fluorescence to predominate.

It is important to note that the binding in these studies occurs in entirely different conditions than those utilized for binding strength experiments. Herein the

cells are alive, and binding occurs in complete growth medium supplemented with calcium. To determine binding strength/dissociation constants, the binding occurs in PBS supplemented with calcium, where the cells are fixed with glutaraldehyde and, thus, no longer alive, which could deactivate the import mechanisms.

Chapter 3: Applicability of Existing Fusion Proteins to Pancreatic Cancer

Katrin P. Guillen, Antonietta Restuccia, Carla Kurkjian, and Roger G. Harrison.

Abstract

Objectives: The bleak prognosis associated with pancreatic cancer (PDAC) drives the need for the development of novel treatment methodologies. Here, we evaluate the applicability of three enzyme prodrug therapies for PDAC, which are simultaneously targeted to the tumor, tumor vasculature, and metastases via annexin V. In these therapies, annexin V is fused to an enzyme, creating a fusion protein that converts non-toxic drug precursors, prodrugs, into anticancer compounds while bound to the tumor, therefore mitigating the risk of side effects.

Methods: The binding strength of fusion proteins to the human PDAC cell lines Panc-1 and Capan-1 was measured via streptavidin- horseradish peroxidase binding to biotinylated fusion proteins. Cytotoxic efficacy was evaluated by treatment with saturating concentrations of fusion protein followed by varying concentrations of the corresponding prodrug plus docetaxel.

Results: All fusion proteins exhibited strong binding to PDAC cells, with dissociation constants between 0.02-1.15 nM. Cytotoxic efficacy was determined to be very good

for two of the systems, both of which achieved complete cell death on at least one cell line at physiologically attainable prodrug concentrations.

Conclusions: Strong binding of fusion proteins to PDAC cells and effective cytotoxicity demonstrate the potential applicability of enzyme prodrug therapy to the treatment of PDAC.

Introduction

Pancreatic cancer (PDAC) remains a lethal and treatment refractory disease with a 5-year survival rate below 6%.[103] Due to a complete lack of early diagnostic markers, patients usually present with locally advanced or metastatic disease, leaving little possibility for surgical resection.[136] The current standard of treatment for PDAC, chemotherapy with gemcitabine, increases survival by approximately 5 weeks but is accompanied by severe side effects.[137] Clearly, there exists an urgent need for the development of effective, targeted treatment options for PDAC.

Enzyme prodrug therapy (EPT) is an attractive candidate for the treatment of PDAC as it creates high intratumoral concentrations of anti-cancer drugs/compounds while greatly reducing the risk of side effects associated with systemic administration. To enact EPT, we utilize fusion proteins that consist of a targeting protein, capable of binding to the tumor/tumor vasculature, linked to an enzyme, capable of converting prodrugs into cytotoxic drugs. EPT is a two-step process, as shown in Figure 27: (i) First the fusion protein (FP) is administered via the bloodstream and allowed to bind to the tumor vasculature and to the tumor cells after transport through the gaps found in leaky tumor vasculature. (ii) After any unbound fusion protein is allowed to clear from the bloodstream (typically <8 h),[126] the prodrug is then introduced into the system and interacts with the enzyme bound to the tumor/tumor vasculature. The drug created upon enzymatic conversion of the prodrug is subsequently free to diffuse across cell membranes and enact its cytotoxic effects, as well as diffuse to surrounding cells to create a bystander effect.
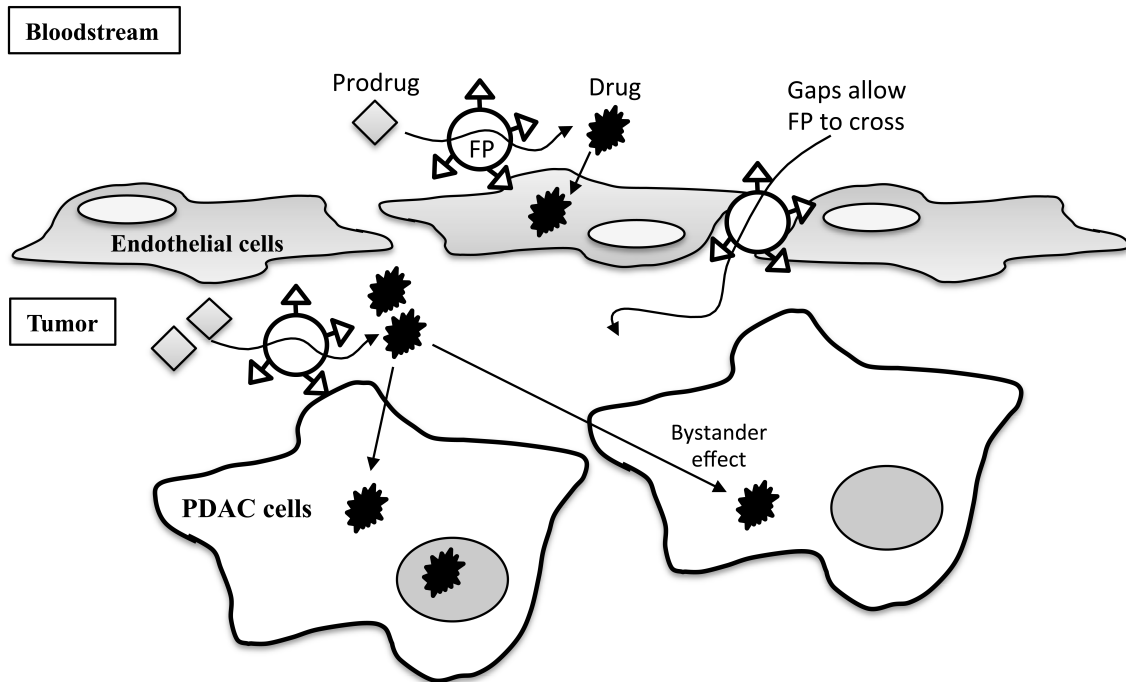
Figure 27: EPT mechanism of action for PDAC

Schematic representation of enzyme prodrug therapy. First, the targeting portion ($\triangle$) of the fusion protein (FP) binds to endothelial cells of the tumor vasculature and the tumor cells themselves, which is possible due to gaps found in leaky tumor vasculature. Second, after any unbound fusion protein is allowed to clear from the bloodstream, a prodrug ($\blacklozenge$) is administered, which upon interaction with the enzyme portion (O) of the bound fusion protein is converted into an anticancer drug ($\ast$) that is free to move across the cell membrane to enact its killing effects. Drugs are also free to move between cells (bystander effect), and therefore even cells that do not have any fusion protein bound to them can be effectively treated.

Annexin V (AV)-directed EPT is an especially appealing treatment modality for PDAC, as it does not discriminate between the primary tumors, metastases, or tumor

vasculature. This not only allows for the treatment of multiple tumor/metastatic sites simultaneously, but also affords a two-pronged approach to the EPT mechanism of treatment: (i) direct action of drugs on cancer cells, and (ii) action of drugs on endothelial cells of tumor vasculature, damage of which will amplify downstream via the depletion of oxygen, nutrients, and the route of metastatic spread.[75] Vascular targeting may be especially important for PDAC, as vascularity has been associated with significantly decreased time to progression as well as significantly decreased median survival.[73]

The targeting protein of AV-directed EPT, AV, has a strong affinity to phosphatidylserine, an anionic plasma membrane phospholipid that is tightly segregated to the inner leaflet in healthy cells but is robustly and consistently expressed on the outer leaflet of tumor cells, their metastases, and the endothelial cells of tumor vasculature.[2,38,113] Phosphatidylserine has been identified as a potential biomarker for PDAC, and has been shown to be a viable and safe target for PDAC in subcutaneous and orthotropic xenografts in athymic *nu/nu* mice.[138,139] Importantly, the dense desmoplastic stroma surrounding PDAC tumors, a hallmark drug delivery barrier for PDAC, contains abnormal endothelium-lined vessels,[16] which can be targeted by AV. Phosphatidylserine expression on endothelial cells of tumor vasculature makes this an attractive targeting approach since unlike tumor specific antigen targeting wherein the endothelial cells present a potential barrier to tumor drug delivery, tumor endothelial cells serve to augment treatment efficacy.[75] Additionally, AV-directed EPT has the potential to overcome the distribution limitations of antibody-directed EPT,[20] and unlike

gene-directed EPT/ virus-directed EPT this approach does not require the development of safe and effective vectors to achieve clinical translation.[24]

The addition of low-dose docetaxel, a taxoid with tubulin polymerizing properties,[140] has the potential to increase the efficacy of AV-directed EPT via its capacity to increase the expression of phosphatidylserine on the outer cell leaflet of tumor cells/vasculature. A single subtoxic dose has been shown to increase phosphatidylserine exposure on tumor endothelium *in vivo* by approximately 70% without causing apoptosis or changing phosphatidylserine exposure on normal endothelium.[34] Docetaxel in combination with AV-directed EPT has been shown to increase EPT cytotoxic efficacy *in vitro* for prostate cancer cells without any cytotoxic effects of docetaxel alone.[141]

We have developed three distinct AV-directed EPT systems,[39,116,117] each containing a different enzyme, as follows:

(1) L-methioninase (MT) – Converts the relatively nontoxic prodrug L-selenomethionine (SM) to toxic methylselenol, which generates the reactive oxygen species α-ketobutyrate and ammonia.[77] MT also converts the amino acid methionine to methanethiol, thereby creating a dual cytotoxic strategy, since most cancer cells have upregulated methionine dependence.[78] PDAC cells have shown evidence of sensitivity to methionine depletion,[142] and sensitivity to gene-directed EPT treatment with MT.[143]

(2) Purine nucleoside phosphorylase (PNP) – Converts the purine nucleoside analogue fludarabine (9-β-D-arabinofuranosyl-2-fluoroadenine 5'-monophosphate, FD) into highly cytotoxic 2-fluoroadenine (2-FA); 2-FA

incorporates into DNA/RNA and effectively kills dividing and nondividing cells.[80] PDAC has shown sensitivity to gene-directed EPT approaches utilizing PNP[81] and to virus-directed EPT with PNP/FD.[144]

(3) Cytosine deaminase (CD) – Converts the prodrug 5-fluorocytosine (5-FC) to 5-fluorouracil (5-FU), metabolites of which misincorporate into DNA/RNA and inhibit the nucleotide synthesis enzyme thymidylate synthetase.[83] PDAC has shown sensitivity towards virus- and gene- directed EPT approaches with CD/5-FC.[22,145]

Upon fusion of these enzymes to AV, the resulting fusion proteins are referred to as MT-AV, PNP-AV, and CD-AV, respectively.

We have previously reported the vascular targeting and killing capabilities of each of these systems on non-confluent human abdominal aorta endothelial cells (HAAE-1) as mimics of tumor vasculature *in vitro*.[39,116,117] We have also validated the safety and efficacy of the MT-AV system *in vivo* for the treatment of MDA-MB-231 breast cancer xenografts in mice.[126]

To date, the efficacy of our AV-directed EPT systems on PDAC remains unexplored. Although phosphatidylserine is robustly and consistently expressed by solid tumors, their vasculature, and their metastases, the level of phosphatidylserine exposure varies between cell lines of different cancer types,[38] as well as between cell lines of the same cancer type, including PDAC.[138] Therefore, AV-directed EPT efficacy cannot be assumed to be tumor-type independent. To this end, in the current study we investigated the *in vitro* binding strength and anticancer activity of three AV-

directed EPT systems combined with low-dose docetaxel for two diverse PDAC cell lines to evaluate the potential applicability of AV-directed EPT to PDAC.

Materials and Methods

Expression and purification of fusion proteins

All fusion proteins were expressed and purified as described previously.[39,116,117] Briefly, the polymerase chain reaction (PCR) was used to amplify the genes encoding each enzyme and AV, as well as a fusion site containing a six residue flexible linker and an N- or C-terminal His$_6$ tag with a HRV 3C protease cleavage site immediately downstream or upstream, respectively. Plasmids containing each fusion protein were created via transformation of NovaBlue competent cells and then expressed in *E.coli* BL21 (DE3) cells. Recombinant fusion proteins were produced and purified according to the procedure of Zang *et al.* using immobilized metal (Ni^{2+}) affinity chromatography.[127] The His$_6$ tag was removed during purification by cleavage with HRV 3C protease (Merck, Darmstadt, Germany). Fusion proteins were lyophilized and stored at -80 °C.

Cell culture

Human pancreatic epithelioid carcinoma cell line, Panc-1, and human pancreatic adenocarcinoma cell line, Capan-1, were obtained from the American Type Culture Collection (ATCC, Manassas, VA). Panc-1 cells were cultured in Dulbecco's Modified Eagle's Medium (ATCC) supplemented with 10% fetal bovine serum (FBS), 100 U/ml penicillin, and 100 µg/ml streptomycin (both from Atlanta Biologics, Flowery Branch,

GA). Capan-1 cells were cultured in Iscove's Modified Dulbecco's Medium (ATTC),

supplemented with 20% FBS, 100 U/ml penicillin, and 100 μg/ml streptomycin. All

cells were maintained at 37 °C in a 5% CO_2 atmosphere. Cells were passaged at 70-

80% confluence, 1-3 times per week, <12 times during the course of experiments.

In vitro binding assays

Cells were plated at 50 x 10^3 cells/well in 24-well cell culture plates and allowed to

grow to 90% confluence. Dissociation constants were determined as described

previously.[39,116,117] Briefly, cells were fixed with glutaraldehyde, treated with bovine

serum albumin, and incubated with varying concentrations (0-20 nM) of biotin-labeled

fusion proteins, which after washing were then allowed to react with streptavidin-

horseradish peroxidase. Subsequently, binding was quantified with the chromogenic

substrate o-phenylenediamine by measuring absorbance at 450 nm. To determine

specific binding, the above procedure was conducted in the presence of 2 mM Ca^{2+}

(total binding) and in the absence of Ca^{2+} with 5 mM EDTA added to chelate any

residual calcium present (non-specific binding). All experiments contained a blank

subjected to the same procedure but with 0 nM fusion protein.

In vitro enzyme prodrug cytotoxicity

Panc-1 cells were plated at 25 x 10^3 cells/well on 24-well plates, and Capan-1 cells were

plated at 2.5 x 10^3 cells/well on plates coated with 0.1 % w/v gelatin, which was

determined to be necessary to sustain Capan-1 cells in culture for the duration of EPT

treatment. Culture medium was supplemented with 2 mM Ca^{2+}, since AV binding to

phosphatidylserine is calcium-dependent. Medium for MT-AV EPT also contained

0.02 mM pyridoxal phosphate (co-factor). Cells were treated with sub-toxic

concentrations of docetaxel (Biotang, Waltham, MA) 24 h post plating and 24 h prior to

the beginning of EPT treatment at concentrations previously determined to have no

effect on cell viability or growth rate (200 pM for Panc-1 cells and 50 pM for Capan-1

cells). To mimic *in vivo* EPT, cells were treated with a saturating concentration of

fusion protein (100 nM) every 3 days for 2 h at 37 °C in accordance with previous

binding stability studies.[39,116,117] Each day medium was replaced with medium

containing varying concentrations of prodrug (SM and 5-FC from Fisher Scientific,

Waltham, MA and FD from VWR, Radnor, PA) or drug analog (2-FA from Fisher

Scientific and 5-FU from Sigma-Aldrich, St. Louis, MO) both containing appropriate

concentrations of docetaxel. An Alamar Blue (Invitrogen, Grand Island, NY) assay was

preformed every 2 days to measure cell viability.[128] Cells were incubated with 10%

Alamar Blue in fresh medium for 4 h at 37 °C, and supernatant fluorescence (530/590

nm) was read on a microtiter plate reader. Cells were washed twice after each Alamar

Blue assay and three times after each fusion protein incubation before prodrug/drug

treatments were added. All studies were carried out over a 6-day treatment cycle.

Data analysis

All treatments were run in triplicate. Dissociation constants were obtained using Prism

5 software (GraphPad, La Jolla, CA). Statistical significance was determined with

Prism 5 via a one-way ANOVA employing the Tukey-Kramer multiple comparisons

test.

Results

Binding strength of fusion proteins to phosphatidylserine on cell surface

The binding strength of each fusion protein to phosphatidylserine on the surface of

Panc-1 and Capan-1 cells was measured by subtracting non-specific binding (EDTA)

from total binding (Ca^{2+}) to obtain specific binding. Representative data for MT-AV

binding to Panc-1 cells is shown in Figure 28. The data were then fit to a one-site, non-

competitive binding model to determine dissociation constants (K_d) for specific binding,

which are presented in Table 3 for all fusion proteins binding to both cells lines.

AV-directed EPT cytotoxicity

Simulated EPT was carried out over a 6-day treatment period with various

concentrations of corresponding prodrug for each EPT system. No treatment controls

(0 μM prodrug/drug) were run without docetaxel (notated "w/o doc") to confirm

docetaxel alone had no effect on cell viability. Each EPT system included controls of

prodrug treatment alone at all concentrations investigated. For the PNP-AV and CD-

AV systems, controls with matched concentrations of the drug generated by the EPT

system were also included (for the MT-AV system, the resulting drug cannot be

obtained as it has a very short half life).[146] Percent cell viability was determined by

comparing cell viability on days 2, 4, and 6 to viability on day 0 on a per well basis,

averaged per triplicate. Statistical significance was established by comparing cells

treated with EPT, prodrug alone, or drug controls to their corresponding control groups

treated with 0 nM concentrations of the drug/prodrug on the same day (#, $p < 0.05$; *, p

< 0.01; and **, $p < 0.001$). Additionally, 0 μM prodrug/drug with and without
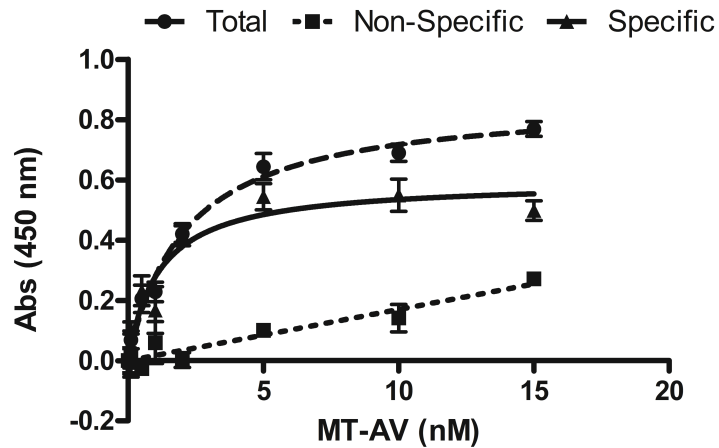
Figure 28: MT-AV binding to Panc-1 cell surface

Representative binding curves for MT-AV binding to phosphatidylserine expressed on the external surface of Panc-1 cells. Total binding ($\bullet$) was measured in the presence of 2 mM Ca^{2+} and non-specific binding ($\blacksquare$) was measured in the absence of Ca^{2+} (with 5 mM EDTA) for increasing concentrations of MT-AV (0-15 nM). Specific binding ($\blacktriangle$) was obtained by subtracting non-specific from total binding. Data presented as mean ± SE (n = 3).

Table 3: Dissociation constants for PDAC cell lines

Dissociation constants for fusion proteins binding to Panc-1 and Capan-1 cells. Data presented as K_d ± SE nM (n=3).

Cell line	Fusion protein		
	MT-AV	PNP-AV	CD-AV
Panc-1	1.15 ± 0.38	0.03 ± 0.04	0.09 ± 0.08
Capan-1	0.38 ± 0.15	0.02 ± 0.02	0.90 ± 0.10

docetaxel were compared, matched for experimental day; we found that docetaxel (200 pM on Panc-1 and 50 pM on Capan-1) did not significantly affect cell viability throughout any of the experiments.

MT-AV + SM EPT treatment showed highly cytotoxic effects at low concentrations for Panc-1 cells (Figure 29a). On day 6, cells treated with a concentration of 100 µM SM exhibited only 9% residual viability. EPT efficacy increased with increasing SM concentrations, resulting in only 3% viability by day 6 for 250 µM SM concentrations, compared to 500 µM SM where only 3% viability remained by day 4 and by day 6 viability dropped to 0%. For all SM concentrations, SM alone showed no cytotoxic effects.

MT-AV + SM treatment of Capan-1 cells (Figure 29b) showed good efficacy but required higher concentrations of SM for effective killing than Panc-1 cells. Large cytotoxic effects were seen at 500 µM SM concentrations, at which viability dropped below 15% by day 4. At this SM concentration, SM alone began to display growth inhibitory effects on Capan-1 cells, as percent viability did not increase with time.

PNP-AV + FD EPT treatment on Panc-1 cells (Figure 30a) exhibited strong cytotoxic effects, but higher concentrations of FD were necessary for complete killing of Panc-1 than Capan-1 cells. By day 6, FD concentrations of 3 µM caused 8% residual viability and for 20 µM FD only 2% viability remained. PNP-AV EPT effectively mimicked the effects of the drug 2-FA at concentrations of FD $\geq$ 3 µM. Even at the highest concentration (20 µM), FD alone showed no harmful or growth inhibitory effects on Panc-1 cells.
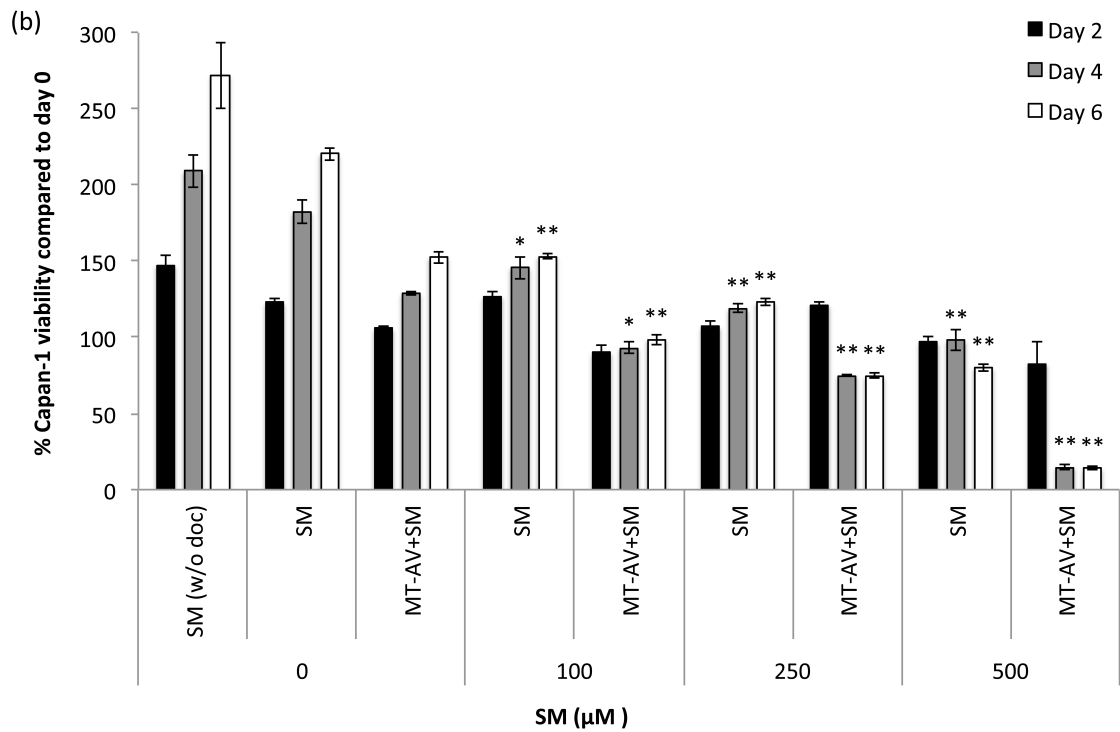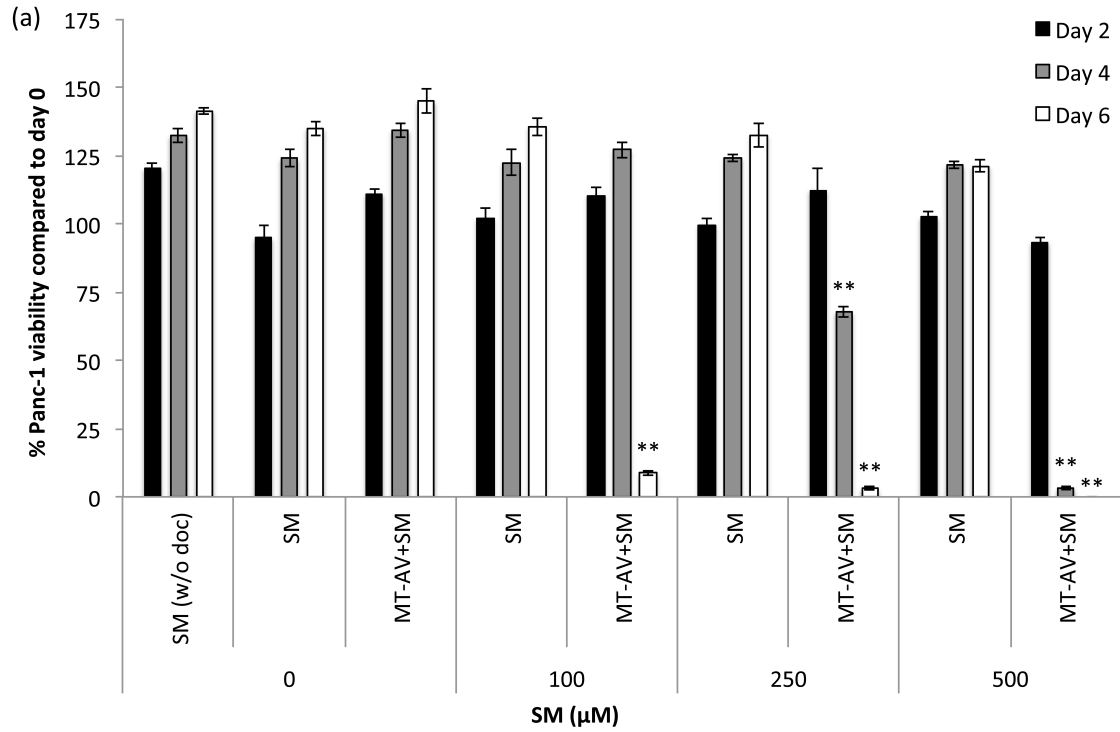
Figure 29: MT-AV + SM EPT efficacy on PDAC cell lines

Effect of MT-AV + SM EPT treatment on (a) Panc-1 and (b) Capan-1 cells plus docetaxel, except where noted ("w/o doc"). Cell viability was assessed using Alamar Blue assay at the beginning of the experiment (day 0) and on days 2, 4 and 6. Results are presented as percent viability compared to day 0. Cells treated with varying concentrations of SM were compared their corresponding control group treated with 0 nM of SM on the same day, and significant differences are denoted by * ($p < 0.01$) and ** ($p < 0.001$). Data presented as mean ± SE (n = 3).
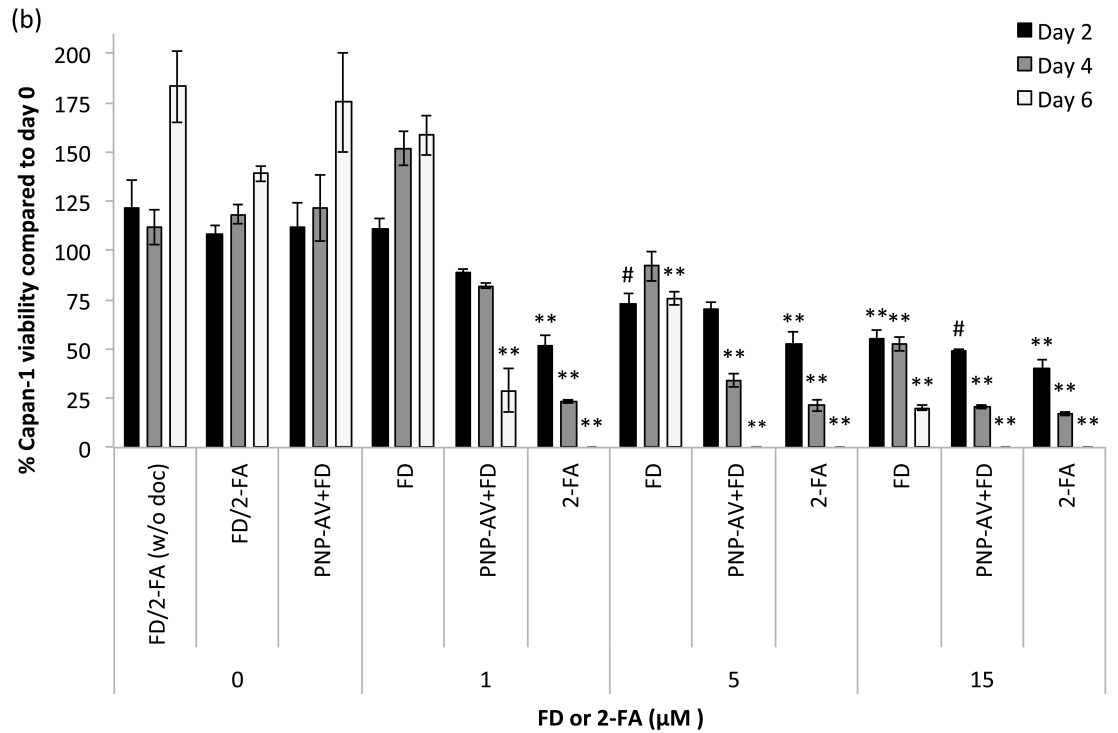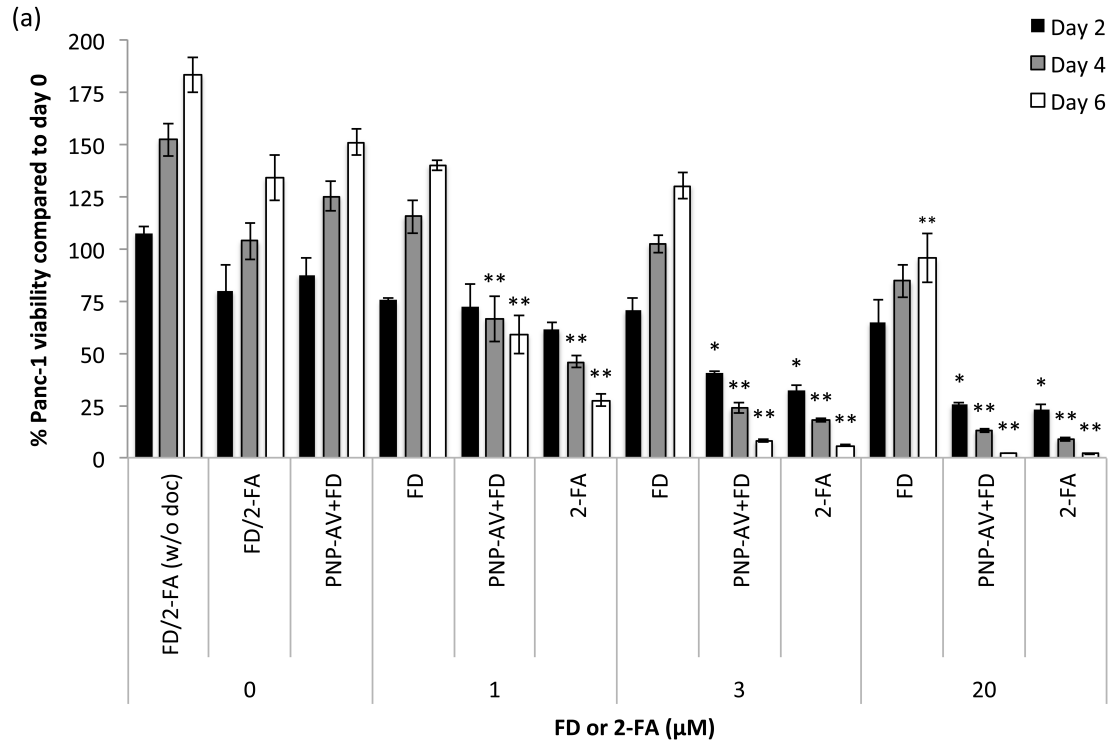
Figure 30: PNP-AV + FD EPT efficacy on PDAC cell lines

Effect of PNP-AV + FD treatment on (a) Panc-1 and (b) Capan-1 cells plus docetaxel, except where noted ("w/o doc"). Cells treated with varying concentrations of FD or 2-FA were compared their corresponding control groups treated with 0 nM concentrations on the same day, and significant differences are denoted by # ($p < 0.05$), * ($p < 0.01$), and ** ($p << 0.001$). Data presented as mean ± SE (n = 3).

For Capan-1 cells, PNP-AV + FD created effective treatment (Figure 30b), resulting in 0% cell viability at FD concentrations of 5 μM and above by day 6, and was as effective throughout the study as 2-FA treatment at FD concentrations ≥ 5 μM. FD alone, however, also started exhibiting slight cytotoxic effects at concentrations ≥ 5 μM, although significantly less than EPT treatment or 2-FA. The effect of the prodrug FD alone was dose-dependent, and by day 6, 15 μM FD resulted in 20% residual viability.

CD-AV + 5-FC EPT treatment on Panc-1 cells (Figure 31a) showed an effect at concentrations as low as 500 μM, and were comparable to the efficacy of 5-FU drug treatment throughout all experimental days. By day 6, EPT treatment with 10,000 μM concentrations of 5-FC exhibited only 17% residual viability, with no cytotoxic or growth inhibitory effects of 5-FC treatment alone.

CD-AV + 5-FC treatment effects were less pronounced on Capan-1 than Panc-1 cells (Figure 31b). EPT effects were found to be dose-dependent; at low concentrations (500 μM 5-FC) the CD-AV EPT resulted in cell viability of 87% by day 6 while at the highest concentration (10,000 μM 5-FC), viability of Capan-1 cells decreased to 51% by day 6. CD-AV+5-FC treatment efficacy was not comparable to drug treatment with 5-FU, as 5-FU was more effective at all concentrations. 5-FC treatment alone did not
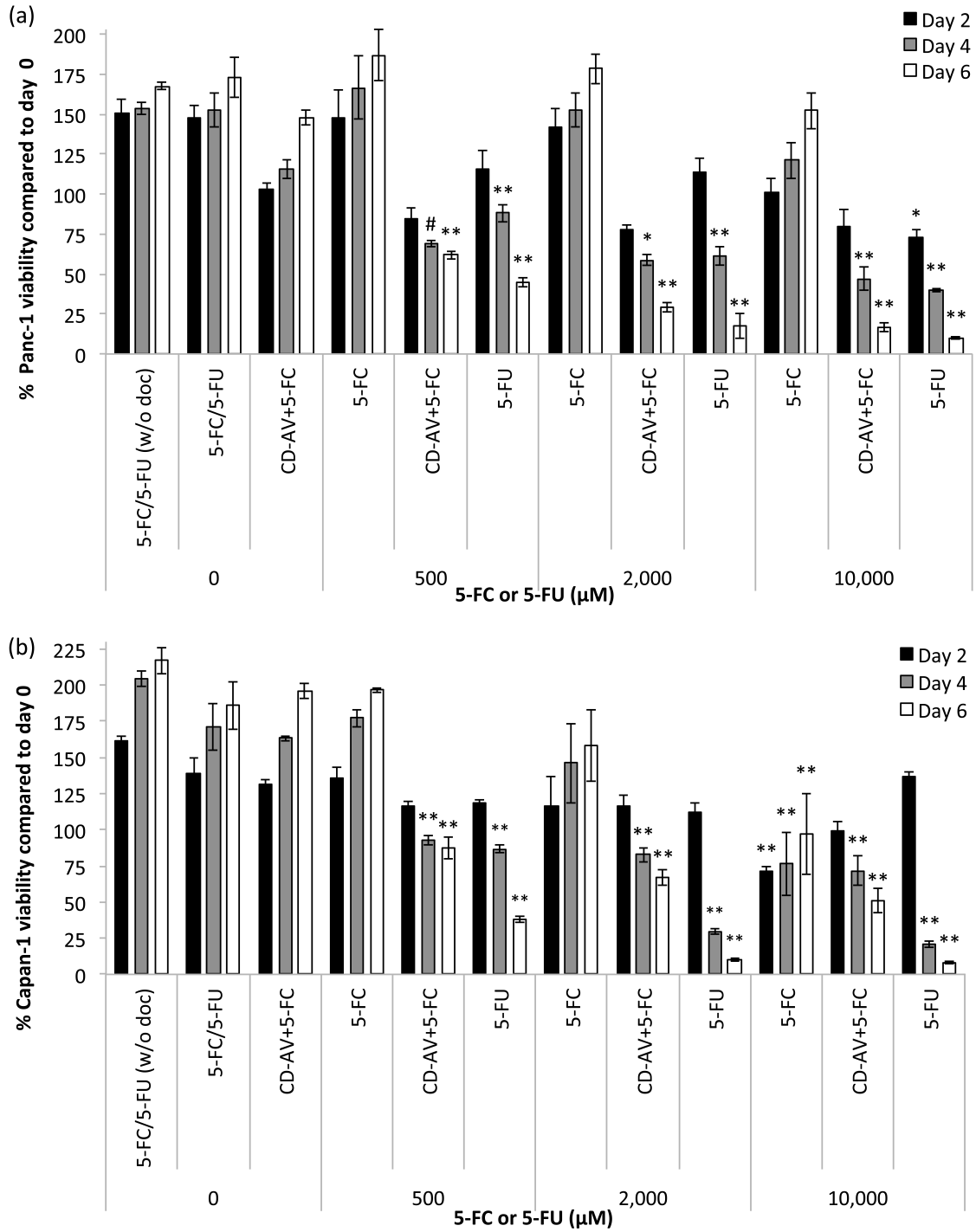
Figure 31: CD-AV + 5-FC EPT efficacy on PDAC cell lines

Effect of CD-AV + 5-FC EPT treatment (a) Panc-1 and (b) Capan-1 cells plus

docetaxel, except where noted ("w/o doc"). Cells treated with varying concentrations of

5-FC or 5-FU were compared their corresponding control groups treated with 0 nM concentrations on the same day, and significant differences are denoted by # ($p < 0.05$), * ($p < 0.01$), and ** ($p < 0.001$). Data presented as mean ± SE (n = 3).

show any cytotoxic effects until a concentration of 10,000 μM, where an initial drop in viability occurred but growth ensued again thereafter.

Discussion

The MT-AV system emerged from this study as an effective potential treatment option, since near complete killing at low prodrug concentrations was achieved for both PDAC cell lines investigated. The median lethal dose (LD_{50}) of SM *in vivo* for female nude mice is 12.5 mg/kg, which translates to ~1100 μM *in vitro*, indicating that a feasible treatment window exists. The generation of reactive oxygen species by the MT-AV system is an unconventional approach to cell killing that has not been extensively investigated for PDAC, and has potential for combination with chemotherapy regimens, as it will continue to be effective even as chemoresistance develops.

PNP-AV EPT displayed good killing efficacy at very low FD concentrations for both Capan-1 and Panc-1 cells, and, therefore, also emerged as a potential treatment option. The prodrug of the PNP-AV system, FD, exhibited a substantial cytotoxic effect on Capan-1 cells, which is consistent with previous results for MCF-7 human breast adenocarcinoma cells.[117] Although these *in vitro* results for FD alone seem promising, the effect of FD alone was found to be insufficient in a phase II clinical trial

for breast cancer.[147] Since 2-FA is more toxic than FD, PNP-AV EPT has the potential to strengthen the antitumor effect of FD.

As the CD-AV system displayed the slowest killing velocity, lowest killing efficacy, and required a high concentration of prodrug to create killing effects, this therapy was the least attractive of the three EPT systems investigated. However, 5-FU treatment has been shown to be of some benefit for PDAC,[148] including in combination therapy for second line treatment.[149] Thus, replacing 5-FU with CD-AV+5-FC in combination regimens could potentially mitigate negative systemic side effects.

We found that each of the prodrugs alone had little to no effect on Panc-1 cells, whereas for Capan-1 cells the prodrugs alone created cytotoxicity for FD and 5-FC and growth inhibitory effects for SM at the highest concentrations tested. We believe this occurred because Capan-1 cells have a much longer doubling time[150] and are, therefore, more susceptible to treatment with prodrugs alone.

All fusion proteins showed tight binding to both cell lines with pM to low nM range dissociation constants. These K_d values are less than those observed previously for AV binding to phosphatidylserine (2.7-15.5 nM).[60,61] The multimeric structure of each fusion protein likely allows for multiple AV to phosphatidylserine bonds per fusion protein, and we believe this contributes to the observed strong binding of fusion proteins to phosphatidylserine. To address the vascular targeting capabilities of these fusion protein systems, we have previously shown that all three systems bind tightly to phosphatidylserine expressing human abdominal aorta endothelial cells (HAAE-1) *in vitro*, with dissociation constants ranging from 0.5-1.5 nM.[39,116,117]

We aimed to take advantage of the phosphatidylserine exposure effect of docetaxel without unleashing its broad-spectrum antitumor properties, as to establish the benefit of docetaxel only with respect to fusion protein binding. This was in fact demonstrated, as all of the no treatment controls with docetaxel did not shown any significant deviations in viability compared to the no treatment controls without docetaxel. In clinical trials, docetaxel has elicited disease-stabilizing effects and objective tumor responses both as monotherapy and in combination with gemcitabine in patients with PDAC.[151,152] We propose that docetaxel in combination with AV-directed EPT may prove synergistic in the clinic as the phosphatidylserine exposing and cytotoxic effects would be utilized simultaneously.

All three of the EPT systems studied contain bacterial enzymes. This is beneficial as native enzymes will not activate the prodrugs utilized and drug accumulation will be confined to the tumor site. However, bacterial enzymes may elicit an immune response, especially with repeated administration, but, regardless, some bacterial enzymes have been successfully tested in humans, such as carboxypeptidase G2.[153] Immunogenicity of the enzyme in each EPT system may be addressed by one of three methods: (i) PEGylating the entire fusion protein to restrict immune recognition,[154] (ii) mutating the active site of human analogs of the bacterial enzyme to confer activity towards the corresponding prodrug,[131,132] or by (iii) genetically modifying the immunogenic epitopes found on the bacterial enzyme.[153]

Since all of the EPT systems investigated are targeted via AV, the concern exists that in a clinical setting the intravenously administered fusion proteins could bind to activated platelets, which also express phosphatidylserine. However, we believe that

AV-directed EPT would be relatively safe because the fraction of activated platelets is less than 0.5% of total platelets present in the bloodstream.[3] To date, phosphatidylserine tumor targeting has been safely utilized in murine models,[34,126] including PDAC,[138,139] without any noticeable platelet-binding mediated side effects.

In conclusion, we were able to demonstrate strong binding and significant cytotoxic effects, including complete cell killing, with three distinct annexin V-directed EPT systems on two diverse pancreatic cancer cell lines. These results suggest that AV-directed EPT treatment, especially the MT-AV system, could be useful for treating vascularized PDAC, while mitigating the side effects associated with systemic administration of chemotherapeutics.
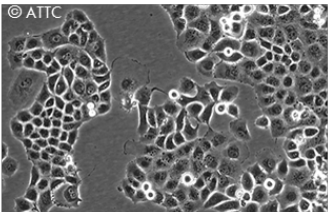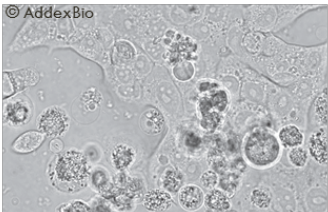
Additional Figures

Diversity of pancreatic cell lines

Pancreatic adenocarcinoma cell lines with highly variable characteristics were utilized to test binding strength and cytotoxic efficacy of our FPs. Importantly, both Panc-1 and Capan-1 cell lines are KRAS mutants, a mutation found in over 90% of all pancreatic tumors that leads to unchecked growth. KRAS mutations lead to increased cell survival, proliferation, cell motility (implicated in metastasis), and increases in vesicular trafficking and cell cycle progression.   Additional characteristics of each cell line investigated are presented in Table 4.[150]

Table 4: Differences between Panc-1 and Capan-1 PDAC cell lines

Cell Line	Panc-1	Capan-1
Image		
K-ras	Mutant	Mutant
p53	Mutant	Mutant
p16	Mutant	Mutant
DPC4/smad4	Wild Type	Mutant
Doubling Time	Fast	Slow
Cellular Polymorphism	Grade 3	Grade 1
Nuclear Polymorphism	Grade 3	Grade 2
Source	Primary Tumor	Liver Metastasis

Effect of docetaxel alone on PDAC cell lines

The data utilized to determine docetaxel treatment concentrations is shown in Figure 32a for Panc-1 cells and Figure 32b for Capan-1 cells. Cells were plated as described in the enzyme prodrug cytotoxicity methods section. After 24 h, complete growth medium was replaced with complete growth medium containing varying concentrations of docetaxel. Alamar blue assays were utilized to determine viability on Days 0, 2, 4, and 7 for Panc-1 cells and on Days 0, 2, 4, and 6 for Capan-1 cells. All data is presented as % viability compared to day 0.
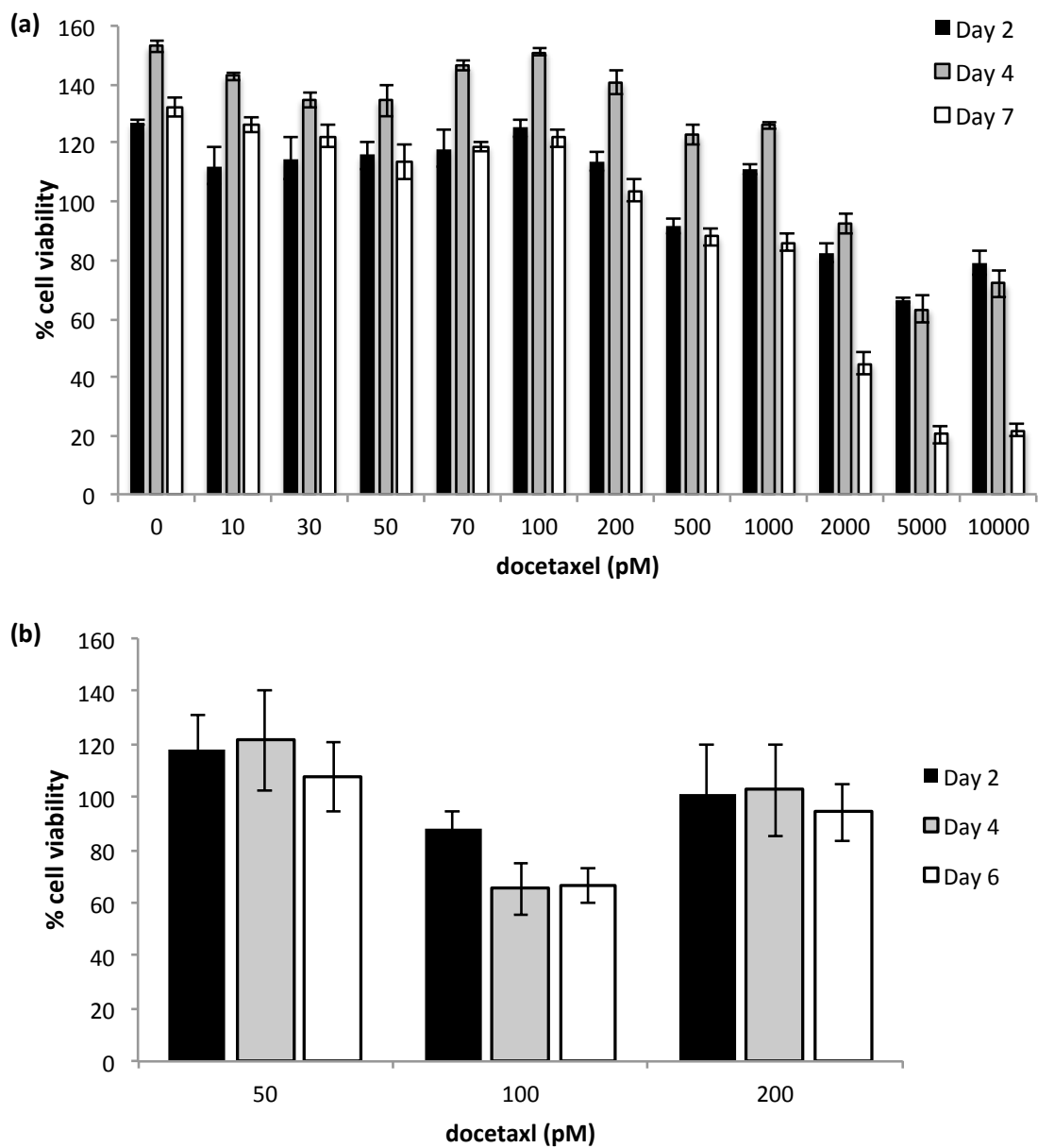
Figure 32: Effect of docetaxel on Panc-1 cell and Capan-1 cells

Cytotoxic effect of increasing docetaxel concentrations on (a) Panc-1 cell and (b) Capan-1 cells. Cells were treated daily with growth medium containing docetaxel and viability was measured via Alamar Blue assay and compared to viability on day 0. From this treatment concentrations (200 pM for Panc-1 and 50 pM for Capan-1) were determined. Data presented as mean ± SE (n = 3).

Binding strength curves

Curves not selected as the published "sample curve" are presented in Figure 33 for

Panc-1 cells and Figure 34 for Capan-1 cells.
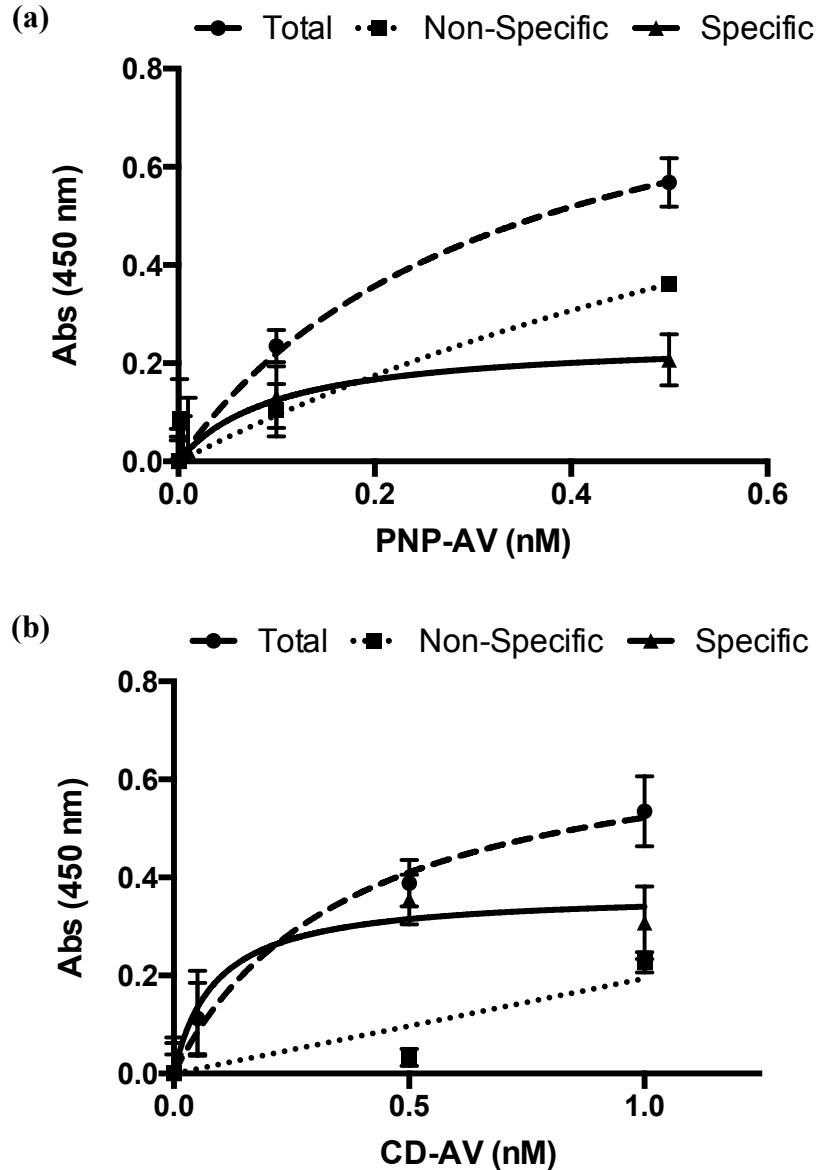
Figure 33: PNP-AV and CD-AV binding to Panc-1 cell surface

Panc-1 cells were incubated with increasing concentrations of (a) biotin labeled PNP-AV and (b) biotin labeled CD-AV, with total binding ($\bullet$) measured in the presence of 2 mM Ca^{2+} and non-specific binding ($\blacksquare$) measured in the absence of Ca^{2+} with 5 mM EDTA to chelate any residual Ca^{2+}. Specific binding ($\blacktriangle$) was obtained by subtracting non-specific from total binding. Data presented as mean ± SE (n = 3).

(a)

(b)
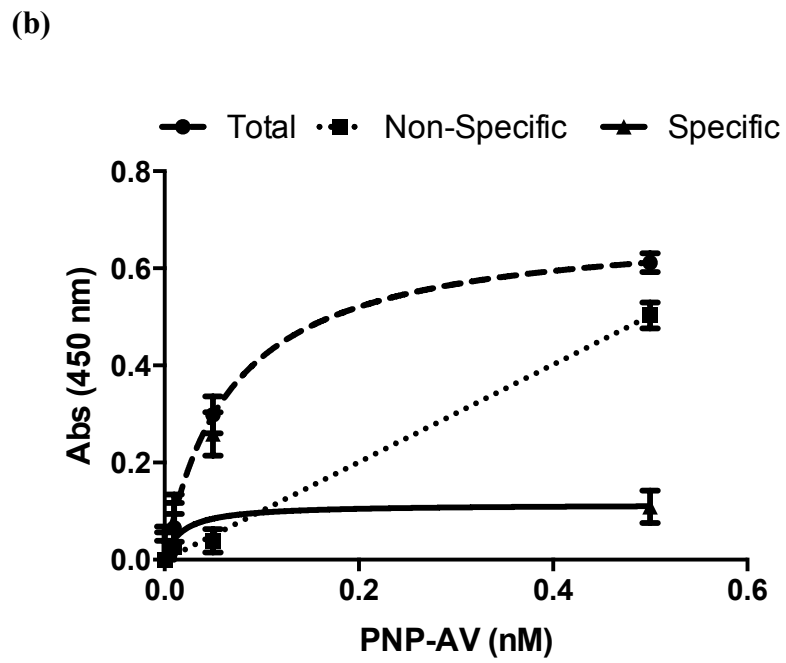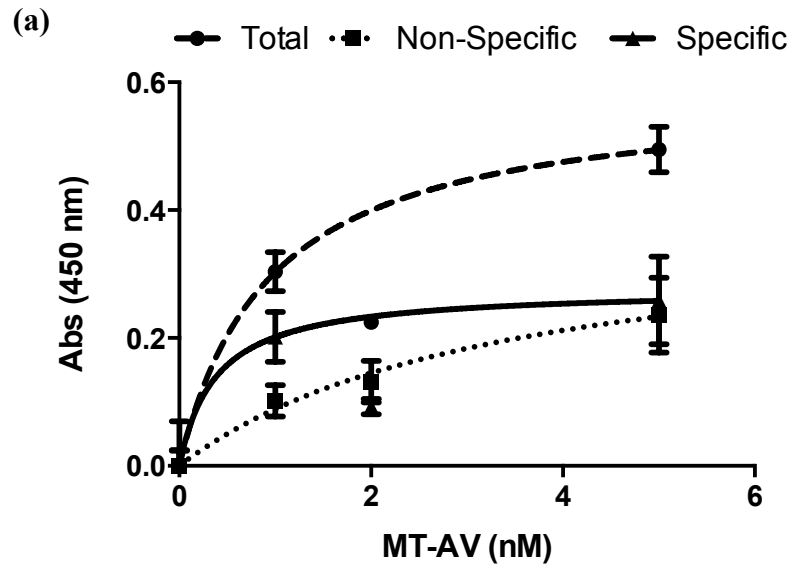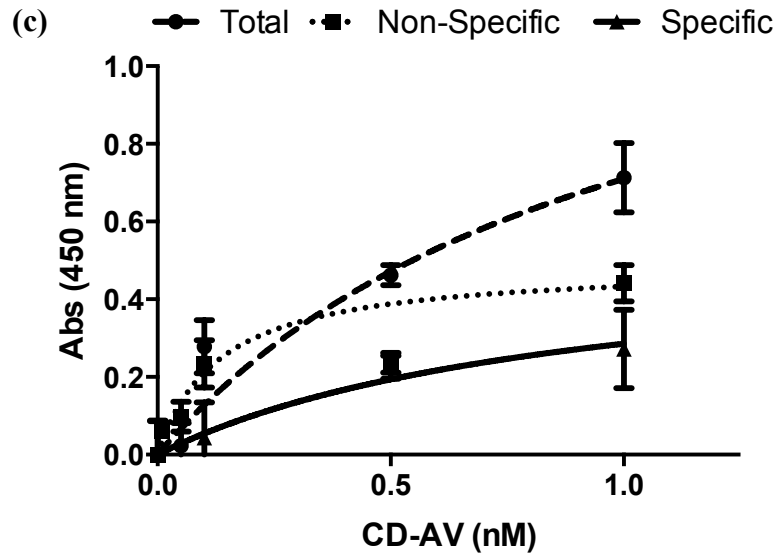
Figure 34: MT-AV, PNP-AV, and CD-AV binding to Capan-1 cell surface

Capan-1 cells were incubated with increasing concentrations of (a) biotin labeled MT-AV (b) biotin labeled PNP-AV and (b) biotin labeled CD-AV, with total binding ($\bullet$) measured in the presence of 2 mM Ca^{2+} and non-specific binding ($\blacksquare$) measured in the absence of Ca^{2+} with 5 mM EDTA to chelate any residual Ca^{2+}. Specific binding ($\blacktriangle$) was obtained by subtracting non-specific from total binding. Data presented as mean ± SE (n = 3).

Additional Data: Docetaxel Effect on FP Binding to Panc-1 Cells

Introduction

We were interested in determining if the increases in protein binding observed for

prostate cancer cells (Chapter 2, additional data) with the addition of docetaxel would

also be observable for Panc-1 pancreatic cancer cells. Prior to commencing large-scale

EPT studies, we utilized flow cytometry to investigate differences in binding afforded

by docetaxel, and this data was in part used to justify the inclusion of docetaxel in all of

the EPT studies published in *Pancreas*.

Methods

All FPs were labeled with FITC (Thermo Scientific, Waltham, MA, USA) according to

the manufacturer's instructions. Cells were plated, allowed to adhere, and then selected

wells were treated with 200 pM docetaxel 24 h prior to FP binding. Cells were

incubated with varying saturating concentrations (~2 times the K_D values) of FITC-

labeled FPs at 37 °C for 2 h in medium augmented with 2mM Ca^{2+}. After a thorough

wash, cells were trypsinized, transferred to 1.5 ml microcentrifuge tubes, and

centrifuged at 100 x g for 5 min. Cells were resuspended in FACS buffer and kept on

ice. Data was collected on a BD Accuri C6 and presented as mean fluorescence per

10,000 gated events.

Results

All FPs exhibited an increase in binding in the presence of docetaxel. Mean

fluorescence (FLU) per 10,000 events as a measure of total FP binding in the presence

and absence of 200 pM docetaxel are shown for all three fusion proteins in Figure 35. Both PNP-AV and MT-AV binding increased by approx. 25%, while CD-AV binding increased by 94% on average.

Discussion

Since all FPs displayed increases in total binding with the addition of docetaxel, this led us to conclude that docetaxel will be advantageous to all three EPT systems for Panc-1 cells.

Unlike for PC-3 prostate cancer cells, MT-AV system binding did increase in the presence of docetaxel. This may indicate that the response of these two cell lines to docetaxel results in different spatial patterns of additional PS exposure, one of which is amenable to increased MT-AV binding and one that is not. MT-AV is the only tetramer investigated and consistently binds the least strongly of all three-fusion proteins, regardless of cell line. This may also mean that it is most susceptible to spatial differences in PS exposure, such as raft vs. random distributions of PS on the surface of cancer cells.

Surprisingly, the only difference to achieve statistical significance was that of MT-AV ($p = 0.0945$). However, we propose that the introduction of docetaxel increases the diversity of PS expressed within the cell population as (a) not all cells express the same number of PS residues to begin with and (b) not all cells will respond to docetaxel treatment identically. Therefore the initial diversity of PS expression density on the outer leaflet is magnified with docetaxel exposure and contributes to the large standard errors observed.

Clearly, more work on how PS exposure is altered under low-concentration docetaxel conditions is needed to fully elucidate this mechanism of enhanced binding capacity. However, this work does provide a logical rationale for including docetaxel with annexin-directed fusion proteins.
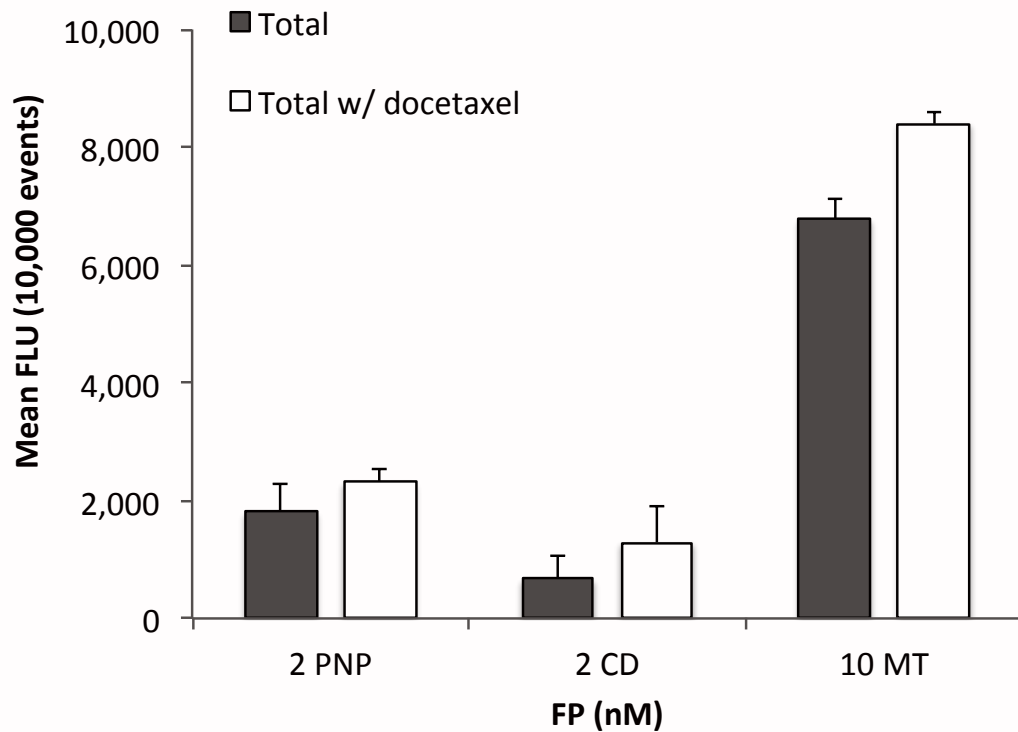
Figure 35: FPs binding to Panc-1 cells in the presence and absence of docetaxel

FITC-labeled FPs were allowed to bind to Panc-1 cells in the presence and absence of docetaxel in order to investigate docetaxel modulated increases in total FP binding. All FPs were incubated with Panc-1 cells at concentrations approx. twice their K_D values, and all FPs displayed increases in binding capacity with the addition of docetaxel. Data presented as mean ± SE (n = 3).

Additional Data: Binding Strength of FPs to BxPC-3 Cells

Introduction

At the initiation of this project, we intended to utilize BxPC-3 human pancreatic adenocarcinoma cells as a third cell line to increase the diversity of PDAC cell lines evaluated. However, it was found that BxPC-3 cells could not be kept in culture for > 3 days. However, all fusion proteins were shown to bind to BxPC-3 cells.

Methods

BxPC-3 cells (ATCC) were cultured in RPMI-1640 medium (ATCC) supplemented with 10% FBS, 100 U/ml penicillin, and 100 μg/ml streptomycin. Cells were cultured as described previously. Cells were plated at 50 k/well for binding strength assays, which were executed as described in the main methods section.

Results

Binding strength curves for all three fusion proteins are presented in Figure 36 and dissociation constants are presented in Table 5.

Discussion

All fusion proteins exhibited strong binding to the BxPC-3 cell surface.

(a)

Total · · Non-Specific · · Specific

(b)

Total · · Non-Specific · · Specific
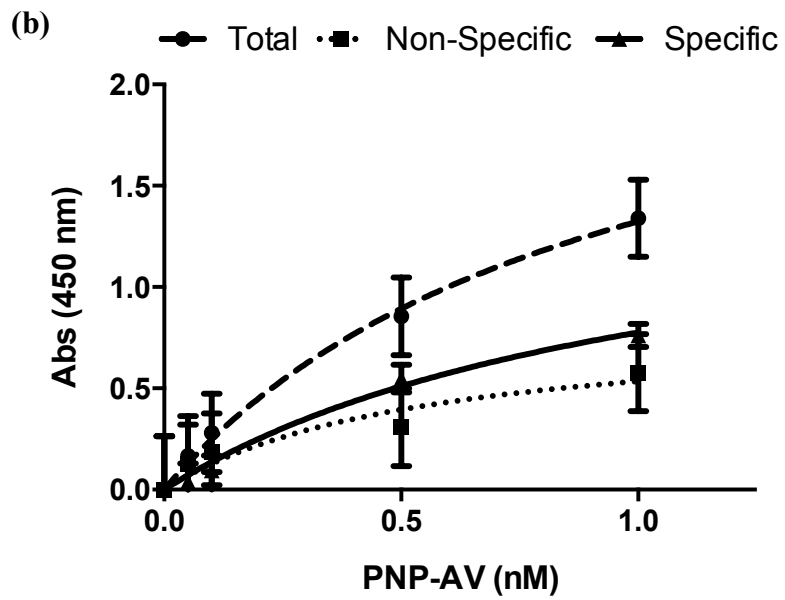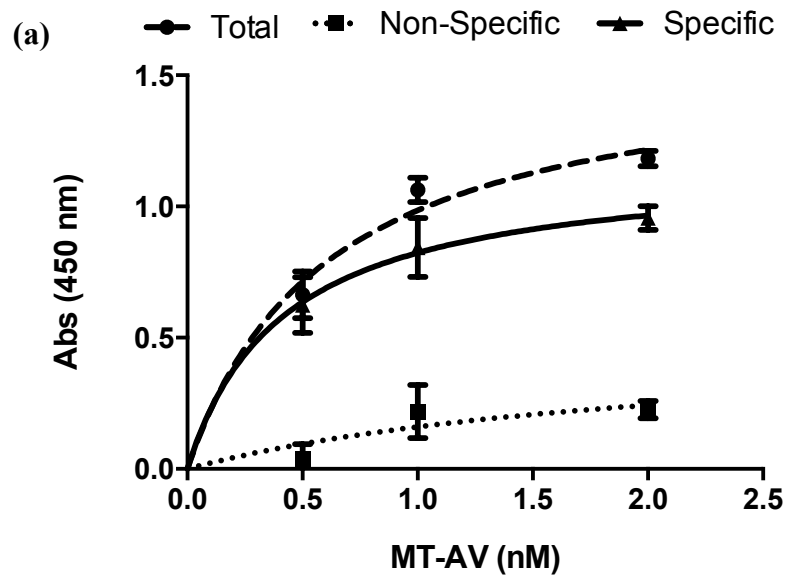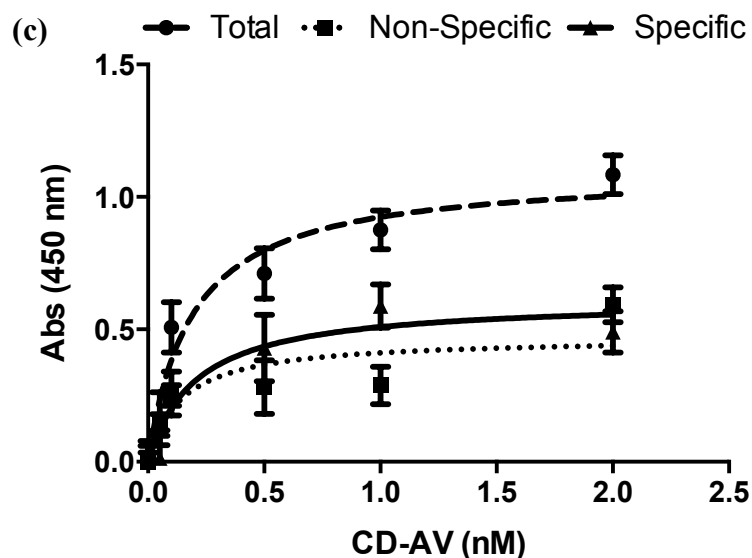
Figure 36: MT-AV, PNP-AV, and CD-AV binding to BxPC-3 cell surface

Bx-PC3 cells were incubated with increasing concentrations of (a) biotin labeled MT-AV (b) biotin labeled PNP-AV and (c) biotin labeled CD-AV, with total binding ($\bullet$) measured in the presence of 2 mM Ca^{2+} and non-specific binding ($\blacksquare$) measured in the absence of Ca^{2+} with 5 mM EDTA to chelate any residual Ca^{2+}. Specific binding ($\blacktriangle$) was obtained by subtracting non-specific from total binding. Data presented as mean ± SE (n = 3).

Table 5: Dissociation constants for bx-PC3 PDAC cell line

Dissociation constants for fusion proteins binding to bx-PC-3 cells. Data presented as K_d ± SE nM (n=3).

Cell line	Fusion protein		
	MT-AV	PNP-AV	CD-AV
Bx-PC3	0.419 ± 0.071	1.090 ± 0.470	0.204 ± 0.115

Chapter 4: Development and Evaluation of Annexin-Directed β-Glucuronidase

The following manuscript is slated for submission to the *British Journal of Cancer* as "Annexin-Directed β-Glucuronidase for the Targeted Treatment of Vascular Solid Tumors". The authors are Katrin P. Guillen, Eliza A. Ruben, and Roger G. Harrison.

Abstract

Background: To improve the clinical relevance of annexin-directed enzyme prodrug therapy (EPT), we have created fusion proteins centered about the human enzyme β-glucuronidase (βG), which can convert innocuous prodrugs into chemotherapeutics. By targeting βG to phosphatidylserine on tumor cells, the tumor vasculature, and metastases via annexin, we aim to create high-dose, combination chemotherapy only within the tumor environment, thereby mitigating side effects.

Methods: Genes for human annexin A1 orA5 were fused to genes for human wt or 16a3 mutant βG. Fusion proteins were expressed in fed-batch CHO suspension cultures and chromatographically purified. Enzyme kinetics were measured. Binding was visualized via confocal microscopy and quantitated via dissociation constants and stability assays. Cytotoxic efficacy was determined for the prodrug SN-38 glucuronide.

Results: All fusion constructs achieved > 95% purity with yields up to 740 μg/L. Activity of mutant fusions was significantly improved at pH 7.4. Nanomolar range dissociation constants were observed, 0.98-3.0 nM for A1-16a3 and 0.34-1.1 nM for

A5-16a3, along with cell line dependent stability. The A5-16a3 fusion protein in combination with SN-38 glucuronide was as effective as SN-38.

Conclusions: Annexin-βG fusion proteins provide a powerful, new EPT modality with promising clinical potential based on their fully human design and combination therapy capability.

Keywords: enzyme prodrug therapy, SN-38, phosphatidylserine, vascular targeted

Background

It remains difficult to exploit the full potential of chemotherapeutics due to the manifestation of dose-limiting side effects during treatment, which stem from a lack of specificity towards neoplastic disease. Enzyme prodrug therapy (EPT) has the potential to increase the potency of chemotherapeutics while mitigating side effects by generating localized, high-dose therapy within solid tumors [5]. However, many EPT systems are highly immunogenic, create relatively small therapeutic windows, and are limited to a single target approach by a lack of prodrug variety.

The ability to affect multiple targets is an increasingly important strategy contrasting the highly-selective, single-target approach of the magic-bullet era [1]. The enzyme β-glucuronidase (βG) presents a promising avenue for EPT, as cell-surface tethered βG can effect a multi-target approach through its capability to simultaneously activate topoisomerase inhibitors, alkylating agents, histone deacetylase inhibitors, and anthracyclines. More prodrugs for βG are currently being developed, facilitating further target expansion [155].

β-glucuronidase is a lysosomal enzyme, which cleaves glucuronide acid moieties. Since βG prodrugs contain hydrophilic glucuronic acid moieties, they do not readily diffuse across cell membranes, greatly reducing prodrug systemic toxicities with respect to their drug equivalents. Further, the sequestration of βG within lysosomes allows for the use of human βG in EPT, without risk of prodrug conversion by endogenous βG or immunogenicity, a significant concern for the non-human enzymes commonly utilized in EPT [156]. The known 16a3 mutant form of βG, containing six

point mutations, confers increased activity to βG in less-acidic environments, and, thus, further enhances βG suitability for EPT [157].

Substantial effort has been directed towards localizing suitable EPT enzymes to tumor cells, βG or otherwise, but many approaches suffer distribution limitations or are currently unsafe for clinical use [158,21]. In an effort to surpass these limitations, we target βG to surface exposed phosphatidylserine. Phosphatidylserine is an anionic plasma membrane phospholipid asymmetrically found exclusively on inner leaflet under non-pathological conditions. However, malignant cells, their metastases, the tumor vasculature, and cultured tumor cells all explicitly and significantly externalize phosphatidylserine, due to a loss of lipid asymmetry, without cell damage or external activators present, making outer leaflet phosphatidylserine a promising malignant cell fingerprint [38]. Further, the feasibility of phosphatidylserine targeting has been validated by the clinical success of Bavituximab, a phosphatidylserine binding antibody [4].

Phosphatidylserine targeting also adds another layer to the multi-effect approach as it enables cell-surface tethering of βG to both cancer cells and the tumor vasculature, without displaying preference to either. Vascular damage is especially covetable since endothelial cells pose an easily accessible target, are more genetically stable than malignant cells, and damage amplifies downstream [75]. Breast [70], colon [74], and pancreatic [73] tumors all heavily rely on vascularization making them suitable targets for annexin-directed EPT.

To target phosphatidylserine we utilize the proteins annexin A1 and A5, both of which strongly and specifically bind to phosphatidylserine. Although A5 displays stronger binding than A1 to phosphatidylserine, A5 along has been shown to trimerize

causing endocytosis, whereas A1 binds in monomeric fashion forming a halo-like effect around the cell [50,47]. This distinction may be important for annexin-directed EPT systems, especially those that require external presence of the enzyme, such as for βG, as any increases in internalization would be directly linked to decreases in system performance. It remains unclear if A5 internalization still occurs in A5 fusion proteins, since fusion creates significant steric hindrance to trimerization. Thus, both A1 and A5 in fusion merit investigation.

Annexin-βG fusion proteins enact EPT via a two-step administration scheme, as shown in Figure 37. First, the fusion protein is delivered to the tumor via the bloodstream, bypassing healthy tissue, but binding to tumor endothelial cells and primary tumor cells via uptake through gaps in leaky tumor vasculature. After unbound fusion proteins are allowed to clear, the prodrug is administered systemically and converted to its drug equivalent upon interaction with surface tethered βG at the tumor site. Now free to diffuse across cell membranes, the drugs generated create both direct and bystander effects.

Producing βG in sufficient quantities for translational work remains a challenge. Human βG requires a mammalian production system to provide the post-translational modifications necessary to confer activity to βG, as without glycosylation βG remains inactive [159]. Especially for βG in fusion constructs, yields are generally very low [160,161], not reported, or the product is simply not purified. The best reported yield to date for βG in fusion is 3-5 mg/L[162], but scalability of this particular production method is hampered by the adherent nature of the cells utilized.
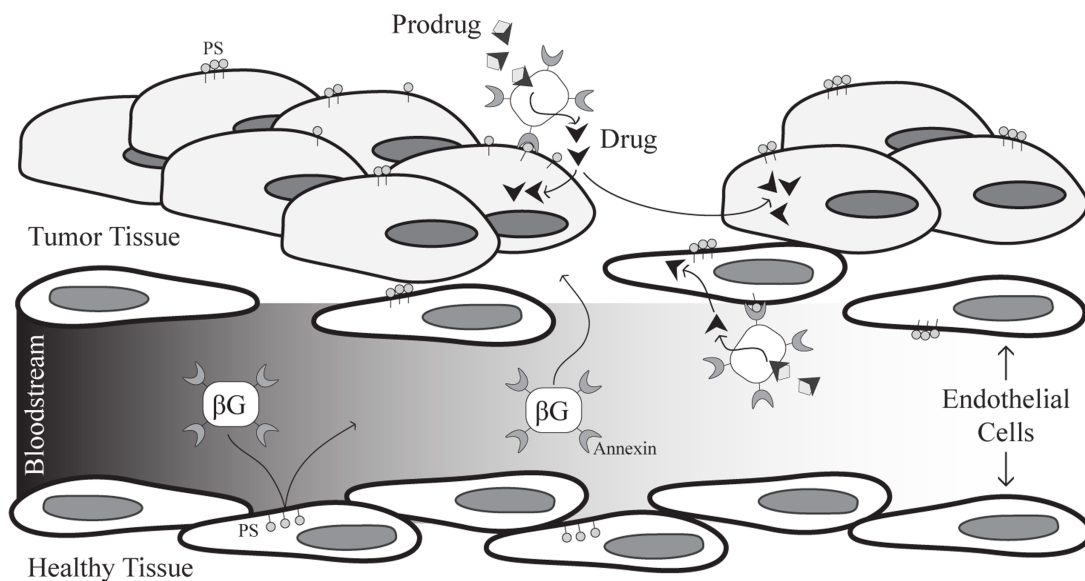
Figure 37: Overview of how annexin-βG fusion proteins enact EPT

Annexin-βG fusion proteins are systemically administered and bind to phosphatidylserine encountered on tumor cells and tumor endothelial cells. Once any residual fusion protein has been cleared from circulation, a prodrug, containing a hydrophilic glucuronide, is systemically administered but does not readily diffuse across cell membranes, remaining relatively innocuous. Prodrug glucuronide moieties are cleaved upon interaction with bound βG in the tumor microenvironment, and resulting drugs are then free to diffuse across cell membranes and exact their cytotoxic effects as well as diffused into cells without bound fusion protein (bystander effect).

Herein, we present two novel annexin-16a3 mutant βG fusion proteins and investigate their *in vitro* EPT efficacy across multiple human cancer cell lines when combined with the glucuronide of SN-38, a topoisomerase I inhibitor. SN-38 has shown efficacy in a PEGylated form against triple-negative, previously-treated breast

cancer in a phase II clinical trial [92], is the active metabolite of CPT-11 (irinotecan), the standard of care for first and second line treatment of colon cancer [9], and warrants further investigation for pancreatic cancer based on outcomes of FOLFIRINOX regimen trials [163]. By utilizing annexin-βG fusion proteins to generate SN-38, a powerful, clinically relevant drug, we aim to unveil a promising new tumor-type independent EPT modality. We also present a novel suspension culture based production method for βG fusion proteins, therefore making production readily scalable to help enhance the translational potential of annexin-βG fusion proteins.

Methods

Cell culture

Adherent CHO Flp-In cells were maintained in Ham's F-12 with 2 mM L-glutamine supplemented with 100 μg/ml Zeocin[TM] to maintain Flp-In genotype prior to transfection, replaced with 600 μg/ml hygromycin B post-transfection, all from Life Technologies (Grand Island, NY, USA). Once adapted to suspension culture, transfected CHO Flp-In cells were maintained in SFM4CHO medium with L-glutamine from GE Healthcare (Little Chalfont, Buckinghamshire, UK), supplemented with 1:300 anti-clumping agent (Life Technologies) and 1x sodium hypoxanthine and thymidine (Corning Life Sciences, Tewksbury, MA, USA), at 37 °C, 5% CO_2, and 110 rpm. No antibiotic selective pressure was applied to CHO suspension cultures as this suppressed protein yield; however, protein production was maintained ≥ 16 passages post adaptation.

119

HT-29 colorectal adenocarcinoma cells, MCF-7 breast adenocarcinoma, and Panc-1 pancreatic epithelioid carcinoma were obtained from ATCC (Manassas, VA, USA) and maintained in McCoy's 5A, Eagle's minimum essential medium with 0.01 mg/ml recombinant human insulin (Life Technologies), or in Delbecco's Modified Eagles Medium, respectively, all from ATCC. Human abdominal aorta endothelial cells (HAAE-1) were obtained from the Coriell Cell Repositories (Camden, NJ, USA) and cultured on 0.1 % w/v gelatin in F-12K medium (ATCC) with 0.03 mg/ml endothelial cell growth supplement (Corning) and 0.1 mg/ml heparin. All adherent cell culture medium contained 10% fetal bovine serum and penicillin (100 U/ml)/streptomycin (100 mg/ml) both from Atlanta Biologics (Flowery Branch, GA, USA). Cells were cultured at 37 °C and 5% CO_2, not beyond the tenth passage, sixth for HAAE.

Genetic construction

To create fusion genes, the human clone A5 (Accession: NM_001154), a generous gift from Dr. Stuart Lind at the University of Colorado, A1 (BC035993), wild type βG (BC014142), and a custom synthesized 16a3 mutant βG [157], all from Life Technologies, were amplified via polymerase chain reaction with the Phusion High Fidelity PCR kit from New England Biolabs (NEB, Ipswich, MA, USA) utilizing tailed primers synthesized by Integrated DNA Technologies (San Jose, CA, USA). The 16a3 mutant βG sequence, primer sequences, and thermal cycles are given in appendix E, appendix B, and appendix A.12.3, respectively. Resulting amplicons contained a His_6 purification tag/HRV 3C cleavage site on the A1/A5 N-terminal and EciI digestion sites

120

on the C-terminal of A1/A5 and the N-terminal of βG. The native βG signal sequence was removed, but the C-terminal propeptide was maintained intact to promote enzyme catalytic activity [164]. Amplicons were EciI digested and fused with T4 ligase, both from NEB, according to manufacturer's protocols. Fusions were gel-extracted before ligation into the pSecTag/FRT/V5/HIS/TOPO TA vector (Life Technologies) via the large-insert protocol with 20 μl volume. Sequence verified plasmids were then co-transfected with pOG44 (1:9 w/w) into Cho Flp-In cells with Lipofectamine 3000, both from Life Technologies, and true transfectants were selected via hygromycin B for > 3 weeks.

Fusion protein production and purification

Adherent stable CHO cells lines were adapted sequentially to suspension culture. Fusion proteins were produced in 2-week fed batch cultures in 1-2 L volumes, split between 500 ml Erlenmeyer flasks (200 ml/flask). Cells were seeded at $2.5\text{-}3\text{x}10^5$ cells/ml and were fed with 0.7% Cell Boost 2 on day 4 and 0.35% on day 7 [165]. Fusion proteins were extracted from cell-free culture supernatants via immobilized metal affinity chromatography (IMAC) on two HisTrap Excel columns in series following GE protocol, but with 0 mM imidazole in the wash buffer and 100 mM in the elution buffer. Collected elutant peak was titrated to 0.9 M ammonium sulfate (Sigma Aldrich, Buchs SG, Switzerland), precipitant removed via centrifugation, and further purified via hydrophobic interaction chromatography (HIC) on a HiTrap butyl sepharose HP column. Fusion protein containing fractions from HIC were pooled and concentrated using an Amicon Ultra-15 centrifugal filter (EMDMillipore, Darmstadt, Germany, 50kDa cutoff) prior to gel filtration chromatography (GFC) on a Superdex 200 Increase

column; GFC flow rate was set to 0.2 ml/min for high-resolution separation and eluted into Tris buffered saline (TBS, 20 mM Tris, 150 mM NaCl, pH 8.0). GFC fractions containing pure fusion proteins, as determined by reducing SDS-PAGE with Imperial stain (Thermo Scientific, Waltham, MA, USA), were pooled, quantitated via Bradford assay (Bio-Rad, Hercules, CA, USA), flash frozen in LN_2, and stored at -80 °C. All columns were obtained from GE Healthcare. HIC and GFC were preformed on an ÄKTA Pure M1 system (GE Healthcare).

Western dot blot

One μg of pure fusion protein was blotted onto a nitrocellulose membrane and dried for 4 h. Membrane was blocked overnight with 1% bovine serum albumin (BSA) in TBS with 0.05% Tween 20, at 4 °C with gentle agitation. Blots were stained with 1:200 dilutions of βG (sc-25827), A1 (sc-11387), or A5 (sc-8300) rabbit polyclonal antibodies for 2 h at room temperature (RT). Blots were washed, then incubated with either goat anti-rabbit IgG-HRP (sc-2004) at a 1:5000 dilution or HisDetector Nickel-HRP conjugate (1:50), obtained from KPL (Gaithersburg, MD, USA). Blots were washed, developed with 3, 3', 5, 5' – tetramethylbenzidine (TMB) solution, and imaged on a Bio-Rad ChemiDoc MP CCD imaging system with a chemiluminescent filter. All antibodies were obtained from Santa Cruz Biotechnology (Dallas, TX, USA).

Activity assay

βG enzymatic activity was measured via the fluorescence of the product 4-methylumbelliferone (4-MU) created through βG conversion of the substrate 4-

methylumbelliferyl β-D-glucuronide (4-MUG) from Life Technologies. Varying

concentrations of 4-MUG were reacted with 0.5 μg of fusion protein in reaction buffer

(50 mM bis-tris, 50 mM triethanolamine, 100 mM acetic acid, and 100 ng/ml BSA) at a

pH of either 4.5 or 7.4. 4-MU florescence was monitored continuously on a mircotiter

plate reader at 360/460 nm over 1 h, and quantitated by comparison to 4-MU standards

(Sigma Aldrich). Linear range data was analyzed via Michaelis-Menten kinetics with

Prism 6 software (GraphPad, La Jolla, CA, USA).

Binding visualization

MCF-7 cells were plated at 150 k cells/coverslip, allowed to adhere overnight, and then

fixed with glutaraldehyde to preserve cell morphology. Biotin-labeled hA5-16a3 (100

mM) was allowed to bind. Cells were then thoroughly washed, followed by staining

with Streptavidin-Alexa-488 at 4 μg/ml to visualize cell-surface bound protein, Cell

Mask Deep Red at 2 μg/ml to indicate the cell membrane, and Hoechst 33258 at 10

μg/ml to mark nucleic acids. All flourophores were acquired from Life Technologies.

Fluorescence was preserved in fluoro-gel and confocal images acquired immediately

following preparation on a Lecia-SP8 confocal laser-scanning microscope (Buffalo

Grove, IL, USA), at 63x in glycerol in both XY and YZ planes.

Dissociation constants and binding stability

O-phenylenediamine color development was utilized to quantitate streptavidin-

horseradish peroxidase binding to biotin-labeled fusion proteins bound to cell surface in

the presence and absence of Ca^{2+} to determine total and non-specific binding

respectively, as reported previously [141]. A similar assay was applied over 3 days to determine binding stability on live cells, as an indicator of internalization. Cells were seeded 10-20 k/well in 96-well plates, allowed to adhere, and then treated with 100 nM fusion proteins on day 0 (except controls without protein), thoroughly washed, and then incubated with the appropriate growth medium containing 2 mM Ca^{2+} until measurement day. Each day, data minus control, to account for non-specific binding, was compared to day 0.

<div align="center">Simulated EPT</div>

In vitro efficacy of fusion proteins was evaluated with the prodrug SN-38 glucuronide (SN-38G) obtained from Toronto Research Chemicals (TRC, Toronto, CA). Cells were plated at 1-10 k/well in 96-well plates, such that each cell line achieved 90% confluence by day 6, and allowed to adhere overnight. Every 2 days, cells were measured by Alamar Blue assay (10%, 4 h, Life Technologies) to determine viability, thoroughly washed, incubated with 100 nM fusion protein for 2 h (or TBS vehicle), thoroughly washed again, and then treated with varying concentrations of prodrug, for 3 total treatment cycles over 6 days. Controls were fusion protein alone, prodrug alone, and for SN-38G, the drug analog, SN-38 (TRC). Fractional viability was averaged per triplicate and compared to day 0. LC_{50} values were determined for day 6 by fitting a sigmoidal dose response curve with Prism 6 software for data normalized to the day 6 control. QIC_{50} values, indicative of the therapeutic window, were computed as LD_{50} prodrug/LC_{50} A5-16a3 plus prodrug.

Statistical analysis

All data was collected in triplicate and analyzed with Prism 6 software. Activity assay

data was compared via unpaired t-tests for unequal variances. A two-way ANOVA was

utilized with Sidak's post hoc comparisons matched by day for binding stability and

Dunnett's post hoc comparisons to the control, matched by day, for simulated EPT.

Results

Pure fusion proteins produced in high-yield, scalable cultures

Genes were fused to form the constructs hA1-βG, hA1-16a3, and hA5-16a3, and ligated

into the pSecTag vector, as shown in Figure 38A. Maximum yields obtained from

stable CHO Flp-In producer cell lines grown in fed-batch suspension cultures were 140

μg/l for hA1-βG and 740 μg/l for the optimized mutant constructs, hA1-16a3 and hA5-

16a3. Fusion proteins were predicted to take a tetrameric form in which the βG core is

spatially separated from annexins by a $(SG_4)_2$ linker, taken from a T cell

immunologically inert peptide [166] to create fully human fusion proteins, as modeled in

Figure 38B with PyMol 1.2 [167]. Reducing SDS-PAGE, shown in Figure 38C, indicates

that > 95% purity was achieved, as determined by densitometry analysis in ImageJ64

[168]. Fusion proteins migrated above their predicted monomeric molecular weights,

indicative of the heavy glycosylation on βG [159] and the single N-linked biantennary

glycosylation site found on A1 [169], as opposed to A5 which is non-glycosylated.

Identity of purified constructs was confirmed via dot blot, as shown in Figure 38D.
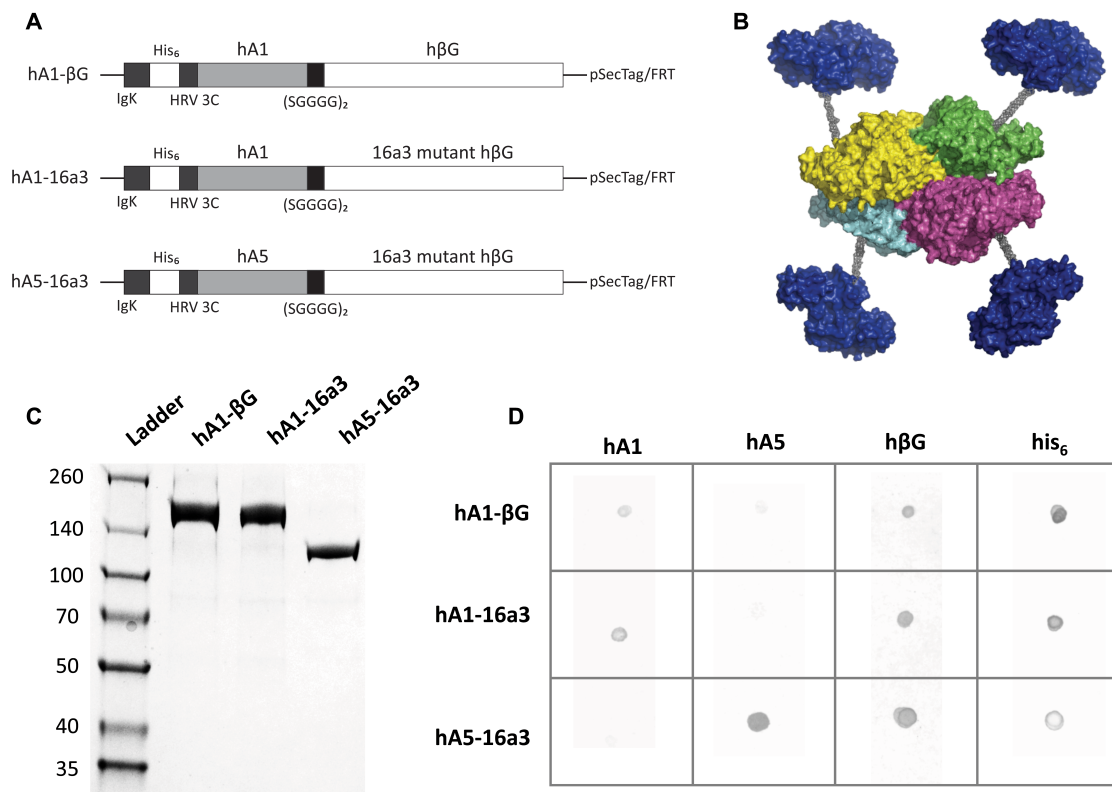
Figure 38: Characterization of the three annexin- βG fusion proteins created

(**A**) Schematic of human (h) annexin-βG fusion constructs. (**B**) Theoretical representation of hA5 (RCSB Protein Data Bank (PDB): 1AVH) fused to hβG (PDB: 3HN3). The hβG monomers (shown in cyan, yellow, green, and fuchsia) make up the core of the fusion protein. The flexible linkers (shown in grey extrude out from the hβG core and spatially separate hA5 (shown in blue) from hβG. This allows for binding of hA5 to phosphatidylserine to occur while preserving the accessibility of the hβG active site. Annexin-βG fusion constructs are produced as annexin-βG monomers, which then associate into quaternary structure, driven by the tetramer preference of hβG. (**C**) Reducing SDS-PAGE of annexin-βG fusion constructs, 2 μg, on 8-16% tris-glycine gel stained with Imperial stain. (**D**) Colorimetric (TMB) dot blots of 1 μg purified annexin-βG fusion proteins stained for hA1, hA5, hβG, and His$_6$.

126

16a3 mutation confers significantly improved activity at physiological pH

We determined whether introducing the 16a3 mutation improved activity of fusion proteins by measuring enzyme activity at pH 4.5 and 7.4. The resulting kinetic constants are presented in Table 6. Introducing the 16a3 mutation generally left the Michaelis-Menten constant (K_m) unchanged but increased the maximum enzyme velocity (V_{max}) and the turnover number (k_{cat}). hA1-βG retained 2.0 % specific activity at a pH of 7.4, whereas hA1-16a3 retained 7.8 % and hA5-16a3 retained 28.3 %, both significant increases (p < 0.01).

Annexin-directed binding is cell-surface associated displaying low nanomolar

dissociation constants with limited differences in A1 vs. A5 stability

Utilizing confocal microscopy we visualized hA5-16a3 binding to phosphatidylserine on the MCF-7 cell surface in both XY and YZ planes, shown in Figure 39 A-D and E-H, respectively. As shown, bound hA5-16a3 presence tracked excellently with the cell membrane, indicating a cell-surface based interaction.

To quantitate binding, we measured total and non-specific binding over a range of fusion protein concentrations, with and without Ca^{2+} respectively, from which specific binding was determined, as shown for hA1-16a3 binding to phosphatidylserine on the Panc-1 cell surface in Figure 40A. Dissociation constants (K_D) for specific binding were obtained via a single-site non-competitive binding model and are summarized in Figure 40B. Consistently, hA5-16a3 exhibited lower K_D values (0.34-1.1 nM) than hA1-16a3 (0.98-3.0 nM) for all cell lines.

Table 6: Kinetic constants of annexin-βG fusion proteins at pH 4.5 and 7.4, as determined by Michaelis-Menten kinetics.

Increased specific activity is afforded to fusion proteins via the 16a3 βG mutation. Significance of mutant activity vs. wild-type activity is shown as [**], $p \leq 0.01$, as determined by unpaired t-tests for unequal variances. Substrate is 4-methylumbelliferyl β-D glucuronide. Data shown as mean ± standard error (SE) (n = 3).

Fusion Protein	pH	Specific Activity (mmol/h/mg)	V_{max} (nmol/s)	K_m (mM)	k_{cat} (s^{-1})
hA1-βG	4.5	18.98 ± 2.77	2.64 ± 0.05	0.036 ± 0.002	1,214 ± 24
	7.4	0.38 ± 0.045	0.053 ± 0.001	0.249 ± 0.067	26.5 ± 3.0
hA1-16a3	4.5	15.84 ± 1.30	2.20 ± 0.13	0.029 ± 0.006	1,014 ± 61
	7.4	1.24 ± 0.09 [**]	0.172 ± 0.008	0.481 ± 0.067	79.3 ± 3.8
hA5-16a3	4.5	87.62 ± 6.74	12.17 ± 0.68	0.071 ± 0.013	5,473 ± 305
	7.4	24.76 ± 1.41 [**]	3.44 ± 0.07	0.333 ± 0.025	1,546 ± 32
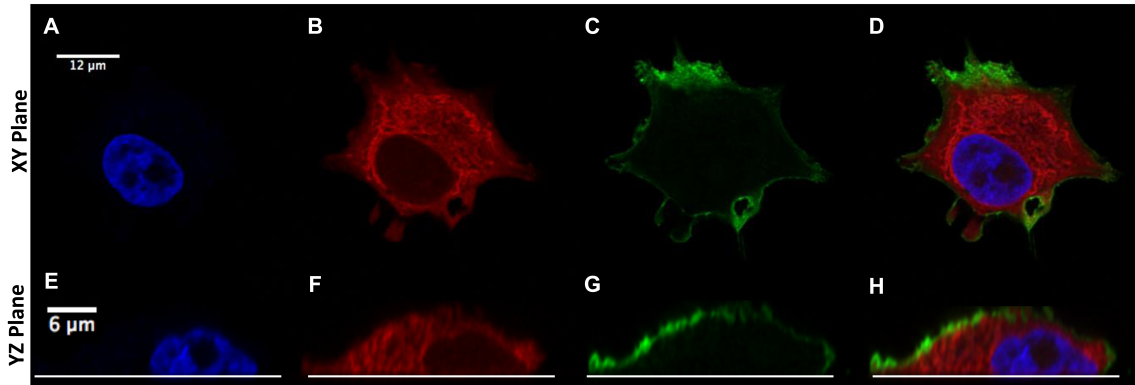
Figure 39: Confocal microscopy visualization of hA5-16a3 binding to phosphatidylserine on MCF-7 cell surface

First row depicts **(A)** Hoechst **(B)** Cell Mask Deep Red, **(C)** streptavidin-AlexaFlour 488 bound to biotin labeled hA5-16a3, and **(D)** composite image of a-d, all in the XY plane. Scale bar for a-d is 12 μm. Second row depicts the same cell in the YZ plane stained with **(E)** Hoechst **(F)** Cell Mask Deep Red, **(G)** streptavidin-AlexaFlour 488 bound to biotin labeled hA5-16a3, and **(H)** composite image of e-g. Cover slip is depicted as a white line. Scale bar for e-h is 6 μm.
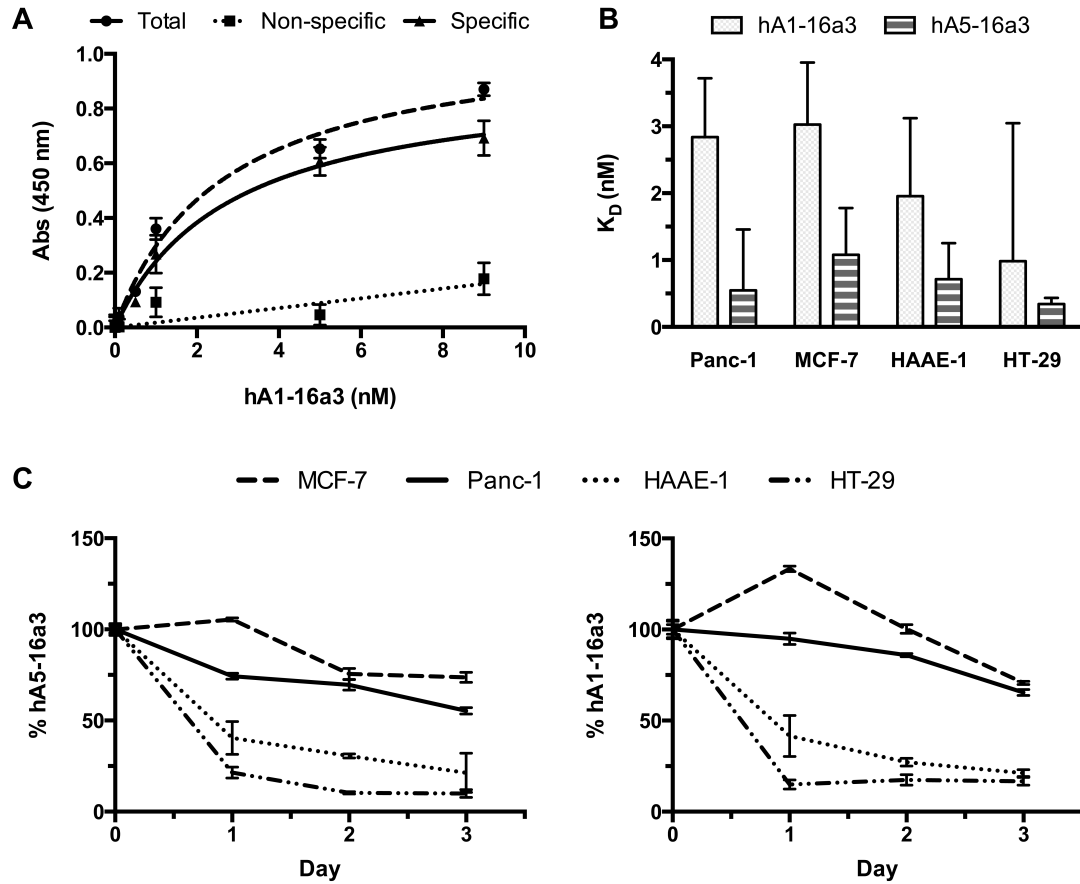
Figure 40: Quantitative binding analysis of hA1-16a3 and hA5-16a3

(A) Binding of hA1-15a3 to phosphatidylserine exposed on the surface of Panc-1 cells. Total binding ($\bullet$) was measured in PBS with 2 mM Ca^{2+} and non-specific binding ($\blacksquare$) was measured in PBS without Ca^{2+}, but with 5 mM EDTA to chelate any residual Ca^{2+}, for increasing concentrations of hA1-16a3 (0-9 nM). Specific binding ($\blacktriangle$) was obtained by subtracting non-specific from total binding. (B) Specific binding dissociation constants (K_D) for fusion proteins binding to all cell lines. (C) Binding stability presented as percent of bound protein remaining on each day compared to day 0, over a 3-day period. All data presented as mean ± SE (n = 3).

Binding stability was determined in the presence Ca^{2+} over 3 days, as shown in Figure 40C. The MCF-7 and Panc-1 cell lines displayed excellent stability, with hA1-16a3 retaining significantly more ($p < 0.001$) bound protein than hA5-16a3 on days 1 and 2, but detectable differences disappearing by day 3. Contrastingly, HT-29 and HAAE-1 cells exhibited large initial drops in stability; however, bound protein was not significantly different for hA1-16a3 vs. hA5-16a3, matched for cell line, on any day.

hA5-16a3 combined with SN-38 glucuronide is as effective as the drug SN-38

We simulated EPT *in vitro* to establish the efficacy of hA1/hA5-16a3 combined with the prodrug SN-38 glucuronide against a human pancreatic (Panc-1) cancer cell line along with non-confluent endothelial cells (HAAE-1), which mimic tumor vasculature. Day 6 dose-response curves for hA5-16a3 + SN-38G and all appropriate controls are presented in Figure 41. hA5-16a3 + SN-38 was statistically indistinguishable from the SN-38 drug control for both Panc-1 and HAAE-1 cell lines at and beyond day 4, with a therapeutic index (QIC_{50}) ranging from 2-50. Full simulated EPT data sets for all days are given in supplemental materials, including data for hA1-16a3 + SN38-G, which was excluded from day 6 dose-response curves as it was quickly determined to be much less effective than hA5-16a3.
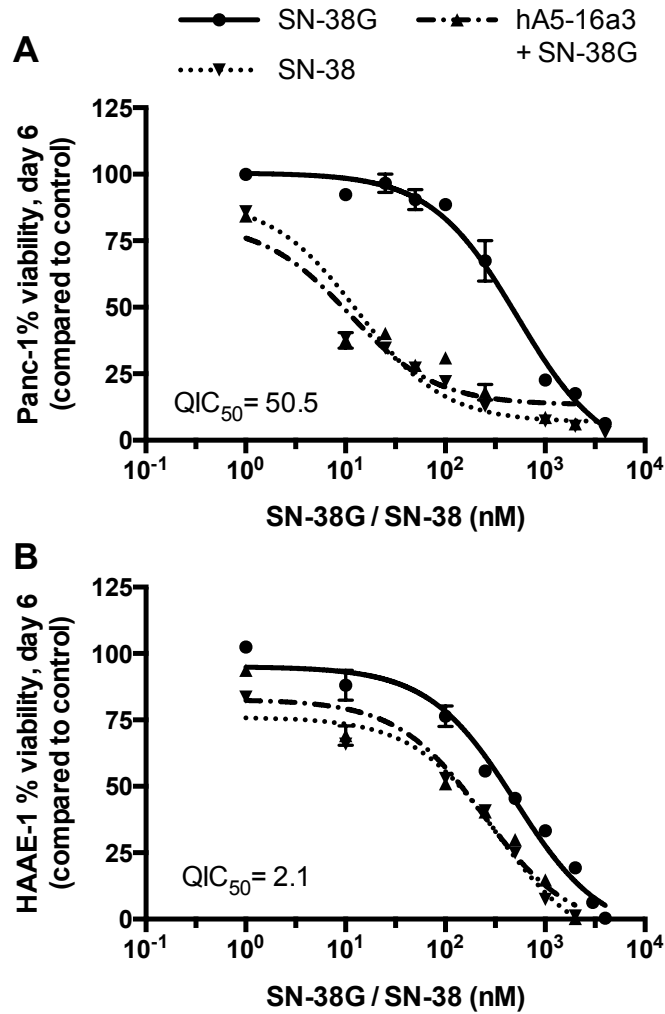
Figure 41: Dose response curves of fusion proteins in combination with SN-38G on day 6 of simulated EPT treatment

hA5-16a3 + SN-38G with SN-38G and SN-38 controls shown for **(A)** Panc-1 and **(B)** HAAE-1 cell lines. All data were normalized to a control matched for day 6 and fit with a three-parameter dose response curve (hill-slope = 1). Data presented as mean ± SE (n = 3).

Discussion

Herein we present two novel annexin-βG fusion proteins that enable high-dose, on-site

combination chemotherapy. The hA5-16a3 construct emerged as the best candidate for

translation, matching SN-38 toxicity when combined with SN-38 glucuronide. We also

lend significant evidence for the tumor-type independence of the annexin-directed EPT

approach as hA5/A1-16a3 showed strong targeting and killing capabilities towards

multiple human cancer cell lines as well as endothelial cells, which mimic tumor

vasculature.

A5-16a3 binding matched previously reported K_D values of AV alone binding to

cell surface phosphatidylserine, ranging from 0.1 to 2 nM [170,171]. As expected, A1-16a3

exhibited higher K_D values than A5-16a3. However, A1-16a3 displayed lower K_D

values for cultured cells expressing phosphatidylserine than previously reported for A1

alone binding to immobilized lipid bilayers containing phosphatidylserine, approx. 39

nM [48]. In previous studies, we noted remarkably lower dissociation constants for

hexamer fusion conformations [117], but similar dissociation constants for another

tetrametic annexin fusion protein [116], suggesting that (i) dissociation constants for

annexin fusion proteins are determined by the quaternary structure of the fusion, and (ii)

hexameric fusions are able to bind with higher avidity than tetramer structures due to

the spatial conformation of annexins.

Internalization mediated by A5 did not emerge as a significant factor to favor

use of A1 vs. A5 for annexins in fusion. For cell lines where hA5-16a3 and hA1-16a3

showed less stability, bound protein retention did not differ for A1 vs. A5, suggesting

that internalization is occurring at similar rates mediated by general endocytosis and not

the proposed novel portal to cell entry for A5 induced by trimerization. For cell lines where both hA5-16a3 and hA1-16a3 exhibited remarkable stability, hA1-16a3 did show markedly less internalization initially; however, by day 3 differences in bound protein retention were no longer significant. The lack of evidence for the reduced internalization of A1 fusions compared to A5 fusions, paired with the lower K_D and higher activity seen in A5 fusions, strongly favors further investigation of the A5-16a3 construct.

The annexin-βG fusion proteins produced herein are the largest annexin fusion proteins proposed to date, measuring approximately 30 nm in diameter. This significant size, allows annexin-βG fusions to benefit from passive targeting via the enhanced permeability and retention effect [41]. Active targeting for particles below 50 nm have been shown to further boost this effect, suggesting that annexin-βG fusions will experience enhanced targeting once translated *in vivo.*

Activity retention at a physiological pH was significantly improved by the introduction of the 16a3 mutation. hA5-16a3 retained 28% specific activity at a pH of 7.4, based on specific activity at a pH of 4.5, which matched previously reported activity retention values for the 16a3 βG mutation [157]. hA1-16a3 retained less specific activity than hA5-16a3, falling short of previously reported values but still displaying significant improvement. Unexpectedly, hA5-16a3 also displayed higher specific activity at pH 4.5 than hA1-16a3. We propose that both of these differences are due to post-translational processing difficulties that arise due to the glycosylation site on A1, upstream of βG, which is not present on A5, as post-translational processing is essential for the establishment of βG enzymatic activity.

The production method delineated is the first suspension-based approach published for βG fusions and is completely devoid of serum within the production environment. Suspension-based production will play an important role in translating the βG platform towards the clinic, as suspension cultures readily scale to bioreactors for large-scale production.

Promising designer prodrugs for βG are currently being developed, which will afford even greater potency to this EPT system. One such prodrug is a duocarmycin SA analog [172], which selectivity binds the N3 of adenine in AT rich-minor DNA groove regions. Duocarmycin SA is one of the strongest known anticancer compounds, but even analogs trigger severe myelotoxicity [173,174]. However, βG mediated prodrug to drug conversion within the tumor site mitigates the side effects associated with systemic administration and may allow for the clinical use of duocarmycin SA analogs, alone, or in combination with other βG generated chemotherapeutics. Duocarmycin SA analog prodrugs have demonstrated remarkable efficacy against CL1-5 lung cancer xenografts via βG gene-directed EPT [175], and are capable of producing astounding therapeutic windows approaching 10^6 [102].

In conclusion, the fully human hA5-16a3 fusion protein shows promise via both its tumor-type independent targeting mechanism and enzyme flexibility with respect to prodrug selection, with proven binding and killing capacities across multiple human cancer cell lines. While many enzyme prodrug therapy approaches show promise, most cannot be readily translated due to immunogenicity or are confined to a single-agent approach, and thus lack potency. hA5-16a3 based therapy presents no known immune risk while producing on-site combination chemotherapy, and, therefore, we propose that

the hA5-16a3 fusion protein is one of the strongest clinical candidates for enzyme prodrug therapy developed to date.

Conflict of Interest

No conflicts of interest are declared.

Additional Figures

Full temporal cytotoxicity plots

Cytotoxicity plots showing cell growth/death for all days are presented in Figure 42.

These plots will be published as supplementary material to the article.
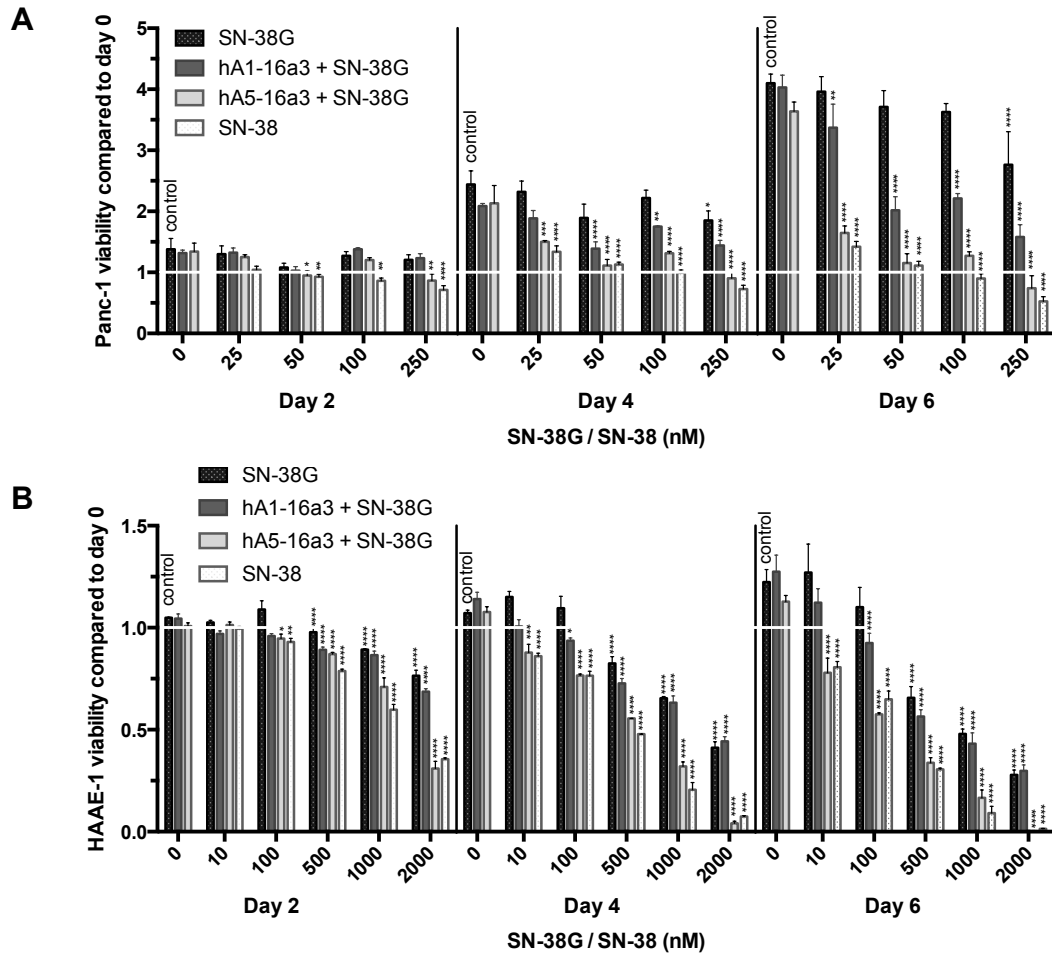
Figure 42: Time-dependent simulated EPT results for SN-38G combined with hA5-16a3 or hA1-18a3

Results are presented for **(A)** Panc-1 and **(B)** HAAE-1 cell lines for days 2, 4, and 6 as fractional viability compared to day 0, without normalization to show growth vs. time. Statistical analysis was conducted via Dunnett's post hoc comparisons to the control, matched by day, following a two-way ANOVA, with ****, $p \leq 0.0001$; ***, $p \leq 0.001$; **, $P \leq 0.01$; and *, $p \leq 0.05$. For determination of efficacy differences between SN-38 and hA5-16a3 + SN-38G, Dunnett's post hoc tests were also utilized, and no statistical differences were present by day 4 for all cell lines. All data presented as mean ± SE (n = 3).

Kinetic constant determination curves

Substrate concentration vs. enzyme velocity curves for all three βG fusion proteins are shown in Figure 43 for pH 4.5 and pH 7.4. From these curves, K_m, k_{cat}, and V_{max} were determined using GraphPad Prism 6 as described in Appendix A.19. A graphical comparison of specific activity is presented in Figure 44.
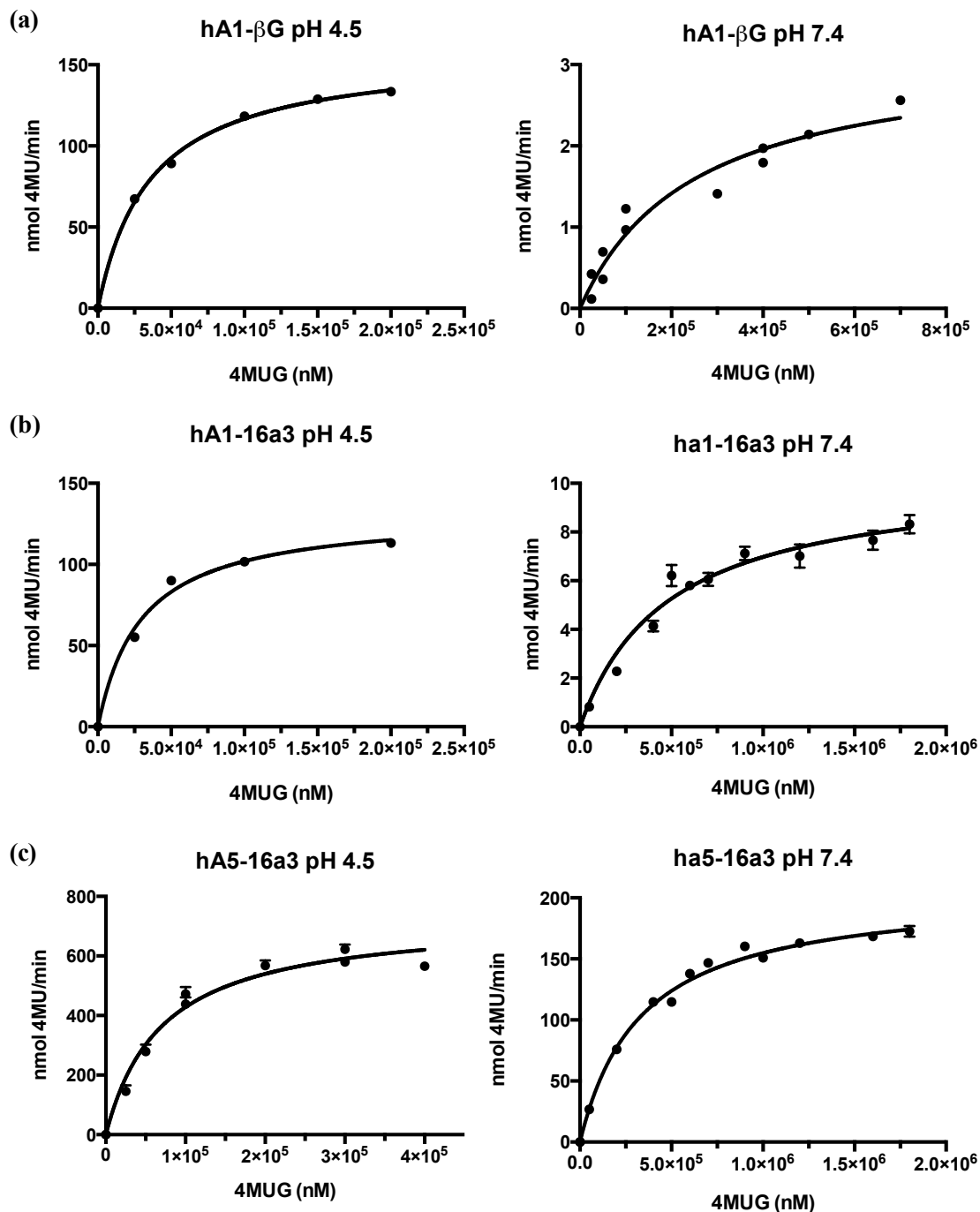
Figure 43: Velocity vs. substrate concentration for βG fusion proteins

To determine K_m, k_{cat}, and V_{max} data were plotted at substrate (4-MUG) concentration vs. velocity of product conversion (nmol 4-MU/min) for **(A)** hA1- βG, **(B)** hA1-16a3, and **(C)** hA5-16a3 at a pH of 4.5 and 7.4. Data shown as mean ± SE (n=3).
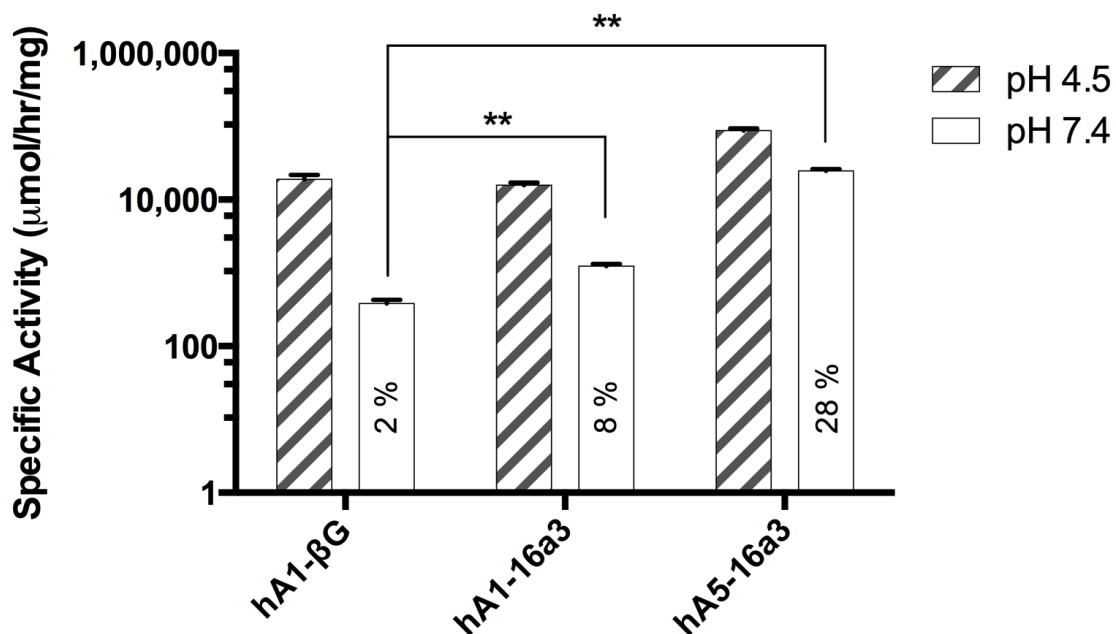
Figure 44: Specific activity of wild type and 16a3 mutant βG in fusion

Increased specific activity is afforded to fusion proteins via the 16a3 βG mutation. Fusion proteins (0.5 µg) were incubated with varying concentrations of 4-methylumbelliferyl β-D-glucuronide (4MUG) at 37 °C for 1 h in either pH 4.5 or pH 7.4 reaction buffer. 4MU production was monitored continuously via fluorescence (360/460 nm). Specific activity was computed from V_{max}, as determined by Michaelis-Menten kinetics. Percent of specific activity retained at a pH of 7.4 compared to a pH of 4.5 is indicated within each bar for each fusion protein. Significance of mutant activity vs. wild type activity is shown as **, $p \leq 0.01$, as determined by unpaired t-tests for unequal variances. Data shown as mean ± SE (n=3).

Binding strength curves not selected as the published "sample curve" are shown for

hA5-16a3 binding to Panc-1 cells in Figure 45, for hA1-16a3 and hA5-16a3 binding to

MCF-7 cells in Figure 46, for hA1-16a3 and hA5-16a3 binding to non-confluent

HAAE-1 cells in Figure 47, and for hA1-16a3 and hA5-16a3 binding to HT-29 cells in

Figure 48.
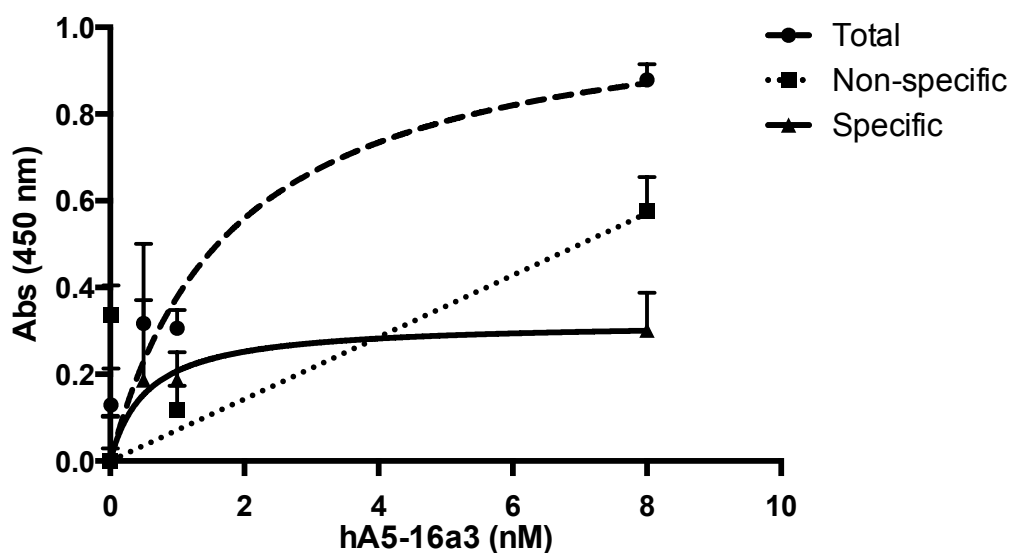
Figure 45: hA5-16a3 binging to PS on Panc-1 cell surface

Panc-1 cells were incubated with increasing concentrations of biotin labeled hA5-16a3,

with total binding (●) measured in the presence of 2 mM Ca^{2+} and non-specific binding

(■) measured in the absence of Ca^{2+} with 5 mM EDTA to chelate any residual Ca^{2+}.

Specific binding (▲) was obtained by subtracting non-specific from total binding. Data

presented as mean ± SE (n = 3).
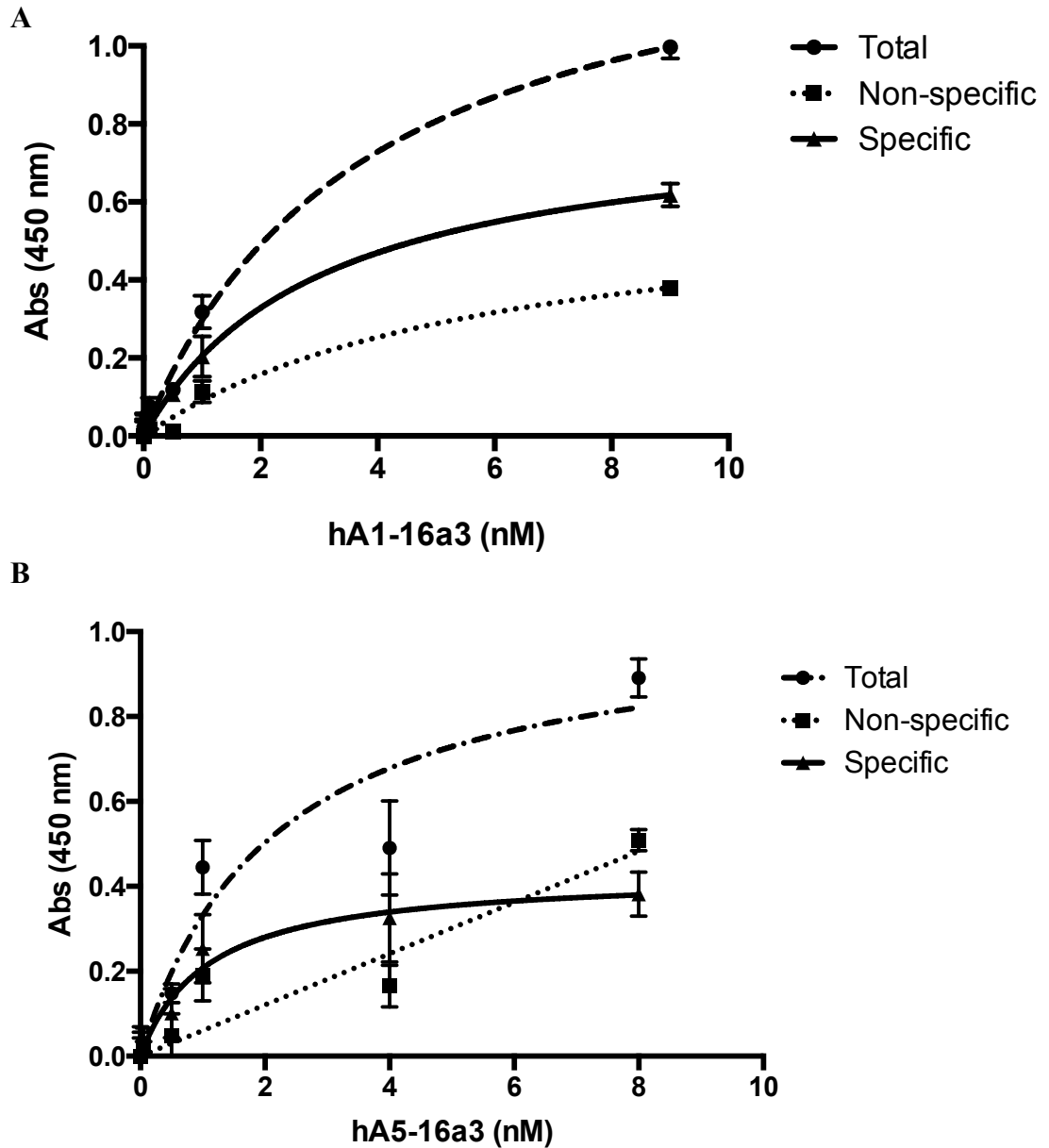
Figure 46: hA1-16a3 and hA5-16a3 binging to PS on MCF-7 cell surface

MCF-7 cells were incubated with increasing concentrations of biotin labeled **(A)** hA1-16a3 and **(B)** hA5-16a3, with total binding (●) measured in the presence of 2 mM Ca^{2+} and non-specific binding (■) measured in the absence of Ca^{2+} with 5 mM EDTA to chelate any residual Ca^{2+}. Specific binding (▲) was obtained by subtracting non-specific from total binding. Data presented as mean ± SE (n = 3).
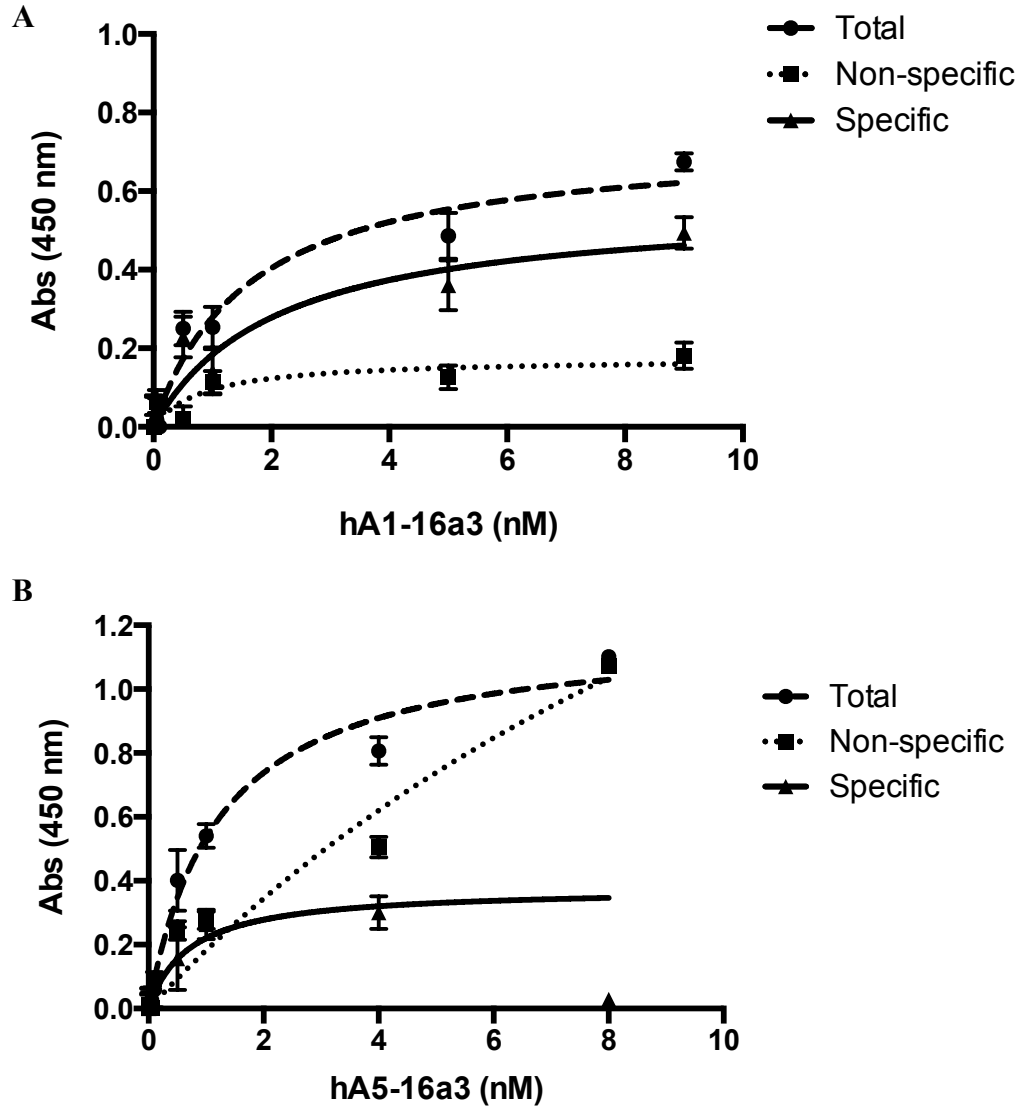
Figure 47: hA1-16a3 and hA5-16a3 binging to PS on HAAE-1 cell surface

Non-confluent HAAE-1 cells, as mimics of tumor vasculature, were incubated with increasing concentrations of biotin labeled **(A)** hA1-16a3 and **(B)** hA5-16a3, with total binding (●) measured in the presence of 2 mM Ca^{2+} and non-specific binding (■) measured in the absence of Ca^{2+} with 5 mM EDTA to chelate any residual Ca^{2+}. Specific binding (▲) was obtained by subtracting non-specific from total binding. Data presented as mean ± SE (n = 3).
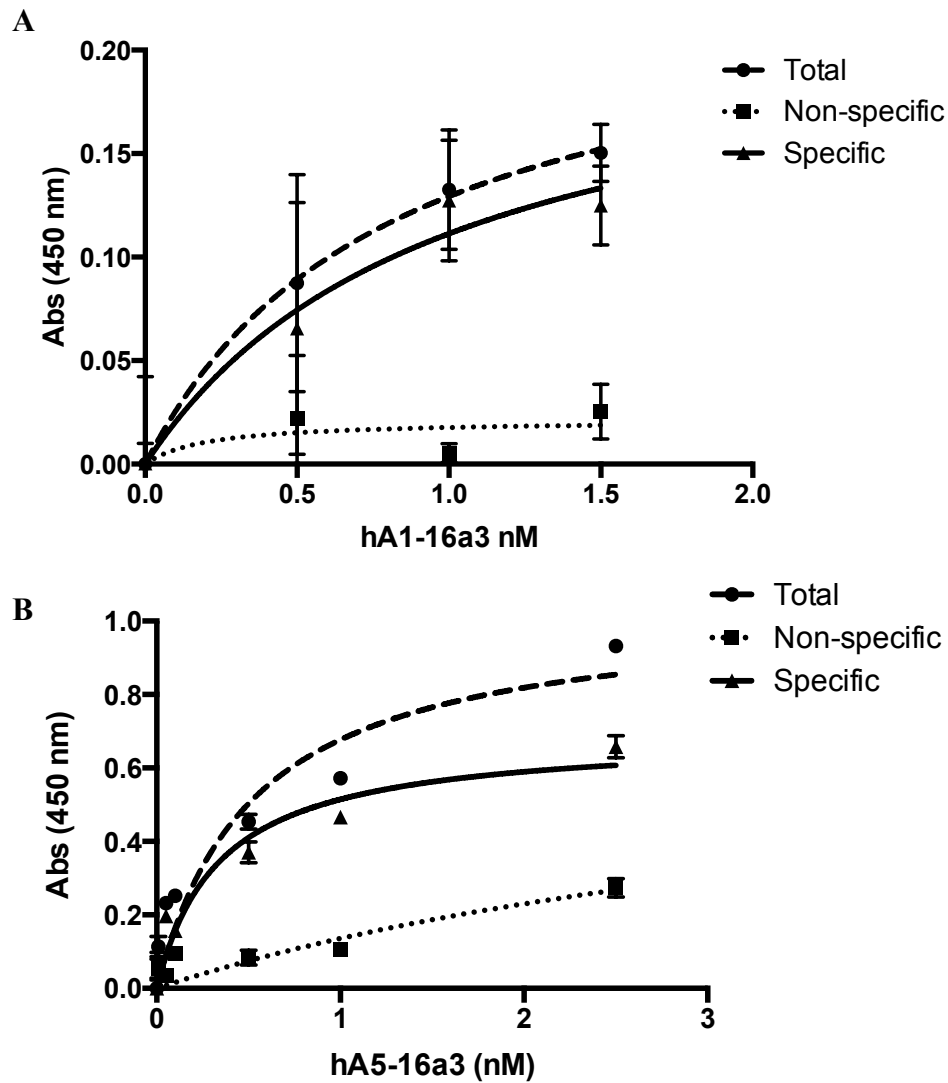
Figure 48: hA1-16a3 and hA5-16a3 binging to PS on HT-29 cell surface

HT-29 cells were incubated with increasing concentrations of biotin labeled **(A)** hA1-16a3 and **(B)** hA5-16a3, with total binding (●) measured in the presence of 2 mM Ca^{2+} and non-specific binding (■) measured in the absence of Ca^{2+} with 5 mM EDTA to chelate any residual Ca^{2+}. Specific binding (▲) was obtained by subtracting non-specific from total binding. Data presented as mean ± SE (n = 3).

Chapter 5: Final Conclusions and Future Directions

Final Conclusions

Three main conclusions emerge from the work presented within this dissertation. (i) Annexin-directed enzyme prodrug therapy is tumor-type independent not only in theory, but likely also in practice, specifically for prostate, pancreatic, breast, and colon cancer, with strong evidence that this property will carry over to more cancer cell lines as well. (ii) Cells can be effectively primed with docetaxel to become more susceptible to annexin-directed enzyme prodrug therapy, and these effects are robust enough to be seen in a simulated *in vitro* setting. Therefore, tumor priming should be strongly considered in a translational setting. (iii) While previously developed fusion proteins based on non-human enzymes show constant, patterned efficacy in a cell culture environment, it is the novel β-glucuronidase based fusion proteins that present the most-promising avenue for translational annexin-directed enzyme prodrug therapy. β-glucuronidase fusion proteins are the first to allow for combination, on-site chemotherapy of FDA approved drugs within the same enzyme platform, while also promising to be non-immunogenic due to their fully human nature.

From the applicability studies of existing fusion proteins to prostate and pancreatic cancer, we were able to conclude that the cytotoxic mechanism employed in annexin-directed enzyme prodrug therapy is likely tumor-type independent in spite of varying expression levels of phosphatidylserine, the target, both between different tumor types and within the same tumor type. When combined with results from previous work, the efficacy of annexin-directed EPT has now been established on a total of eight cell lines, which are 4T1, MCF-7, MDA-MB-231, PC-3, Panc-1, Capan-1, HT-

146

29, and HAAE-1. We believe this wealth of data firmly establishes the broad-spectrum applicability of annexin-directed EPT to solid tumors.

For the previously existing systems, which all utilize non-human enzymes, the cytotoxic efficacy consistently followed the pattern: MT-AV $\geq$ PNP-AV $>>$ CD-AV, with both MT-AV and PNP-AV effecting complete cell death for at least one cell line. Furthermore, the PNP-AV system consistently displayed matched cytotoxic efficacy with its drug analog. Unfortunately, the least cytotoxic system, CD-AV, generates the only FDA approved drug, 5-flourocytosine, in this initial batch of fusion proteins. However, we conclude that the MT-AV and PNP-AV systems could harbor significant clinical potential, once their immunogenicity is addressed. This is especially true for the MT-AV system since its mechanism of killing is not chemotherapeutic in nature, but instead relies on reactive oxygen species induced cell damage, a relative novelty in the realm of cancer treatment approaches.

Within the applicability studies just discussed, we also investigated the cell-priming effects of the FDA approved, small-molecule drug docetaxel for its capabilities to enhance the receptiveness of cells to annexin-directed EPT via increased target expression. We were able to conclude that docetaxel increases binding for fusion proteins in a manner that is dependent on both the multimeric structure of the fusion protein and the cell line. Docetaxel consistently increased fusion protein binding for five of six instances investigated across two cell lines and three fusion proteins. Furthermore, during simulated enzyme prodrug therapy *in vitro*, we were able to show up to 35% additional cell killing when very low dose docetaxel was combined with annexin-directed enzyme prodrug therapy treatment. Thus, the overwhelming majority

of the data lead to the conclusion that docetaxel is generally beneficial for increasing the efficacy of annexin-directed enzyme-prodrug therapy. Further, we propose that the higher doses of docetaxel typically utilized in the clinic could prove synergistic with our enzyme-prodrug systems, as higher doses will elicit a cytotoxic effect alongside the cell priming effect.

Having lent considerable evidence to the tumor-type independence of annexin-directed enzyme prodrug therapy via the above applicability studies, we designed and developed a novel family of fusion proteins centered about the human enzyme β-glucuronidase. Importantly, β-glucuronidase opens up an entire new realm of combination chemotherapy, including FDA approved drugs, within the same enzyme platform. Furthermore, β-glucuronidase fusion proteins are fully human constructs, and, thus, likely non-immunogenic and a significant improvement upon the non-human nature of the enzymes utilized previously. We also developed a new suspension based, fully scalable production method, which once translated to a bioreactor setting will readily allow for the production of the quantities of fusion protein necessary for translation. The β-glucuronidase fusion protein hA5-16a3 emerged as particularly promising, with high yields of pure product and approximately 30% activity retention at a pH of 7.4, making it therapeutically relevant in the tumor microenvironment. Further, hA5-16a3 displayed excellent cell surface binding capabilities with dissociation constants in the low-nanomolar range, and when combined with the prodrug SN-38G resulted in cytotoxicity on par with the matched drug, SN-38. We thus conclude, that the novel β-glucuronidase fusion proteins developed, especially hA5-16a3, greatly improve the translational potential of annexin-directed enzyme prodrug therapy.

Future Directions

We propose that rapid translation of the hA5-16a3 fusion protein is merited as this construct presents a significant and powerful push forward in the field of enzyme prodrug therapy. With the problem of scalable production solved, the fully human hA5-16a3 fusion protein is an outstanding potential candidate for clinical trials in the foreseeable future. While many enzyme prodrug therapy approaches have been successful in animal models, most cannot be readily translated to humans due to immunogenicity, while others lack the potency necessary for strong clinical impact. To date, only one enzyme prodrug therapy approach has entered clinical trials. This approach was antibody-directed utilizing the enzyme carboxypeptidase G2 to generate benzoic acid alkylating drugs, and treatment resulted in evidence of colorectal tumor response, but treatment was discontinued after just two weeks due to patient antibody response.[176] hA5-16a3 based therapy presents no known immune risk while producing on-site combination chemotherapy and is therefore one of the strongest clinical candidates for enzyme prodrug therapy developed to date.

It has been suggested that high doses of alkylating agents present a plausible method for overcoming acquired drug resistance, due in part to the capacity for large-scale cell death within short timeframes.[176,5] Currently, hA5-16a3 can generate three alkylating compounds, SN-38, pHAM, and a seco-duocarmycin SA analog, along with other chemotherapeutics initiating different, diverse cell death pathways. This allows for hA5-16a3 based therapy to be tailored to the patient's genotype via prodrug selection. This is important as genotype-based treatment approaches are emerging as

the gold standard of patient care as seen by the shift towards tumor board based treatment decisions.

The path towards translating hA5-16a3 to the clinic consists of two mouse model phases. The hA5-16a3 construct as it currently exists should be tested in human xenografts for efficacy. The mA5-16a3 construct (m for murine), which is already prepared for production, should be examined in immune-competent mice for both efficacy and immunogenicity. These studies should focus on combinations of prodrugs within the βG platform, and possibly also investigate the βG platform in combination with immune-stimulants or anti-angiogenesis drugs. In order to produce protein in sufficient quantities for these mouse model studies, we propose that a bioreactor should be designed to facilitate large-scale protein production

Throughout the work presented, we have established the collaborations that will be essential in driving hA5-16a3 into the clinic. Dr. Eliza Ruben, who manages the protein production core facility at the University of Oklahoma, will be instrumental in executing the large-scale purification processes as she has expertise to make these purifications simple and efficient. Continued collaboration with Dr. Lutz Tietze of the Georg-August-University Göttingen, who generously provided the seco-CBI-DMAI prodrug, will allow for our continued experimentation with novel super-prodrugs.

Lastly, tumor type independence has been significantly established for not only the βG platform, but also all non-human annexin-directed EPT systems previously developed. This opens up a large window for clinical translation across the spectrum of solid tumors and serves to push annexin-directed enzyme prodrug therapy further towards to ultimate goal of impacting the lives of patients.

References

1. Frantz S. Drug discovery: Playing dirty. Nature. 2005 Oct 13;437(7061):942–3.

2. Ran S, Thorpe PE. Phosphatidylserine is a marker of tumor vasculature and a potential target for cancer imaging and therapy. Int J Radiat Oncol. 2002 Dec 1;54(5):1479–84.

3. Schneider DJ, Sobel BE. Lack of early augmentation of platelet reactivity after coronary intervention in patients treated with bivalirudin. J Thromb Thrombolysis. 2009 Jul 1;28(1):6–9.

4. Tabagari D, Nemsadze G, Jincharadze M, Janjalia M, Shan JS. Phase II study of bavituximab plus docetaxel in patients with locally advanced or metastatic breast cancer. ASCO Meet Abstr. 2009 May 20;27(15S):3005.

5. Begent R, Sharma S, Chester K. Antibody-Dependent Enzyme Prodrug Therapy (ADEPT). In: Kontermann R, Dübel S, editors. Antibody Engineering [Internet]. Springer Berlin Heidelberg; 2010 [cited 2013 Jun 6]. p. 431–51. Available from: http://link.springer.com/protocol/10.1007/978-3-642-01144-3_28

6. John RM, Ross H. Economic value of disability-adjusted life years lost to cancers: 2008. J Clin Oncol. 2010;28.

7. Garcia M, Jemal A. Global Cancer Facts and Figures 2011. Atlanta GA Am Cancer Soc. 2011;

8. Siegel R, Ma J, Zou Z, Jemal A. Cancer statistics, 2014. CA Cancer J Clin. 2014 Jan 1;64(1):9–29.

9. Vanhoefer U, Harstrick A, Achterrath W, Cao S, Seeber S, Rustum YM. Irinotecan in the Treatment of Colorectal Cancer: Clinical Overview. J Clin Oncol. 2001 Mar 1;19(5):1501–18.

10. Verweij J, de Jonge MJA. Achievements and future of chemotherapy. Eur J Cancer. 2000 Aug;36(12):1479–87.

11. Morgan G, Ward R, Barton M. The contribution of cytotoxic chemotherapy to 5-year survival in adult malignancies. Clin Oncol. 2004 Dec;16(8):549–60.

12. Moss RA, Lee C. Current and emerging therapies for the treatment of pancreatic cancer. OncoTargets Ther. 2010 Sep 7;3:111–27.

13. Tannock IF. Conventional cancer therapy: promise broken or promise delayed? The Lancet. 1998;351:SII9–16.

14. Scheel C, Weinberg RA. Cancer stem cells and epithelial–mesenchymal transition: Concepts and molecular links. Semin Cancer Biol. 2012 Oct;22(5–6):396–403.

15. Johnstone RW, Ruefli AA, Lowe SW. Apoptosis: A Link between Cancer Genetics and Chemotherapy. Cell. 2002 Jan 25;108(2):153–64.

16. Kong X, Li L, Li Z, Xie K. Targeted Disruption of Orchestration between Stroma and Tumor Cells in Pancreatic Cancer: Molecular Basis and Therapeutic Implications. Cytokine Growth Factor Rev. 2012 Dec;23(6):343–56.

17. Schroeder A, Heller DA, Winslow MM, Dahlman JE, Pratt GW, Langer R, et al. Treating metastatic cancer with nanotechnology. Nat Rev Cancer. 2012 Jan;12(1):39–50.

18. Marusyk A, Polyak K. Cancer Cell Phenotypes, in Fifty Shades of Grey. Science. 2013;339(6119):528–9.

19. Sharma SK, Bagshawe KD. Antibody-Directed Enzyme Prodrug Therapy (ADEPT) for Cancer. In: Reddy LH, Couvreur P, editors. Macromolecular Anticancer Therapeutics [Internet]. Springer New York; 2010 [cited 2013 Jun 6]. p. 393–406. Available from: http://link.springer.com/chapter/10.1007/978-1-4419-0507-9_11

20. Del Vecchio S, Reynolds JC, Carrasquillo JA, Blasberg RG, Neumann RD, Lotze MT, et al. Local distribution and concentration of intravenously injected 131I-9.2.27 monoclonal antibody in human malignant melanoma. Cancer Res. 1989;49:2783–9.

21. Xu G, McLeod HL. Strategies for Enzyme/Prodrug Cancer Therapy. Clin Cancer Res. 2001 Nov 1;7(11):3314–24.

22. Miller CR, Williams CR, Buchsbaum DJ, Gillespie GY. Intratumoral 5-fluorouracil produced by cytosine deaminase/5-fluorocytosine gene therapy is effective for experimental human glioblastomas. Cancer Res. 2002;62:773–80.

23. Singh Y, Palombo M, Sinko PJ. Recent trends in targeted anticancer prodrug and conjugate design. Curr Med Chem. 2008;15:1802–26.

24. Ekblad M, Halldén G. Adenovirus-based therapy for prostate cancer. Curr Opin Mol Ther. 2010;12:421–31.

25. Satchi R, Connors TA, Duncan R. PDEPT: polymer-directed enzyme prodrug therapy. Br J Cancer. 2001 Sep;85(7):1070–6.

26. Fejerskov B, Zelikin AN. Substrate Mediated Enzyme Prodrug Therapy. PLoS ONE. 2012 Nov 13;7(11):e49619.

27. Theys J, Pennington O, Dubois L, Anlezark G, Vaughan T, Mengesha A, et al. Repeated cycles of Clostridium-directed enzyme prodrug therapy result in sustained antitumour effects in vivo. Br J Cancer. 2006 Oct 3;95(9):1212–9.

28. Lehouritis P, Springer C, Tangney M. Bacterial-directed enzyme prodrug therapy. J Controlled Release. 2013 Aug 28;170(1):120–31.

29. Greco O, Dachs GU. Gene directed enzyme/prodrug therapy of cancer: Historical appraisal and future prospectives. J Cell Physiol. 2001;187(1):22–36.

30. Schellekens H. Immunogenicity of therapeutic proteins: Clinical implications and future prospects. Clin Ther. 2002 Nov;24(11):1720–40.

31. Hunt MA, Dachs GU, Currie MJ. Vascular targeted gene therapy in cancer treatment. In: Gustafsson WB, editor. New Gene Therapy and Cancer Research. Nova Science Publishers, Inc.: New York, NY, USA; 2008.

32. Ran S, Downes A, Thorpe PE. Increased exposure of anionic phospholipids on the surface of tumor blood vessels. Cancer Res. 2002;62:6132–40.

33. Riedl S, Rinner B, Asslaber M, Schaider H, Walzer S, Novak A, et al. In search of a novel target — Phosphatidylserine exposed by non-apoptotic tumor cells and metastases of malignancies with poor treatment efficacy. Biochim Biophys Acta BBA - Biomembr. 2011 Nov;1808(11):2638–45.

34. Huang X, Bennett M, Thorpe PE. A Monoclonal Antibody that Binds Anionic Phospholipids on Tumor Blood Vessels Enhances the Antitumor Effect of Docetaxel on Human Breast Tumors in Mice. Cancer Res. 2005 May 15;65(10):4408–16.

35. Torchilin VP. Delivery of protein and peptide drugs in cancer. Imperial College; 2006.

36. Zwaal RFA, Comfurius P, Bevers EM. Surface exposure of phosphatidylserine in pathological cells. Cell Mol Life Sci CMLS. 2005 May 1;62(9):971–88.

37. Brown GC, Neher JJ. Eaten alive! Cell death by primary phagocytosis: "phagoptosis." Trends Biochem Sci. 2012 Aug;37(8):325–32.

38. Riedl S, Rinner B, Asslaber M, Schaider H, Walzer S, Novak A, et al. In search of a novel target-Phosphatidylserine exposed by non-apoptotic tumor cells and metastases of malignancies with poor treatment efficacy. Biochim Biophys Acta BBA-Biomembr. 2011;1808(11):2638–45.

39. Van Rite BD, Harrison RG. Annexin V-targeted enzyme prodrug therapy using cytosine deaminase in combination with 5-fluorocytosine. Cancer Lett. 2011 Aug 1;307(1):53–61.

40. Stuart MJ, Nagel RL. Sickle-cell disease. The Lancet. 9;364(9442):1343–60.

41. Farokhzad OC, Langer R. Impact of Nanotechnology on Drug Delivery. ACS Nano. 2009 Jan 27;3(1):16–20.

42. Raynal P, Pollard HB. Annexins: the problem of assessing the biological role for a gene family of multifunctional calcium- and phospholipid-binding proteins. Biochim Biophys Acta BBA - Rev Biomembr. 1994 Apr 5;1197(1):63–93.

43. Moss SE, Morgan RO. The annexins. Genome Biol. 2004 Mar 31;5(4):219.

44. Gerke V, Moss SE. Annexins: From Structure to Function. Physiol Rev. 2002 Apr 1;82(2):331–71.

45. Gerke V, Creutz CE, Moss SE. Annexins: linking Ca2+ signalling to membrane dynamics. Nat Rev Mol Cell Biol. 2005;6(6):449–61.

46. Lemmon MA. Membrane recognition by phospholipid-binding domains. Nat Rev Mol Cell Biol. 2008 Feb;9(2):99–111.

47. Janshoff A, Ross M, Gerke V, Steinem C. Visualization of Annexin I Binding to Calcium-Induced Phosphatidylserine Domains. ChemBioChem. 2001;2(7-8):587–90.

48. Kastl K, Ross M, Gerke V, Steinem C. Kinetics and Thermodynamics of Annexin A1 Binding to Solid-Supported Membranes: A QCM Study†. Biochemistry (Mosc). 2002 Aug 1;41(31):10087–94.

49. Ernst JD, Mall A, Chew G. Annexins Possess Functionally Distinguishable Ca2+ and Phospholipid Binding Domains. Biochem Biophys Res Commun. 1994 Apr 30;200(2):867–76.

50. Kenis H, van Genderen H, Bennaghmouch A, Rinia HA, Frederik P, Narula J, et al. Cell surface-expressed phosphatidylserine and annexin A5 open a novel portal of cell entry. J Biol Chem. 2004;279:52623–9.

51. Zwaal RF., Comfurius P, Bevers EM. Lipid–protein interactions in blood coagulation. Biochim Biophys Acta BBA - Rev Biomembr. 1998 Nov 10;1376(3):433–53.

52. Arur S, Uche UE, Rezaul K, Fong M, Scranton V, Cowan AE, et al. Annexin I Is an Endogenous Ligand that Mediates Apoptotic Cell Engulfment. Dev Cell. 2003 Apr;4(4):587–98.

53. Fan X, Krahling S, Smith D, Williamson P, Schlegel RA. Macrophage Surface Expression of Annexins I and II in the Phagocytosis of Apoptotic Lymphocytes. Mol Biol Cell. 2004 Jun 1;15(6):2863–72.

54. Parente L, Solito E. Annexin 1: more than an anti-phospholipase protein. Inflamm Res. 2004 Mar 1;53(4):125–32.

55. Blume KE, Soeroes S, Waibel M, Keppeler H, Wesselborg S, Herrmann M, et al. Cell Surface Externalization of Annexin A1 as a Failsafe Mechanism Preventing Inflammatory Responses during Secondary Necrosis. J Immunol. 2009 Dec 15;183(12):8138–47.

56. Lim LHK, Pervaiz S. Annexin 1: the new face of an old molecule. FASEB J. 2007 Apr 1;21(4):968–75.

57. Oh P, Li Y, Yu J, Durr E, Krasinska KM, Carver LA, et al. Subtractive proteomic mapping of the endothelial surface in lung and solid tumours for tissue-specific therapy. Nature. 2004 Jun 10;429(6992):629–35.

58. Schrama D, Reisfeld RA, Becker JC. Antibody targeted drugs as cancer therapeutics. Nat Rev Drug Discov. 2006 Feb;5(2):147–59.

59. Hsiang C-H, Tunoda T, Whang YE, Tyson DR, Ornstein DK. The impact of altered annexin I protein levels on apoptosis and signal transduction pathways in prostate cancer cells. The Prostate. 2006;66(13):1413–24.

60. Van Heerde W, Poort S, Van't Veer C, Reutelingsperger C, De Groot PG. Binding of recombinant annexin V to endothelial cells: effect of annexin V binding on endothelial-cell-mediated thrombin formation. Biochem J. 1994;302:305–12.

61. Van Heerde WL, Sakariassen KS, Hemker HC, Sixma JJ, Reutelingsperger C, de Groot PG. Annexin V inhibits the procoagulant activity of matrices of TNF-stimulated endothelium under blood flow conditions. Arterioscler Thromb Vasc Biol. 1994;14:824–30.

62. Van Genderen HO, Kenis H, Hofstra L, Narula J, Reutelingsperger CPM. Extracellular annexin A5: Functions of phosphatidylserine-binding and two-dimensional crystallization. Biochim Biophys Acta BBA - Mol Cell Res. 2008 Jun;1783(6):953–63.

63. Gerke V, Moss SE. Annexins: From Structure to Function. Physiol Rev. 2002 Apr 1;82(2):331–71.

64. Huber R, Römisch J, Paques EP. The crystal and molecular structure of human annexin V, an anticoagulant protein that binds to calcium and membranes. EMBO J. 1990 Dec;9(12):3867–74.

65. Bouter A, Gounou C, Berat R, Tan S, Gallois B, Granier T, et al. Annexin-A5 assembled into two-dimensional arrays promotes cell membrane repair. Nat Commun. 2011 Apr;2:270.

66. Folkman J. What Is the Evidence That Tumors Are Angiogenesis Dependent? J Natl Cancer Inst. 1990 Jan 3;82(1):4–7.

67. Ribatti D, Vacca A, Dammacco F. The Role of the Vascular Phase in Solid Tumor Growth: A Historical Review. Neoplasia. 1999 Oct;1(4):293–302.

68. Carmeliet P, Jain RK. Molecular mechanisms and clinical applications of angiogenesis. Nature. 2011 May 19;473(7347):298–307.

69. Weidner N, Folkman J, Pozza F, Bevilacqua P, Allred EN, Moore DH, et al. Tumor angiogenesis: a new significant and independent prognostic indicator in early-stage breast carcinoma. J Natl Cancer Inst. 1992;84(24):1875–87.

70. Bosari S, Lee AKC, DeLellis RA, Wiley BD, Heatley GJ, Silverman ML. Microvessel quantitation and prognosis in invasive breast carcinoma. Hum Pathol. 1992 Jul;23(7):755–61.

71. Franck Lissbrant I, Stattin P, Damber J-E, Bergh A. Vascular density is a predictor of cancer-specific survival in prostatic carcinoma. The Prostate. 1997;33(1):38–45.

72. Weidner N, Carroll PR, Flax J, Blumenfeld W, Folkman J. Tumor angiogenesis correlates with metastasis in invasive prostate carcinoma. Am J Pathol. 1993;143(2):401.

73. Masaki T, Ohkawa S, Amano A, Ueno M, Miyakawa K, Tarao K. Noninvasive assessment of tumor vascularity by contrast-enhanced ultrasonography and the prognosis of patients with nonresectable pancreatic carcinoma. Cancer. 2005 Mar 1;103(5):1026–35.

74. Takahashi Y, Tucker SL, Kitadai Y, et al. Vessel counts and expression of vascular endothelial growth factor as prognostic factors in node-negative colon cancer. Arch Surg. 1997 May 1;132(5):541–6.

75. Liu Y, Deisseroth A. Tumor vascular targeting therapy with viral vectors. Blood. 2006 Apr 15;107(8):3027–33.

76. Oh P, Li Y, Yu J, Durr E, Krasinska KM, Carver LA, et al. Subtractive proteomic mapping of the endothelial surface in lung and solid tumours for tissue-specific therapy. Nature. 2004 Jun 10;429(6992):629–35.

77. Esaki N, Tanaka H, Uemura S, Suzuki T, Soda K. Catalytic action of L-methionine .gamma.-lyase on selenomethionine and selenols. Biochemistry (Mosc). 1979 Feb 1;18(3):407–10.

78. Cellarier E, Durando X, Vasson M, Farges M, Demiden A, Maurizis J, et al. Methionine dependency and cancer treatment. Cancer Treat Rev. 2003;29:489–99.

79. Gandhi V, Plunkett W. Cellular and clinical pharmacology of fludarabine. Clin Pharmacokinet. 2002;41(2):93–103.

80. Plunkett W, Gandhi V, Huang P, Robertson L, Yang L, Gregoire V, et al. Fludarabine: pharmacokinetics, mechanisms of action, and rationales for combination therapies. Semin Oncol. 1993;20:2–12.

81. Deharvengt S, Wack S, Uhring M, Aprahamian M, Hajri A. Suicide gene/prodrug therapy for pancreatic adenocarcinoma by E. coli purine nucleoside phosphorylase and 6-methylpurine 2'-deoxyriboside. Pancreas. 2004;28:672–80.

82. Parker WB, Allan PW, Shaddix SC, Rose LM, Speegle HF, Gillespie GY, et al. Metabolism and Metabolic Actions of 6-Methylpurine and 2-Fluoroadenine in Human Cells. Biochem Pharmacol. 1998 May 15;55(10):1673–81.

83. Longey D. 5-fluorouracil, mechanisms of action and clinical strategies. Nat Rev Cancer. 2003;3:330–8.

84. Kawato Y, Aonuma M, Hirota Y, Kuga H, Sato K. Intracellular Roles of SN-38, a Metabolite of the Camptothecin Derivative CPT-11, in the Antitumor Effect of CPT-11. Cancer Res. 1991 Aug 15;51(16):4187–91.

85. Huang P-T, Chen K-C, Prijovich ZM, Cheng T-L, Leu Y-L, Roffler SR. Enhancement of CPT-11 antitumor activity by adenovirus-mediated expression of β–glucuronidase in tumors. Cancer Gene Ther. 2011 Jun;18(6):381–9.

86. Mürdter TE, Friedel G, Backman JT, McClellan M, Schick M, Gerken M, et al. Dose Optimization of a Doxorubicin Prodrug (HMR 1826) in Isolated Perfused Human Lungs: Low Tumor pH Promotes Prodrug Activation by β-Glucuronidase. J Pharmacol Exp Ther. 2002 Apr 1;301(1):223–8.

87. De Graaf M, Nevalainen TJ, Scheeren HW, Pinedo HM, Haisma HJ, Boven E. A methylester of the glucuronide prodrug DOX-GA3 for improvement of tumor-selective chemotherapy. Biochem Pharmacol. 2004 Dec 1;68(11):2273–81.

88. Chen K-C, Wu S-Y, Leu Y-L, Prijovich ZM, Chen B-M, Wang H-E, et al. A humanized immunoenzyme with enhanced activity for glucuronide prodrug activation in the tumor microenvironment. Bioconjug Chem. 2011;22(5):938–48.

89. Tietze LF, Schuster HJ, Krewer B, Schuberth I. Synthesis and Biological Studies of Different Duocarmycin Based Glycosidic Prodrugs for Their Use in the Antibody-Directed Enzyme Prodrug Therapy. J Med Chem. 2008;52(2):537–43.

90. Thomas M, Rivault F, Tranoy-Opalinski I, Roche J, Gesson J-P, Papot S. Synthesis and biological evaluation of the suberoylanilide hydroxamic acid (SAHA) β-glucuronide and β-galactoside for application in selective prodrug chemotherapy. Bioorg Med Chem Lett. 2007 Feb 15;17(4):983–6.

91. Ramesh M, Ahlawat P, Srinivas NR. Irinotecan and its active metabolite, SN-38: review of bioanalytical methods and recent update from clinical pharmacology perspectives. Biomed Chromatogr BMC. 2010 Jan;24(1):104–23.

92. Osborne CR, O'Shaughnessy JA, Steinberg MS, Holmes FA, Kim HS, Kocs DM, et al. Final analysis of Phase 2 study of EZN-2208 (PEG-SN38) in metastatic breast cancer (MBC) demonstrates activity in patients with triple negative breast cancer (TNBC) and in platinum pretreated patients. Am Soc Preclin Oncol Poster [Internet]. 2012 [cited 2015 Jan 29];1017. Available from: https://enzon.com/files/PEG-SN38-6.pdf

93. Kelly WK, Richon VM, O'Connor O, Curley T, MacGregor-Curtelli B, Tong W, et al. Phase I Clinical Trial of Histone Deacetylase Inhibitor Suberoylanilide Hydroxamic Acid Administered Intravenously. Clin Cancer Res. 2003 Sep 1;9(10):3578–88.

94. (EBCTCG) EBCTCG. Comparisons between different polychemotherapy regimens for early breast cancer: meta-analyses of long-term outcome among 100 000 women in 123 randomised trials. The Lancet. 2012 Feb 10;379(9814):432–44.

95. Chen Y, Chen Y. Nitrogen Mustard Derivatives [Internet]. US20140303218 A1, 2014 [cited 2015 Feb 2]. Available from: http://www.google.com/patents/US20140303218

96. Emadi A, Jones RJ, Brodsky RA. Cyclophosphamide and cancer: golden anniversary. Nat Rev Clin Oncol. 2009 Nov;6(11):638–47.

97. Tietze LF, Schuster HJ, Schmuck K, Schuberth I, Alves F. Duocarmycin-based prodrugs for cancer prodrug monotherapy. Bioorg Med Chem. 2008 Jun 15;16(12):6312–8.

98. Zitvogel L, Apetoh L, Ghiringhelli F, Kroemer G. Immunological aspects of cancer chemotherapy. Nat Rev Immunol. 2008 Jan;8(1):59–73.

99. Wyatt MD, Wilson DM. Participation of DNA repair in the response to 5-fluorouracil. Cell Mol Life Sci CMLS. 2009;66(5):788–99.

100. De M, Nl G, K K-H, Dd VH. Central nervous system toxicity with fludarabine. Cancer Treat Rep. 1986 Dec;70(12):1449–50.

101. Ding X, Herzlich AA, Bishop R, Tuo J, Chan C-C. Ocular toxicity of fludarabine: a purine analog. Expert Rev Ophthalmol. 2008 Feb 1;3(1):97–109.

102. Tietze LF, von Hof JM, Müller M, Krewer B, Schuberth I. Glycosidic Prodrugs of Highly Potent Bifunctional Duocarmycin Derivatives for Selective Treatment of Cancer. Angew Chem Int Ed. 2010;49(40):7336–9.

103. Siegel R, Naishadham D, Jemal A. Cancer statistics, 2012. CA Cancer J Clin. 2012;62(1):10–29.

104. Freytag SO, Stricker H, Movsas B, Kim JH. Prostate cancer gene therapy clinical trials. Mol Ther. 2007;15:1042–52.

105. Gottesman MM, Fojo T, Bates SE. Multidrug resistance in cancer: role of ATP-dependent transporters. Nat Rev Cancer. 2002;2:48–58.

106. Hersh MR, Kuhn JG, Phillips JL, Clark G, Ludden TM, Hoff DD. Pharmacokinetic study of fludarabine phosphate (NSC 312887). Cancer Chemother Pharmacol. 1986;17:277–80.

107. Meikle SR, Matthews JC, Brock CS, Wells P, Harte RJA, Cunningham VJ, et al. Pharmacokinetic assessment of novel anti-cancer drugs using spectral analysis and positron emission tomography: a feasibility study. Cancer Chemother Pharmacol. 1998;42:183–93.

108. Cheung WY, Fralick R, Cheng S. The confused cancer patient: a case of 5-fluorouracil–induced encephalopathy. Curr Oncol. 2008;15:234–6.

109. Bissery MC, Nohynek G, Sanderink GJ, Lavelle F. Docetaxel (Taxotere): a review of preclinical and clinical experience. Part I: Preclinical experience. Anticancer Drugs. 1995;6:339–55.

110. Matthews EJ, Kruhlak NL, Benz RD, Contrera JF. Assessment of the health effects of chemicals in humans: I. QSAR estimation of the maximum recommended therapeutic dose (MRTD) and no effect level (NOEL) of organic chemicals based on clinical trial data1. Curr Drug Discov Technol. 2004;1:61–76.

111. Bigler SA, Deering RE, Brawer MK. Comparison of microscopic vascularity in benign and malignant prostate tissue. Hum Pathol. 1993 Feb;24(2):220–6.

112. Bevers E, Comfurius P, Zwaal R. Regulatory mechanisms in maintenance and modulation of transmembrane lipid asymmetry: pathophysiological implications. Lupus. 1996;5:480–7.

113. Utsugi T, Schroit AJ, Connor J, Bucana CD, Fidler IJ. Elevated expression of phosphatidylserine in the outer membrane leaflet of human tumor cells and recognition by activated human blood monocytes. Cancer Res. 1991;51:3062–6.

114. Sparreboom A, van Tellingen O, Nooijen WJ, Beijnen JH. Preclinical pharmacokinetics of paclitaxel and docetaxel. Anticancer Drugs. 1998;9(1):1–17.

115. Tannock IF, De Wit R, Berry WR, Horti J, Pluzanska A, Chi KN, et al. Docetaxel plus prednisone or mitoxantrone plus prednisone for advanced prostate cancer. N Engl J Med. 2004;351:1502–12.

116. Van Rite BD, Lazrak YA, Pagnon ML, Palwai NR, Neves LFF, McFetridge PS, et al. Enzyme prodrug therapy designed to target l-methioninase to the tumor vasculature. Cancer Lett. 2011;301:177–84.

117. Krais JJ, De Crescenzo O, Harrison RG. Purine Nucleoside Phosphorylase Targeted by Annexin V to Breast Cancer Vasculature for Enzyme Prodrug Therapy. PLoS ONE. 2013 Oct 3;8(10):e76403.

118. Hori H, Takabayashi K, Orvis L, Carson DA, Nobori T. Gene Cloning and Characterization of Pseudomonas putida l-Methionine-α-deamino-γ-mercaptomethane-lyase. Cancer Res. 1996 May 1;56(9):2116–22.

119. Poirson-Bichat F, Gonfalone G, Bras-Goncalves R, Dutrillaux B, Poupon M. Growth of methionine-dependent human prostate cancer (PC-3) is inhibited by ethionine combined with methionine starvation. Br J Cancer. 1997;75:1605–12.

166

120. Zhao R, Domann FE, Zhong W. Apoptosis induced by selenomethionine and methioninase is superoxide mediated and p53 dependent in human prostate cancer cells. Mol Cancer Ther. 2006;5:3275–84.

121. Parker WB, Allan PW, Shaddix SC, Rose LM, Speegle HF, Gillespie GY, et al. Metabolism and metabolic actions of 6-methylpurine and 2-fluoroadenine in human cells. Biochem Pharmacol. 1998;55:1673–81.

122. Sorscher EJ, Peng S, Bebok Z, Allan PW, Bennett Jr LL, Parker WB. Tumor cell bystander killing in colonic carcinoma utilizing the Escherichia coli DeoD gene to generate toxic purines. Gene Ther. 1994;1(4):233–8.

123. Singh PP, Joshi S, Russell PJ, Verma ND, Wang X, Khatri A. Molecular Chemotherapy and Chemotherapy: A New Front against Late-Stage Hormone-Refractory Prostate Cancer. Clin Cancer Res. 2011;17:4006–18.

124. Xie X, Guo J, Kong Y, Xie GX, Li L, Lv N, et al. Targeted expression of Escherichia coli purine nucleoside phosphorylase and Fludara® for prostate cancer therapy. J Gene Med. 2011;13:680–91.

125. Voeks D, Martiniello-Wilks R, Madden V, Smith K, Bennetts E, Both GW, et al. Gene therapy for prostate cancer delivered by ovine adenovirus and mediated by purine nucleoside phosphorylase and fludarabine in mouse models. Gene Ther. 2002;9:759–68.

126. Van Rite BD, Krais JJ, Cherry M, Sikavitsas VI, Kurkjian C, Harrison RG. Antitumor Activity of an Enzyme Prodrug Therapy Targeted to the Breast Tumor Vasculature. Cancer Invest. 2013 Oct;31(8):505–10.

127. Zang XP, Palwai NR, Lerner MR, Brackett DJ, Pento JT, Harrison RG. Targeting a methioninase-containing fusion protein to breast cancer urokinase receptors inhibits growth and migration. Anticancer Res. 2006;26:1745–51.

128. O'Brien J, Wilson I, Orton T, Pognan F. Investigation of the Alamar Blue (resazurin) fluorescent dye for the assessment of mammalian cell cytotoxicity. Eur J Biochem. 2000;267:5421–6.

129. Cao S, Durrani FA, Rustum YM. Selective modulation of the therapeutic efficacy of anticancer drugs by selenium containing compounds against human tumor xenografts. Clin Cancer Res. 2004;10:2561–9.

130. Yang Y, Huang F, Ren Y, Xing L, Wu Y, Li Z, et al. The anticancer effects of sodium selenite and selenomethionine on human colorectal carcinoma cell lines in nude mice. Oncol Res Featur Preclin Clin Cancer Ther. 2009;18:1–8.

131. Afshar S, Asai T, Morrison SL. Humanized ADEPT comprised of an engineered human purine nucleoside phosphorylase and a tumor targeting peptide for treatment of cancer. Mol Cancer Ther. 2009 Jan 1;8(1):185–93.

132. Stone E, Paley O, Hu J, Ekerdt B, Cheung N-K, Georgiou G. De Novo Engineering of a Human Cystathionine-γ-Lyase for Systemic l-Methionine Depletion Cancer Therapy. ACS Chem Biol. 2012 Nov 16;7(11):1822–9.

133. Yang Z, Wang J, Lu Q, Xu J, Kobayashi Y, Takakura T, et al. PEGylation confers greatly extended half-life and attenuated immunogenicity to recombinant methioninase in primates. Cancer Res. 2004;64:6673–8.

134. Ishii H, Mori T, Shiratsuchi A, Nakai Y, Shimada Y, Ohno-Iwashita Y, et al. Distinct localization of lipid rafts and externalized phosphatidylserine at the surface of apoptotic cells. Biochem Biophys Res Commun. 2005 Feb 4;327(1):94–9.

135. Nuutila J, Lilius E-M. Flow cytometric quantitative determination of ingestion by phagocytes needs the distinguishing of overlapping populations of binding and ingesting cells. Cytometry A. 2005;65A(2):93–102.

136. Löhr M. Is it possible to survive pancreatic cancer? Nat Clin Pract Gastroenterol Hepatol. 2006;3(5):236–7.

137. Wang Z, Li Y, Ahmad A, Banerjee S, Azmi AS, Kong D, et al. Pancreatic cancer: understanding and overcoming chemoresistance. Nat Rev Gastroenterol Hepatol. 2010;8:27–33.

138. Chu Z, Abu-Baker S, Palascak MB, Ahmad SA, Franco RS, Qi X. Targeting and Cytotoxicity of SapC-DOPS Nanovesicles in Pancreatic Cancer. PLoS ONE. 2013 Oct 4;8(10):e75507.

139. Beck AW, Luster TA, Miller AF, Holloway SE, Conner CR, Barnett CC, et al. Combination of a monoclonal anti-phosphatidylserine antibody with gemcitabine

strongly inhibits the growth and metastasis of orthotopic pancreatic tumors in mice. Int J Cancer. 2006;118(10):2639–43.

140. Bissery M-C, Nohynek G, Sanderink G-J, Lavelie F. Docetaxel (Taxotere (R)) a review of preclinical and clinical experience. Part I: preclinical experience. Anticancer Drugs. 1995;6(3):339–55.

141. Guillen KP, Kurkjian C, Harrison RG. Targeted enzyme prodrug therapy for metastatic prostate cancer–a comparative study of L-methioninase, purine nucleoside phosphorylase, and cytosine deaminase. J Biomed Sci. 2014;21(1):65.

142. Palwai NR, Zang X-P, Harrison RG, Benbrook D, Pento JT. Selective growth inhibition of cancer cells by L-methioninase-containing fusion protein targeted to the urokinase receptor. Pharmacology. 2009;84(5):271–5.

143. Miki K, Xu M, Gupta A, Ba Y, Tan Y, Al-Refaie W, et al. Methioninase cancer gene therapy with selenomethionine as suicide prodrug substrate. Cancer Res. 2001;61:6805–10.

144. Bossow S, Grossardt C, Temme A, Leber M, Sawall S, Rieber E, et al. Armed and targeted measles virus for chemovirotherapy of pancreatic cancer. Cancer Gene Ther. 2011;18:598–608.

145. Simpson GR, Han Z, Liu B, Wang Y, Campbell G, Coffin RS. Combination of a fusogenic glycoprotein, prodrug activation, and oncolytic herpes simplex virus for enhanced local tumor control. Cancer Res. 2006;66(9):4835–42.

146. Suzuki KT, Kurasaki K, Ogawa S, Suzuki N. Metabolic transformation of methylseleninic acid through key selenium intermediate selenide. Toxicol Appl Pharmacol. 2006;215:189–97.

147. Mittelman A, Ashikari R, Ahmed T, Savona S, Arnold P, Arlin Z. Phase II trial of fludarabine phosphate (f-ara-AMP) in patients with advanced breast cancer. Cancer Chemother Pharmacol. 1988;22(1):63–4.

148. Sultana A, Smith CT, Cunningham D, Starling N, Neoptolemos JP, Ghaneh P. Meta-Analyses of Chemotherapy for Locally Advanced and Metastatic Pancreatic Cancer. J Clin Oncol. 2007 Jun 20;25(18):2607–15.

149. Yoo C, Hwang JY, Kim J-E, Kim TW, Lee JS, Park DH, et al. A randomised phase II study of modified FOLFIRI.3 vs modified FOLFOX as second-line therapy in patients with gemcitabine-refractory advanced pancreatic cancer. Br J Cancer. 2009 Oct 13;101(10):1658–63.

150. Sipos B, Möser S, Kalthoff H, Török V, Löhr M, Klöppel G. A comprehensive characterization of pancreatic ductal carcinoma cell lines: towards the establishment of an in vitro research platform. Virchows Arch. 2003;442:444–52.

151. Androulakis N, Kourousis C, Dimopoulos MA, Samelis G, Kakolyris S, Tsavaris N, et al. Treatment of Pancreatic Cancer With Docetaxel and Granulocyte Colony-Stimulating Factor: A Multicenter Phase II Study. J Clin Oncol. 1999 Jun 1;17(6):1779–1779.

152. Sherman WH, Fine RL. Combination Gemcitabine and Docetaxel Therapy in Advanced Adenocarcinoma of the Pancreas. Oncology. 2001;60(4):316–21.

153. Mayer A, Sharma SK, Tolner B, Minton NP, Purdy D, Amlot P, et al. Modifying an immunogenic epitope on a therapeutic protein: a step towards an improved system for antibody-directed enzyme prodrug therapy (ADEPT). Br J Cancer. 2004 May 25;90(12):2402–10.

154. Veronese FM. Peptide and protein PEGylation: a review of problems and solutions. Biomaterials. 2001;22(5):405–17.

155. Tranoy-Opalinski I, Legigan T, Barat R, Clarhaut J, Thomas M, Renoux B, et al. β-Glucuronidase-responsive prodrugs for selective cancer chemotherapy: An update. Eur J Med Chem. 2014 Mar 3;74:302–13.

156. Andrady C, Sharma SK, Chester KA. Antibody-enzyme fusion proteins for cancer therapy. Immunotherapy. 2011;3(2):193–211.

157. Chen C-P, Hsieh Y-T, Prijovich ZM, Chuang H-Y, Chen K-C, Lu W-C, et al. ECSTASY, an adjustable membrane-tethered/soluble protein expression system for the directed evolution of mammalian proteins. Protein Eng Des Sel. 2012 Jul 1;25(7):367–75.

158. Beckman RA, Weiner LM, Davis HM. Antibody constructs in cancer therapy. Cancer. 2007 Jan 15;109(2):170–9.

159. Shipley JM, Grubb JH, Sly WS. The role of glycosylation and phosphorylation in the expression of active human beta-glucuronidase. J Biol Chem. 1993 Jun 5;268(16):12193–8.

160. Biela BH, Khawli LA, Hu P, Epstein AL. Chimeric TNT-3/Human Beta-Glucuronidase Fusion Proteins for Antibody-Directed Enzyme Prodrug Therapy (ADEPT). Cancer Biother Radiopharm. 2003 Jun 1;18(3):339–53.

161. Boado RJ, Pardridge WM. Genetic engineering of IgG-glucuronidase fusion proteins. J Drug Target. 2010 Apr;18(3):205–11.

162. Wu C-H, Balasubramanian WR, Ko Y-P, Hsu G, Chang S-E, Prijovich ZM, et al. A simple method for the production of recombinant proteins from mammalian cells. Biotechnol Appl Biochem. 2004;40(2):167–72.

163. Conroy T, Gavoille C, Samalin E, Ychou M, Ducreux M. The Role of the FOLFIRINOX Regimen for Advanced Pancreatic Cancer. Curr Oncol Rep. 2013 Jan 23;15(2):182–9.

164. Islam MR, Grubb JH, Sly WS. C-terminal processing of human beta-glucuronidase. The propeptide is required for full expression of catalytic activity, intracellular retention, and proper phosphorylation. J Biol Chem. 1993 Oct 25;268(30):22627–33.

165. Han YK, Ha TK, Lee SJ, Lee JS, Lee GM. Autophagy and apoptosis of recombinant Chinese hamster ovary cells during fed-batch culture: Effect of nutrient supplementation. Biotechnol Bioeng. 2011 Sep 1;108(9):2182–92.

166. Chang TW, Yu L. Hybrid with interferon-beta and an immunoglobulin Fc joined by a peptide linker. 5,908,626, 1999.

167. Schrödinger, LLC. The PyMOL Molecular Graphics System, Version 1.3r1. 2010.

168. Schneider CA, Rasband WS, Eliceiri KW. NIH Image to ImageJ: 25 years of image analysis. Nat Methods. 2012 Jul;9(7):671–5.

169. Goulet F, Moore KG, Sartorelli AC. Glycosylation of annexin I and annexin II. Biochem Biophys Res Commun. 1992 Oct 30;188(2):554–8.

170. Schutters K, Reutelingsperger C. Phosphatidylserine targeting for diagnosis and treatment of human diseases. Apoptosis. 2010 Sep 1;15(9):1072–82.

171. Neves LFF, Krais JJ, Rite BDV, Ramesh R, Resasco DE, Harrison RG. Targeting single-walled carbon nanotubes for the treatment of breast cancer using photothermal therapy. Nanotechnology. 2013 Sep 20;24(37):375104.

172. Tietze LF, Schmuck K, Schuster HJ, Müller M, Schuberth I. Synthesis and Biological Evaluation of Prodrugs Based on the Natural Antibiotic Duocarmycin for Use in ADEPT and PMT. Chem – Eur J. 2011;17(6):1922–9.

173. Hurley LH, Lee CS, McGovren JP, Warpehoski MA, Mitchell MA, Kelly RC, et al. Molecular basis for sequence-specific DNA alkylation by CC-1065. Biochemistry (Mosc). 1988;27(10):3886–92.

174. Puyo S, Montaudon D, Pourquier P. From old alkylating agents to new minor groove binders. Crit Rev Oncol Hematol. 2014;89(1):43–61.

175. Chen K-C, Schmuck K, Tietze LF, Roffler SR. Selective Cancer Therapy by Extracellular Activation of a Highly Potent Glycosidic Duocarmycin Analogue. Mol Pharm. 2013 May 6;10(5):1773–82.

176. Napier MP, Sharma SK, Springer CJ, Bagshawe KD, Green AJ, Martin J, et al. Antibody-directed Enzyme Prodrug Therapy: Efficacy and Mechanism of Action in Colorectal Carcinoma. Clin Cancer Res. 2000 Mar 1;6(3):765–72.

177. GraphPad Curve Fitting Guide [Internet]. [cited 2015 Jan 15]. Available from: http://www.graphpad.com/

Appendix A: Protocols

A.1 - Prokaryotic fusion protein production & purification

For the production and purification of MT-AV, CD-AV, and PNP-AV.

Day before starting, autoclave the following items:

- 1 liter LB medium

- 4-liter Erlenmeyer flask (with aluminum foil on top)

- 125 ml Erlenmeyer flask (with aluminum foil on top)

- 100 ml beaker (with aluminum foil on top)

- All size tips

- 1.5 ml centrifuge tubes

- 1 liter DI water

A.1.1 Production

1) Culture 5 μl of *E. coli* BL21 (DE3) harboring pET- 30 Ek/LIC (MT-AV and CD-AV) or pET303CT (PNP-AV) with the fusion gene of interest in 10 ml of LB medium containing selection antibiotic in a 125 ml Erlenmeyer flask overnight at 37 ^{o}C, 200 rpm.

   - LB medium: 1 liter DI H_2O + 10 g tryptone + 5 g yeast extract + 5 g NaCl.

   - For MT-AV and CD-AV: Add 35 mg kanamycin to the 1 L of LB medium before taking out the 10 ml for the initial culture.

   - For PNP-AV: Add 100 mg carbenicillin to the 1 L of LB medium before taking out the 10 ml for the initial culture.

2) Add 10 ml of the cell culture to 1 liter of fresh culture medium + appropriate antibiotic and incubate at 37 $^\circ$C, 200 rpm. Take 1.5 mL of medium before adding the bacteria, as a blank. Grow culture to mid-log phase => OD_{600} = 0.5.

- Take a 1.5 ml sample of just the LB medium. Label 1.5 ml tube 'LB.'

- Transfer entire volume of medium to 4-L flask.

- After approx. 15 h of shaking, measure optical density at 600 nm (absorbance) using a clear 96 well plate and microtiter plate reader of sample vs LB medium => using 250 µl samples of each. When OD_{600nm} = 0.5, then proceed to next step.

3) Add isopropyl β-D-thiogalactopyranoside (IPTG) to a final concentration of 0.4 mM (96 mg IPTG) to 1-liter solution in 4L flask and incubate at 30°C with shaking (180 rpm) for 5 h to induce protein expression. IPTG stimulates the production of fusion protein. IPTG activates the promoter in the plasmid that will start the transcription of the gene that follows the promoter.

4) Harvest the cells by centrifugation for 10 min at 1000 x g, at 4°C.

- Use 50 ml "unbreakable" ultracentrifuge tubes (VWR).

- After first centrifuge, pour out supernatant, add more culture to same 8 tubes. Bacteria will be stuck to side of tubes so inverting to pour out is not a problem. Can put the 4 tubes in -20 $^\circ$C freezer for overnight storage.

5) Resuspend the cell pellet in 40 ml of sonication buffer.

- 0.05 mM N- p-tosyl-L-phenylalanine chloromethyl ketone (TPCK) - (-20 $^\circ$C) => 0.704 mg.

- 1 mM phenylmethylsulfonyl fluoride (PMSF) - (shelf) => 6.968 mg.

- 1% HPLC ethanol - (flammables) => 400 μl.

- 0.02 mM pyridoxal phosphate – (-20ºC) => 400 μl of 2 mM.

- 0.01% β-mercaptoethanol – (bench top) => 4 μl.

- 0.02 M sodium phosphate dibasic – (shelf) => 113.6 mg.

- Correct to pH 7.4 – using HCl.

- Dissolve TPCK and PMSF in ethanol in microcentrifuge tube, then add to beaker.

- Make this buffer in the 100 ml beaker.

- Add to centrifuge tubes, and vortex to resuspend cell pellets.

- Pour contents of the tubes back into the 100 ml beaker.

6) Lyse the cells by sonication at 4 °C for 30 sec at 4.5 watts then allow it to cool for 30 sec on ice. This cycle was repeated for 4 times (= 5 times total) for a total sonication time of 2.5 min on power level 4.

   - Clean sonicator tip w/ ethanol before use.

   - Put beaker in tub w/ ice while sonicating.

7) Centrifuge the lysate obtained at 12,000 x g for 30 min to remove the cell debris and take the supernatant.

A.1.2 Purification

1) After taking supernatant sample, add imidazole (40 mM) and NaCl (500 mM) to the lysate to reduce non-specific protein binding prior to loading column.

   - 40 mM imidazole => use 0.0817 g

   - 500 mM NaCl => use 1.168 g

2) Equilibrate a 5 ml HisTrap chromatography column with immobilized Ni^{+2} using Wash Buffer 1.

3) Feed the soluble protein fraction into the column.

4) Wash the column with 70 column volumes of Wash Buffer 2 to remove unwanted proteins and endotoxin (350 ml).

5) Wash the column with 20 column volumes of Wash Buffer 1 to wash the protein until the pen reaches the baseline (100 ml). Flow thru contains unwanted proteins.

6) Elute the protein using elution buffer.

7) Dialyze eluted protein for 3 hours against 2 liters of dialysis buffer to make it suitable for N-terminal His-tag cleavage.

8) Before continuing, need to regenerate the column using this procedure:

   - 25 ml of 1 M KCl => make 200 ml, so use 14.91 g

   - 25 ml of 1 M NaOH => make 200 ml, so use 8.0 g

   - 25 ml of DI Water

   - 25 ml of 1 M HPLC grade ethanol (1.46 ml ethanol + 23.54 ml DI water)

9) Measure the concentration of protein (Bradford protein assay).

10) Cleave the N-terminal His-tag by adding HRV 3C protease at 10 U/mg of protein with the recommended 10X buffer provided (stored @ -20 ºC). Incubate for 16h at 4ºC with gentle shaking, in the dark. HRV 3C protease comes as 2 U/µl and we want to use it at 10 U/mg protein.

11) Add imidazole (40 mM) and NaCl (500 mM) to the cleaved protein solution.

12) Equilibrate the HisTrap column with Wash Buffer 1.

13) Feed the cleaved protein solution to the HisTrap HP (5 ml) column. Collect peak as it contains protein of interest.

14) Run wash buffer 1 through column until baseline is reached. Continue collecting peak.

15) Elute uncleaved protein with elution buffer. This contains both uncleaved protein and HRV 3C (contains a His_6 tag).

16) Dialyze purified protein for 3 hours against 2 liters of dialysis buffer.

17) Regenerate the column as above.

18) Optional: Pass the sample thru a 0.2 μm cellulose-acetate filter using a syringe.

19) If necessary: Concentrate the protein using a 150 kDa, 20 ml protein concentrator (Millipore #89921).

20) Aliquot purified protein into cryovials and flash freeze in the liquid nitrogen tank prior to freeze-drying.

21) Freeze dry flash frozen proteins overnight.

A.1.3 Buffers

MT-AV requires the addition of pyridoxal phosphaste during purification. For all other FPs, omit pyridoxal phosphate. For MT-AV purification, prepare 30 ml of 2 mm pyridoxal phosphate – enough for entire purification.

<u>Wash buffer 1 (500 ml)</u>

- 20 mM sodium phosphate dibasic => use 1.42 g

- 40 mM imidazole => use 1.362 g

- 500 mM NaCl => use 14.61 g

- (0.02 mM pyridoxal phosphate => use 5 ml of 2 mM)

- Correct this to pH 7.4

Wash buffer 2 (300 ml) – For endotoxin removal

- 20 mM sodium phosphate dibasic => use 0.8517 g

- 40 mM imidazole => use 0.817 g

- 500 mM NaCl => use 8.766 g

- (0.02 mM pyridoxal phosphate => use 3 ml of 2 mM)

- 0.1% Trition X-114 => 3 ml

- Correct this to pH 7.4

Elution buffer (300 ml)

- 20 mM sodium phosphate dibasic => use 0.8517 g

- 500 mM imidazole => use 10.212 g

- 500 mM NaCl => use 8.766 g

- (0.02 mM pyridoxal phosphate => use 3 ml of 2 mM)

- Correct this to pH 7

Dialysis buffer (2L) => pH 7.4

- 20 mM sodium phosphate dibasic => 5.678 g

- 100 mM NaCl => use 11.688 g

- (0.02 mM pyridoxal phosphate => 20 ml of 2 mM)

A.2 - Bradford assay

For determining protein concentration, when extinction coefficients are unknown.

1. Add the following to a 96-well plate:

    a. 10 µl of protein sample

    b. 200 µl of 1x Quick Start Bradford Dye Reagent (Bio-Rad)

2. Gently shake to mix – either in plate reader or on shaker at room temperature.

3. Incubate at room temperature for 10 min.

4. Measure the absorbance at 595 nm.

5. Compare with the standard curve (Figure 49) to calculate the protein concentration.

$$\frac{mg}{mL} = \left(\frac{(A_{595} - A_{H_2O}) - 0.021}{1.1047} \right)$$
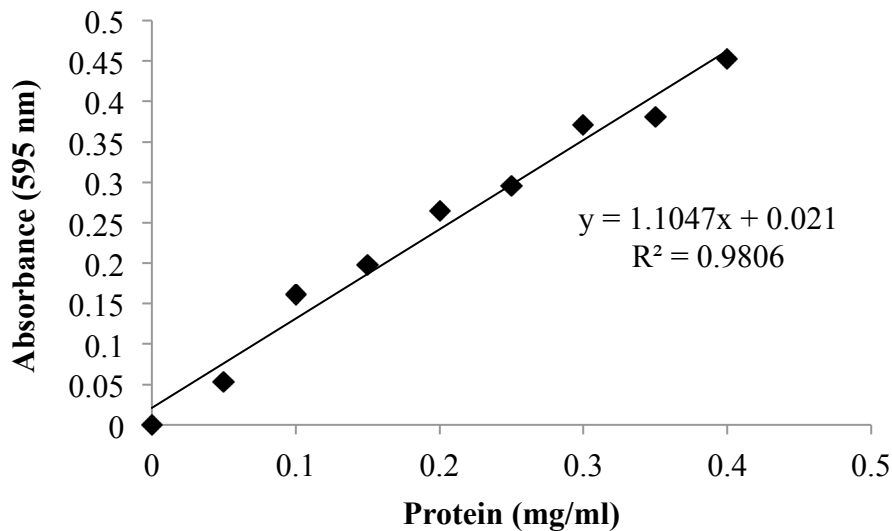
Figure 49: Bradford assay standard curve

The chart shows Absorbance (595 nm) on the y-axis versus Protein (mg/ml) on the x-axis, with the fit:

$$y = 1.1047x + 0.021$$
$$R^2 = 0.9806$$

A.3 - Biotin labeling FPs

For creating biotinylated constructs for downstream use in binding assays and confocal microscopy. Biotin used is SureLINK Chromophoric Biotin (KPL).

1) Using a Spectrum Labs 1ml float-a-lyzer G2 (20 kDa) dialyze protein into conjugation buffer if protein contains Tris, imidazole, glycine, or primary amines as these will inhibit biotin-labeling reaction.

2) Prepare a stock solution of 20 mg/ml (25 nmol/μl) SureLINK Chromophoric Biotin in anhydrous DMF immediately prior to use.

   a. 1 mg dissolved in 50 μL

3) Using a 100-fold excess of biotin for conjugation, add the appropriate volume of biotin stock solution.

$$\mu l \ of \ 20 \ {}^{mg}\!/_{ml} \ stock = \frac{1000 \times (mg \ of \ protein) \times 100}{protein \ MW \ (kDa) \times 25 \ nmole/\mu l}$$

4) Incubate at room temperature for 2 h with gentle shaking, in the dark.

5) Remove the unconjugated chromophoric biotin by dialysis using a 20 kDa, 1 ml float-a-lyzer G2 in 2L dialysis buffer at 4 $^{\circ}$C with gentle stirring. Same cassette may be reused, as long as it has not been allowed to dry out. Run dialysis for 4 hours. Change dialysate and run overnight.

6) Bradford or Qubit to determine concentration, aliquot, and store at -80°C in the dark

Dialysis Buffer (2 L) – pH to 7.4

- 100 mM sodium phosphate dibasic (28.392 g)

- 150 mM NaCl (17.532 g)

A.4 - Binding strength assay

The binding strength of each FP to PS on cancer cells can be analyzed via the dissociation constant (K_d), or simply the concentration at which half saturation of binding occurs. To measure K_d, cells seeded in 24-well plates were incubated with biotinylated FPs at varying concentrations. Biotin was then allowed to react with streptavidin-HRP, and after washing, bound strep-HRP was reacted with OPD with color developed measured on a plate reader. Strep-HRP cannot pass through the cell membrane, and therefore gives us a true measure of binding to the outside of the cell. To determine specific binding, the experiment was run in the presence of Ca^{2+} or in the presence of EDTA, a metal chelating agent, as shown in Figure 50. Results are fit to a one-site, non-competitive binding model using GraphPad Prism 5 or 6.

Procedure:

1) Grow cells in T-75 flasks until they reach 80-85% confluence.

2) Transfer 5×10^4 cells/well to 48 wells on two 24-well plates. Grow cells to 90% confluence.

3) Fix the cells in all 48 wells by adding 200 μl/well PBS buffer containing 0.25% glutaraldehyde. Remove before proceeding.

4) Quench excess aldehyde groups by incubating with 200 μl/well of 50 mM NH_4Cl, diluted in PBS buffer for 5 minutes at room temperature. Remove after incubation period.

5) Wash 2x with 300 μl/well PBS.

6) Incubate for 1h (37 °C, 5% Co_2) with 300 μl/well of PBS + 0.5% BSA.

7) Dilute fusion protein-biotin conjugate in 0.5% BSA diluted in PBS buffer at predetermined concentrations (usually 0-12 nM). Make 2 sets, one in EDTA and one in Ca^{2+}. Add 300 µl to wells, using triplicates of each concentration. The blank for each set will receive no FP. Incubate for 2 hours at 37 °C, 5% CO_2.

8) Wash aggressively 4 times with 300 µl of 0.5% BSA diluted in PBS buffer plus either Ca^{2+} or EDTA.

9) Add 300 µl of Streptavidin-HRP (2 µg/ml) and incubate for 1 h at room temperature. (Streptavidin-HRP is stored at 4 °C)

10) Wash 4 times with 300 µl of PBS buffer, pus either EDTA or Ca^{2+}.

11) Add 300 µl of the chromogenic substrate o-phenylenediamine (OPD) to each well. (OPD is in -20 °C freezer). The OPD solution is made with phosphate citrate buffer (1 capsule in 100 ml DI water). Prior to use, add 40 µl of 30% H_2O_2. Weigh out the desired amount of OPD with a concentration of 0.4 mg/ml.

   a. Add one capsule of phosphate-citrate buffer to 100 mL DI in beaker and stir (no more than 30 min prior to use of OPD)

   b. Weigh 0.4 mg/mL OPD and place in foil coated tube

      i. 6.4 mg for 16 mL buffer

   c. Add 40 µL of 30% H_2O_2 to buffer

   d. Stir for 30 seconds

   e. Add required amount of buffer to OPD

   f. Mix by inversion

12) Incubate for 20 mins at room temperature and in the dark to minimize OPD color change. Keep unused OPD solution as a control. If the leftover OPD solution turns yellow, experiment is void.

13) Transfer 100 µl of the supernatant to 96-well plates.

14) Measure absorbance at 450 nm.

Analysis:

1) The BioTek plate reader acquisition software will give means/triplicate and standard deviations. Using the correlated table (0 nM must be set as a blank), the acquisition software will subtract off the baseline (0 nM) for you.

2) In Excel or GraphPad, subtract non-specific binding from total binding to obtain specific binding. Determine the standard deviation of specific binding using error propagation.

3) Divide all standard deviations by the square root of the number of samples to obtain standard errors. Arrange data columns as follows, with row values matched for concentration: total binding, total biding standard error, non-specific binding, non-specific biding standard error, specific binding, and specific biding standard error.

4) Copy and paste values into GraphPad Prism.

5) Run analysis

    a. Non-linear regression

    b. Single-site, non-competitive binding model

    c. Least squares fit with automatic outlier elimination

6) Prism will calculate the dissociation constants (K_d) for total, non-specific, and specific binding along with errors. Total and specific binding should converge, whereas non-specific binding is generally linear as a function of fusion protein concentration and therefore the K_d should be ambiguous (not-converged). Report the K_d for the specific binding curve.
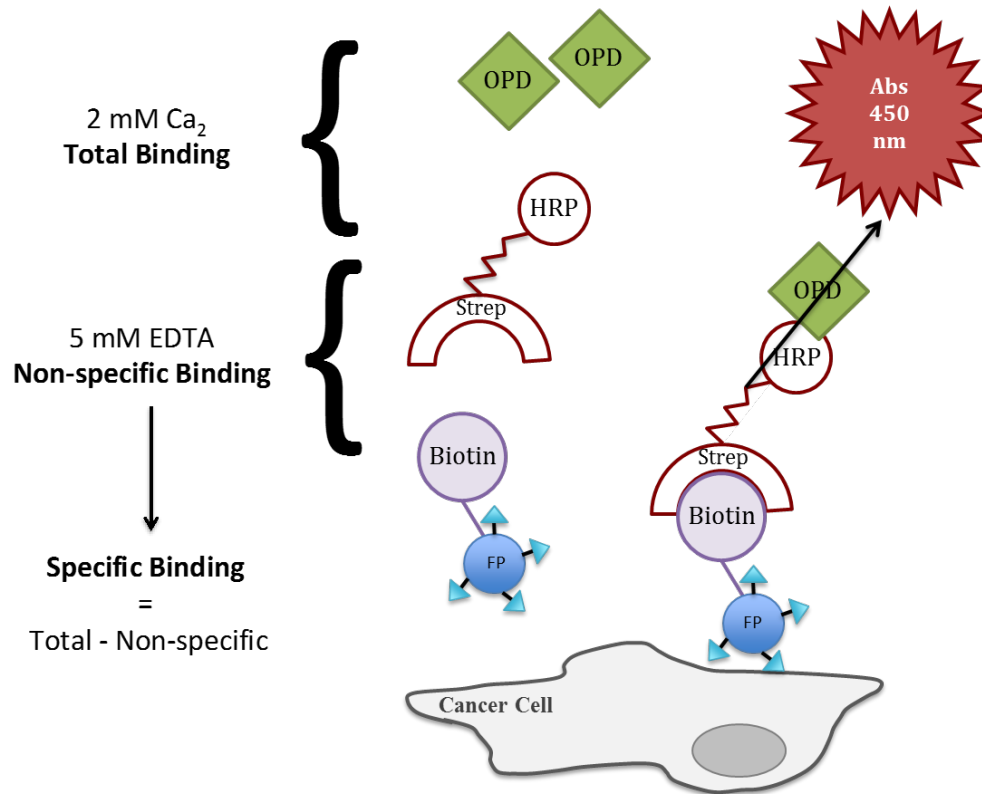
Figure 50: Schmatic of method for determining binding strength of FPs to PS on cell surface

To determine the binding strength of each FP to PS on cancer cells, FPs were biotinylated and incubated at varying concentrations with cells seeded in 24-well plates. Biotin was then allowed to react with streptavidin-HRP, and after washing bound strep-HRP was reacted with OPD. To determine specific binding, the experiment was run in the presence of Ca^{2+} or in the presence of EDTA, a metal chelating agent. Results were fit to a one-site, non-competitive binding model.

A.5 - Live cell binding stability assay

The binding stability assay is used to determine how much FP remains bound to live cancer cells over a 3-day period. This assay utilizes the same detection method as the binding strength assay, but measurements are taken on 3 consecutive days, as shown in Figure 51. To control for non-specific binding, all cells, regardless of cell type, were plated in gelatin. This is especially important since non-specific binding of strep-HRP to the plate will change as confluence increases over the course of 3 days, due to the difference in plate surface area available for strep-HRP binding. Gelatin essentially negates this effect by blocking non-specific binding of strep-HRP to the plate.

Procedure:

1) Grow cells in T-75 flasks using until they reach 80-85% confluence.

2) Plate at $5x10^3$-$10x10^3$ cells/well in 6 wells (per fusion protein to be tested) on four 96-well plates, all in gelatin. Each plate will correspond to a different experimental day (0-4). Grow cells to 80% confluence, approx. 48 h.

3) Add 75 µl CA medium (regular growth medium with 2 mM Ca^{2+}) containing 100 nM biotinylated fusion protein to three wells on each plate. Incubate for 2 h at 37 ^{o}C, 5% CO_2.

4) Wash 4x with 100 µl CA medium. Add 300 µl CA medium to all wells.

On each day (0, 1, 2, and 3):

1) Aspirate, then add 75 µl CA medium with 0.25% glutaradlehyde to each well.

   a. Incubate for 5 min at room temperature.

189

b. Remove medium.

2) Add 75 μL CA medium with 50 mM ammonium chloride.

    a. Incubate for 5 minutes at room temperature.

    b. Remove medium.

3) Wash 3 times with 100 μl CA medium.

4) Add 75 μl Streptavidin/HRP (2 μg/mL). Incubate for 1 hour at room temperature.

5) Wash 4 times with 100 μl of CA medium.

6) Add 100 μl of the chromogenic substrate o-phenylenediamine (OPD) to each well. The OPD solution is made with phosphate citrate buffer (1 capsule in 100 ml DI water). Prior to use, add 40 μl of 30% H_2O_2. Weigh out the desired amount of OPD with a concentration of 0.4 mg/ml.

    a. Add one capsule of phosphate-citrate buffer to 100 mL DI in beaker and stir (no more than 30 min prior to use of OPD).

    b. Weigh 0.4 mg/mL OPD and place in foil coated tube.

    c. Add 40 μL of 30% H_2O_2 (glass fridge) to buffer.

    d. Stir for 30 seconds.

    e. Add required amount of buffer to OPD.

    f. Mix by inversion.

7) Incubate for 20 minutes at room temperature and in the dark to minimize OPD color change.

8) Transfer 80 μl of the supernatant to 96-well plates. Measure absorbance at 450 nm.
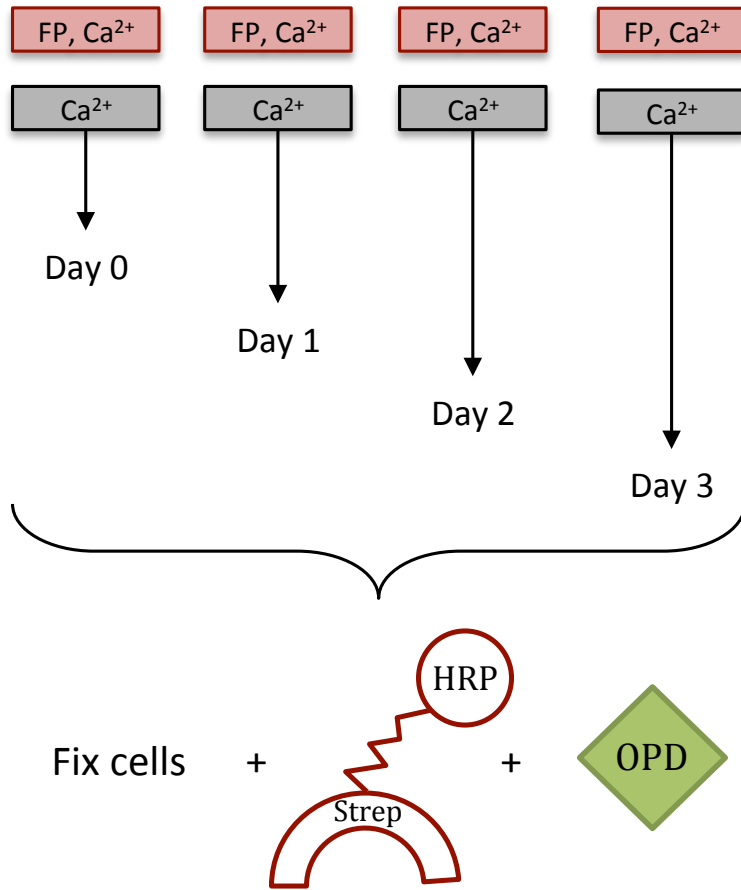
Figure 51: Schematic of method for determination of binding stability on live cells

A.6 - Cytotoxicity assay – Simulated *in vitro* EPT

A.6.1 MT-AV, PNP-AV, and CD-AV cytotoxicity studies

To examine how our fusion proteins preform as anti-cancer therapies, we simulated

EPT *in vitro*. This method was utilized for both prostate cancer applicability studies

(Chapter 2) and pancreatic cancer applicability studies (Chapter 3) for the fusion

proteins MT-AV, PNP-AV, and CD-AV. An overview of the treatment strategy is

presented in Figure 52.

1) [Day -2] Plate cells in complete growth medium the appropriate density in 24-well

    plates in a plating volume of 1 ml. Allow cells to adhere overnight.

    a. PC-3: 50 x 10^3 cells/well

    b. Panc-1: 25 x 10^3 cells/well

    c. Capan-1: 2.5 x 10^3 cells/well on 0.1 % w/v gelatin

        i. Treat each well with 300 μl gelatin, let sit for 10 minutes at RT, and

          then remove immediately prior to plating.

2) Prepare FP medium:

    a. To complete growth medium for each cell line, add 2 mM Ca^{2+}, since AV

        binding to phosphatidylserine is calcium-dependent. All steps other than

        initial plating will be carried out in this calcium containing FP medium.

        i. F12K – 0.1697 g $CaCl_2$

        ii. DMEM – 0.1338 g $CaCl_2$

        iii. IMEM – 0.1532 g $CaCl_2$

b. For medium for MT-AV EPT also add 0.02 mM pyridoxal phosphate. This is 0.00275 g pyridoxal phosphate per 555 ml media stock.

3) [Day -1] After cells have adhered overnight (not simultaneously with plating as cells WILL NOT attach), selected wells are treated with 300 µl/well of docetaxel at a concentration determined to have no effect on cell viability or growth rate.

   a. PC-3: 50 pM

   b. Panc-1: 200 pM

   c. Capan-1: 50 pM

4) [Day 0] **Measure cell viability:**

   a. Replace growth medium with 300 µl of FP medium. Perform an Alamar Blue assay to determine cell viability.

      i. Add 10% (30 µl) of Alamar Blue.

      ii. Incubate for 4 hours at 37 °C.

      iii. Transfer 250 µl to an opaque 96-well plate

      iv. Read fluorescence: excitation – 530 nm; emission – 590 nm.

      v. NO CELLS well is blank, 0 uM on 2 plates without FP is 100% viability

   b. Wash 2 times using 300 µl of FP suitable medium.

5) [Day 0] **Bind fusion protein:**

   a. Add 300 µl of FP media containing 100 nM fusion protein to 21 wells. To control wells (prodrug or drug alone) add 300 µl of FP media.

   b. Incubate for 2 hours at 37 °C.

   c. Wash aggressively 3 times using 300 µl of FP suitable medium.

193

6) [Day 0] **Treat with prodrug/drug:**

    a. Remove medium from wells. Add 300 µl/well of FP suitable containing varying concentrations of prodrug/drug.

7) Studies are carried out over a 3, 6, or 9-day treatment cycle which is executed as shown in Table 7. For each step follow same procedure as Day 0.

    a. AB = Alamar Blue assay to measure cell viability

    b. FP = Bind fusion protein

    c. T = Treat with drug prodrug

8) To analyze data, compute % viability per well and check for significance compared to matched control via a one-way ANOVA with Tukey-Kramer multiple comparisons on GraphPad Prism.

A.6.2 hA1-16a3 and hA5-16a3 cytotoxicity studies

To examine how βG fusion proteins functioned as anti-cancer therapeutics, a similar

technique was used as for the pancreatic and prostate applicability studies (A.6.1),

Figure 52. However, the plates utilized and the dosage-timing was altered.

1) [Day -1] Plate cells in complete growth medium at 2.5-10 x 10^3 cells/well in 96-well

   plates in a plating volume of 200 ml. Allow cells to adhere overnight.

   i. Use only the inside wells, as evaporation will occur in the outside

      wells, particularly in the corners. Fill all unused wells with 300 μl

      PBS. (leave three empty for AB blank)

   ii. Treat plates for HAAE-1 with 100 μl gelatin, let sit for 10 minutes at

       RT, and then remove immediately prior to plating.

2) Prepare FP medium:

   a. To complete growth medium for each cell line, add 2 mM Ca^{2+}, since AV

      binding to phosphatidylserine is calcium-dependent. All steps other than

      initial plating will be carried out in this calcium containing FP medium.

      i. F12K – 0.1697 g $CaCl_2$

      ii. DMEM – 0.1338 g $CaCl_2$

      iii. EMEM – 0.1338 g $CaCl_2$

      iv. McCoy's 5A - 0.1983 g $CaCl_2$

3) [Day 0, 2, 4] **Measure cell viability:**

   a. Replace growth medium with 100 μl of FP medium. Perform an Alamar

      Blue assay to determine cell viability.

i. Add 10% (10 µl) of Alamar Blue.

   ii. Incubate for <u>4 hours</u> at 37 °C.

   iii. Transfer 80 µl to an opaque 96-well plate

   iv. Read fluorescence: excitation – 530 nm; emission – 590 nm.

   v. NO CELLS well is blank, 0 uM on 2 plates without FP is 100% viability

   b. Wash 2 times using 100 µl of FP suitable medium.

4) [Day 0, 2, 4] **Bind fusion protein:**

   a. Add 75 µl of FP media containing 100 nM fusion protein to appropriate wells. To control wells (prodrug or drug alone), add 75 µl of FP media.

   b. Incubate for <u>2 hours</u> at 37 °C.

   c. Wash aggressively 3 times using 100 µl of FP suitable medium.

5) [Day 0, 2, 4] **Treat with prodrug/drug:**

   a. Remove medium from wells. Add 150 µl/well of FP suitable containing varying concentrations of SN-38G/SN-38 (prodrug/drug).

6) [Day 6] **Measure cell viability.**

7) Studies were carried out over a 6-day treatment cycle, as shown in Table 7.

8) Analyze data by calculating % viability on a per well basis in GraphPad, then compare to control using a two-way ANOVA with Dunnett's post hoc comparisons to the control matched for experimental day. Dunnett's post hoc test can also be used to compare FP + prodrug to the drug, matched for experimental day, to determine if differences in efficacy exist.
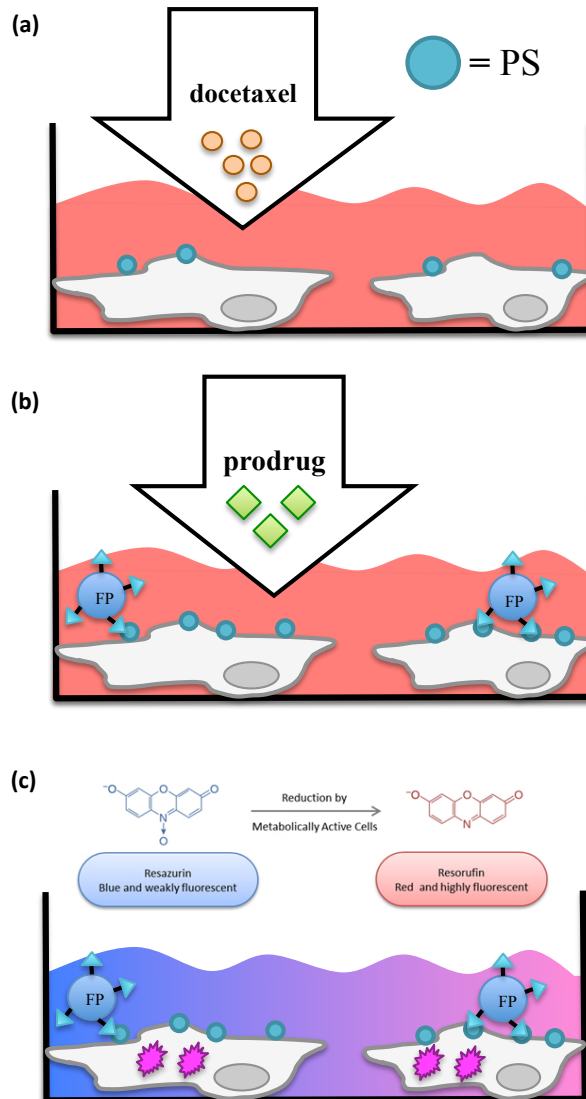
Figure 52: Schematic overview of cytotoxicity assay methodology

(a) Cancer cells were seeded in 24-well plates. Selected wells were treated for 24 h with docetaxel to increase PS expression on the outer leaflet. (b) A saturating concentration (100 nM) of FP was incubated with cells for 2 h every 2-3 days. Residual FP was removed, and cells were then treated with varying concentrations of prodrug. (c) FP in contact with the prodrug, creates cytotoxic drugs (✳). Cell viability was assessed every 1, 2, or 3 days, depending on the protein studied, via the Alamar Blue assay which turns from blue to pink indicating cell viability, as illustrated.

Table 7: Treatment cycles for 3, 6, and 9 day simulated EPT studies

Treatment cycles used for simulated in vitro EPT. "AB" indicates Alamar Blue assay "FP" indicates fusion protein treatment, and "T" indicates prodrug/drug treatments were applied.

	MT-AV, PNP-AV, CD-AV			βG
Day	3 Days	6 Days	9 Days	6 Days
Day 0	AB, FP, T	AB, FP, T	AB, FP, T	AB, FP, T
Day 1	T	T	T	
Day 2	T	AB, T	T	AB, FP, T
Day 3	AB	FP, T	AB, FP, T	
Day 4		AB, T	T	AB, FP, T
Day 5		T	T	
Day 6		AB	AB, FP, T	AB
Day 7			T	
Day 8			T	
Day 9			AB	

A.7 - FITC labeling FPs

FITC Source: Thermo Scientific, Catalog # 46424

Conjugation buffer:

- 50 mM borate buffer

- pH 8.5

Procedure:

1) Dissolve ~1 mg of FP in 0.5 ml of conjugation buffer.

2) Dissolve FITC in DMF at 10 mg/ml. Mix well to completely dissolve the FITC.

3) Add 15- to 20-fold molar excess of FITC to 0.5 ml of FP solution and immediately mix the reaction.

4) Incubate for 1 hour at room temperature in the dark with gentle shaking.

5) Remove excess and hydrolyzed FITC by dialysis (in the dark)

    a. Two, 4-hour dialyses

Dialysis buffer (2L):

- 20 mM sodium phosphate dibasic (5.678 g)

- pH 7.4

A.8 - Flow cytometry: Docetaxel modulated total and specific FP binding

To determine binding of FPs to cancer cells via flow cytometry, FITC labeled FPs are incubated with cells in 24-well plates at various concentrations. Akin to binding strength assays, this procedure can be executed in the presence of Ca^{2+} (total binding) or the in absence of Ca^{2+} with EDTA added to chelate any residual Ca^{2+} (non-specific binding). If docetaxel treatment enhanced FP binding, we would expect to measure more fluorescence intensity, as shown in Figure 53a for PC-3 cells.

Medium:

- Plating = Complete growth medium (with FBS and P/S)

- Doc = Complete medium with docetaxel (stored in DMSO at 100 uM at -20 °C)

    o 50 pM for PC-3 cells

    o 200 pM for Panc-1 cells

- Ca = Plating with 2 mM Ca^{2+} (0.16317 g $CaCl_2$ / 555 ml Media)

- EDTA = Plating + 5 mM EDTA

Procedure:

1) Plate cells in plating medium at 50-100k/well. Incubate overnight at 37 °C, 5% CO_2.

2) Treat selected wells with 300 μl of Doc medium per well. Incubate at 37 °C, 5% CO_2 for 24 h. Exchange medium on control plate with 300 μl FP media per well.

3) Aspirate media. Add 300 μl of CA or EDTA medium to each well containing FITC labeled FPs in desired concentrations. Incubate at 37 °C, 5% CO_2 for 2 hours.

4) Prepare flow samples:

a. Aspirate, wash 3-4 times with Ca/EDTA medium to remove all non-bound FP.

b. Wash 2x with PBS

c. Add 200 μl trypsin/well, incubate 3-4 minutes at 37 °C.

d. Gently loosen cells, add 500 μl Ca or EDTA media to quench

e. Transfer cells to 1.5 ml Eppendorf tube

f. Microcentrifuge for 5 minutes are 100 x g.

g. Aspirate (Carefully, cell pellets will usually not be very visible)

h. Resuspend in 300 μl appropriate FACS buffer

i. Keep cells on ice and in the dark

5) Run Sample on BD Accuri C6

a. Agitate each sample before loading. Check for clumps, as these will clog the flow cytometer.

b. Threshold = 80,000

c. Use excitation of 488 nm (blue laser) and filter set (FL1) 533/30 nm, see Figure 53b

d. Count 5,000 to 10,000 events at slow or medium flow rates

FITC Spectrum (fluorescein isothiocyanate)

- Excitation = 492 (Use blue laser)

- Emission = 520 (Use 533/30 filter, as shown in Figure 53b).

FACS Buffer

- 1x PBS/DPBS

- 0.5% BSA

- 2 mM Ca^{2+} or 5 mM EDTA
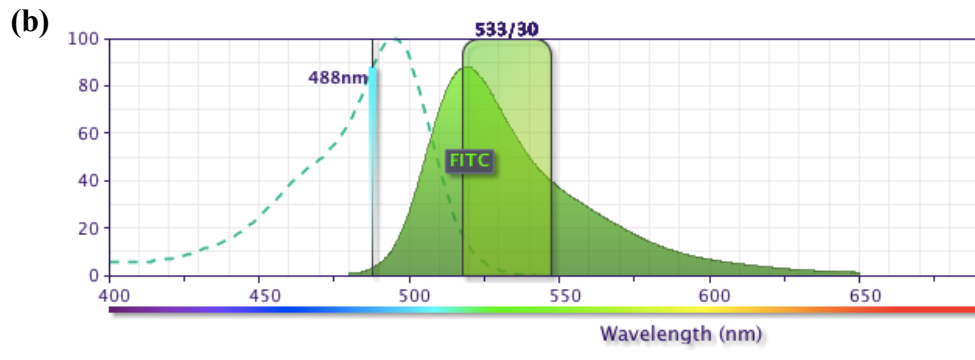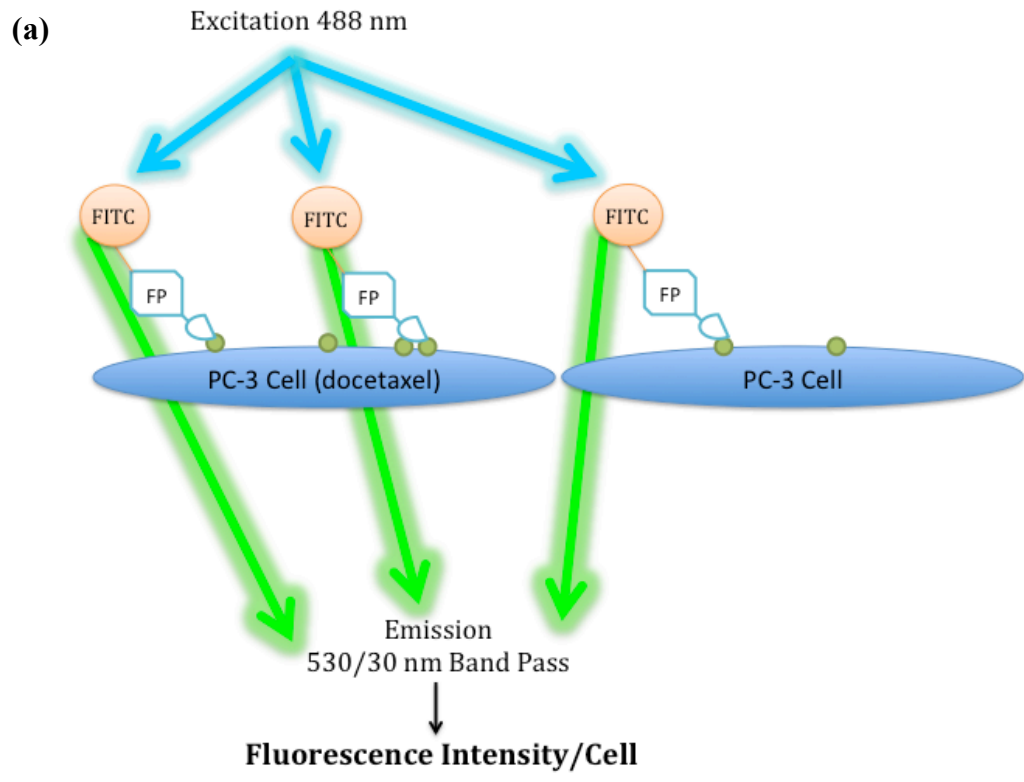
Figure 53: (a) Schematic of flow cytometry FP binding analysis method and (b) FITC spectrum

Image source: Invitrogen Spectraviewer

A.9 - Flow cytometry: Internal vs. external FP binding analysis

Since FITC labeled FPs are free to move across the cell membrane, flow cytometry also allows for the examination of internal vs. external binding by the inclusion of Trypan Blue in the FACS buffer, a well-established method for quenching external fluorescence. By subtracting internal fluorescence (measured in the presence of Trypan Blue) from total fluorescence (measured without Trypan Blue), we are able to compute external fluorescence and therefore measure external binding without inhibiting any internalization that may be occurring.

Medium:

- Plating = Complete growth medium (with FBS and P/S)
- CA = Plating with 2 mM Ca^{2+}

Procedure:

1) Plate cells in plating medium at 50-100k/well. Incubate overnight at 37 °C, 5% CO_2.

2) Aspirate media. Add 300 μl CA media to each well containing FITC labeled FP in desired concentrations. Incubate at 37 °C, 5% CO_2 for 2 hours.

3) Prepare Flow samples:

    a. Aspirate, wash 3-4 times with CA medium to remove all non-bound FP.

    b. Wash 2x with PBS.

    c. Add 200 μl trypsin/well, incubate 3-4 minutes at 37 °C.

    d. Gently loosen cells, add 500 μl CA media to quench trypsin.

    e. Transfer cells to 1.5 ml Eppendorf tube.

    f.   Microcentrifuge for 5 minutes are 100 x g.

    g.   Aspirate (carefully, cell pellets will usually not be very visible).

    h.   Resuspend in 300 μl FACS buffer.

    i.   Keep cells on ice and in the dark.

4)   Run sample on BD Accuri C6

    a.   Agitate each sample before loading. Check for clumps, as these will clog the flow cytometer.

    b.   Threshold = 80,000

    c.   Use excitation of 488 nm (blue laser) and filter set (FL1) 533/30 nm, see Figure 53.

    d.   Count 5,000 to 10,000 events at slow or medium flow rates.

FACS Buffer (total fluorescence)

- 1x PBS/DPBS

- 0.5% BSA

- 2 mM Ca^{2+}

FACS Buffer (internal fluorescence)

- 1x PBS/DPBS

- 0.5% BSA

- 2 mM Ca^{2+}

- 1.2 mg/ml Trypan Blue

A.10 - Preparation of LB plates and broth

A.10.1 LB agar plates

1) Prepare agar as 120 ml of agar mixture in a 500 ml Erlenmeyer flask as shown in Table 8. Swirl the mixture to combine. Mixture will not completely dissolve, but anything left on the glass will burn.

2) Cover the flask with aluminum foil and tape down (DO NOT SEAL) with autoclave tape. Autoclave for 20 minutes.

3) Allow solution to cool to 55 °C in water bath.

4) Add the appropriate amount of antibiotic to the solution and swirl.

5) Pour ~20 ml of agar per 10 cm petri dish.

    a. Pour slowly to avoid bubbles. If bubbles do occur, an inverted Bunsen burner flame can be quickly passed over plate to eliminate these.

    b. Work close to flames of Bunsen burner at all times.

6) Place lids over plate. Let dry for 1 h, until solidified. Invert and let dry overnight.

7) Store at 4°C, with parafilm wrapped around the edges.

8) Use within 1-2 months.

A.10.1 LB broth

1) Combine all components in a 100 ml or a 1L glass bottle, as per the compositions shown in Table 9.

2) Autoclave. Let cool to RT. Add appropriate amount of antibiotic.

Table 8: LB agar plate composition

LB Agar Plates	500 ml (g)	120 ml (g)
NaCl	5	1.2
Tryptone	5	1.2
Yeast Extract	2.5	0.6
Agar	7.5	1.8
Autoclave, then add		
Carbenicillin (100 µg/ml)	/	0.012
Chloramphenicol (25 µg/ml)	/	120 µl of 25 mg/ml stock
Yield		8-10 plates

Table 9: LB broth composition

LB Broth	1L (g)	100 ml (g)
NaCl	5	0.5
Tryptone	10	1
Yeast Extract	5	0.5
Autoclave, then add		
Carbenicillin (100 µg/ml)	0.1	0.01
Chloramphenicol (25 µg/ml)	/	100 µl of 25 mg/ml stock

A.11 - Agarose gel electrophoresis

For separating and visualizing DNA by size, as well as for gel extraction:

1. Dissolve 0.5g agarose into 40 ml of 1x TE buffer in 250 ml beaker (1.25% gel).

2. Add 4 μl of Syber Safe Dye (10,000x).

    a. Omit if using EtBR for gel extraction.

3. Microwave (covered with paper towel) 1:25 minutes (full power) or until rolling boil occurs. Caution – Will be hot! Wrap paper towel around beaker when handling to avoid burns.

4. Cool 3 minutes with shaking (by hand if shaker is in the 4 °C fridge).

    a. If using EtBR for gel extraction, add 2.5 μl of 10 mg/ml EtBR after 2.5 minutes of shaking. Wear double gloves, goggles, and lab coat when handling EtBR.

5. Poor, set for 30-45 min to 1hr. Store at 4 °C, wrapped in plastic for up to 3 days.

    a. After pouring, air bubbles can be removed by poking with pipette tip.

6. Prepare gel for loading

    a. Remove edge pieces and comb

    b. Cover with 1X TE buffer. Make sure wells don't contain air bubbles.

7. Load

    a. 1 μl dye + 2 μl DNA/ladder + 3 μl DI H_2O

    b. Load on negative (black) side.

8. Run at 95 V for 25-40 minutes depending on BPs in product of interest.

    a. 1-3 kBP runs well at 35 minutes

    b. Run large plasmids/gel extractions for 45 minutes.

9. Turn off power supply.

10. View the gel using the UV box. Wear the UV mask!!!

TAE Buffer:

- 1 mM EDTA

- 40 mM Tris

- Acetic acid

- pH 8.0

For 1 liter of 10X TAE Buffer:

- 3.722g EDTA

- 48.456 g Tris

- 11.4 ml of glacial acetic acid

- Diluted in distilled water and pH to 8.0

A.12 - Construction of β-glucuronidase fusion proteins

To produce genes for A1-βG, A1-16a3, and A5-16a3, we expanded individual genes with specially designed tailed primers, digested to create sticky ends, fused these ends, and then cleaned up the final product. An overview of the construction procedure is presented in Figure 54. Products were verified via agarose gel electrophoresis for correct size at appropriate time points during construction.

Note: We originally made three different versions of A1-βG, which are A1-$_s$βG$_p$, A1-$_{ns}$βG$_p$, and A1-$_{ns}$βG. Native βG has a 22 amino acid, N-terminal, signal sequence (notated by "s" with constructs sans the signal sequence notation by "ns" "for no signal") that targets βG to the lysosomes, but is removed during early post-translational processing. Native βG also has an 18 amino acid, C-terminal, propeptide sequence (notated by "p") that is removed by protetolytic cleavage late during or post its delivery to lysosomes.[164] If the propeptide is removed, native βG shows a decrease in catalytic activity, although no decrease in stability.[164] Past fusion attempts have found that excluding the propeptide increases secreted yield, but shows diminished activity.[161]

A.12.1 Expand commercial clones

hA1 and hβG were commercially obtained from Life Technologies, with hA5 already on hand. Clone IDs and sequences can be found in Appendix D.

1) To expand glycerol stock, scrape (with pipette tip) off top of glycerol stock and streak onto agar plate with appropriate selection antibiotic. While scarping, and at ALL OTHER TIMES, keep the glycerol stock on ice.

a. hβG is in the pOTB7 vector with is resistant to chloramphenicol, but hA1 (pDNR-LIB) and hA5 are both stored in vectors resistant to carbenicillin.

b. Grow overnight at 37 °C, inverted.

2) Transfer single colonies into 50 ml of LB broth continuing appropriate selection antibiotic in a 200 ml Erlenmeyer flask, capped loosely with foil. Culture at 37 °C with 200 rpm shaking for 16-18 hours, until OD reaches 0.8-1.

a. To measure OD – 600 nm absorbance vs. blank (LB broth) in 250 μl samples.

3) Extract and purify plasmid according to Qiagen Plasmid Plus Midi Kit using vacuum manifold. Elutes up to 250 μg Plasmid DNA into 100 μl.

4) Measure DNA quantity on Invitrogen Qubit. Follow manufacturer's protocol.

5) Store in 30 μg aliquots at -20C.

a. Sequence verify (OMRF) before fusing/transfecting

A.12.2 Mutant hβG clones

Mutant hβG was custom synthesized via the GeneArt service through Invitrogen and optimized for expression in CHO cells. Vector and sequence information can be found in Appendix E. Purified plasmids as well as corresponding glycerol stocks were purchased so no expansion was necessary. The 5 μg of lyophilized clones were simply resuspended in 50 μl PCR grade water, aliquoted, and stored at -20°C.
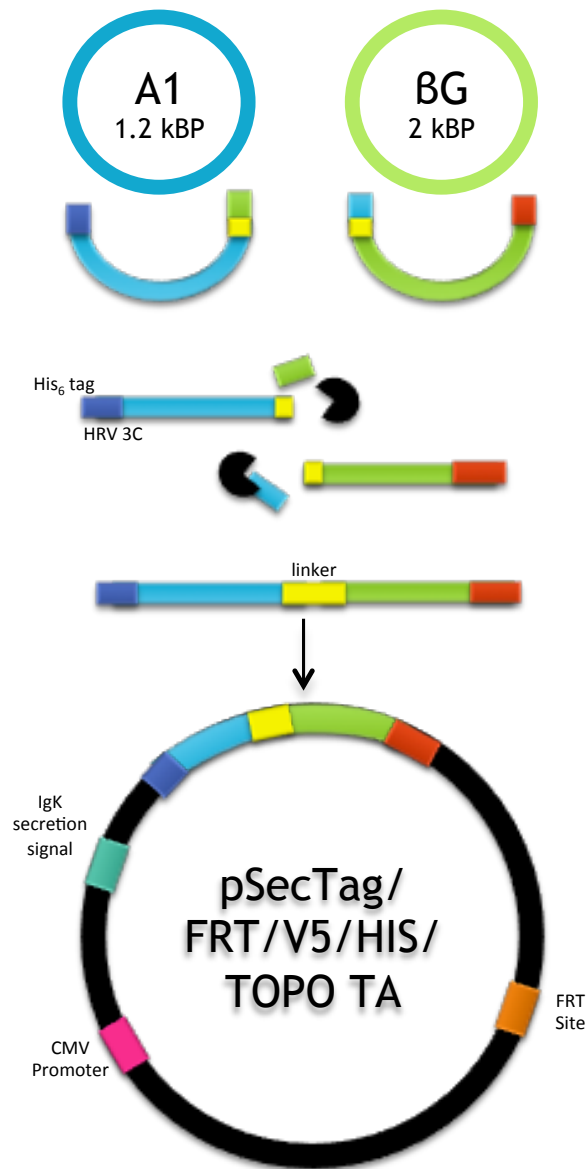
Figure 54: A1-βG construction and ligation into pSecTag diagram

Genes for hA1/hA5 and wild-type/mutant hβG were amplified separately with tailed primers to introduce a His_6 tag with a downstream HRV3C site for ease of tag cleavage (shown in dark blue), a non-immunogenic linker (shown in yellow), and both ends of an EciI restriction site (shown in lime green and light blue), as well as a stop codon on the C-terminal of hβG. Genes were then digested with EciI, shown in black, and fused with T4 ligase to create a fusion gene ready for vector ligation

A.12.3 PCR amplification of individual clones

Primers: All primer formulations can be found in Appendix B. Primers were

reconstituted in TAE buffer, as recommended by IDT to a concentration of 50 μM.

Stocks were further diluted in TAE buffer to a concentration of 10 μM for use in PCR

reactions. All stocks were stored in aliquots at -20 °C. Note: Primers are very large and

must be thoroughly mixed after thawing.

PCR set up: NEB's Phusion High Fidelity PCR kit was used for all PCR reactions. For

all PCR reactions, components were added to PCR tubes in order of decreasing volume.

Phusion PCR Polymerase was added last and kept on ice at all times. Once complete,

PCR set ups were thoroughly mixed before thermal cycling commenced. Successful

PCR conditions for each DNA target are shown in Table 10 for hA1 and hA5, in Table

11 for all versions of wild type hβG, and in Table 12 for mutant hβG.

PCR product verification: All PCR products were cleaned up with the Qiagen PCR

Clean Up Kit (eluted in 50 μl) and verified via agarose gel electrophoresis with the NEB

2 kBP DNA ladder. Sample agarose gels for hA1, hA5, and the 16a3 mutant amplicons

can be found Figure 55a.

A.12.4 EciI digestion

To create sticky ends on the C-terminal of A1 or A5 and on the N-terminal of the

selected hβG construct:

1) Combine, on ice:

a. 40 μl of A1, A5, or selected variety of hβG (~200 ng/μl)

b. 5 μl 10x NEB CutSmart Buffer

c. [Last] 5 μl of EciI

d. Mix thoroughly.

2) Cut by incubating at 37 °C for 60 minutes, followed by inactivation at 65°C for 20 minutes. Run in thermal cycler.

3) Purify digested genes with Qiagen PCR Clean Up Kit (elute in 50 μl).

A.12.5 T4 ligation

In order to fuse the sticky ends use T4 ligase as follows:

1) Combine on ice:

a. 30 μl EciI digested A1 or A5

b. 30 μl EciI digested hβG (any variety)

c. 7.4 μl 10x T4 buffer

d. [Last] 6 μl of 10x T4 ligase

e. Mix thoroughly

2) Ligate by incubating at 37 °C for 240 minutes (4 h), followed by inactivation at 65 °C for 10 minutes. A sample agarose gel of pre-gel extraction fusion constructs is shown in Figure 55a.

a. Note: A 2 h ligation will yield much less fused product.

3) Purify via gel extraction:

a. Load all fused product onto an ethidium bromide (EtBR) agarose gel.

b. Run gel.

c. While wearing double gloves, goggles, lab coat, face shield, and closed toed shoes, use a clean sharp scalpel to excise the correct fused fragment.

d. Follow Qiagen Gel Extraction Purification Kit protocol for purify.

e. Measure DNA quantity with Qubit.

f. Store at 4°C for short periods of time (days), but best if used immediately.

4) Samples of post-gel extracted fused constructs are shown in Figure 55b for hA1-16a3 and hA5-16a3.

Table 10: hA1 and hA5 PCR amplification – concentrations and thermal cycle conditions

Input (for hA1)	Volume (ul)	Initial [uM]	Final [uM]	Target []
dNTPs	1	10 mM	200	200 uM
Forward Primer	2.5	10	0.5	
Reverse Primer	2.5	10	0.5	(0.2-1uM) 0.5 uM
Plasmid (hA1)	1	0.5 (ug/ul)?	0.01	1 pg -10 ng
HF Buffer	10	5x	1x	1x
DMSO	1.5		3%	3%
Phusion (Add Last)	0.75			1U/50 ml
PCR Grade H2O	30.75			
Total	50			

3 Step PCR		# clcyles	Temp (C)	Time
	Initial Denaturation	1	98	3 min
Amplification	Denaturation		98	10 sec
	Annealing	35	52 - hA5, 58 - hA1	15 sec
	Extension		72	30 sec
	Final Extension	1	72	10 min
	Cooling	1	4	∞

Table 11: hβG (± signal, ± propeptide) Two-Step PCR amplification –

concentrations and thermal cycle conditions

Input (for BG) 1x +/- Pro	Volume (ul)	Initial [uM]	Final [uM]	Target []
dNTPs	1	10 mM	200	200 uM
Forward Primer	2.5	10	0.5	
Reverse Primer	2.5	10	0.5	(0.2-1uM) 0.5 uM
Plasmid (hBG)	1	0.5 (ug/ul)?	0.01	1 pg -10 ng
Buffer	10	5x	1x	1x
DMSO	1.5		3%	3%
Phusion (Add Last)	0.75			1U/50 ml
PCR Grade H2O	30.75			
Total	50			

2 Step PCR		# clcyles	Temp (C)	Time
	Initial Denaturation	1	98	3 min
Amplification	Denaturation	35	98	10 sec
	Extension		72	30 sec
	Final Extension	1	72	10 min
	Cooling	1	4	∞

Table 12: h16a3 βG mutant (propeptide) PCR amplification – concentrations and thermal cycle conditions

Input (for 16a3)	Volume (ul)	Initial [uM]	Final [uM]	Target []
dNTPs	1	10 mM	200	200 uM
Forward Primer	2.5	10	33.33	(0.2-1uM) 0.5
Reverse Primer	2.5	10	33.33	uM
Plasmid (hA1)	1	0.5 (ug/ul)?	0.01	1 pg -10 ng
HF Buffer	10	5x	1x	1x
DMSO	1.5		3%	3%
Phusion (Add Last)	0.75			1U/50 ml
PCR Grade H2O	30.75			
Total	50			

3 Step PCR		# clcyles	Temp (C)	Time
	Initial Denaturation	1	98	3 min
Amplification	Denaturation		98	10 sec
	Annealing	35	67-72	15 sec
	Extension		72	30 sec
	Final Extension	1	72	10 min
	Cooling	1	4	∞

 * 67-72 was a run as a temperature gradient and all temperatures were found to be equally successful
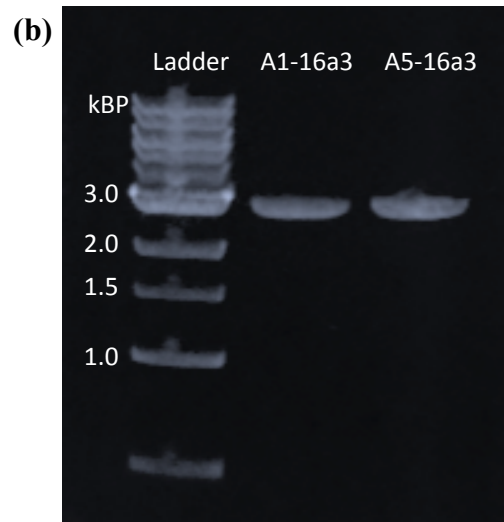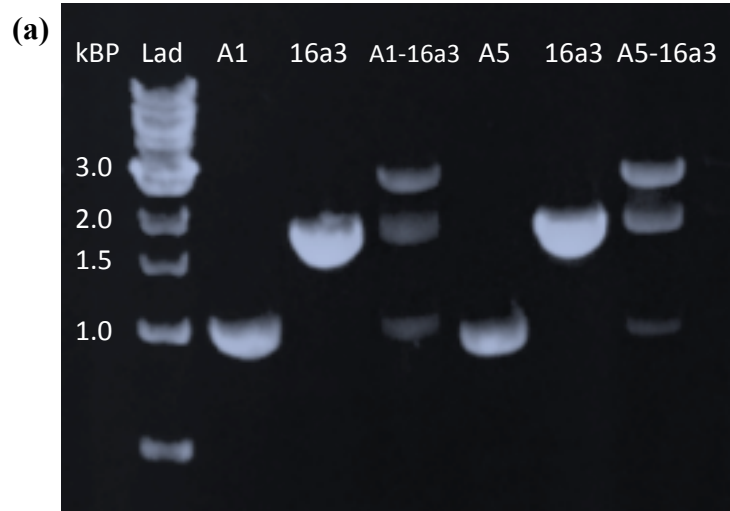
Figure 55: Pre (a) and post (b) gel extraction agarose gels of hA1-16a3 and hA5-6a3

A.13 - pSecTag/FRT Vector Ligation

We chose to ligate our fused genes into the pSecTag/FRT/V5-His-TOPO® Vector because it carries a CMV mammalian promoter, an SV40 mammalian promoter enhancer, an FRT site for the creation of stable producer cell lines, and most importantly a IgK secretion signal that will ensure our fusion proteins end up outside of the cell for easy harvest as opposed to degraded in the lysosomes, since hβG is generally shuttled there.

We did run into some issues with this vector: (i) The storage and shipping conditions are of paramount importance. This vector is shipped pre-linearized, but even slight changes in temperature will cause it to bind to itself, therefore making it unusable for ligations. This vector must be stored in the back of the -20°C freezer and should never be removed (as in you will need to pipette while the tube is still in the freezer). (ii) Although the vector cloning is in theory directionally independent, we did notice that for some constructs there was a strong preference for backwards insertion. Due to these issues, we completed two different restriction digests, and only sent plasmids that showed correct fragments for both digests to sequencing at OMRF. More time investment, but much cheaper.

To ligate our fused genes, we utilized a version of a protocol different from Invitrogen's published protocol provided with the vector. This is because our insert is relatively large. The following protocol has been adapted from an FAQ response on Invitrogen's website, specific to inserts of large size.

Adding 3' A- overhangs: Since we use a HF Phusion polymerase for amplification, our fused genes have blunt ends. However, the vector ligation relies on 3' A overhangs which are left by all Taq polymerases. This step must be done immediately before ligation, otherwise the 3' A overhangs will simply fall off.

1) Combine, on ice:

    a. 5 μl of DNA input (~50 ng/μl)

    b. 0.7 μl 10x NEB Taq buffer

    c. 0.5 μl dNTPs

    d. [Last] 0.5 μl NEB Taq

    e. Mix thoroughly.

2) Incubate in thermal cycler at 72°C for 20 minutes, then cool to 4°C.

3) Calculate final concentration, since DNA has been diluted.

Ligate into PsecTag vector:

1) Combine (in this order):

    a. 14.9 μl PCR grade H_2O

    b. 3.7 5 μl provided salt solution in vector box

    c. Mix thoroughly.

    d. Add in 0.5 μl of DNA.

    e. Add in ~ 0.9 μl of vector .

        i. May change a little depending on DNA concentration – aim to keep insert:vector molar ratio at 1:1.

        ii. Remember to pipette this vector IN THE FREEZER.

    f.   Mix gently.

        i.   Total reaction volume = 20 μl

2) Incubate at room temperature for 30 minutes.

Transform ligated vector into Top10 *E. coli:*

1) In an ice water bath, without submerging the vial, thaw one vial of Top10 competent *E. coli cells.*

2) Add 20 μl for the ligation reaction (all of it) to the vial of cells. DO NOT PIPETTE UP AND DOWN TO MIX. Mix gently by swirling.

3) Incubate on ice for 10 minutes.

4) Heat shock the cells for 30 seconds (and only 30 seconds) in the 42 °C water bath.

5) Immediately place tubes back on ice.

6) Add 250 μl SOC outgrowth medium to vial.

7) Cap tube tightly and incubate horizontally at 37 °C, 200 rpm for 1 h.

8) Plate 50 μl of cells in SOC into 50 μl of fresh SOC medium on agar plates with carbenicillin. Grow overnight, up-side down, at 37 °C.

9) The next morning, lift individual colonies, and transfer into 5 ml of LB broth with carbenicillin in round-bottomed culture tubes. Grow overnight at 37°C, 200 rpm.

10) Extract plasmids (but save 100 μl for potential glycerol stocks, at 4 °C, if clones are correct) and purify (24 at a time) with the Qiagen Miniprep Kit. Using the vacuum manifold significantly simplifies this task.

BamHI restriction digest

1) Make a reaction stock solution, on ice (given for 26 digest reactions):

   a. 15.6 μl 10x NEB 4 Buffer

   b. 136.5 μl PCR grade water

   c. 3.9 μl BamHI

   d. Mix thoroughly

2) For each plasmid combine, on ice:

   a. 3 μl plasmid

   b. 6 μl reaction stock

3) Incubate for 30 minutes at 37 °C in thermal cycler.

4) Add 2 μl loading dye to each sample, and run on agarose gel.

5) Depending on the fragments, we can tell if the insert is forwards of backwards as shown in diagram in Figure 56a. Sample restriction digests for hA1-16a3 are shown in Figure 57.

EciI restriction digest: Take positive clones from BamHI digest and further analyze them with an EciI restriction digest.

1) Make a reaction stock solution, on ice (given for 5 digest reactions):

   a. 3.12 μl 10x CutSmart Buffer

   b. 3.9 μl EciI

   c. 24.28 μl PCR grade water

   d. Mix thoroughly

2) For each plasmid combine, on ice:

       a. 3 μl plasmid

       b. 6 μl reaction stock

3) Incubate for 60 minutes at 37 °C in thermal cycler.

4) Add 2 μl loading dye to each sample, and run on agarose gel.

5) Depending on the fragments, we can tell if the insert is present as shown in

    diagram in Figure 56b. Sample EciI restriction digests are shown in Figure 58.

What we expect to see with BamHI

Fused Psec	hA1 16a3	hA1 16a3 BKW	hA5 16a3	hA5 16a3 BKW
	7175		7097	
		5459		5459
5185				
		2044		1966
	679	679	679	679
	328		328	

(b) **What we expect to see with EciI**

Fused	hA1 16a3	hA5 16a3
	2276	2276
2040	2040	2040
1526	1526	1526
	1366	1288
828	828	828
633		
146*	146*	146*

Figure 56: Theoretical Restriction Digests with BamHI and EciI

Theoretical restriction digests are shown for BamHI and EciI. (a) To verify insert directionality, since pSecTag ligation is direction independent, we used BamHI restriction digest analysis of clones (typically 24 at a time). The lack of a 2107 kBP fragment was determined to be a good indicator of correct directionality. (b) To further verify insert presence, EciI restriction digests were preformed on positive clones from BamHI digests. Fragments at 1906 and 1366 kDa were used as indicators of insert presence within the vector. * Indicates that the fragment is likely too small to be seen on the agarose gel.
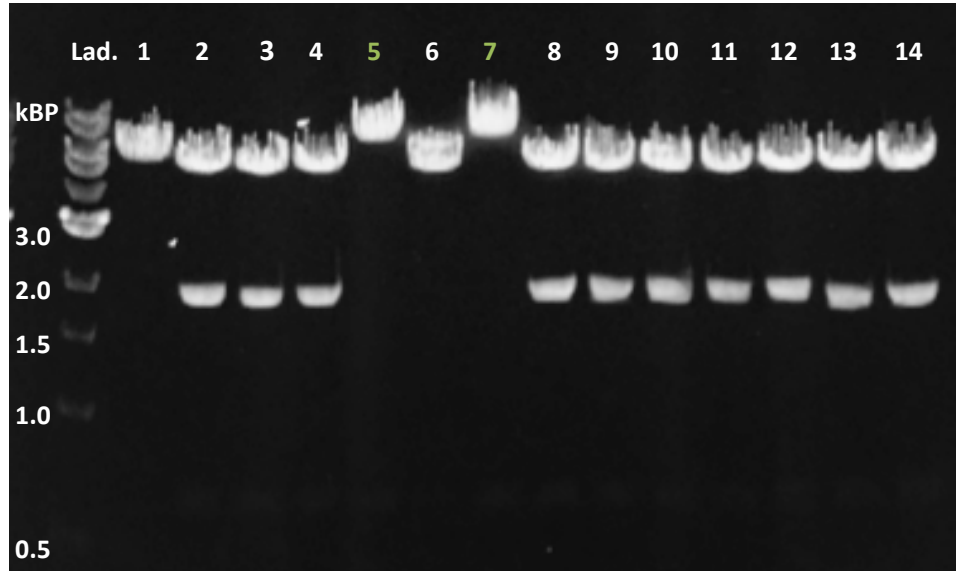
Gel #1 (0.4g Agarose in 40 m, 95V, 40 min)		Result
Lane 0	NEB 1kb	/
Lane 1	Clone A1 1	Fused
Lane 2	Clone A1 2	BWK
Lane 3	Clone A1 3	BWK
Lane 4	Clone A1 4	BWK
Lane 5	Clone A1 5	Correct
Lane 6	Clone A1 6	Fused
Lane 7	Clone A1 7	Correct
Lane 8	Clone A1 8	BWK
Lane 9	Clone A1 9	BWK
Lane 10	Clone A1 10	BWK
Lane 11	Clone A1 11	BWK
Lane 12	Clone A1 12	BWK
Lane 13	Clone A5 1	BWK
Lane 14	Clone A5 2	BWK
A1	% ligated	83%
	% forward	20%

Figure 57: Sample agarose gel of BamHI digests pSecTag ligation

hA1-16a3 ligated into pSecTag vector and digested with BamHI. Results identify 2 positive clones in lanes 5 and 7 as seen by the lack of a band around 2 kBP and a band around 7 kBP as opposed to the backwards ligations with a band around 5 kBP.

226
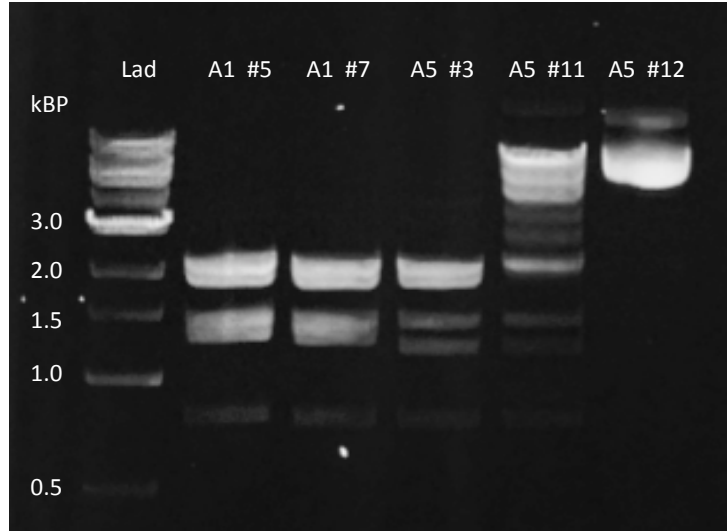
Gel #3 (0.4g Agarose in 35 ml)		Result
Lane 0	NEB 1kb	/
Lane 1	Clone A1 5	Correct
Lane 2	Clone A1 7	Correct, Seq
Lane 3	Clone A5 3	Correct, Seq
Lane 4	Clone A5 11	Incorrect
Lane 5	Clone A5 12	Incorrect

Figure 58: Sample agarose gel of EciI digests post pSecTag ligation

Clones identified as correct by BamHI digests for hA1-16a3 (lanes 1-2) and hA5-16a3 (lanes 3-5) digested with EciI for secondary confirmation. Both A1-16a3 clones show correct retraction digest fragments, but only A5-16a3 #3 shows correct pattern. Sequences for both clones sequenced turned out to be 100 % correct.

A.14 - CHO FLP-IN transfection/selection

In order to create stable, constitutively expressing, cell lines, we embedded out genes in pSecTag vectors into the FRT site in CHO Flp-In cells. When purchased form Invitrogen, these cells contain a single FRT genomic recombination site that has been shown to be integrated into a highly transcriptionally active genomic locus. CHO Flp-In cells are resistant to the antibiotic Zeocin, until they are transfected, at which point they become Zeocin sensitive by hygromycin B resistant. An overview of the transfection process is provided in Figure 59. To integrate our gene of interest into the CHO cell genone, CHO Flp-In cells were co-transfected with our genes of interest in the pSecTag vector and POG44, which generates Flp-In recombinases upon transfection that then recombine the pSecTag vector into the FRT site in the Flp-In cells. Details of this genomic recombination event are shown in Figure 60. This recombination event inserts an ATG codon upstream of the hygromycin B resistance gene allowing successfully transfected cells to be easily identified under antibiotic selective pressure. Since there is only one FRT site/cell, there is no need for selection by limiting dilution. Once selection is complete (> 3 weeks), cells are ready to be scaled up for protein production in suspension culture.

CHO Flp-In cell culture:

    1) Maintain CHO cells in T-75 flasks at 37°C and 5% CO_2 in:

        a) Ham's 12 Medium

        b) 10 % FBS

        c) 1% P/S

d) 2 mM L-glutamine

e) 100 μg/ml Zeocin

2) Cells are split 1:5-1:10 every 2-3 days or medium exchanged. Word of caution: these cells grow very fast.

Transfection

1) **[Day -1]** Plate Cho Flp-In cells at a density of 7.5×10^5 cells/35 mm cell culture dish (2 ml plating volume) in complete growth medium with Zeocin. Allow to adhere overnight at 37 °C and 5% CO_2.

2) For pilot transfections, appropriate controls need to be included, as shown in Figure 61. To determine the effect on s, ns, and p species on transfection efficiency and ensuing yield, each A1-hβG variety was transfected with either 3.75 μl of Lipofectamine 3000, or 7.5 μl Lipofectamine 3000, as recommended by the manufacturer and as shown in Figure 61. When preforming pilot transfections, be sure to plate enough cells to include all controls.

3) **[Day 0]** Per dish:

a) Combine 125 μl of Opti-MEM medium with 7.5 μl of Lipofectamine 3000. Vortex for 2-3 seconds to combine.

b) Prepare master mix of DNA

   i. 125 μl Opti-MEM medium

   ii. 5 μl of P3000 reagent

   iii. 2.5 μg of DNA total: Flp-In transfections require a ratio of 9:1 of POG44:pSecTag as we want recombination to be a relatively rare

229

event. This means we need 2.25 µg of POG44 and only 0.25 µg of the pSecTag vector containing our gene of interest.

    iv. Mix well.

  c) Add 125 µl diluted DNA to 125 µl diluted Lipofectamine 3000.

  d) Incubate 5 minutes at RT.

  e) Aspirate medium from cells and wash with PBS 2x.

  f) Add 2 ml of F12 medium with FBS and L-glutamine, but without any antibiotics (No Zeocin, no hygromycin B, and no P/S) to each well.

  g) Add 250 µl of DNA-Lipofectamine 3000 complexes to cells.

  h) Incubate for 24 h at 37 °C and 5% CO_2.

4) **[Day 1]** After 24 hours, replace medium on all plates with F12 medium with FBS and L-glutamine, but without any antibiotics (No Zeocin, no hygromycin B, and no P/S).

5) **[Day 2]** After another 24 h, transfer cells to T-75 flaks (1 plate/flask) and begin hygromycin B selection.

  a) Wash cells with 1 ml PBS.

  b) Lift cells using 1 ml trypsin/plate for 5-7 minutes.

  c) Quench with 2 ml F-12 + FBS.

  d) Centrifuge and aspirate off old medium.

  e) Resuspend in F-12 + FBS + P/S + L-glutamine + 600 µg/ml of hygromycin B.

6) **[Days 3-21]:** Observe as cells begin to form foci as shown in Figure 62. Add fresh complete growth medium with hygromycin B every 2-3 days. Once cells

reach 70-80% confluence, begin splitting 1:3-1:10 every 1-5 days, depending on cells growth.

7) If conducting pilot studies, control vs. transfected viability can be tracked on 24 well plates using the same selection conditions as in the T-75 flasks, by measuring cell viability via a presto blue assay (10 minute incubation time) on 24 well plates, as shown in Figure 61.

During transfection optimization, we found that 7.5 μl Lipofectamine 3000 greatly increased transfection efficiency with minimal effect on cell health during transfection, as shown in Figure 63. We also found that constructs that include the signal sequence preform much worse post transfection, Figure 63, although they can eventually be coaxed to grow under selective pressure. However, we felt that this data was sufficient to exclude the signal sequence from all future constructs.
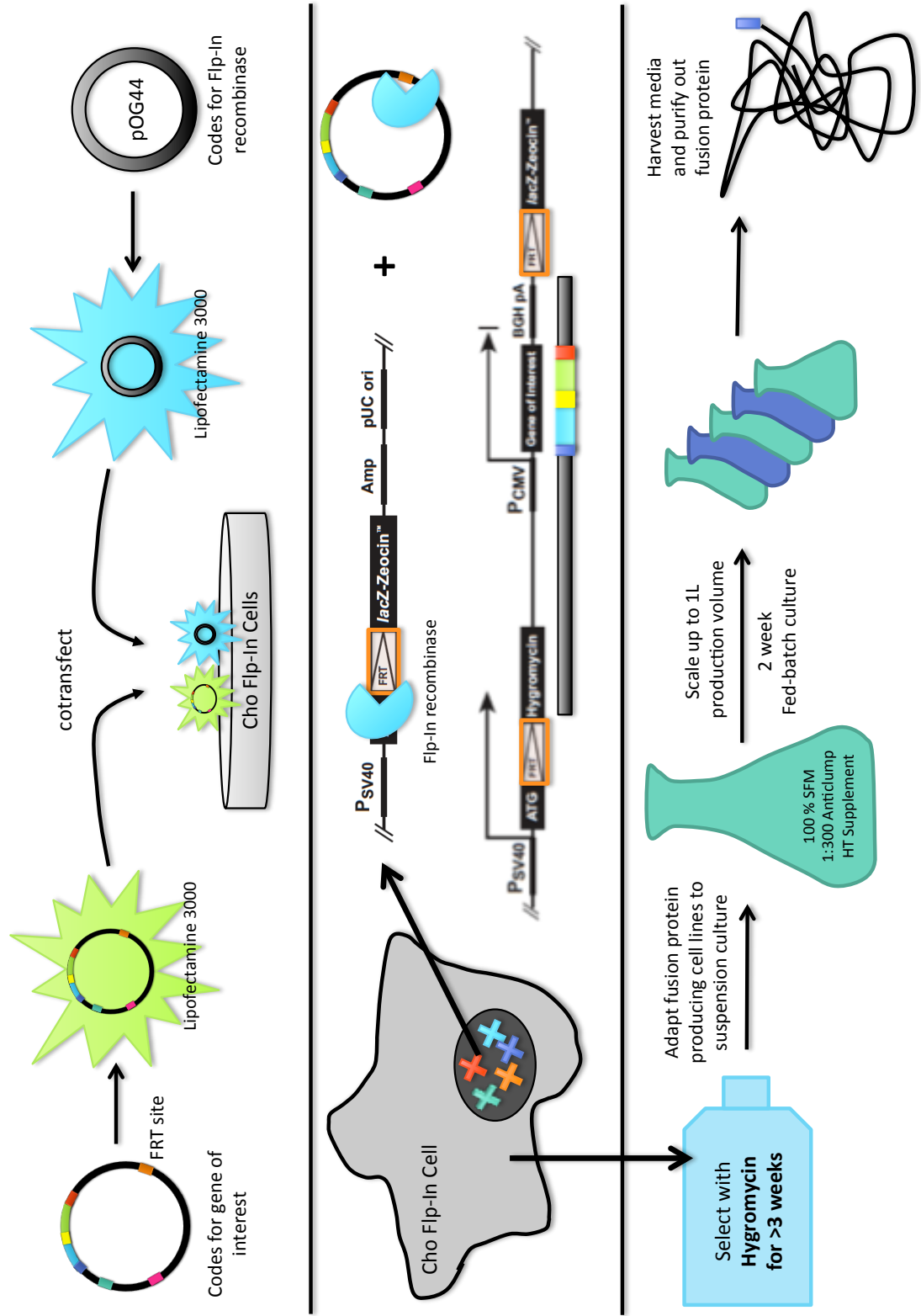
Figure 59: Schematic overview of transfection /selection /production of β-glucuronidase fusion proteins

1. pFRT/*lac*Zeo is stably transfected into the mammalian cells of interest to generate the Zeocin™-resistant Flp-In™ Host Cell Line(s)

Expression of *lacZ* and Zeocin™ fusion gene

P_SV40 ATG FRT *lacZ*-Zeocin™ Amp pUC ori Flp-In™ Host Cell Line

2. The pcDNA5/FRT expression vector containing your gene of interest (GOI) is cotransfected with pOG44 into the Flp-In™ Host Cell Line.

+ pOG44
+ pcDNA5/FRT

P_SV40 ATG FRT *lacZ*-Zeocin™ Amp pUC ori Flp-In™ Host Cell Line
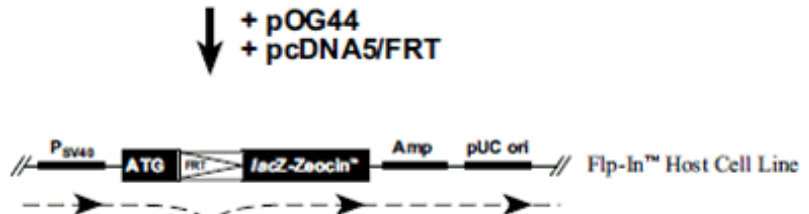
3. The Flp recombinase expressed from pOG44 catalyzes a homologous recombination event between the FRT sites in the host cells and the pcDNA5/FRT expression vector.

pcDNA5/FRT Expression Vector

GOI BGH pA FRT Hygromycin pUC ori Amp P_CMV
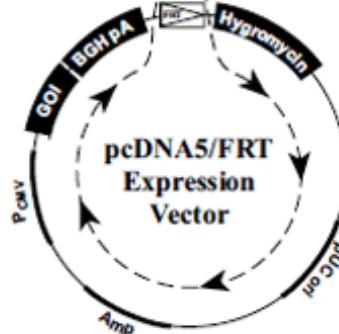
4. Integration of the expression construct allows transcription of the gene of interest (GOI) and confers hygromycin resistance and Zeocin™ sensitivity to the cells.

Expression of hygromycin   Expression of your gene

P_SV40 ATG FRT Hygromycin pUC ori Amp P_CMV GOI BGH pA FRT *lacZ*-Zeocin™ Amp pUC ori

Flp-In™ Expression Cell Line
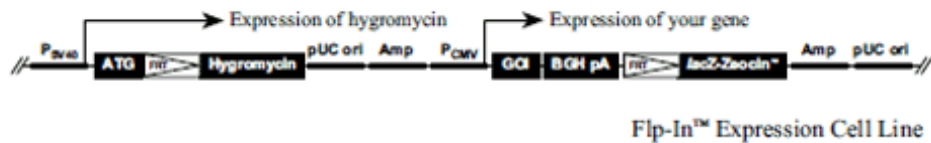
Figure 60: Genomic events of Flp-In recombination post transfection (Invitrogen)

FRT is a genomic integration site. CHO Flp-In cells have been transfected to contain an FRT site. When co-transfected with a Flp-In recombinase vector (pOG44), pSecTag containing hA1-βG can be integrated into the genome and stably expressed after selection with hygromycin B, resistance to which is conferred to the cells upon integration of an ATG start codon directly upstream of the hygromycin B site from the pSecTag vector. Image Source: Invitrogen.

233
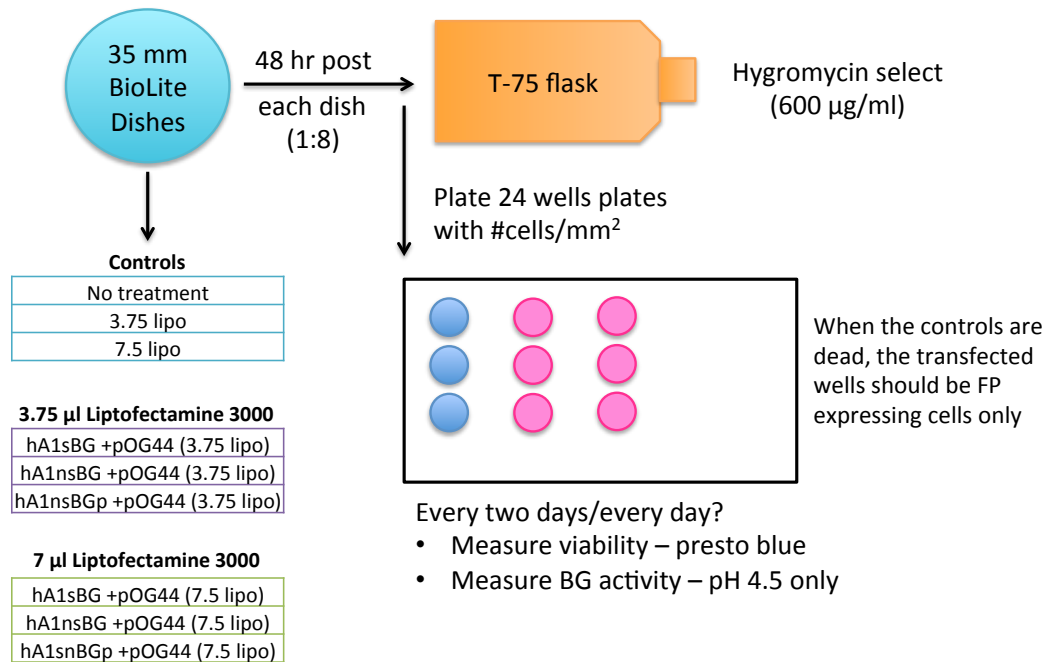
Figure 61: Cho Flp-In Transfection Optimization Set-Up

Cho Flp-In cells were plated on 35 mm cell culture treated dishes in medium containing Zeocin, and allowed to adhere. To test different Lipofectamine 3000 concentrations as well as the effect of signal (s and ns) and the propeptide (p), we transfected 9 different conditions including controls sans DNA. After 48 hours, cells were transferred to T-75 flasks and hygromycin B selection began. To track post transfection viability differences, we also mimicked T-75 flask cultures on 24 well plates that were monitored via the presto blue assay, for which results are shown in Figure 63.
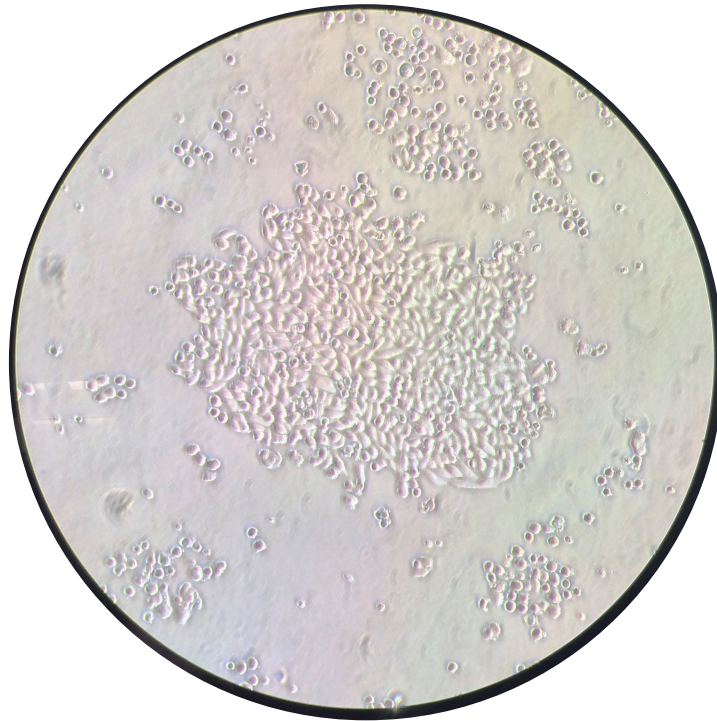
Figure 62: hA1nsBGp transfected CHO FLP-IN cells

Cho Flp-In cells cotransfected with hA1nsBGp and POG44 with 7.5 μl Lipofectamine

3000 formed foci in culture under high selective pressure with 600 μg/ml hygromycin

B. Cells are shown in T-75 flasks on day 8 post transfection. Cells were imaged with

an iPhone on Dr. Nollert's light microscope.
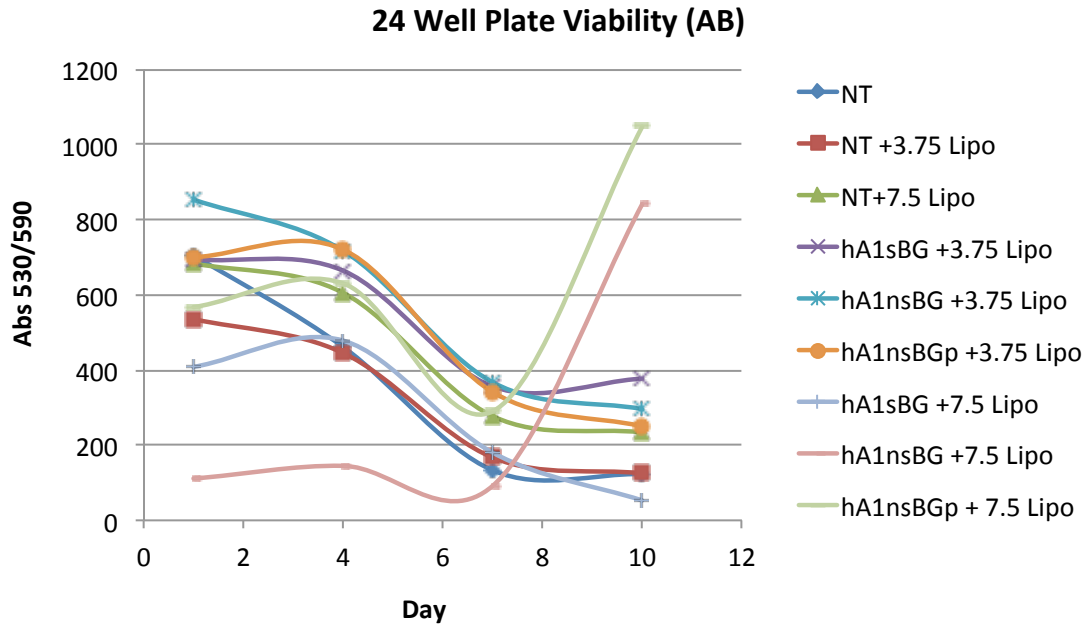
Figure 63: CHO Flp-In post-transfection viability under selective pressure

We tracked viability of $hA1_s\beta G_p$, $hA1_{ns}\beta G_p$, and $hA1_{ns}\beta G$ in 24-well plates post transfection under hygromycin B selective pressure. Day 0 indicates 48 hours post-transfection, when cells were transferred to either T-75 flasks or the 24-well plate in the appropriate ratio. 7.5 μl Lipofectamine 3000 was much more effective than 3.75 μl Lipofectamine 3000 for $hA1_{ns}\beta G_p$, and $hA1_{ns}\beta G$ and was utilized in all future transfections. $hA1_s\beta G_p$, which contains the signal sequence, did not fare as well, but the 3.75 μl Lipofectamine transfection did eventually grow, but these latter cells were simply stored as stocks, and no further work was conducted without removing the signal sequence.

A.15 - Production of β-glucuronidase fusion proteins

Cell line: CHO Flp-In Cells co-transfected with PSecTag/Insert and POG44 (1:9),

selected for > 3 weeks in 600 μg/ml hygromycin B.

Adaptation:

1) Thaw frozen adherent stocks as per standard protocol. Grow cells to 80%
   confluence, switching complete medium (F-12 + FBS + P/S + 2 mM L-
   glutamine + 600 μg/ml hygromycin B) every two days.

2) Split cells 1:3 into 3 T-75 flasks, each containing 10 ml complete medium and 5
   ml SFM4CHO medium *without* HT supplementation or anticlumping agent
   (AC). Grow to 80% confluence, replacing media every 2 days. This should not
   take more than 1-2 days. CHO cells grow very rapidly.

3) Lift cells (quench with 100% complete F12 medium), centrifuge, resuspend in
   50 ml complete SFM4CHO (with L-glutamine and sodium bicarbonate, then add
   20 ml 50x HT supplement, or 10 ml 100x HT, and 1:333 AC (3 ml into 1L)) in
   3x E-125 flasks. Incubate at 37 °C, 110 RPM, and 5% CO_2.

4) Count cells every two days. If cells are not ready to be passaged by day 2-3,
   centrifuge and resuspend in new complete SFM4CHO.

Passaging: The goal is to keep the cell density between **$3x10^5$ to $3x10^6$ cells/ml** prior to

the inoculation of large-scale suspension cultures. Cells can be passaged as early as

$1x10^6$. Suspension cultures only need to be centrifuged once every 1-3 passages, more

frequently if they were recently thawed or adapted. There are two options for passaging cells:

1) Dilution: Simply dilute cells into fresh complete SFM4CHO complete medium to obtain a density of $3x10^5$.

2) Complete media exchange: Centrifuge cells (~1000 for 5 min), then resuspend in appropriate flask/volume

   a. E-125: 30-50 ml

   b. E-250: 75-100 ml

   c. E-500: 150-200 ml

Cryopreservation: Cells adapted to SFM4CHO cells are be cryopreserved in a 1:1 ratio of fresh and conditioned SFM4CHO, with 7.5% DMSO added. Cells should be cryopreserved such that one vial yields $3x10^5$ cells/ml in 50 ml in a 125 ml Erlenmeyer flask.

Fed batch culture:

Used to produce protein over 2 weeks in 1 L cultures (preferably 5x E-500 flasks).

Note - If using a new cell line or new conditions, count cells frequently, i.e. on days 0, 2, 4, 6, 8, 10, 12, and 14, and take a 500 μl sample for activity assay etc. Be sure to centrifuge sample (microcentrifuge in D-201) to remove cells; set centrifuge dial to 2000 rcf (~1000 x g) for 5 min.

1) Initiation: Seed cells at 3×10^5 cells/ml in 180 ml media. For hA5-16a3 cells, cultures appear to preform better at a slightly lower seeding density of 2.5×10^5 cells/ml. These cells should have been passaged 1-2 times since thawing, and have had AT LEAST ONE complete media exchange since thawing, but two is preferable. Cells should be in the logarithmic growth phase, with a doubling time of approx. 20 h. Count cells! Do not skip counting cells. If you do not count cells, cultures will underperform or crash out. Also, play special attention to seeding density. Slight changes will drastically affect cultures. After counting cells, use this formula:

$$\text{ml suspension cells into E500} = \frac{\left(3 \times 10^5 \left(\frac{\text{target cells}}{\text{ml}}\right)\right) * 180 \text{ ml}}{\text{cell culture density} \left(\frac{\text{cells}}{\text{ml}}\right)}$$

$$\frac{\text{ml SFM media}}{\text{E500 flask}} = (180 \text{ ml}) - \text{ml suspension cells}$$

2) Feeding: On day 4 (log growth phase) feed with 20% (so for an E-500 flask, this is 40 ml), and on day 9 (steady phase) feed with 10% (20 ml for E-500 flask).[165] Feedings of 50 ml at Day 4 appear to work just as well with no follow-up feeding at day 9, but further optimization may be possible.

   a. How to prepare Cell Boost 2 (3.5% w/v)

      i. Weigh out 35 g Cell Boost 2.

      ii. Dissolve in 900 ml sterile DI water (use beaker).

      iii. Stir for 30 minutes.

      iv. Titrate to 1000 ml.

      v. Vacuum filter (in laminar flow hood).

<div align="right">
vi.   Add 1:300 (3 ml/L) anticlumping agent.

vii.   Store at 4 °C.
</div>

3) <u>Harvest:</u> Transfer cells to 50 ml tubes (will need at least 20). Centrifuge (D-211) at 2500 rcf for 10 minutes. Pour off supernatant into 1 L glass bottle. Pour down the side to avoid bubbles. Store at 4 °C in the dark until ready for purification. Do not store for > 4 h.

Sample fed-batch production curves for cell count, cell viability, and βG activity are shown in Figure 64. Cells begin clumping around day 4, causing to apparent drops in cell density. However, viability remains above 85% until day 14, and βG activity continues to increase throughout the culture duration.

Troubleshooting:

1) **Slow growing cells post thawing** – passage 1:1 with complete medium exchange every 2 days. Check expiration dates on medium, HT, AC. If cells do not grow, try a vial from a different cryopreservation batch or simply adapt a new adherent vial to suspension culture.

2) **Shaker keeps turning off** – Check to make sure the switch is flipped up. Down is the timer setting, and the shaker will shut off automatically.

3) **Cells crash out after 3-4 days** – If your large-scale suspension cultures look white but without an odor and appear normal, but highly populated under the microscope, then may have been seeded seeded too high. If there are too many

<div align="center">240</div>

cells to begin with, they grow too quickly and are unable to cope with the lack of nutrients, so they crash out, and very little protein is produced.

4) **Contamination** – If your flasks are white and smell terribly awful it time to toss, disinfect, use new media, and possibly make more Cell Boost 2. These cells grow for very long timeframes without antibiotics. Losing all flasks is a sign of systemic trouble. Losing 1 out of 8 occurs occasionally, and does generally not indicate a systemic issue. Make sure you spray everything with EtOH a lot, just avoid spraying the filter caps.

5) **Cryopreservation** – Although cells should keep their inserts under cryopreservation for > 1 year, we noticed that this may not be the case as cells were only stored successfully for approx. 4 months. When in doubt, adapt new adherent cells, since antibiotic selection is present in adherent but not suspension culture.
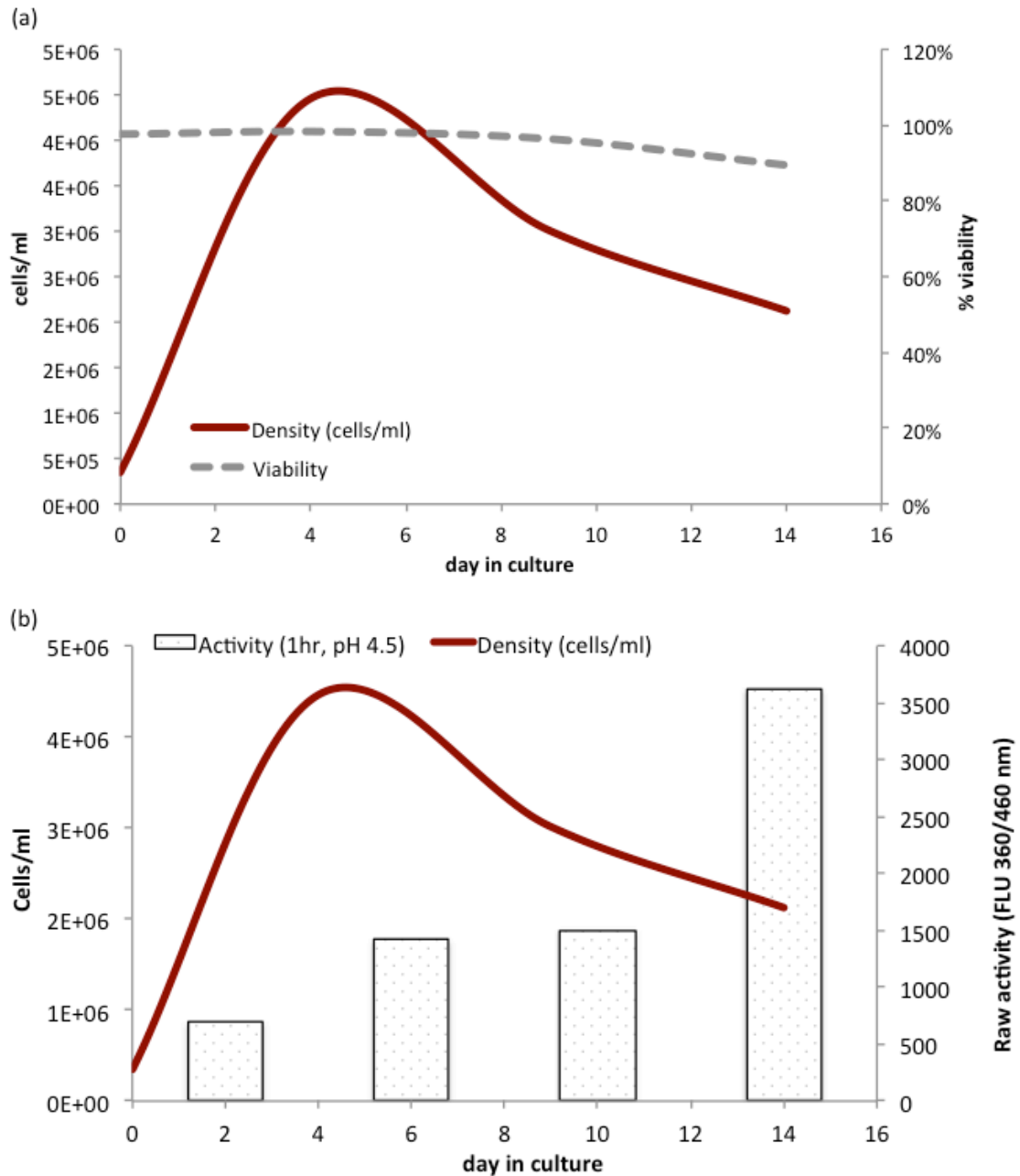
Figure 64: Sample βG production curves

Production curves, (a) cell count and viability and (b) cell count and βG activity are shown for hA1-16a3. This was a 2 L fed-batch production run. Cells were counted on a hemocytometer using the Trypan Blue dye exclusion method for viability determination.

A.16 - Purification of β-glucuronidase fusion proteins

Purification of βG constructs is achieved via a three-step purification scheme, an overview of which is given in Figure 65, commonly referred to in the literature as **CIP**:

1) **C**apture – Proteins are captured via their N-terminal His$_6$ tag from cell-free suspension culture supernatant (SFM4CHO medium) via immobilized metal affinity chromatography (IMAC) with a GE 5 ml HisTrap Excel column. This reduces the volume from 1L to approximately 30-50 ml and puts the protein in a well-defined environment. Excel columns are the only commercially available columns for the purification of protein directly from cell-free-mammalian cell supernatants. GE HisTrap HP columns as well as CloneTech HisTALON Superflow cartridges will strip entirely when subjected to mammalian cell culture supernatant and therefore cannot be utilized for this type of capture.

2) **I**ntermediate – Hydrophobic interaction chromatography (HIC) on a GE 5 ml butyl sepharose high performance column is utilized to further separate out unwanted species via hydrophobic interactions in the presence of high salt concentrations. This step serves to remove by removing bulk impurities from out target protein.

3) **P**olishing – Final cleanup is achieved with gel filtration chromatography (GFC) on a GE Superdex 200 column. Proteins purity is then verified via SDS-PAGE.

4) **Storage** – Proteins are flash frozen in TBS buffer in cyrovials with liquid nitrogen, and then stored at -80 °C.
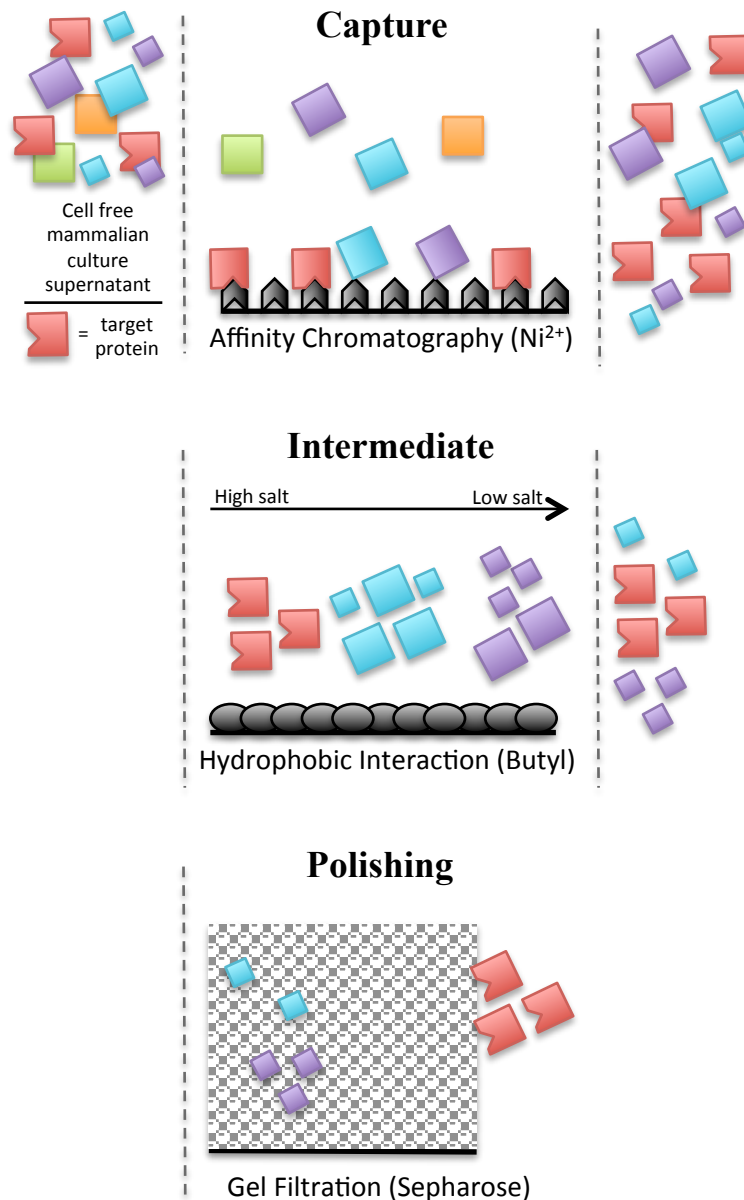
Figure 65: Overview of CIP purification procedure for βG proteins

βG proteins in cell-free culture supernatant are first captured with Ni²⁺ affinity chromatography, which places them in a well-defined, small volume environment. Next, βG proteins are taken to the brink of precipitation and further purified by hydrophobic interaction chromatography to separate out bulk impurities. Lastly, βG proteins are polished with gel filtration to yield a clean final product with purity > 95%.

A.16.1 Step 1: Capture – IMAC (HisTrap Excel)

1) (Optional) Throughout the chromatography take 100 µl samples of:

    a. IP = Input

    b. FT = Flow Through

    c. W = Wash (~150 ml)

    d. E = Elution (collect ~30 ml)

2) Prepare the column (switch the pump off every time connections are made or buffers are being switched).

    a. Set pump to 3 (~ 1ml/min). Chart speed to 6 cm/h.

    b. Run DI water through the pump to remove any air bubbles.

    c. Attach column connector (red).

    d. Run pump.

    e. Drip into column, attach column (make sure it's still blue).

    f. Run pump.

    g. Connect column to monitor.

    h. Run 30 ml of equilibration buffer through column.

        i. During this, make sure ABS 280 reaches and maintains a steady baseline.

3) (Optional) If purifying > 1L of culture, it is beneficial to use two 5 ml columns in series for maximum capture of target protein. Simply attach 2nd column to first column, and proceed with set up as specified in step 2. ***Note****: using two columns will cause some broadening of the elution peak.*

4) Load sample.

a. Set pump to 3 (~ 1 ml/min), 3.5 (~ 1.5 ml/min), or 4 (~ 1.75 ml/min).

b. Load sample. Cover with parafilm. Load will take ~ 12-18 h depending on volume.

    i. Make sure tubing is close to bottom of bottle.

    ii. If cell–free supernatants sit at 4 °C for >12 hours, they WILL clog the column. These samples can be tediously vacuum filtered to resolve this (use a low protein binding membrane), but filters clog after 100-200 ml.

    iii. Check columns occasionally to make sure they do not clog for other reasons. If backpressure does increase significantly, drop down to a lower pump setting to help coax loading/washing to continue.

    iv. If running columns in series and a clog occurs, remove columns from series set up and work with each column individually. Cap column not currently being run.

c. Make sure recorder sees protein, then switch chart speed to 0.3 cm/h.

d. Take last bit of sample and transfer to 50 ml tube for easier loading.

5) Wash

a. Set pump to 3, chart speed to 3 cm/h.

b. Rinse tubing in DI water, then load equilibration buffer.

c. Collect wash fraction in 50 ml tube.

d. Wash until ABS 280 reaches a steady baseline (usually 100-200 ml).

6) Elute

a. Set pump to 2, chart speed to 6 cm/h.

b. Dip tubing into DI water to clean, load elution buffer.

c. Once pen starts to go up, count 10-15 drops, then collect the next 30-40 ml, or more if the peak is still going.

d. Elutant will still be relatively yellow. The dye in the SFM medium appears to stick to the secreted proteins.

e. Continue to elute until ABS 280 levels off or if sufficient protein has been collected, begin i500 (see page 249) cleaning step immediately.

7) Cleaning the column

a. Run 20-50 ml for i500 elution buffer (see page 249) through until Abs 280 levels off.

b. Load 10 ml 1M NaOH. Let sit overnight, and then run 25 more ml through.

c. Load 1.5 M NaCl – 25 ml.

d. Load 30% Isopropanol – 25 ml.

e. Store in 20% EtOH.

A sample IMAC chromatograph, along with activity analysis and an SDS-PAGE gel of fractions, is shown in Figure 66.

Unlike His_6 IMAC purifications previously conducted on GE HisTrap HP columns, purification on HisTrap Excel columns does not yield a clean product, and further purification methods must be employed. Increased purity is generally achieved by including 0-50 mM imidazole in the wash buffer. However, we found that even very low amounts of imidazole in the wash buffer caused elution of the majority of the target

protein (Figure 67). After consulting with GE, we learned that at 460 kDa and 4/5 N-linked glycosylation sites, our annexin-βG fusion proteins are outside of the limits of proteins size and extent of glycosylation, which can interfere with binding and increases apparent protein size, investigated by GE for Excel columns. From correspondence with Lars Anderson at GE (08/07/2014):

> "With such a large protein as 460 kDa, the size is likely to aggravate the lower affinity of Ni Sepharose excel compared to "ordinary" Ni Sepharose HP or FF. The size gives slow diffusion; a lower ability to reach ligands in small bead pores."

The main difference between the HP columns utilized for all bacterial fusion protein purifications is how strongly the nickel ions are bound to the IMAC resin (Figure 68) so that the mammalian cell culture supernatant does not strip the ions off the resin. As each nickel ion only has a finite binding capacity, less binding capacity remains available to bind the target protein. For smaller, less glycosylated proteins, cleaner purifications may be possible. Nevertheless, we found that IMAC excel purifications were a simple, efficient, and quick step for capture of annexin-βG fusion proteins from cell free supernatants.

IMAC Buffers (HisTrap Excel)

Equilibration buffer (500 mL)

1. 20 mM sodium phosphate dibasic => use 1.42 g

2. 500 mM NaCl => use 14.61 g

3. pH 7.4

Elution buffer i100 (500 mL)

1. 20 mM sodium phosphate dibasic => use 1.42 g

2. 100 mM imidazole => use 3.404 g

3. 500 mM NaCl => use 14.61 g

4. pH 7.4

Elution buffer i500 (500 mL)

1. 20 mM sodium phosphate dibasic => use 1.42 g

2. 100 mM imidazole => use 17.02 g

3. 500 mM NaCl => use 14.61 g

4. pH 7.4
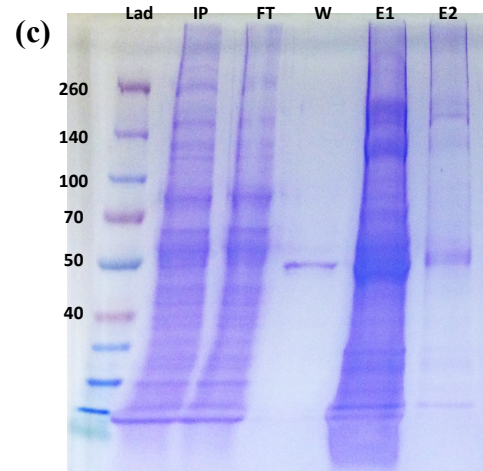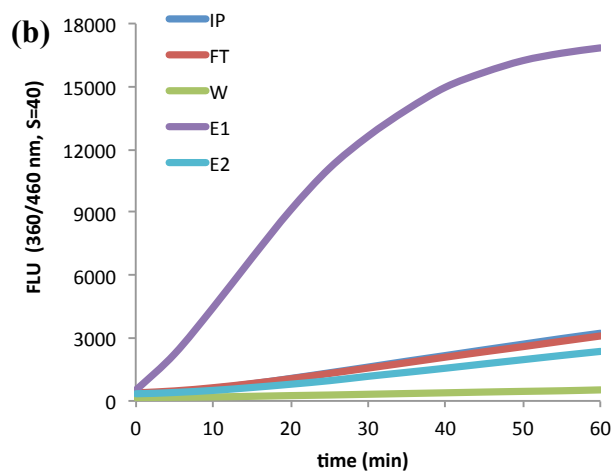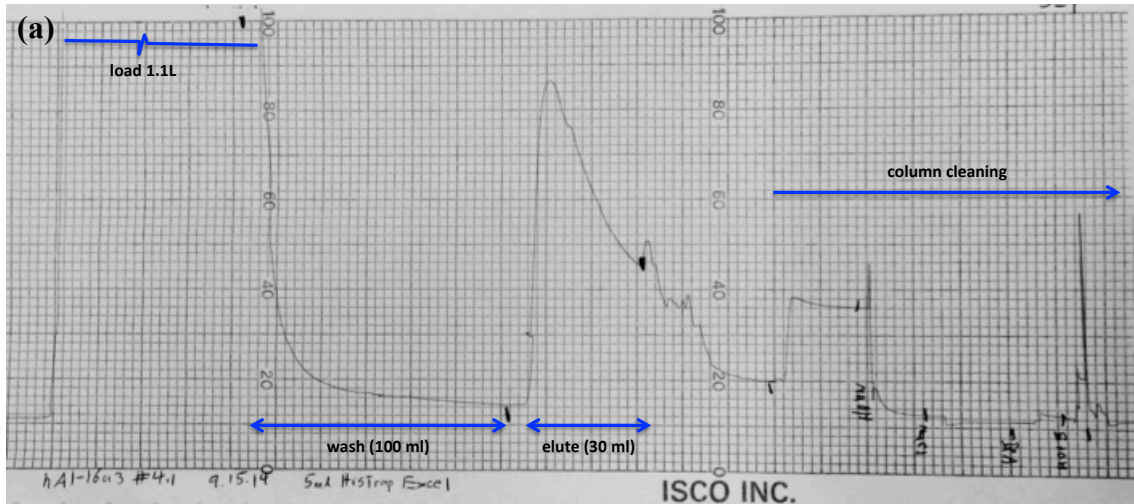
Figure 66: Sample βG IMAC chromatograph, SDS-PAGE, and activity assay

(a) Chromatograph of hA1-16a3 IMAC Excel purification. A 5-ml GE HisTrap Excel column was utilized. For this purification, 1.1L of fed-batch culture (day 13) was loaded onto the column, washed with equilibration buffer, and then eluted with i100 elution buffer. Only the first 30 ml of the elution were transitioned into HIC. (b) Raw fluorescence values (FLU) indicating βG activity in IMAC fractions for hA1-16a3: IP, input; FT, flow through; W, wash with equilibration buffer; E1, i100 elution (30 ml); and E2, i100 elution not retained. (c) SDS-PAGE of IMAC purification fractions for hA1-16a3, with same abbreviations as for activity assay in (b).
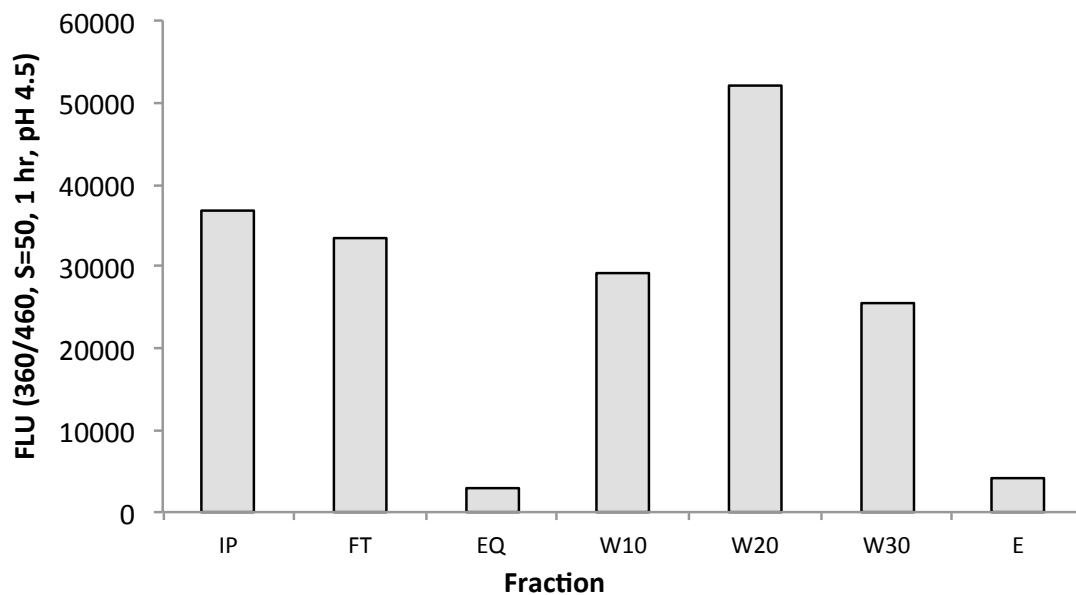
Figure 67: Effect of imidazole in wash buffer for IMAC on HisTrap Excel columns

Stepwise wash of hA1-βG on HisTrap Excel column in 10 mM imidazole increments. EQ is equilibration buffer, which contains 0 mM imidazole. W10-W30 contain 10 mM to 30 mM imidazole respectively, and E contains 500 mM imidazole. 0-30 mM imidazole is the concentration range of imidazole in wash buffer recommended by GE. However, we found that even 10 mM imidazole in the wash buffer will release all of the protein of interest from the HisTrap Column. Additions of up to 1.5 M NaCl (strengthens His_6 to Ni^{2+} binding) and 1 M urea (slight denaturing conditions) did not alter this occurrence. Therefore we conclude that it is the large and highly glycosylated nature of these fusion proteins that causes release in low concentrations of imidazole and not a His_6 tag availability issue. Based on this data, all washes were and should continue to be conducted in EQ buffer.
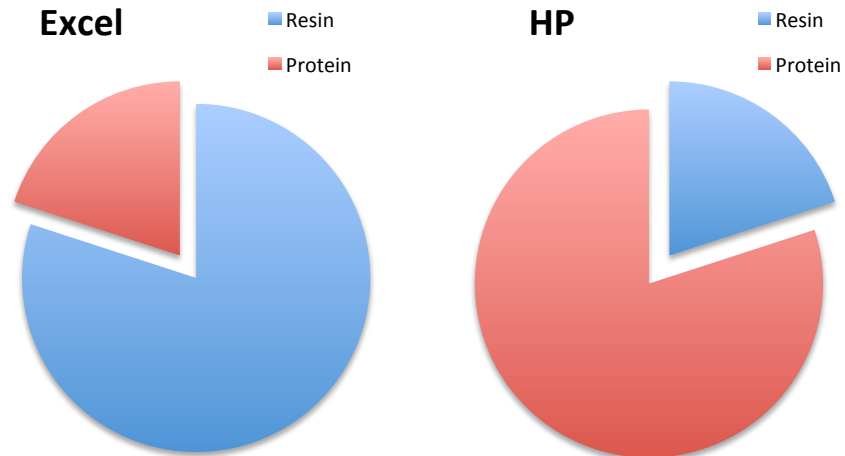
Figure 68: Nickel binding capacity distribution in GE IMAC Excel vs. HP columns

Representation of the differences in how Ni^{2+} binding capacity is utilized in HisTrap Excel and HisTrap HP columns. Excel columns were designed to be able to pull His tagged mammalian proteins directly from cell-free mammalian cell culture supernatant. However, mammalian cell culture supernatant is known for stripping Ni^{2+} ions from resins/columns. The solution to this is a stronger binding of the Ni^{2+} ions to the resin. However, Ni^{2+} ions only have a finite binding capacity, and therefore once bound more strongly to the resin, less of the binding capability remains unused and therefore able to capture the target protein.

A.16.2 Step 2: Intermediate – HIC (Butyl Sepharose HP)

HIC, to remove bulk impurities, must be preceded with a partial precipitation of the protein solution, as the hydrophobic interactions that drive HIC are only present at high salt concentrations. We used a 0.9 M ammonium sulfate concentration, as this precipitates out the relatively little of our target protein (as measured by βG activity, shown in Figure 69). Note that increasing βG activity is measured in the supernatant as the ammonium sulfate concentration is increased – this is likely only an effect of the ammonium sulfate carrying its own background signal in the activity assay. Figure 69 in itself is not conclusive. Thus, we attempted HIC with 0.7 and 0.9 M ammonium sulfate concentrations, and better separations were obtained with 0.9 M ammonium sulfate.

Note: For consistency and reproducibility, Sigma Aldrich Catalog # A5132 ammonium sulfate (reagent Plus with ≥ 99.0% purity) must be utilized for precipitation and in HIC buffers. Armesco proteomics grade ammonium sulfate was found to have disastrous consequences on the HIC separation process.

Ammonium sulfate precipitation:

1) Pour IMAC elutant (as is, no dialysis necessary) into a high-G tolerance tube. Place tube in a glass freeze-drying vial so that it remains upright and place a mini-stir bar in the tube.

2) Very slowly (over at least 10 minutes) add in the appropriate amount of ammonium sulfate to titrate sample to 0.9 M, while stirring. NEVER remove

the tube from the stir plate to add in the ammonium sulfate. High local

concentrations can easily cause the target protein to precipitate out.

3) After all ammonium sulfate has been added, place sample on stir plate at 4 °C,

and let precipitation run to completion overnight. The timescale for some

proteins to precipitate is hours, so this step should not be greatly abbreviated.

4) Centrifuge for 20 min at 15,000 x g at $r_{avergae}$ (14,000 RCF on our centrifuge).

HIC: All HIC was conducted by Eliza Ruben in the protein production core on the GE

Healthcare ÄKTA pure M1.

1) Equilibrate column with loading buffer.

2) Load sample onto column (pass through 2x).

    a. Flow rate = 1 ml/min

3) Wash with 3x CV of loading buffer.

    a. 5 ml column = 15 ml

    b. Flow rate = 1 ml/min

4) Run a 32x CV (column volume) gradient from 0.9 M ammonium sulfate

(loading buffer) to 0 M ammonium sulfate (elution buffer).

    a. Flow rate = 1 ml/min

    b. 5 ml column = 160 ml

5) Collect and pool 2 ml fractions containing target protein. Which peaks this

entails varies between protein types.

Sample HIC chromatographs, along with activity analysis and an SDS-PAGE gel of

fractions, are shown in Figure 70 for hA1-βG, Figure 71 for hA1-16a3, and Figure 72

for hA5-16a3. Captions notate which fractions were routinely pooled for downstream

purification.

HIC Buffers (Butyl Sepharose HP)

<u>Loading Buffer (500 mL)</u>

1. 20 mM sodium phosphate dibasic => use 1.42 g

2. 100 mM imidazole => use 3.404 g

3. 500 mM NaCl => use 14.61 g

4. 0.9 M ammonium sulfate => use 59.445 g

5. pH 7.4

6. Sterile filter

** Dissolve ammonium sulfate first in 300 ml of DI H_2O. Then titrate to 500 ml.

<u>Elution buffer (500 mL)</u>

1. 20 mM sodium phosphate dibasic => use 1.42 g

2. pH 7.4

3. Sterile filter
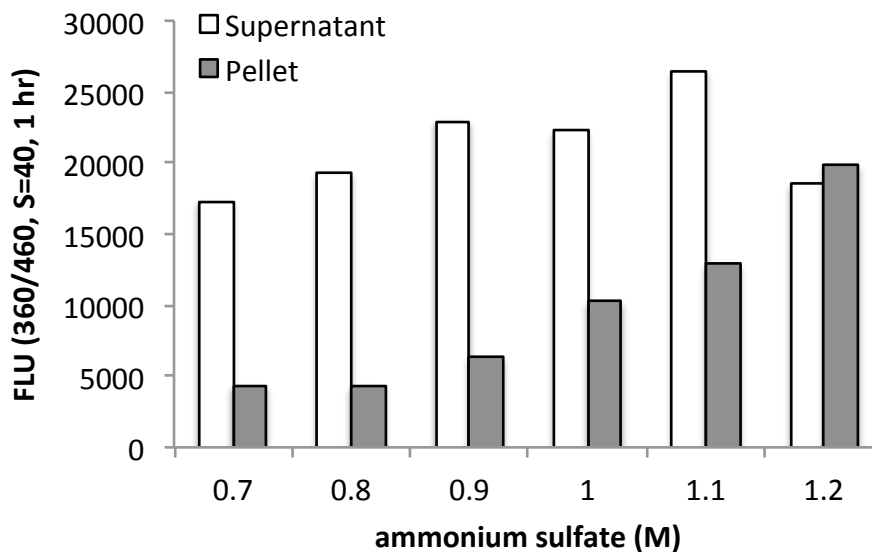
Figure 69: Effect of ammonium sulfate concentration on the precipitation of βG activity

Post IMAC Excel (hA1-16a3 #3.1), 500 μl aliquots of the elution (still in i100 elution buffer) were treated with varying concentrations of ammonium sulfate (0.7-1.2 M). Samples were allowed to precipitate overnight with gentle shaking at 4 ˚C. Activity values are shown in raw fluorescence units (360 nm excitation, 460 nm emission filter, pH 4.5) after 1 hour.
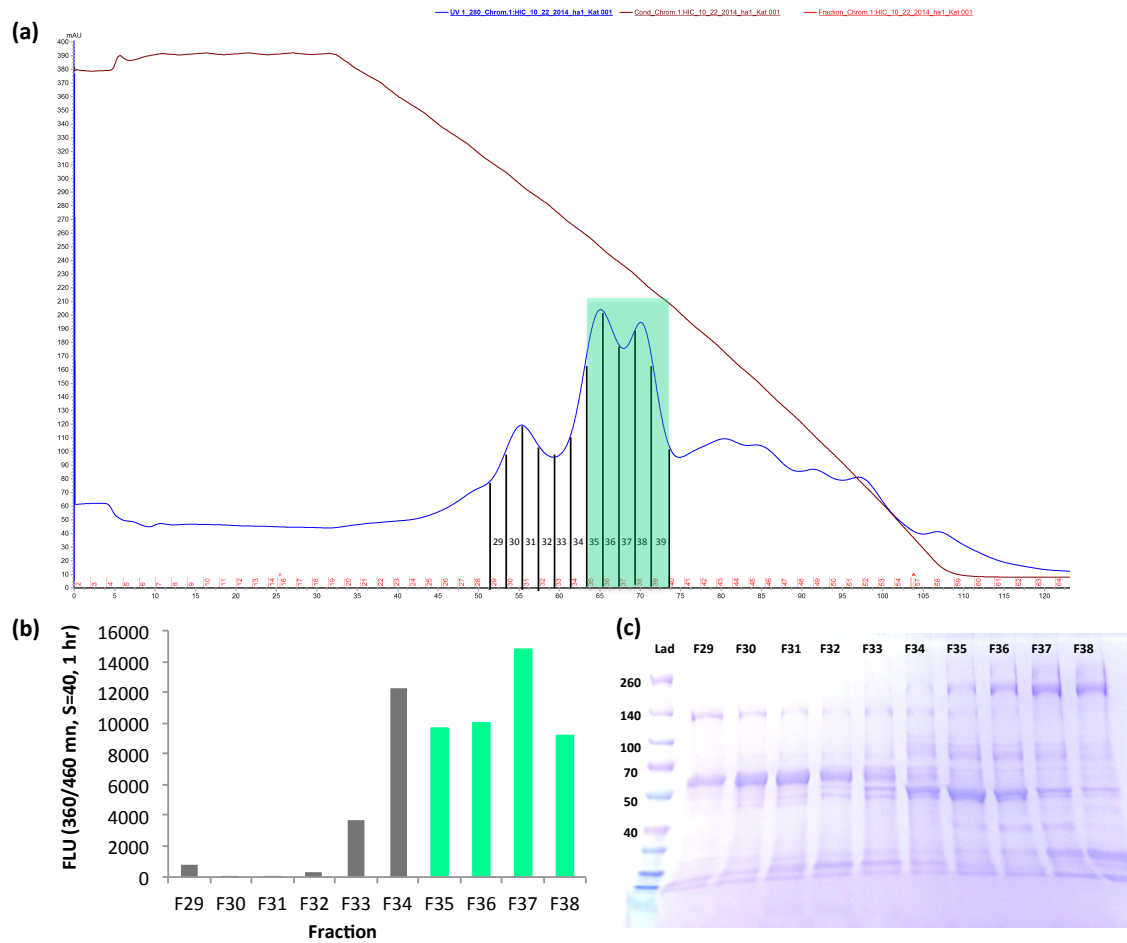
Figure 70: Sample hA1-βG HIC chromatograph, activity assay, and SDS-PAGE

(a) Chromatogram of hA1-βG HIC (Butyl HP) purification with fractions of interest during the 1 h gradient labeled. The red line indicates conductivity, and therefore a decreasing concentration of ammonium sulfate. Chromatograph from a 1 L, 2-week, fed-batch culture. (b) Raw activity values after 1 h at pH 4.5. (c) Reducing SDS-PAGE, showing most of the protein of interest in fractions 35-38. For hA1-βG, fractions 35-39 were routinely pooled prior to GFC.
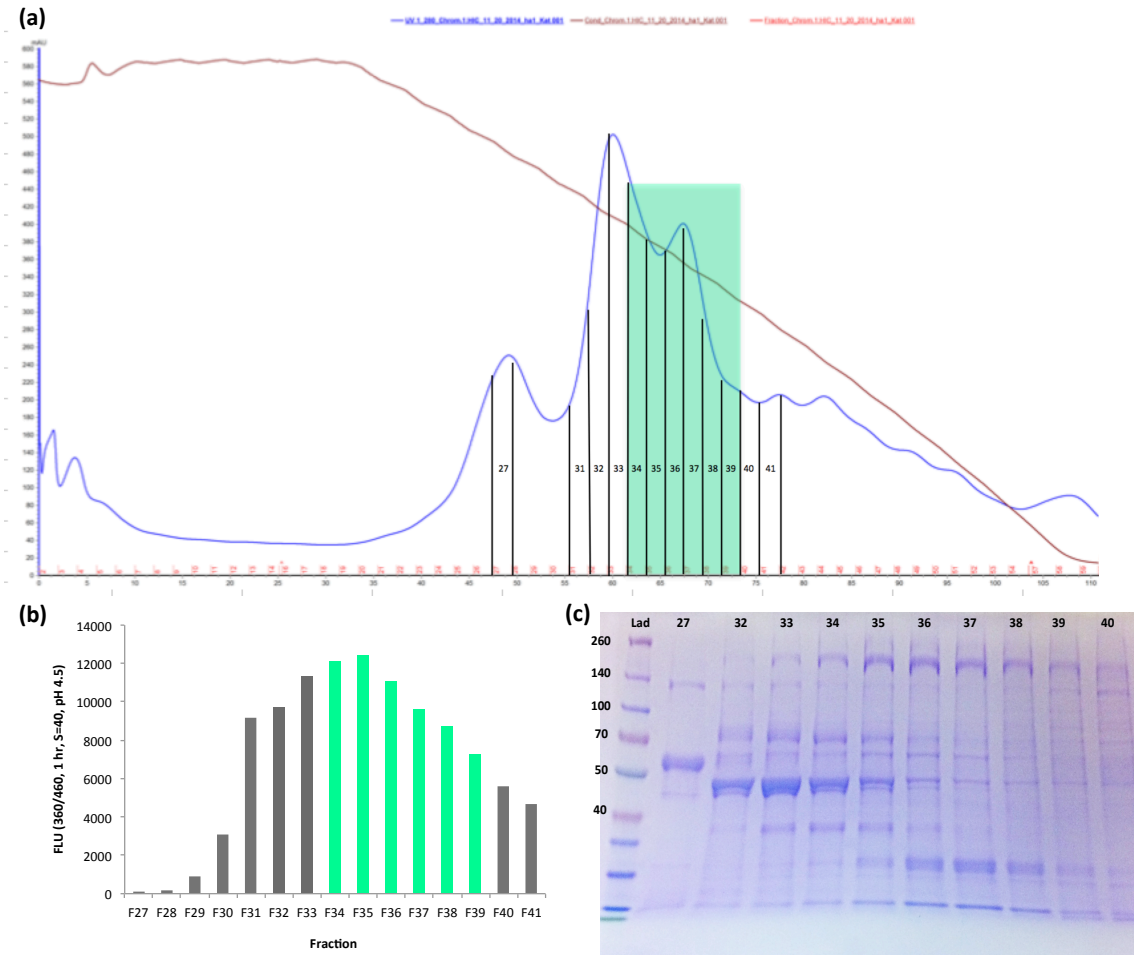
Figure 71: Sample hA1-16a3 HIC chromatograph, activity assay, and SDS-PAGE

(a) Chromatogram of hA1-16a3 HIC (Butyl HP) purification with fractions of interest during the 1 h gradient labeled. The red line indicates conductivity, and therefore a decreasing concentration of ammonium sulfate. Chromatograph from a 1.6 L, 2-week, fed-batch culture. (b) Raw activity values after 1 h at pH 4.5. (c) Reducing SDS-PAGE, showing most of the protein of interest in fractions 33-39. For hA1-16a3, fractions 34-39 were routinely pooled prior to GFC, as indicated by the green highlights. Fraction 33 was excluded due to the large amount of protein species at 45 kDa.
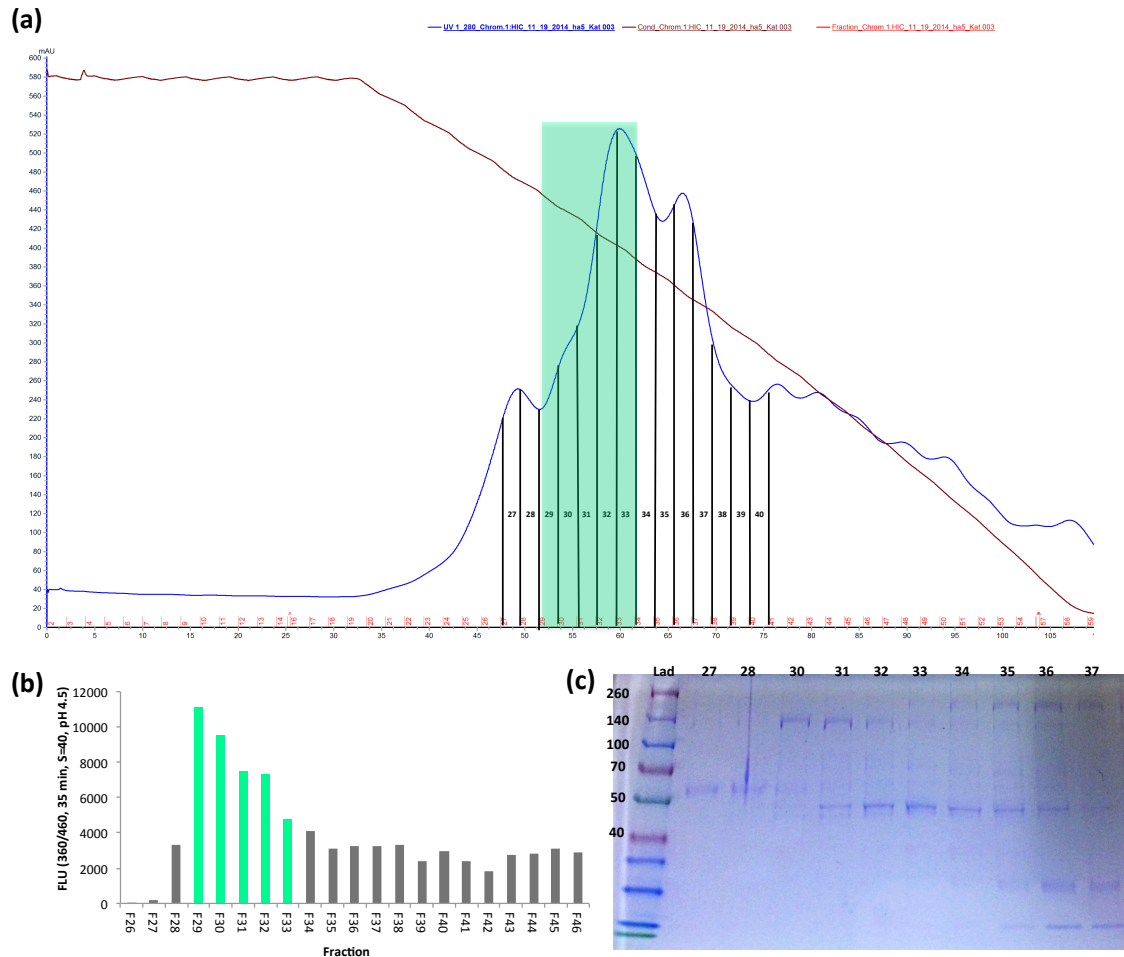
Figure 72: Sample hA5-16a3 HIC chromatograph, activity assay, and SDS-PAGE

(a) Chromatogram of hA5-16a3 HIC (Butyl HP) purification with fractions of interest during the 1 h gradient labeled. The red line indicates conductivity, and therefore a decreasing concentration of ammonium sulfate. Chromatograph from a 1.6 L, 2-week, fed-batch culture. (b) Raw activity values after 1 h at pH 4.5. (c) Reducing SDS-PAGE, showing most of the protein of interest in fractions 30-33. For hA5-16a3, fractions 29-33 were routinely pooled prior to GFC, as indicated by the green highlights.

A.16.3 Step 3: Polishing – GFC (Superdex 200)

After HIC, some small impurities remain, mainly a pesky species around 60 kDa (denatured). Additionally, our target protein resides in an ill-defined and unfavorable buffer condition. The final purification step, and the most commonly utilized polishing step, handily solves both of these issues. GFC simply separates by size, to give us a clean final product.

Concentration: HIC pooled fractions containing protein of interest were concentrated with an Amicon Ultra-15 Centrifugal Filter Unit with a 50 kDa cutoff. Centrifugation conditions were 4000 x g using a fixed angle centrifuge (Avanti J26S, rotor JLA 16.250) for a time of 30 min, or until desired volume is achieved (varies between 500 µl and 1 ml depending on protein concentration).

GFC: All GCF was completed at the protein production core by Eliza Ruben on the GE Healthcare ÄKTA pure M1.

1) Concentrated HIC fractions are loaded onto the Superdex 200.
2) TBS buffer (tris buffered saline, pH 8.0) is used to elute off protein as a flow rate between 0.2-0.4 ml/min. Flow rates influence resolution of separation, as shown in Figure 73.

Peaks of interest were verified to contain pure target protein via reducing SDS-PAGE. All clean fractions were pooled, aliquoted into cyrovials, and flash frozen in liquid nitrogen, before storage at -80 °C. Sample GFC chromatographs, along with an SDS-PAGE gel of fractions are shown in Figure 74 for hA1-βG (also includes activity

analysis), Figure 75 for hA1-16a3, and Figure 76 for hA5-16a3. Captions notate fractions pooled for experimental use.
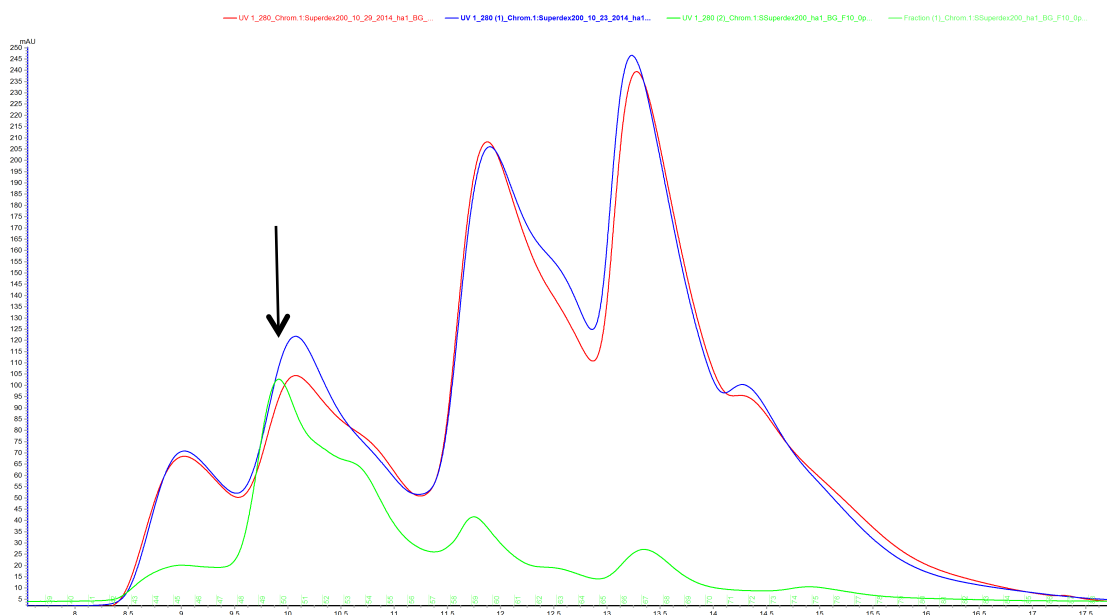
Figure 73: The effect of flow rate on GFC resolution.

All GFC traces shown are hA1-βG purifications, however with varying flow rates: blue (0.4 ml/min) > red (0.3 ml/min) > green (0.2 ml/min). Protein of interest is contained in the front half of the second peak on the blue trace, as indicated by the black arrow. However, lowering the flow rate reveals a plateau that splits this blue peak in half, leading to more accurate capture of the target protein.
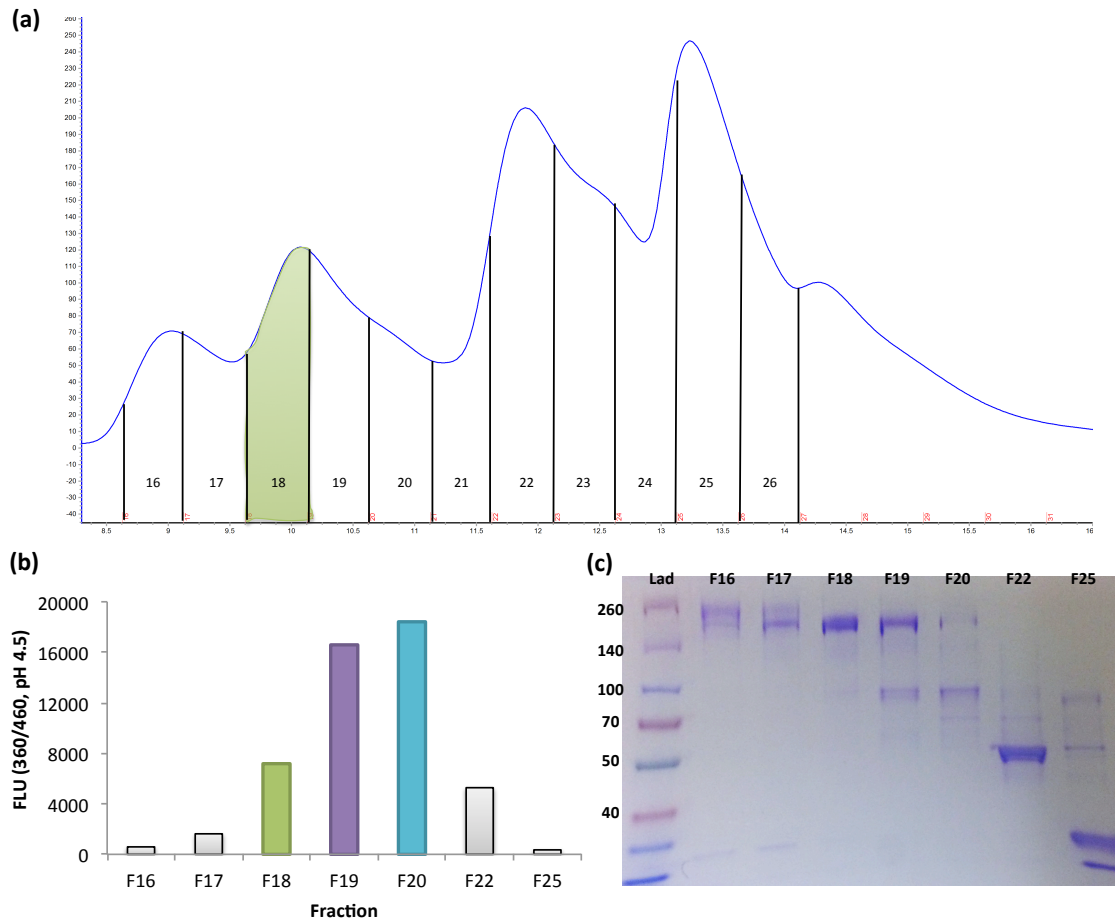
Figure 74: GFC chormatograph, activity data, and SDS-PAGE gel for hA1-βG

(a) GFC chromatograph of hA1-βG (1L culture), run a flow rate of 0.4 ml/min, with 1 ml fractions collected. (b) Activity analysis of selected fractions. We propose that the high activity in fraction F19 and F20 comes not from the hA1- βG fusion protein but from the species at expressing at a kDa of ~80-100, which correlates with un-fused, native βG. (c) SDS-PAGE of selected fractions, showing good purity in fraction 18, which was flash frozen and utilized in experiments.
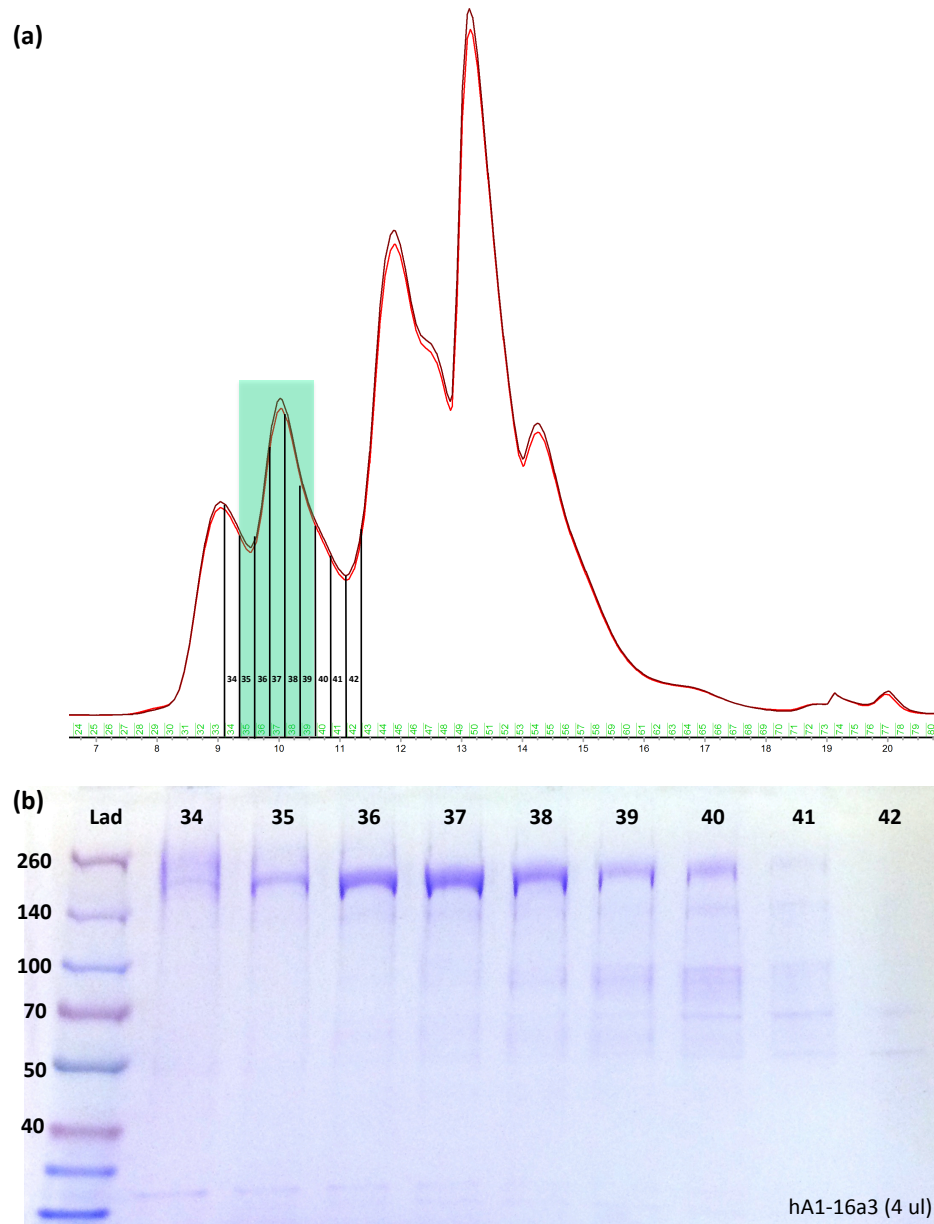
Figure 75: GFC chormatograph and SDS-PAGE gel for hA1-16a3

(a) Overlay (red and maroon traces) of two GFC runs (~0.5 ml injections) for hA1-16a3, run at a flow rate of 0.2 ml/min with 0.5 ml fractions collected. Both runs were from the same HIC purification (1.6 L culture), however there was too much protein to concentrate the entirety. (b) SDS-PAGE of fractions 34-41, showing good purity in the first GFC peak. Fractions 35-39 were pooled, flash frozen, and utilized in experiments.
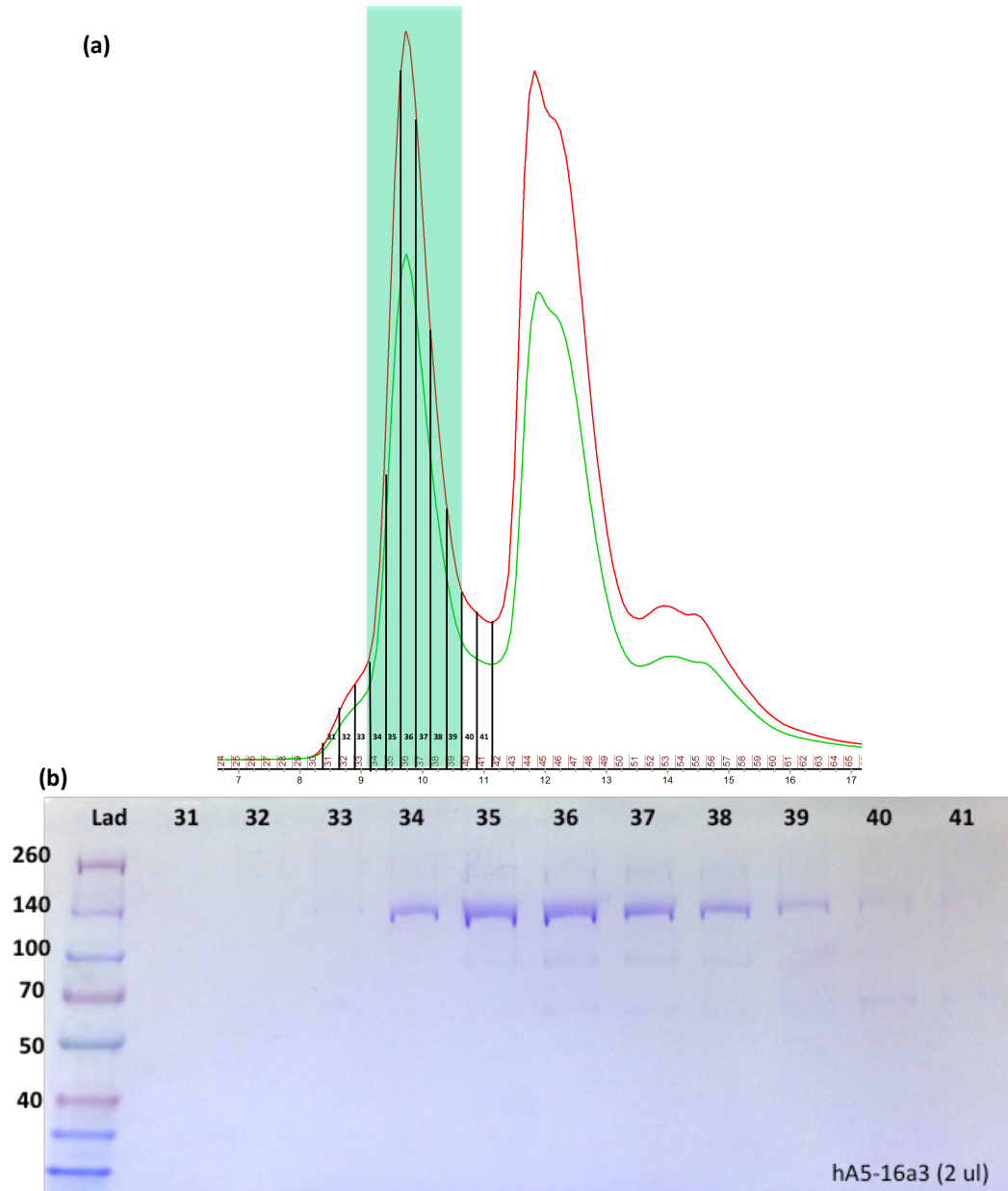
Figure 76: GFC chormatograph and SDS-PAGE gel for hA5-16a3

(a) Overlay (red and green traces) of two GFC runs (~ 0.5 ml injections) for hA5-16a3, run at a flow rate of 0.2 ml/min with 0.5 ml fractions collected. Both runs were from the same HIC purification (1.6 L culture), however there was too much protein to concentrate the entirety. (b) SDS-Page of fractions 31-41, showing good purity in first GFC peak. Fractions 34-39 were pooled, flash frozen, and utilized in experiments.

A.18 - Cell counting

1) For adherent cultures:

   • While passaging, take 20 µl sample after quenching cells and before centrifuging. Note volume. Dilution = 1:1.

2) For suspension cultures, combine (Dilution = 1:5):

   • 75 µl medium

   • 5 µl Trypan Blue (if omitted, replace volume with medium)

   • 20 µl cells

3) Add 10 µl to each side of hemocytometer

   • Count cells in quadrants 1, 2, 3, and 4 as shown in Figure 77

   • Average over both sides

4) Calculate cells/ml

$$\frac{cells}{ml} = Average\ Count \times Dilution\ Factor \times 2500$$
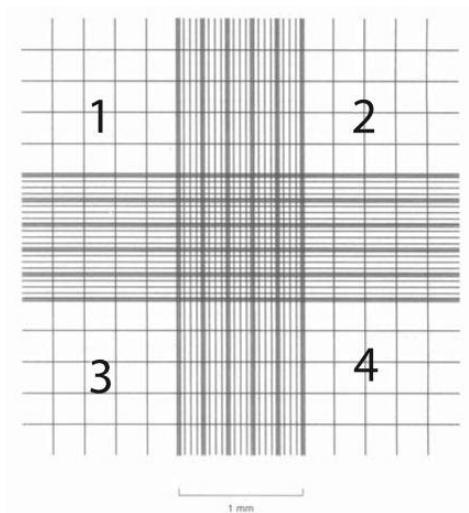
Figure 77: Hemocytometer Layout

Image source: ATCC Cell Culture Technical Resource

A.19 - βG activity assay

This assay is utilized to determine how efficient a βG protein in a given sample is at cleaving a glucuronide moiety. The substrate is 4-methylumbelliferyl-β-D-glucuronide (4-MUG, MW = 352.3 Da) which is converted by βG to 4-methylumbelliferone, sodium salt (4-MU, MW = 198.2), as shown in Figure 78. 4-MU is highly fluorescent at 360 nm excitation, 460 nm emission, allowing us to track accumulation over time in a microtiter plate reader. We were able to obtain 4-MU accumulation data at each time point by transforming observed fluorescence units to 4-MU concentration units via standard curves, presented in Figure 79.   As shown, 4-MU fluorescence is highly dependent on pH, and, thus, it is imperative that different standard curves be generated for each pH condition of interest.
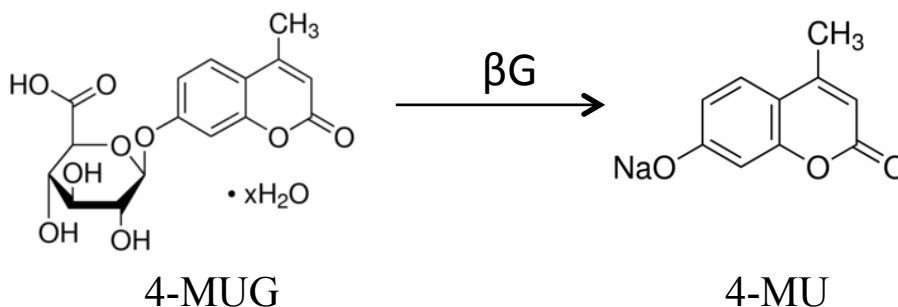
Figure 78: 4-MUG to 4-MU conversion by βG

βG cleaves the glucuronic acid from 4-MUG to create 4-MU, which is fluorescent and, therefore, allows for us to measure its accumulation. Chemical structures from Sigma Aldrich online product catalog.
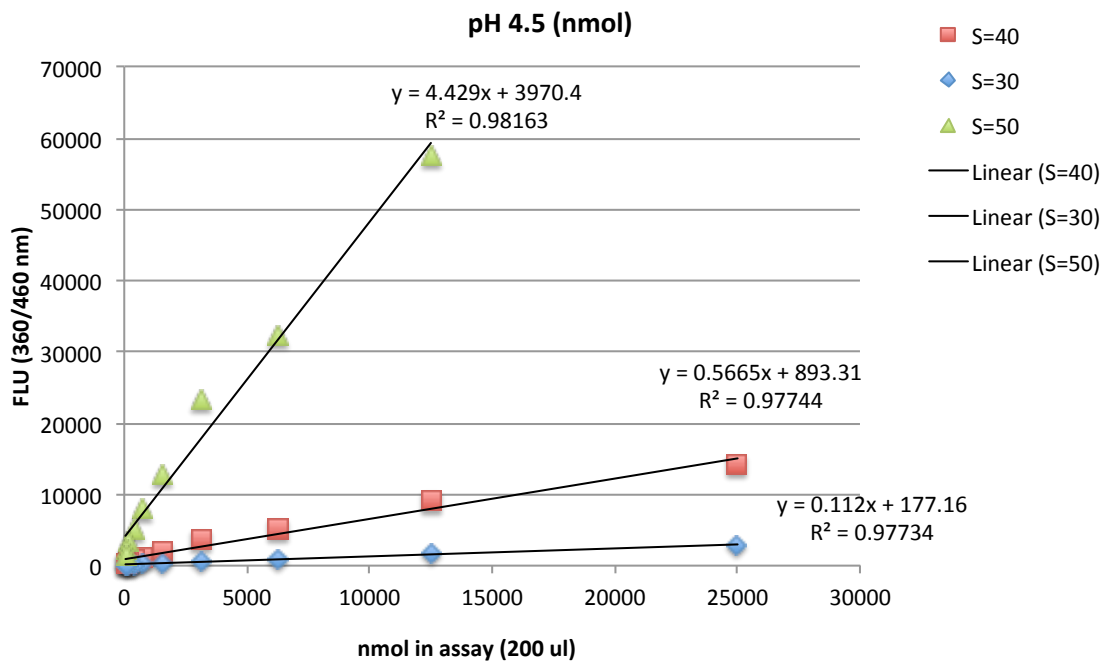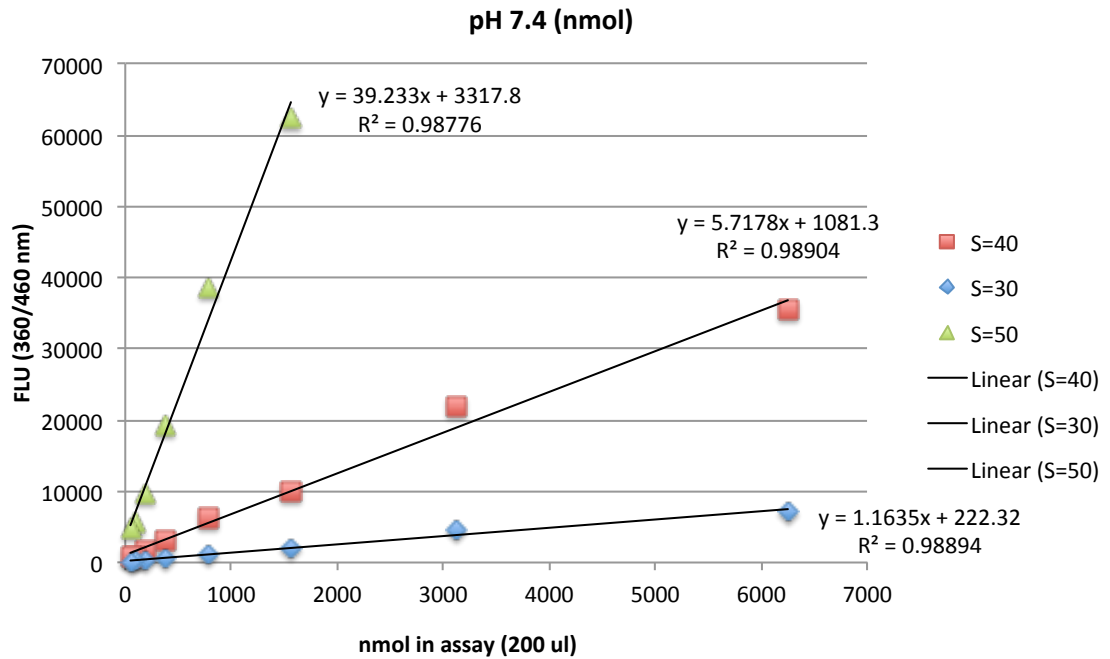
Figure 79: Standard curves to convert FLU (360/460 nm) to nmol 4-MU product

A.19.1 Simple analysis of activity in intermediate samples

Reaction set up for production/purification analysis:

- 140 μl buffer

- 40 μl sample

- 20 μl 1mM 4-MUG in appropriate buffer

    o This is added last, right before loading plate into plate reader.

Plate reader set up (kinetic):

- Pre-heat to 37°C, and run all assays at 37°C.

- FLU 360/460 nm.

- 1 h kinetic with reads every 5 minutes.

- Shaking prior to 1st reading to mix in 4-MUG.

- Sensitivity (S) depends on how much protein we input. Currently,

    o Production is S = 50

    o Purification S = 40 (otherwise we get #####).

For 200 ml of Reaction Buffer:

1) Add the following to 50 ml DI water:

    a. **50 mM Bis tris** (chem shelf) → 2.092g

    b. **50 mM triethanolamine** (chem shelf) → 1.327 ml

        i. This is very difficult to pipette and must be done extremely

            slowly.

    c. **100 mM acetic acid** (flammables cabinet) → 1.148 ml

    d. **100 ng/ml BSA** → 20 μl of 1mg/ml stock

        i. There is some 1 mg/ml stock in the glass fridge, check date. If too old (timescale of weeks), make new stock. BSA (powder) is also in glass fridge. To make stock weigh out BSA, then add exact amount of DI H_2O needed.

2) Titrate to 200 ml.

3) pH to 4.5 or 7.4.

4) Vacuum filter.

5) Store at 4 °C.

To make 4MUG substrate solution:

1) Weight out 4-MUG. Aim to weight out approx. 0.0035 g.

2) MW = 352.3, so to get 1mM solution.

$$\frac{1m\ mol}{L} = \frac{4MUG\ (g)}{buffer\ (ml)} * \frac{352.3g}{mol} * \frac{10^3 mmol}{mol} * \frac{10^3 ml}{L}$$

If we compress this equation, to get 1 mM 4-MUG, we need:

$$ml\ buffer = (2838.49) * (4MUG\ grams\ weighed\ out)$$

3) For pH 7.4, it is sometimes beneficial to use a 2 mM 4-MUG solution, but this is near the solubility limit and higher concentrations are not tolerated.

4) Store at 4 °C in the dark

    a. Stability is debatable in the literature. If running to determine kinetic constants use fresh preparations. However, when stored in buffer, no noticeable difference in assay values was detected over 3 months.

A.19.2 Determining kinetic constants - Theory

To determine the enzymatic constants of interest, we can employ Michaelis-Menten

kinetics. We are interested in finding:

- V_{max} - the maximum enzyme velocity, found by extrapolation.

- K_m - the Michaelis-Menten constant, and the substrate concentration necessary

  to achieve ½ of V_{max}.

- k_{cat} - the tunover number, as in how many molecules the enzyme converts from

  substrate molecules to product molecules per unit time.

  - To compute this we will also need to find E_t, which is the concentration

    of enzyme catalytic sites. For βG there are two catalytic sites per

    protein, which needs to be considered when calculating E_t.

- Specific activity: the amount of product generated per mg protein per unit time.

To enable this analysis, we must collect the initial slopes, phase 2 in the curve in Figure

80a, or reaction rate/velocity, for varying concentrations of substrate (4-MUG), while

keeping protein concentration and assay volume constant. We can then plot the

substrate concentration, [S] verses the linear rate of product formation (the velocity), so

that the curve looks like Figure 80b. Using GraphPad Prism we can then fit this

equation to determine V_{max} and K_m, where Y = velocity and X = substrate

concentration:

$$Y = \frac{V_{max} \times X}{K_m + X}$$

Or, we can constrain E_t, and fit this eqution to get k_{cat}:

$$Y = \frac{E_t \times k_{cat} \times X}{K_m + X}$$

Specific activity can simpy be computed via V_{max}, converted to nmol/h, and adjusted for the amount of protein input into the assay.

When fitting these equations, care must be taken to ensure that all data and constrains are in the proper units. The ones utilied for the βG proteins are:

- Velocity (Y) = nmol 4-MU/min

- Substrate concentraion (X) = nM

- E_t = nmol (this is not nM, it is an absolute count of catalytic sites)

Which makes the output values take on the units:

- V_{max} = nmol 4-MU/min

- K_m = nM

- k_{cat}: = min^{-1}

- Specific activity = nmol/h/mg
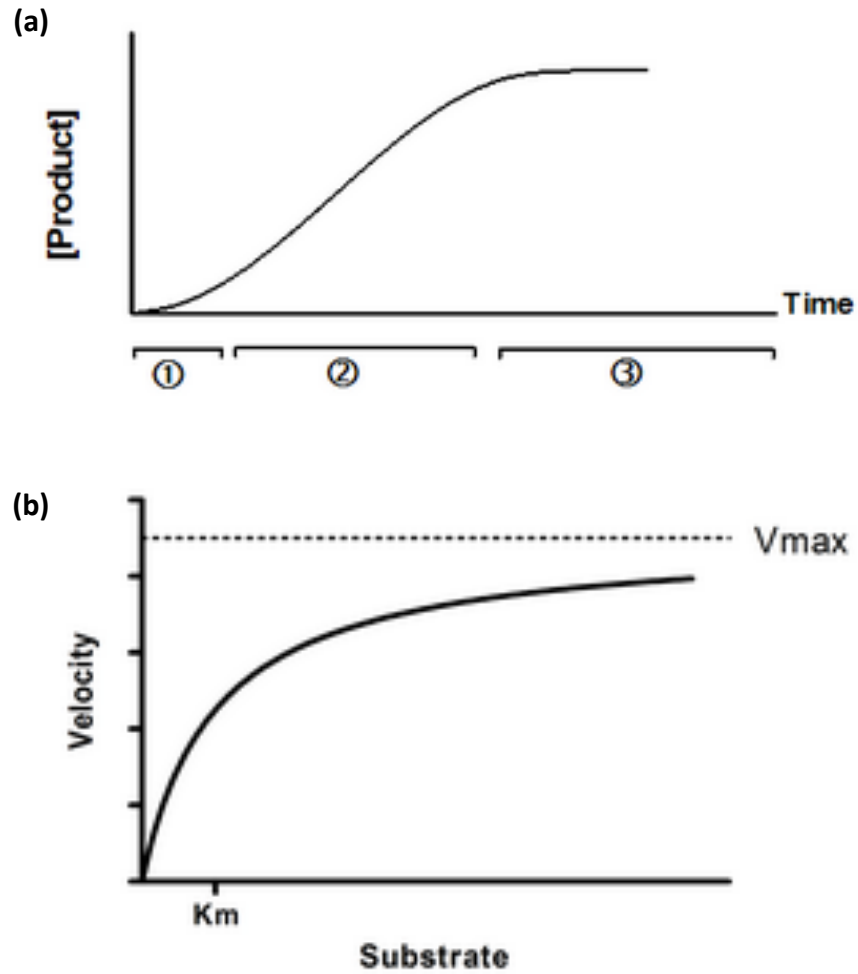
Figure 80: Theoretical curves for kinetic constant determination[177]

(a) The time vs. product curve. This is collected for varying concentrations of substrate, and for each concentration, the linear slope in phase 2 is computed. (b) Each of the linear slopes, or initial rates, is plotted as a function of substrate concentration. Images from GraphPad Curve Fitting Guide.[177]

A.19.3 Determining kinetic constants - Practice

Setting up the reaction

1) Calculate compositions of each well. Each condition will be run in triplicate, so at most six conditions should be set up at a time, or else pipetting speed may begin to influence results. Make a table that looks something like Table 13. Note that total reaction volume is always 200 μl.

2) Pre-heat the plate reader to 37 °C. Set up protocol so that there is a 10 s shake at an intensity of 5, only before the first reading.

3) Set up proceeds like this:

    a. First pipette the buffer (either pH 7.4 or 4.5, never both) into six wells for each substrate concentration of interest. Three of these wells will receive protein and three will receive water (as the baseline for that condition). Each substrate concentration should have a different amount of buffer.

    b. Calculate out how many μl are needed of your sample to equate to 0.5 μg (can also use other concentrations, but need to be consistent throughout). You need to have taken triplicate measurements of the concentration of your protein sample (to establish mean ± SE) in order to compute specific activity later on, as you will need a standard error.

    c. Don't add the protein yet, but do add an equivalent of DI water to three of the six wells for each substrate concentration on the plate.

    d. Add the appropriate amount of 4-MUG to all wells (6x per substrate concentration). Cover with foil immediately.

e. Take the covered plate, protein, pipette, tips, and trash bucket to the pre-heated plate reader. Quickly and accurately (changing tips every time) pipette the protein into the three wells per substrate concentration that are to receive protein. No need to mix as plate reader will shake prior to first reading.

Data Analysis (all in GraphPad Prism 6):

Before beginning Michaelis-Menten analysis:

1) Subtract off the baseline (DI water) individually for each substrate concentration Use Prim manipulations to baseline correct data.

2) Convert measured FLUs into 4-MU concentrations using appropriate standards, Figure 80. Use a custom equation in Prism to easily manipulate data.

3) Fit a linear regression to data for each substrate concentration.

4) Plot the resulting slopes vs. substrate concentration.

5) Convert μl 4-MUG to nM 4-MUG (200 μl assay volume). Use a second custom equation in Prism to achieve this.

6) Once you have a plot of 4-MUG (nM) vs. velocity (nmol 4-MU/min) you are ready to proceed.

Curve Fitting:

4) Double-check all units.

5) Non-lin fit (Michaelis-Menten – least squares) the data to obtain V_{max} and K_m.

6) Non-lin fit (kcat, constrain E_t, least squares) to obtain k_{cat}.

7) Compute specific activity from V_{max} and mg protein input. Error propagation is buit into Prism, so this is best done with column math in a separate Prism file as the error propagations are quite extensive.

Table 13: Sample set-up for βG activity analysis at pH 4.5

μl 1mM 4-MUG (pH 4.5)	μl pH 4.5 Buffer	μl protein	μg protein
0	198.7	1.32	0.50
10	188.7	1.32	(2x, once
20	178.7	1.32	with H2O
40	158.7	1.32	instead of
60	138.7	1.32	protein)
80	118.7	1.32	

A.20 - SDS-PAGE

For visualizing denatured proteins based on size.

Sample Prep:

1) Combine 8 μl of 4x Lamelli loading buffer (Biorad) with 22 μl of each sample.

2) Briefly vortex, incubate at 80 °C for 10 min in thermal block, then cool to RT and briefly centrifuge to collect sample in bottom of tube.

3) Thaw ladder, and centrifuge to collect all 10 μl. Use the Thermo Page Ruler Plus prestained ladder.

Running the gel:

1) Remove pre-cast gel from wrapper and insert (ledge facing in) into gel holder. Place dummy gel in gel holder on the opposite side.

2) Insert gel-holder into the cassette. While pressing down on the plastic by the electrodes, lock the gates.

3) Use a plastic transfer pipette to pipette buffer from the tank across the ledge of the precast gel, making sure each well is filled with buffer and does not contain any bubbles.

4) Pour out some of the running buffer from the tank into a beaker.

5) Load 10-20 μl. (2x 10 μl, with a clear tip) into each well. Load 10 μl of ladder.

6) Insert cassette (with samples loaded) into tank, make sure it is hanging correctly.

7) Pour buffer into the middle of the cassette until it covers the samples.

8) Connect lid, turn on power box, and hit start.

9) Run at 150 V for ~45 minutes. You want the blue to run close to the bottom of the gel. TURN OFF POWER SUPPLY

Staining the gel:

1) <u>TURN OFF POWER SUPPLY.</u> Remove lid, remove cassette (pour buffer back into tank), and unclamp gates to remove the gel. Pry open plastic covering gel and use razor blade to gently cut off lanes.

2) Wash in DI H_2O for 15 minutes (4 °C / RT gentle shaking).

3) Wash in destain for 30 minutes (4 °C / RT gentle shaking).

4) Wash briefly with DI water as residual destain will interfere with staining.

5) Stain with imperial stain (Invitrogen) for 1-2 h 4 °C / RT gentle shaking.

6) Destain in DI H_2O overnight. (4° C / RT gentle shaking).

    a. Toss in a chem-wipe (or two) to soak up the dye that comes off.

    b. Can replace water and chem-wipe after a few hours to speed up process.

7) If there's still high background the next day, use fresh water and add in some destain (10-20%). Destain will eventually strip the imperial stain from the proteins.

To make more destain:

- 40% DI H_2O

- 40% methanol

- 20% acetic acid

- Wear goggles!!!!

A.21 - Dot blot

For the confirmation of purified protein identify.

1) Blot 1 μg of purified protein product (verify purity with SDS-PAGE) onto a small piece of dry nitrocellulose membrane.

2) Let dry at RT for 2-4 h.

3) Block overnight in freshly prepared 1% BSA TBST solution, at 4 °C with gentle shaking.

4) Add primary antibody for 2 h at RT with gentle shaking. If probing for His_6 omit this step.

   - βG rabbit polyclonal (sc-25827) at 1:200

   - A1 rabbit polyclonal (sc-11387) at 1:200

   - A5 rabbit polyclonal (sc-8300) at 1:200

5) Wash 3x 5 min with TBST at RT with gentle shaking.

6) Add secondary HRP-conjugated antibody (in TBST) or HisDetector^{TM} Nickel-HRP conjugate (directly into TBST + BSA) and incubate for 1 h, RT, with gentle shaking.

   - Goat anti-rabbit IgG-HRP (sc-2004) at 1:5000

   - HisDetector^{TM} Nickel-HRP conjugate at 1:50

7) Wash 3x with 3 ml TBST at RT with gentle shaking. 1x 15 min, followed by 2x 5 min.

8) Incubate with 1 ml TMB for up to 15 minutes as color develops.

*Note: Colorimetric blots cannot be stripped and re-probed. Blots will maintain some color, but do fade, so a photo is recommended as a permanent record.

A.22 - Confocal microscopy

For the visualization of biotin labeled fusion proteins binding to PS exposed on the cell surface. Streptavidin cannot cross the cell membrane and, therefore, this method detects only extracellularly bound protein. Schematic of this method is shown in Figure 81.

Slide preparation:

1) Place over slip in 35 mm petri dish. Plate cells at 150k/cover slip in 2 ml of medium. Allow to adhere overnight at 37 °C, 5% CO_2.

2) Fix cells in 1 ml 0.25% glutaraldehyde in PBS + 2 mM Ca^{2+} for 5 min at RT.

3) Quench with 50 mM NH_4Cl in PBS for 5 min at RT.

4) Wash 2 times with 1 ml PBS + 2 mM Ca^{2+}.

5) Incubate with saturating concentration of fusion protein (30 nM) in 1 ml of normal growth medium + 2 mM Ca^{2+} at 37 °C, 5% CO_2.

6) Wash 3 times with 1 ml PBS + 2mM Ca^{2+}.

7) Incubate with Streptavidin-Alexa-488 at 4 µg/ml in 1 ml PBS + 2 mM Ca^{2+} for 1 h at 37 °C, 5% CO_2.

8) Wash 3 times with 1 ml PBS + 2 mM Ca^{2+}.

9) Stain with Cell Mask Deep Red at 2 µg/ml in 1 ml PBS + 2 mM Ca^{2+} 3 times for 5 min at 37 °C, 5% CO_2.

10) Wash 3 times with 1 ml PBS + 2 mM Ca^{2+}.

11) Stain with Hoechst 33258 at 10 µg/ml in 1 ml PBS + 2 mM Ca^{2+} for 30 mins at 37 °C, 5% CO_2.

12) Wash 3 times with growth medium + 2 mM Ca^{2+}.

13) Air dry cover slip for 1 min.

14) Use tweezers to gently lift cover slip, invert, and slowly lower onto 2 drops of fluoro-gel on slide. Let sit in the dark for 10 minutes, before transporting.

Imaging:

Confocal images were captured with the Lecia-SP8 at the Samuel Roberts Noble Microscopy Laboratory under the direction of Ben Smith. Setting used were 63x in glycerol. Images presented were de-convoluted prior to preparation of images for publication in ImageJ.
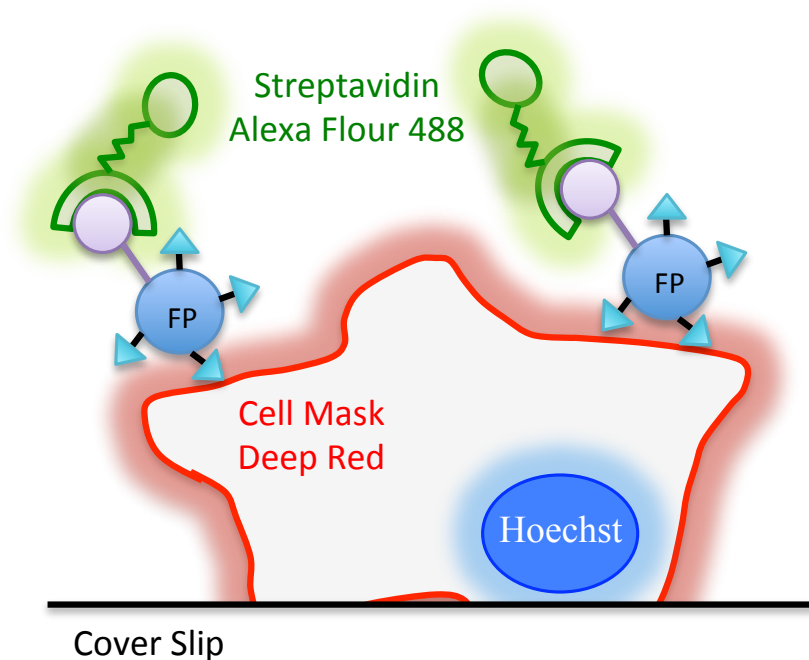
Figure 81: Flourophore staining scheme utilized for confocal imaging

Appendix B: Primers for Human A1/A5-βG

B.1 - Construction primers

Annexin A1 Sense (New)

5' CAT CAC CAT CAC CAT CAC CTT GAA GTC CTC TTT CAG GGA CCC **GCA**

ATG GTA TCA GAA TTC C 3'

Green = His Tag   BP = 61

Purple = HRV 3C Site   CG% = 49.1

Bold = Sequence Overlap   Melting Temp = 69.9 °C

Annexin A1 Antisense

5' TG CTT ACC↓ TCC ACT ACC TCC GCC ACC ACT **GTT TCC TCC ACA AAG**

AGC 3'

Teal = EciI Site   BP = 47

Orange = linker   CG% = 55.3

Bold = Sequence overlap   Melting Temp = 70.9 °C

Annexin A5 Sense

5' CAT CAC CAT CAC CAT CAC CTT GAA GTC CTC TTT CAG GGA CCC **GCA**

CAG GTT CTC AGA GGC 3'

Green = His Tag   BP = 60

Purple = HRV 3C Site   CG% = 55

Bold = Sequence Overlap   Melting Temp = 71.8 °C

Annexin A5 Antisense

5' TG CTT ACC↓ TCC ACT ACC TCC GCC ACC ACT **GTC ATC TTC TCC ACA**

GAG 3'

Teal = EciI Site   BP = 47

Orange = ½ linker   CG% = 55.3

Bold = Sequence overlap   Melting Temp = 70.2 °C

β -glucuronidase (βG) Sense (Signal)

5' ATT TAA ATT TAA GCA GGC GGA GGT AGT GGA GG↓T GGT GGA **GCC**

CGG GGG TCG GCG GTT G 3'

Teal = EciI Site   BP = 58

Orange = ½ Linker   CG% = 58.6

Bold = Sequence overlap   Melting Temp = 74.0 °C

β -glucuronidase (βG) Sense (No Signal)

5' TAA ATT TAA GCA GGC GGA GGT AGT GGA GG↓T GGT GGA **CTG CAG**

GGC GGG ATG CTG TAC C 3'

Teal = EciI Site   BP = 58

Orange = ½ Linker   CG% = 56.9

Bold = Sequence overlap   Melting Temp = 73.0 °C

β-glucuronidase (βG) Antisense (No Propeptide) – Named: hA1BG Extract

Antisense

5' TTA **GGT TTC ATT GGC AAT CTT CCA GTA TCT CTC TCG** 3'

Red = Stop Codon   BP = 37

Bold = Sequence Overlap   CG% = 51.4

                                         Melting Temp = 66.2 °C

β -glucuronidase (βG) Antisense (Propeptide)

5' TCA **AGT AAA CAG GCT GTT TTC CAA ACA TTG** 3'

Red = Stop Codon (native)   BP = 30

Bold = Sequence Overlap   CG% = 36.7

                                         Melting Temp = 58.3 °C

** Kozak sequence w/ ATG Start Codon followed by IgK secretion signal already in PsecTag/FRT vector

** Primers were ordered from IDT and PAGE purified

EciI restriction site:

```
G G C G G A N N N N N N N N N  N N/
C C G C C T N N N N N N N N N/N N
```


Linker is (amino acid): SGGGGSGGGG

DNA linker sequence: AGTGGTGGCGGAGGTAGTGGAGGTGGTGGA

B.2 - Sequencing primers

<u>T7 Primer</u>

TAATACGACTCACTATAGGG (Provided by OMRF)

<u>Human annexin 5 (hA5):</u>

hA5 seq primer 1: TTTTAAGACTCTGTTTGGCA

hA5 seq primer 2: CATACCCTCATCAGAGTCA

<u>Human annexin 1 (hA1):</u>

hA1 seq primer 0: GGATGAAGCAACCATCATT

hA1 seq primer 1: AATACCATCCTTACCACCA

<u>Human native βG and mutant 16a3 βG:</u>

hβG seq primer 1: GAGTGGTGCTGAGGATT

hβG seq primer 2: CAGCCACTACCCCTATGC

Appendix C: pSecTag/FRT/V5-His-TOPO® Vector
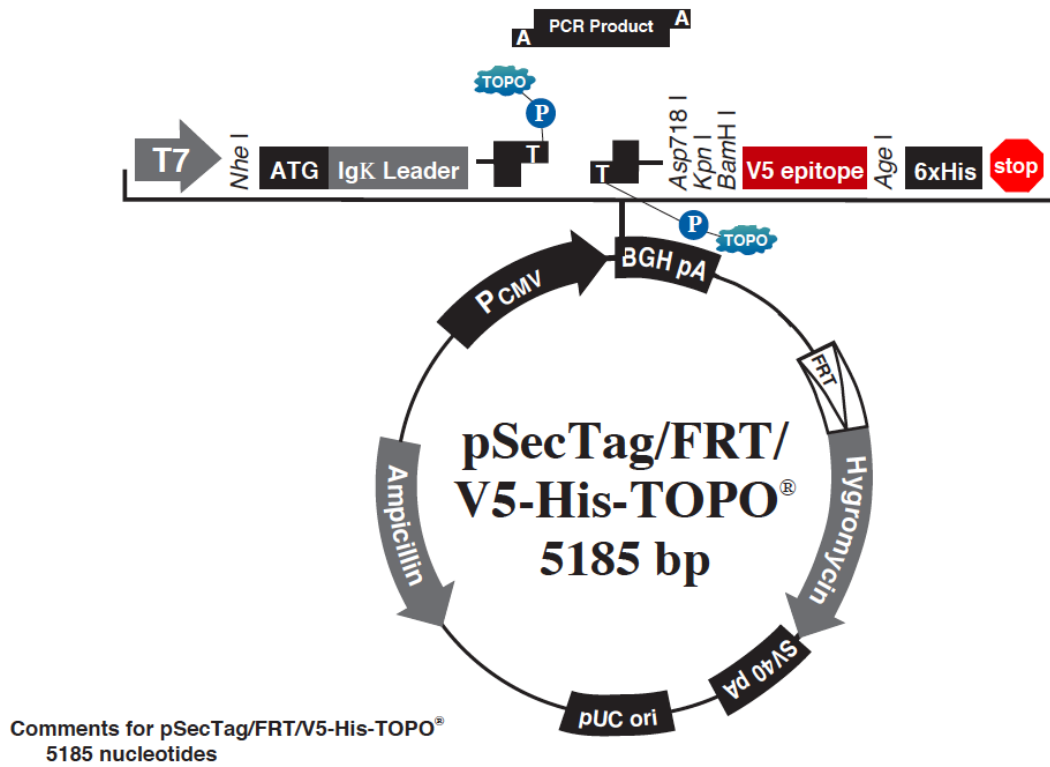
Figure 82: Plasmid map of the pSecTag/FRT/V5-His-TOPO® vector

Image Source: Invitrogen Life Technologies

CMV promoter

721 AAAATCAACG GGACTTTCCA AAATGTCGTA ACAACTCCGC CCCATTGACG CAAATGGGCG

CAAT

CMV forward priming site   TATA   3' end of CMV promoter   putative transcriptional start

781 GTAGGCGTGT ACGGTGGGAG GTCTATATAA GCAGAGCTCT CTGGCTAACT AGAGAACCCA

T7 promoter/priming site   Nhe I

841 CTGCTTACTG GCTTATCGAA ATTAATACGA CTCACTATAG GGAGACCCAA GCTGGCTAGC

Ig K-chain secretion signal

901 CACC **ATG** GAG ACA GAC ACA CTC CTG CTA TGG GTA CTG CTG CTC TGG GTT
          Met Glu Thr Asp Thr Leu Leu Leu Trp Val Leu Leu Leu Trp Val

950 CCA GGT TCC ACT GGT GAC GCG GCC CAG CCG GCC AGG CGC GCG CGC CGT
    Pro Gly Ser Thr Gly Asp Ala Ala Gln Pro Ala Arg Arg Ala Arg Arg

Signal Cleavage Site   Asp718 I   Kpn I   Bam H I

995 ACG AAG CTC GCC CTT ┌─────────┐ AAG GGC GAG CTT GGT ACC GAG CTC GGA
                   G   CGG GAA │ PCR   │ TTC CCG CTC
    Thr Lys Leu Ala Leu │ Product │ Lys Gly Glu Leu Gly Thr Glu Leu Gly
                          └─────────┘   V5 epitope

1040 TCC GAA GGT AAG CCT ATC CCT AAC CCT CTC CTC GGT CTC GAT TCT ACG
     Ser Glu Gly Lys Pro Ile Pro Asn Pro Leu Leu Gly Leu Asp Ser Thr

Age I   Polyhistidine (6xHis) region   Pme I

1088 CGT ACC GGT CAT CAT CAC CAT CAC CAT TGA GTT TAAACCCGCT GATCAGCCTC
     Arg Thr Gly His His His His His His ***

BGH reverse priming site

1141 GACTGTGCCT TCTAGTTGCC AGCCATCTGT TGTTTGCCCC TCCCCCGTGC

Figure 83: Sequence details of ligation site for the pSecTag/FRT/V5-His-TOPO vector

Image Source: Invitrogen Life Technologies

286

Appendix D: Sequences for Commercially Purchased Clones

D.1 - Human annexin A1 mRNA clone

(IMAGE clone ID: 4662939, Accession: BC035993)

```
1    M   A   M   V   S   E   F   L   K   Q   A   W   F   I   N   E   E   Q   E   20
75   atggcaatggtatcagaattcctcaagcaggcctggtttattgaaaatgaagagcaggaa 134

21   Y   V   Q   T   V   K   S   S   K   G   G   P   G   S   A   V   S   P   Y   P   40
135  tatgttcaaactgtgaagtcatccaaaggtggtcccggatcagcggtgagcccctatcct 194

41   T   F   N   P   S   S   D   V   A   A   L   H   K   A   I   M   V   K   G   V   60
195  accttcaatccatcctcggatgtcgctgccttgcataaggccataatggttaaaggtgtg 254

61   D   E   A   T   I   I   D   I   L   T   K   R   N   N   A   Q   R   Q   Q   I   80
255  gatgaagcaaccatcattgacattctaactaagcgaaacaatgcacagcgtcaacagatc 314

81   K   A   A   Y   L   Q   E   T   G   K   P   L   D   E   T   L   K   K   A   L   100
315  aaagcagcatatctccaggaaacaggaaagcccctggatgaaacactgaagaaagccctt 374

101  T   G   H   L   E   E   V   V   L   A   L   L   K   T   P   A   Q   F   D   A   120
375  acaggtcaccttgaggaggttgttttggctctgctaaaaactccagcgcaatttgatgct 434

121  D   E   L   R   A   A   M   K   G   L   G   T   D   E   D   T   L   I   E   I   140
435  gatgaacttcgtgctgccatgaagggccttggaactgatgaagatactctaattgagatt 494

141  L   A   S   R   T   N   K   E   I   R   D   I   N   R   V   Y   R   E   E   L   160
495  ttggcatcaagaactaacaaagaaatcagagacattaacagggtctacagagaggaactg 554

161  K   R   D   L   A   K   D   I   T   S   D   T   S   G   D   F   R   N   A   L   180
555  aagagagatctggccaaagacataacctcagacacatctggagattttcggaacgctttg 614

181  L   S   L   A   K   G   D   R   S   E   D   F   G   V   N   E   D   L   A   D   200
615  ctttctcttgctaagggtgaccgatctgaggactttggtgtgaatgaagacttggctgat 674

201  S   D   A   R   A   L   Y   E   A   G   E   R   R   K   G   T   D   V   N   V   220
675  tcagatgccagggccttgtatgaagcaggagaaaggagaaaggggacagacgtaaacgtg 734

221  F   N   T   I   L   T   T   R   S   Y   P   Q   L   R   R   V   F   Q   K   Y   240
735  ttcaataccatccttaccaccagaagctatccacaacttcgcagagtgtttcagaaatac 794

241  T   K   Y   S   K   H   D   M   N   K   V   L   D   L   E   L   K   G   D   I   260
```

```
795   accaagtacagtaagcatgacatgaacaaagttctggacctggagttgaaaggtgacatt 854
261   E   K   C   L   T   A   I   V   K   C   A   T   S   K   P   A   F   F   A   E   280
855   gagaaatgcctcacagctatcgtgaagtgcgccacaagcaaaccagctttctttgcagag 914
281   K   L   H   Q   A   M   K   G   V   G   T   R   H   K   A   L   I   R   I   M   300
915   aagcttcatcaagccatgaaaggtgttggaactcgccataaggcattgatcaggattatg 974
301   V   S   R   S   E   I   D   M   N   D   I   K   A   F   Y   Q   K   M   Y   G   320
975   gtttcccgttctgaaattgacatgaatgatatcaaagcattctatcagaagatgtatggt 1034
321   I   S   L   C   Q   A   I   L   D   E   T   K   G   D   Y   E   K   I   L   V   340
1035  atctccctttgccaagccatcctggatgaaaccaaaggagattatgagaaaatcctggtg 1094
341   A   L   C   G   G   N   *                                       347
1095  gctctttgtggaggaaactaa                                           1115
```

D.2 - Human annexin A5 mRNA clone

(Accession: NM_001154)

Note: This clone was a gift from Dr. Stuart Lind at the University of Colorado.

```
  1 M   A   Q   V   L   R   G   T   V   T   D   F   P   G   F   D   E   R   A   D   20
  1 ATGGCACAGGTTCTCAGAGGCACTGTGACTGACTTCCCTGGATTTGATGAGCGGGCTGAT 60

 21 A   E   T   L   R   K   A   M   K   G   L   G   T   D   E   E   S   I   L   T   40
 61 GCAGAAACTCTTCGGAAGGCTATGAAAGGCTTGGGCACAGATGAGGAGAGCATCCTGACT 120

 41 L   L   T   S   R   S   N   A   Q   R   Q   E   I   S   A   A   F   K   T   L   60
121 CTGTTGACATCCCGAAGTAATGCTCAGCGCCAGGAAATCTCTGCAGCTTTTAAGACTCTG 180

 61 F   G   R   D   L   L   D   D   L   K   S   E   L   T   G   K   F   E   K   L   80
181 TTTGGCAGGGATCTTCTGGATGACCTGAAATCAGAACTAACTGGAAAATTTGAAAAATTA 240

 81 I   V   A   L   M   K   P   S   R   L   Y   D   A   Y   E   L   K   H   A   L  100
241 ATTGTGGCTCTGATGAAACCCTCTCGGCTTTATGATGCTTATGAACTGAAACATGCCTTG 300

101 K   G   A   G   T   N   E   K   V   L   T   E   I   I   A   S   R   T   P   E  120
301 AAGGGAGCTGGAACAAATGAAAAAGTACTGACAGAAATTATTGCTTCAAGGACACCTGAA 360

121 E   L   R   A   I   K   Q   V   Y   E   E   E   Y   G   S   S   L   E   D   D  140
361 GAACTGAGAGCCATCAAACAAGTTTATGAAGAAGAATATGGCTCAAGCCTGGAAGATGAC 420

141 V   V   G   D   T   S   G   Y   Y   Q   R   M   L   V   V   L   L   Q   A   N  160
421 GTGGTGGGGGACACTTCAGGGTACTACCAGCGGATGTTGGTGGTTCTCCTTCAGGCTAAC 480

161 R   D   P   D   A   G   I   D   E   A   Q   V   E   Q   D   A   Q   A   L   F  180
481 AGAGACCCTGATGCTGGAATTGATGAAGCTCAAGTTGAACAAGATGCTCAGGCTTTATTT 540

181 Q   A   G   E   L   K   W   G   T   D   E   E   K   F   I   T   I   F   G   T  200
541 CAGGCTGGAGAACTTAAATGGGGGACAGATGAAGAAAAGTTTATCACCATCTTTGGAACA 600

201 R   S   V   S   H   L   R   K   V   F   D   K   Y   M   T   I   S   G   F   Q  220
601 CGAAGTGTGTCTCATTTGAGAAAGGTGTTTGACAAGTACATGACTATATCAGGATTTCAA 660

221 I   E   E   T   I   D   R   E   T   S   G   N   L   E   Q   L   L   L   A   V  240
661 ATTGAGGAAACCATTGACCGCGAGACTTCTGGCAATTTAGAGCAACTACTCCTTGCTGTT 720

241 V   K   S   I   R   S   I   P   A   Y   L   A   E   T   L   Y   Y   A   M   K  260
```

```
721 GTGAAATCTATTCGAAGTATACCTGCCTACCTTGCAGAGACCCTCTATTATGCTATGAAG 780
261 G   A   G   T   D   D   H   T   L   I   R   V   M   V   S   R   S   E   I   D   280

781 GGAGCTGGACAGATGATCATACCCTCATCAGAGTCATGGTTTCCAGGAGTGAGATTGAT 840
281 L   F   N   I   R   K   E   F   R   K   N   F   A   T   S   L   Y   S   M   I   300

841 CTGTTTAACATCAGGAAGGAGTTTAGGAAGAATTTTGCCACCTCTCTTTATTCCATGATT 900
301 K   G   D   T   S   G   D   Y   K   K   A   L   L   L   L   C   G   E   D   D   320

901 AAGGGAGATACATCTGGGGACTATAAGAAAGCTCTTCTGCTGCTCTGTGGAGAAGATGAC 960
321 *                                                          321

961 TAA                                                        963
```

(IMAGE clone ID 4662011, Accession: BC014142)

```
  1 M   A   R   G   S   A   V   A   W   A   A   L   G   P   L   L   W   G   C   A  20
  2 atggcccggggggtcggcggttgcctgggcggcgctcgggccgttgttgtggggctgcgcg 61

 21 L   G   L   Q   G   G   M   L   Y   P   Q   E   S   P   S   R   E   C   K   E  40
 62 ctggggctgcagggcgggatgctgtacccccaggagagcccgtcgcgggagtgcaaggag 121

 41 L   D   G   L   W   S   F   R   A   D   F   S   D   N   R   R   R   G   F   E  60
122 ctggacggcctctggagcttccgcgccgacttctctgacaaccgacgccggggcttcgag 181

 61 E   Q   W   Y   R   R   P   L   W   E   S   G   P   T   V   D   M   P   V   P  80
182 gagcagtggtaccggcggccgctgtgggagtcaggccccaccgtggacatgccagttccc 241

 81 S   S   F   N   D   I   S   Q   D   W   R   L   R   H   F   V   G   W   V   W 100
242 tccagcttcaatgacatcagccaggactggcgtctgcggcattttgtcggctgggtgtgg 301

101 Y   E   R   E   V   I   L   P   E   R   W   T   Q   D   L   R   T   R   V   V 120
302 tacgaacgggaggtgatcctgccggagcgatggacccaggacctgcgcacaagagtggtg 361

121 L   R   I   G   S   A   H   S   Y   A   I   V   W   V   N   G   V   D   T   L 140
362 ctgaggattggcagtgcccattcctatgccatcgtgtgggtgaatggggtcgacacgcta 421

141 E   H   E   G   G   Y   L   P   F   E   A   D   I   S   N   L   V   Q   V   G 160
422 gagcatgagggggggctacctcccccttcgaggccgacatcagcaacctggtccaggtgggg 481

161 P   L   P   S   R   L   R   I   T   I   A   I   N   N   T   L   T   P   T   T 180
482 cccctgccctcccggctccgaatcactatcgccatcaacaacacactcacccccaccacc 541

181 L   P   P   G   T   I   Q   Y   L   T   D   T   S   K   Y   P   K   G   Y   F 200
542 ctgccaccagggaccatccaatacctgactgacacctccaagtatcccaagggttacttt 601

201 V   Q   N   T   Y   F   D   F   F   N   Y   A   G   L   Q   R   S   V   L   L 220
602 gtccagaacacatattttgactttttcaactacgctggactgcagcggtctgtacttctg 661

221 Y   T   T   P   T   T   Y   I   D   D   I   T   V   T   T   S   V   E   Q   D 240
662 tacacgacacccaccacctacatcgatgacatcaccgtcaccaccagcgtggagcaagac 721

241 S   G   L   V   N   Y   Q   I   S   V   K   G   S   N   L   F   K   L   E   V 260
722 agtgggctggtgaattaccagatctctgtcaagggcagtaacctgttcaagttggaagtg 781
```

291

```
261 R   L   L   D   A   E   N   K   V   V   A   N   G   T   G   T   Q   G   Q   L   280
782 cgtcttttggatgcagaaaacaaagtcgtggcgaatgggactgggacccagggccaactt 841

281 K   V   P   G   V   S   L   W   W   P   Y   L   M   H   E   R   P   A   Y   L   300
842 aaggtgccaggtgtcagcctctggtggccgtacctgatgcacgaacgccctgcctatctg 901

301 Y   S   L   E   V   Q   L   T   A   Q   T   S   L   G   P   V   S   D   F   Y   320
902 tattcattggaggtgcagctgactgcacagacgtcactggggcctgtgtctgacttctac 961

321 T   L   P   V   G   I   R   T   V   A   V   T   K   S   Q   F   L   I   N   G   340
962 acactccctgtggggatccgcactgtggctgtcaccaagagccagttcctcatcaatggg 1021

341 K   P   F   Y   F   H   G   V   N   K   H   E   D   A   D   I   R   G   K   G   360
1022 aaacctttctatttccacggtgtcaacaagcatgaggatgcggacatccgagggaagggc 1081

361 F   D   W   P   L   L   V   K   D   F   N   L   L   R   W   L   G   A   N   A   380
1082 ttcgactggccgctgctggtgaaggacttcaacctgcttcgctggcttggtgccaacgct 1141

381 F   R   T   S   H   Y   P   Y   A   E   E   V   M   Q   M   C   D   R   Y   G   400
1142 ttccgtaccagccactacccctatgcagaggaagtgatgcagatgtgtgaccgctatggg 1201

401 I   V   V   I   D   E   C   P   G   V   G   L   A   L   P   Q   F   F   N   N   420
1202 attgtggtcatcgatgagtgtcccggcgtgggcctggcgctgccgcagttcttcaacaac 1261

421 V   S   L   H   H   H   M   Q   V   M   E   E   V   V   R   R   D   K   N   H   440
1262 gtttctctgcatcaccacatgcaggtgatggaagaagtggtgcgtagggacaagaaccac 1321

441 P   A   V   V   M   W   S   V   A   N   E   P   A   S   H   L   E   S   A   G   460
1322 cccgcggtcgtgatgtggtctgtggccaacgagcctgcgtcccacctagaatctgctggc 1381

461 Y   Y   L   K   M   V   I   A   H   T   K   S   L   D   P   S   R   P   V   T   480
1382 tactacttgaagatggtgatcgctcacaccaaatccttggacccctcccggcctgtgacc 1441

481 F   V   S   N   S   N   Y   A   A   D   K   G   A   P   Y   V   D   V   I   C   500
1442 tttgtgagcaactctaactatgcagcagacaaggggggctccgtatgtggatgtgatctgt 1501

501 L   N   S   Y   Y   S   W   Y   H   D   Y   G   H   L   E   L   I   Q   L   Q   520
1502 ttgaacagctactactcttggtatcacgactacgggcacctggagttgattcagctgcag 1561

521 L   A   T   Q   F   E   N   W   Y   K   K   Y   Q   K   P   I   I   Q   S   E   540
1562 ctggccacccagtttgagaactggtataagaagtatcagaagcccattattcagagcgag 1621

541 Y   G   A   E   T   I   A   G   F   H   Q   D   P   P   L   M   F   T   E   E   560
```

292

```
1622 tatggagcagaaacgattgcagggtttcaccaggatccacctctgatgttcactgaagag 1681
 561 Y   Q   K   S   L   L   E   Q   Y   H   L   G   L   D   Q   K   R   R   K   Y   580
1682 taccagaaaagtctgctagagcagtaccatctgggtctggatcaaaaacgcagaaaatac 1741
 581 V   V   G   E   L   I   W   N   F   A   D   F   M   T   E   Q   S   P   T   R   600
1742 gtggttggagagctcatttggaattttgccgatttcatgactgaacagtcaccgacgaga 1801
 601 V   L   G   N   K   K   G   I   F   T   R   Q   R   Q   P   K   S   A   A   F   620
1802 gtgctggggaataaaaaggggatcttcactcggcagagacaaccaaaaagtgcagcgttc 1861
 621 L   L   R   E   R   Y   W   K   I   A   N   E   T   R   Y   P   H   S   V   A   640
1862 cttttgcgagagagatactggaagattgccaatgaaaccaggtatccccactcagtagcc 1921
 641 K   S   Q   C   L   E   N   S   L   F   T   *                              652
1922 aagtcacaatgtttggaaaacagcctgtttacttga                          1957
```

293

Appendix E: Sequence for Human 16a3 β-Glucuronidase Mutant Optimized for Expression in CHO Cells

E.1 - Plasmid map
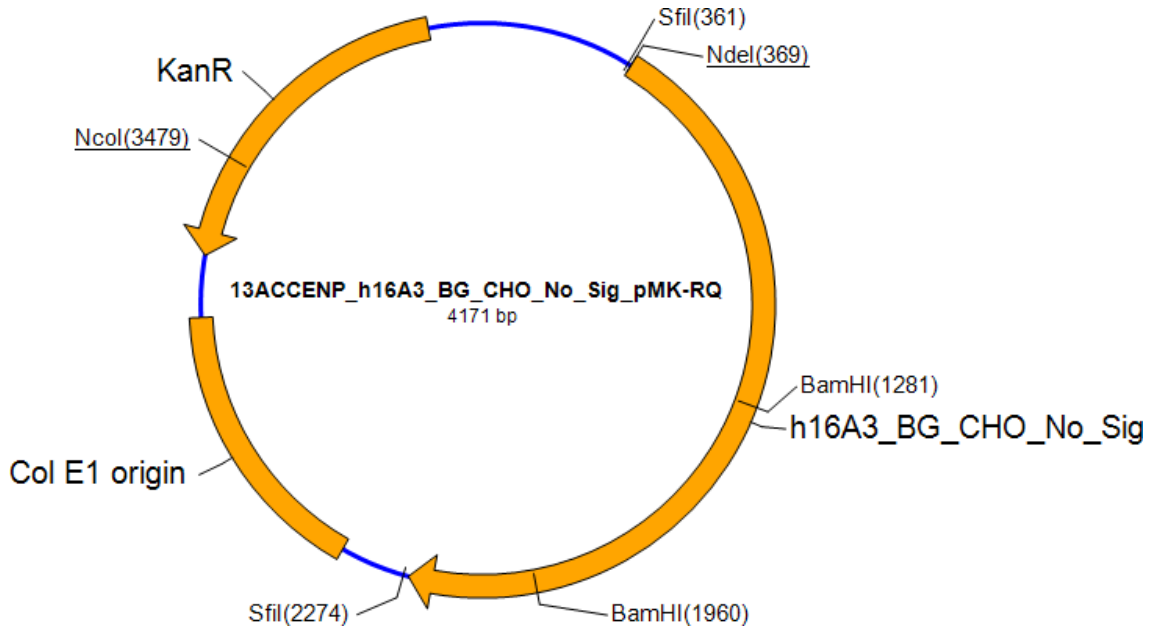
Figure 84: Plasmid map of hβG 16a3 optimized for expression in CHO cells

Plasmid was synthesized via the Invitrogen Gene Art Service and was synthesized without the N-terminal signal sequence but with C-terminal the propeptide sequence. Plasmids were resuspended in 50 μl of DI water, and stored in 5 μl aliquots at -20 °C.

E.2 - Nucleotide sequence

CACTATAGGGCGAATTGAAGGAAGGCCGTCAAGGCCGCATATGCTGCAGGG

CGGGATGCTGTACCCCCAAGAGTCCCCTAGCAGAGAGTGCAAAGAACTGGA

CGGCCTGTGGTCCTTCCGGGCCGACTTCTCCGACAACAGAAGGCGGGGCTT

CGAGGAACAGTGGTACAGACGGCCTCTGTGGGAGTCCGGCCCTACCGTGGA

TATGCCTGTGCCCTCCTCCTTCAACGACATCTCCCAGGACTGGCGGCTGCGG

CACTTTGTGGGATGGGTGTGGTACGAGCGGGAAGTGATCCTGCCTGAGCGG

TGGACCCAGGACCTGAGAACCAGAGTGGTGCTGAGGATTGGCAGCGCCCAC

TCCTACGCCATCGTGTGGGTCAACGGCGTGGACACCCTGGAACACGAGGGC

GGCTACCTGCCTTTCGAGGCCGACATCAGCAACCTGGTGCAAGTGGGCCCT

CTGCCTTCTCGGCTGCGGATCACAATCGCCATCAACAACACCCTGACCCCCA

CCACCCTGCCCCCTGGCACAATCCAGTACCTGACCGACACCTCCAAGTACCC

CAAGGGCTACTTCGTGCAGAACACCTACTTCGATTTCTTCAACTACGCCGGC

CTGCAGCGGAGCGTGCTGCTGTATACCACCCCTACCACCTACATCGACGAC

ATCACCGTGACCACCTCCGTGGAACAGGACTCCGGCCTCGTGAACTACCAG

ATCTCCGTGAAGGGCTCCAACCTGTTCAAGCTGGAAGTGCGGCTGCTGGAC

GCCGAGAACAAGGTGGTGGCTAATGGCACCGGCACCCAGGGCCAGCTGAA

AGTGCCTGGCGTGTCACTGTGGTGGCCCTACCTGATGCACGAGCGGCCTGCC

TACCTGTACTCCCTGGAAGTGCAGCTGACCGCCCAGACCTCTCTGGGCCCTG

TGTCCGACTTCTACACCCTGCCTGTGGGGATCCGCACCGTGGCCGTGACCAA

GTCCCAGTTCCTGATCAACGGCAAGCCCTTCTACTTCCACGGCGTGAACAAG

CACGAGGACGCCGACATTCGGGGCAAGGGCTTCGATTGGCCCCTGCTCGTG

AAGGATTTCAACCTGCTGAGATGGCTGGGCGCCAACGCCTTCAGAACCAGC

CACTACCCCTATGCAGAGGAAGTGATGCAGATGTGCGACAGATACGGCATC

GTCGTGATCGACGAGTGTCCCGGCGTGGGACTGGCCCTGCCTCAGTTCTTCA

ACAACGTGTCCCTGCACCACCACATGCAAGTGATGGAAGAGGTCGTGCGGC

GGGACAAGAACCACCCAGCTGTCGTGATGTGGAGCGTGGCCAACGAGCCTG

CCTCCCACCTGGAATCTGCCGGCTACTACCTGAAGATGGTCATTGCCCACAC

CAAGAGCCTGGACCCCTCTCGGCCTGTGACCTTCGTGTCCTACTCCAATTAC

GCCGCCGACAAGGGCGCTCCCTACGTGGACGTGATCTGTCTGAACCGGTAC

TACGGCTGGTATCACGACTACGGCGACCTGGAACTGATCCAGCTGCAGCTG

GCCACCCAGTTCGAGAACTGGTACAAGAAGTACCAGAAGCCCATCATCCTG

ACCGAGTACGGCGCCGAGACAATCGCCGGCTTCCACCAGGATCCACCCCTG

ATGTTCACCGAGGAATACCAGAAGTCCCTGCTGGAACAGTACCACCTGGGC

CTGGACCAGAAAAGACGGAAATACGTCGTGGGCGAGCTGATCTGGAACTTC

GCCGACTTCATGACCGAGCAGAGCCCTACCAGAGTGCTGGGCAACAAGAAG

GGCATCTTCACCCGGCAGCGGCAGCCTAAGTCTGCCGCCTTTCTGCTGCGAG

AGAGATACTGGAAGATTGCCAATGAAACCCGCTACCCCCACTCCGTGGCCA

AGTCTCAATGTTTGGAAAACAGCCTGTTTACTTGACTGGGCCTCATGGGCCT

TCCTTTCACTGCCCGCTTTCCAG

E.3 - Amino acid sequence

MLQGGMLYPQESPSRECKELDGLWSFRADFSDNRRRGFEEQWYRRPLWESGP

TVDMPVPSSFNDISQDWRLRHFVGWVWYEREVILPERWTQDLRTRVVLRIGSA

HSYAIVWVNGVDTLEHEGGYLPFEADISNLVQVGPLPSRLRITIAINNTLTPTTLP

PGTIQYLTDTSKYPKGYFVQNTYFDFFNYAGLQRSVLLYTTPTTYIDDITVTTSV

EQDSGLVNYQISVKGSNLFKLEVRLLDAENKVVANGTGTQGQLKVPGVSLWW

PYLMHERPAYLYSLEVQLTAQTSLGPVSDFYTLPVGIRTVAVTKSQFLINGKPF

YFHGVNKHEDADIRGKGFDWPLLVKDFNLLRWLGANAFRTSHYPYAEEVMQ

MCDRYGIVVIDECPGVGLALPQFFNNVSLHHHMQVMEEVVRRDKNHPAVVM

WSVANEPASHLESAGYYLKMVIAHTKSLDPSRPVTFVSYSNYAADKGAPYVD

VICLNRYYGWYHDYGDLELIQLQLATQFENWYKKYQKPIILTEYGAETIAGFH

QDPPLMFTEEYQKSLLEQYHLGLDQKRRKYVVGELIWNFADFMTEQSPTRVLG

NKKGIFTRQRQPKSAAFLLRERYWKIANETRYPHSVAKSQCLENSLFT*

Appendix F: Overview of Prodrugs for β-Glucuronidase System

Table 14: (a) Overview of β-glucuronidase prodrug efficacy and (b) commercial availability

(a)

Citation	A/G DEPT	Enyme	Prodrug	In Vivo Effect	Other Comments
Chen 2008	/	hBG	HAMG	/	In vitro only
	/	hBG-S2	SN-38G	/	Prove that S2 is the most active mutant at a pH of 7.4
Chen 2012	ADEPT	hBG	HAMG	No effect	
	ADEPT	hBG-S2	HAMG	Good Effect	Significant slowing of tumor growth (LS174T with 2 treatment cycles)
Chen 2013	GDEPT (sufrace tethered)	hBG	Compound 2	Great Effect	/
Brusselbach 2004	GDEPT (sufrace tethered)	hBG	HMR 1826	Great Effect	/
Houba 2001	ADEPT (conjudated)	hBG (-glycosylation)	DOX-GA3	Regression	1 cycle of treatment
Beila 2004	ADEPT	hBG	DOX-GA3	Good Effect	2 treatment cycles, more effective than dox alone
Fejerskov 2012	SMEPT	hBG	SN-38G	/	80% killing at 1uM in 48 hrs

(b)

Prodrug	Chemical Name	Drug	CAS #	Mechaism of Action	Availibility	Company/Catalog Number	Price
SN-38 Glucuronide		SN-38 (irinotecan metabolite)	121080-63-5	Topoisomerase 1 inhibitor	Commercial	TRC/S589980	$250/ 0.5mg
HMR 1826	N-[4- -Glucuronyl-3-nitrobenzyl-oxycarbomyl]doxorubicin	Doxorubicin	148580-25-0	DNA Binding, Topoisomerase II inhibitor, Cytochrome P450 inhibitor	Commercial	TRC/Custom	20mg / $3600 50mg / $4800
DOX-GA3		Doxorubicin	211364-63-5	DNA Binding, Topoisomerase II inhibitor, Cytochrome P450 inhibitor	Commericial	TRC/Custom	20mg / $3600 50mg / $4800
Compund 2 (Tietze 2010)				Unknown	Collabotare with Dr. Tietze Lab		
HAMG	p-hydroxy aniline mustard β-D-glucuronide	pHAM (p-hydroxy aniline mustard)					

Appendix G: Murine β-Glucuronidase

Since β-glucuronidase is a human protein, translational work can proceed directly to immune competent mouse models. This, however, requires the murine versions of our annexin-βG fusion proteins. These have already been created, transfected, stable cells lines selected for >3 weeks, and cryopreserved as adherent stocks. Cells are ready for adaptation to suspension culture. All necessary information for the murine annexin β-glucuronidase fusion proteins, mA1-16a3 and mA5-16a3 as shown in Figure 85, is presented in this appendix.
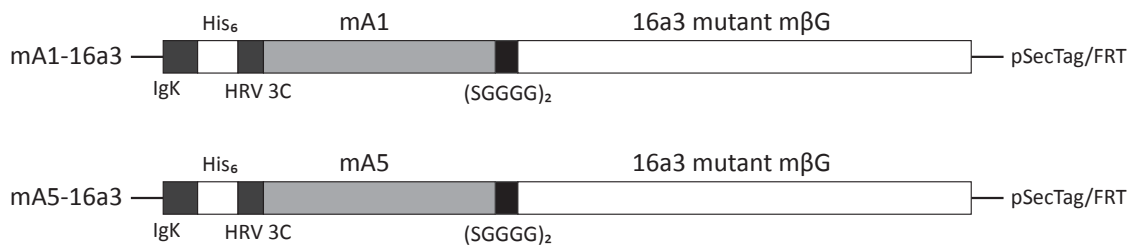
Figure 85: Schematic gene constructions for mA1-16a3 and mA5-16a3

G.1 - 16a3 human and murine β-glucuronidase mutations

Mutations (16a3) between human and murine β-glucuronidase are conserved, but however are not located on the same residue number. Wild type amino acids, mutant amino acids, and their locations in both human and murine βG are presented in Table 15.

Table 15: 16a3 mutation locations for human and murine βG

Human Residue #	Human AA	Mutant AA	Murine AA	Murine AA Residue #
484	N	Y	N	480
503	S	R	S	499
506	S	G	S	502
513	H	D	H	509
538	Q	L	Q	534
539	S	T	S	535

G.2 - Sequences for commercially purchased clones

G.2.1 Murine annexin A1 mRNA clone

(IMAGE clone ID: 3590168, Accession: BC002289)

```
  1 M  A  M  V  S  E  F  L  K  Q  A  R  F  L  E  N  Q  E  Q  E  20
  1 atggcaatggtatcagaattcctcaagcaagcccgttttcttgaaaatcaagaacaggaa 60

 21 Y  V  Q  A  V  K  S  Y  K  G  G  P  G  S  A  V  S  P  Y  P  40
 61 tatgttcaagctgtaaaatcatacaaaggtggtcctgggtcagcagtgagcccctaccct 120

 41 S  F  N  V  S  S  D  V  A  A  L  H  K  A  I  M  V  K  G  V  60
121 tccttcaatgtatcctcggatgttgctgccttgcacaaagctatcatggttaaaggtgtg 180

 61 D  E  A  T  I  I  D  I  L  T  K  R  T  N  A  Q  R  Q  Q  I  80
181 gatgaagcaaccatcattgacattcttaccaagaggaccaatgctcagcgccagcagatc 240

 81 K  A  A  Y  L  Q  E  N  G  K  P  L  D  E  V  L  R  K  A  L  100
241 aaggccgcgtacttacaggagaatggaaagcccttggatgaagtcttgagaaaagccctt 300

101 T  G  H  L  E  E  V  V  L  A  M  L  K  T  P  A  Q  F  D  A  120
301 acaggccacctggaggaggttgttttggctatgctaaaaactccagctcagtttgatgca 360

121 D  E  L  R  G  A  M  K  G  L  G  T  D  E  D  T  L  I  E  I  140
361 gatgaactccgtggtgccatgaagggacttggaacagatgaagacactctcattgagatt 420

141 L  T  T  R  S  N  E  Q  I  R  E  I  N  R  V  Y  R  E  E  L  160
421 ttgacaacaagatctaacgaacaaatcagagagattaatagagtctacagagaagaactg 480

161 K  R  D  L  A  K  D  I  T  S  D  T  S  G  D  F  R  K  A  L  180
481 aaaagagatctggccaaagacatcacttcagatacatctggagactttcggaaagccttg 540

181 L  A  L  A  K  G  D  R  C  Q  D  L  S  V  N  Q  D  L  A  D  200
541 cttgctcttgccaagggtgaccgttgtcaggacttgagtgtgaatcaagatttggctgat 600

201 T  D  A  R  A  L  Y  E  A  G  E  R  R  K  G  T  D  V  N  V  220
601 acggatgccagggctttgtatgaagctggagaaaggagaaaggggacagacgtgaacgtg 660

221 F  T  T  I  L  T  S  R  S  F  P  H  L  R  R  V  F  Q  N  Y  240
661 ttcactacaattctgaccagtaggagctttcctcatcttcgcagagtgtttcagaattac 720

241 G  K  Y  S  Q  H  D  M  N  K  A  L  D  L  E  L  K  G  D  I  260
```

```
 721 ggaaagtacagtcaacatgacatgaacaaagctctggatctggaactgaagggtgacatt 780
 261 E   K   C   L   T   T   I   V   K   C   A   T   S   T   P   A   F   F   A   E   280
 781 gagaagtgcctcacaaccatcgtgaagtgtgccaccagcactccagctttctttgccgag 840
 281 K   L   Y   E   A   M   K   G   A   G   T   R   H   K   A   L   I   R   I   M   300
 841 aagctgtacgaagccatgaagggtgccggaactcgccataaggcattgatcaggattatg 900
 301 V   S   R   S   E   I   D   M   N   E   I   K   V   F   Y   Q   K   K   Y   G   320
 901 gtctcccgttcggaaattgacatgaatgaaatcaaagtatttttaccagaagaagtatgga 960
 321 I   S   L   C   Q   A   I   L   D   E   T   K   G   D   Y   E   K   I   L   V   340
 961 atctctctttgccaagccatcctggatgaaaccaaaggagactatgaaaaaatcctggtg 1020
 341 A   L   C   G   G   N   *                                               347
1021 gctctgtgtggtggaaactag                                               1041
```

```
  1 M   A   T   R   G   T   V   T   D   F   P   G   F   D   G   R   A   D   A   E   20
  1 atggctacgagaggcactgtgactgacttccctggatttgatggcagggctgatgcagaa 60

 21 V   L   R   K   A   M   K   G   L   G   T   D   E   D   S   I   L   N   L   L   40
 61 gtccttcggaaggccatgaaaggcttgggtaccgatgaggacagcatcctgaacctgttg 120

 41 T   S   R   S   N   A   Q   R   Q   E   I   A   Q   E   F   K   T   L   F   G   60
121 acatcccgaagcaatgctcagcgccaggaaattgctcaggagtttaagactctgtttggc 180

 61 R   D   L   V   D   D   L   K   S   E   L   T   G   K   F   E   K   L   I   V   80
181 agggaccttgtggatgacctgaagtctgaactgactggaaagtttgagaagttaattgtg 240

 81 A   M   M   K   P   S   R   L   Y   D   A   Y   E   L   K   H   A   L   K   G   100
241 gctatgatgaagccctcacgactctacgatgcctacgagctgaagcatgctcttaaggga 300

101 A   G   T   D   E   K   V   L   T   E   I   I   A   S   R   T   P   E   E   L   120
301 gctggtacagatgagaaagtattgaccgagattattgcttcaaggacacctgaagaactc 360

121 S   A   I   K   Q   V   Y   E   E   E   Y   G   S   N   L   E   D   D   V   V   140
361 agtgccataaaacaagtttatgaagaagaatatggttccaacctggaagatgatgtggtg 420

141 G   D   T   S   G   Y   Y   Q   R   M   L   V   V   L   L   Q   G   N   R   D   160
421 ggggatacttcagggtactaccaaaggatgttggtggtcctccttcaggggaatagagac 480

161 P   D   T   A   I   D   D   A   Q   V   E   L   D   A   Q   A   L   F   Q   A   180
481 cctgatactgcaattgatgatgctcaagttgaactggatgctcaggcattgttccaggct 540

181 G   E   L   K   W   G   T   D   E   E   K   F   I   T   I   F   G   T   R   S   200
541 ggagagctgaagtggggggacagatgaagaaaaattcatcaccatctttgggacacgcagt 600

201 V   S   H   L   R   R   V   F   D   K   Y   M   T   I   S   G   F   Q   I   E   220
601 gtgtctcatttaagaagagtgtttgacaagtacatgaccatatcaggatttcagattgag 660

221 E   T   I   D   R   E   T   S   G   N   L   E   Q   L   L   L   A   V   V   K   240
661 gaaaccattgatcgggagacctcggggaacttggagcagctgctcctggctgttgtgaag 720

241 S   I   R   S   I   P   A   Y   L   A   E   T   L   Y   Y   A   M   K   G   A   260
721 tctattcggagcatacctgcctaccttgcagagaccctctactatgccatgaagggtgct 780
```

```
261 G   T   D   D   H   T   L   I   R   V   V   V   S   R   S   E   I   D   L   F   280
781 gggacggacgatcacaccctcatcagagtcgtggtgtcgaggagtgagattgacctgttt 840

281 N   I   R   K   E   F   R   K   N   F   A   T   S   L   Y   S   M   I   K   G   300
841 aacataaggaaggagtttaggaagaacttcgccacctccctgtactctatgatcaagggc 900

301 D   T   S   G   D   Y   K   K   A   L   L   L   L   C   G   G   E   D   D   *   320
901 gacacatctggagactataagaaggccctgctgctgctctgcggggggcgaggatgactga 960
```

G.3 - Sequence for murine 16a3 β-glucuronidase mutant optimized for expression in CHO cells
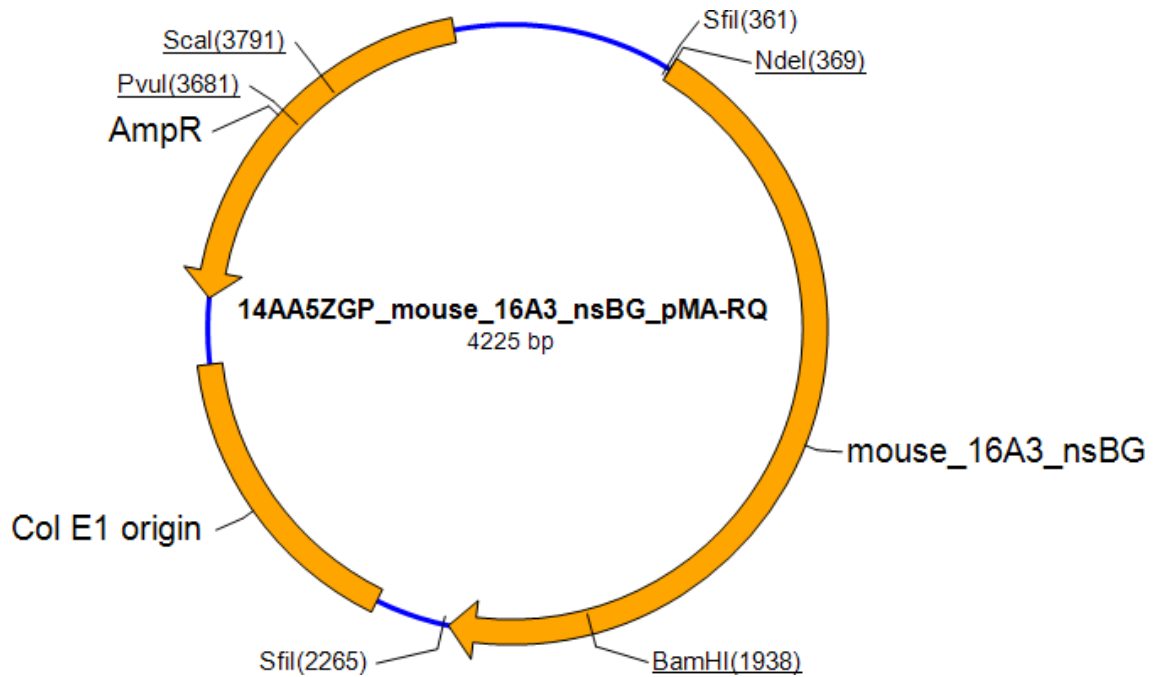
G.3.1 Plasmid map

Figure 86: Plasmid map of mβG 16a3 optimized for expression in CHO cells

Plasmid was synthesized via the Invitrogen Gene Art Service and was synthesized without the N-terminal signal sequence but with C-terminal the propeptide sequence. Plasmids were re-suspended in 50 μl of DI water, and stored in 5 μl aliquots at -20 °C.

CACTATAGGGCGAATTGGCGGAAGGCCGTCAAGGCCGCATATGCTGAAGGG

CGGCATGCTGTTCCCCAAAGAGTCCCCAGCAGAGAGCTGAAGGCTCTGGA

CGGCCTGTGGCACTTCAGAGCCGACCTGTCCAACAACCGGCTGCAGGGCTT

TGAGCAGCAGTGGTACAGACAGCCCCTGCGCGAGTCTGGCCCTGTGCTGGA

TATGCCTGTGCCCTCCTCCTTCAACGACATCACCCAGGAAGCCGCCCTGCGG

GACTTTATCGGCTGGGTGTGGTACGAGAGAGAGGCCATCCTGCCCAGACGG

TGGACCCAGGACACCGACATGAGAGTGGTGCTGCGGATCAACAGCGCCCAC

TACTACGCCGTCGTGTGGGTCAACGGCATCCACGTGGTGGAACACGAGGGC

GGCCATCTGCCTTTCGAGGCCGACATCTCCAAGCTGGTGCAGTCCGGCCCTC

TGACCACCTGTCGGATCACAATCGCCATCAACAACACCCTGACCCCCCACA

CCCTGCCTCCCGGCACCATCGTGTACAAGACCGACACCTCCATGTACCCCAA

GGGCTACTTCGTGCAGGACACCTCCTTCGATTTCTTCAACTACGCCGGCCTG

CACAGATCCGTGGTGCTGTACACCACCCCCACCACCTACATCGACGATATCA

CCGTGATCACCAACGTGGAACAGGACATCGGCCTCGTGACCTACTGGATCT

CCGTGCAGGGCTCCGAGCACTTTCAGCTGGAAGTGCAGCTGCTGGATGAGG

GCGGCAAGGTGGTGGCTCATGGCACCGGAAATCAGGGCCAGCTGCAGGTGC

CCTCCGCTAACCTGTGGTGGCCCTACCTGATGCACGAGCACCCCGCCTACAT

GTACTCCCTGGAAGTGAAAGTGACCACCACCGAGTCCGTGACCGACTACTA

TACCCTGCCCATCGGCATCCGGACCGTGGCCGTGACCAAGTCCAAGTTCCTG

ATCAACGGCAAGCCATTCTATTTTCAAGGCGTGAACAAGCACGAGGACTCC

GACATCCGGGGCAAGGGCTTCGATTGGCCCCTGCTCGTGAAGGACTTCAAC

CTGCTGAGATGGCTGGGCGCCAACTCCTTCCGGACCTCCCACTACCCCTACT

306

CCGAAGAGGTGCTGCAGCTGTGCGACAGATACGGCATCGTCGTGATCGACG

AGTGCCCTGGCGTGGGCATTGTGCTGCCTCAGTCCTTCGGCAACGAGTCCCT

GCGGCATCATCTGGAAGTGATGGAAGAACTCGTGCGGCGGGACAAGAACC

ACCCCGCTGTCGTGATGTGGAGCGTGGCCAACGAGCCTTCCAGCGCCCTGA

AGCCTGCCGCCTACTACTTCAAGACCCTGATCACCCATACCAAGGCCCTGGA

CCTGACCAGACCCGTGACCTTCGTGTCCTACGCTAAGTACGACGCCGACCTG

GGCGCTCCCTACGTGGACGTGATCTGCGTGAACCGGTACTTCGGCTGGTATC

ACGACTACGGCGACCTGGAAGTGATCCAGCCCCAGCTGAACTCCCAGTTCG

AGAACTGGTATAAGACCCACCAGAAGCCCATCATCCTGACCGAGTACGGCG

CCGATGCCATCCCTGGGATCCACGAGGACCCCCCTCGGATGTTCTCCGAGG

AATACCAGAAGCCGTGCTGGAAAACTACCACAGCGTGCTGGACCAGAAAC

GGAAAGAATACGTCGTGGGCGAGCTGATCTGGAACTTCGCCGACTTCATGA

CCAACCAGTCCCCCCTGAGAGTGATCGGCAACAAGAAGGGCATCTTCACCC

GGCAGCGGCAGCCCAAGACCAGCGCCTTTATCCTGAGAGAGCGGTATTGGA

GAATCGCCAACGAGACAGGCGGCCACGGCTCTGGCCCTAGAACCCAGTGTT

TCGGCTCCCGGCCCTTCACCTTCTGACTGGGCCTCATGGGCCTTCCGCTCAC

TGCCCGCTTTCCAG

G.3.3 Amino acid sequence

MLKGGMLFPKESPSRELKALDGLWHFRADLSNNRLQGFEQQWYRQPLRESGP

VLDMPVPSSFNDITQEAALRDFIGWVWYEREAILPRRWTQDTDMRVVLRINSA

HYYAVVWVNGIHVVEHEGGHLPFEADISKLVQSGPLTTCRITIAINNTLTPHTLP

PGTIVYKTDTSMYPKGYFVQDTSFDFFNYAGLHRSVVLYTTPTTYIDDITVITNV

EQDIGLVTYWISVQGSEHFQLEVQLLDEGGKVVAHGTGNQGQLQVPSANLWW

PYLMHEHPAYMYSLEVKVTTTESVTDYYTLPIGIRTVAVTKSKFLINGKPFYFQ

GVNKHEDSDIRGKGFDWPLLVKDFNLLRWLGANSFRTSHYPYSEEVLQLCDRY

GIVVIDECPGVGIVLPQSFGNESLRHHLEVMEELVRRDKNHPAVVMWSVANEP

SSALKPAAYYFKTLITHTKALDLTRPVTFVSYAKYDADLGAPYVDVICVNRYF

GWYHDYGDLEVIQPQLNSQFENWYKTHQKPIILTEYGADAIPGIHEDPPRMFSE

EYQKAVLENYHSVLDQKRKEYVVGELIWNFADFMTNQSPLRVIGNKKGIFTRQ

RQPKTSAFILRERYWRIANETGGHGSGPRTQCFGSRPFTF*

G.4 - Primers for murine A1/A5-βG

G.4.1 Construction primers

Annexin A1 Sense

5' CAT CAC CAT CAC CAT CAC CTT GAA GTC CTC TTT CAG GGA CCC **GCA**

ATG GTA TCA GAA TTC 3'

Green = His Tag   BP = 60

Purple = HRV 3C Site   CG% = 48

Bold = Sequence Overlap   Melting Temp = 69.5 C

Annexin A1 Antisense

5' TG CTT ACC↓ TCC ACT ACC TCC GCC ACC ACT **GTT TCC ACC ACA CAG**

AGC 3'

Teal = EciI Site   BP = 47

Orange = linker   CG% = 57

Bold = Sequence overlap   Melting Temp = 71.7 C

Annexin A5 Sense

5' CAT CAC CAT CAC CAT CAC CTT GAA GTC CTC TTT CAG GGA CCC **GCT**

ACG AGA GGC ACT GTG 3'

Green = His Tag   BP = 60

Purple = HRV 3C Site   CG% = 55

Bold = Sequence Overlap   Melting Temp = 71.6 C

Annexin A5 Antisense

5' TG CTT ACC↓ TCC ACT ACC TCC GCC ACC ACT **GTC ATC CTC GCC CCC**

GCA G 3'

Teal = EciI Site   BP = 48

Orange = ½ linker   CG% = 64.6

Bold = Sequence overlap   Melting Temp = 74.6 C

B-Glucuronidase (16A3_{opt} βG) Sense (No Signal)

5' TAA GCA GGC GGA GGT AGT GGA GG↓T GGT GGA **CTG AAG GGC GGC**

ATG CTG 3'

Teal = EciI Site   BP = 48

Orange = ½ Linker   CG% = 62.5

Bold = Sequence overlap   Melting Temp = 74.1 C

B-Glucuronidase (16A3_{opt} βG) Antisense

5' **TCA GAA GGT GAA GGG CCG GG** 3'

Red = Stop Codon (native)   BP = 20

Bold = Sequence Overlap   CG% = 65

                                    Melting Temp = 61.9 C

T7 Primer

TAATACGACTCACTATAGGG (Provided by OMRF)

Murine annexin 1 (hA1):

mA1 seq primer 1: GAACAGATGAAGACACTCTC

mA1 seq primer 2: AATCCTGGTGGCTCTGTGTG

Murine annexin 5 (hA5):

mA5 seq primer 1: GGATACTTCAGGGTACTACC

mA5 seq primer 2: AGACTATAAGAAGGCCCTG

Murine mutant 16a3 βG):

mBG opt seq primer 1: TCGATTTCTTCAACTACGC

mBG opt seq primer 2: CTGCCTCAGTCCTTCG

Appendix H: KS108 Prodrug Information and LC$_{50}$ Curves

KS108, a seco-duocarmycin SA analog glucuronide prodrug was generously provided
by Dr. Lutz Tietze of the Georg-August-University Göttingen, for study in combination
with the hA5-16a3 βG fusion protein. However, at the time of deposit, data collection
for KS108 had not yet been completed and is therefore not included in Chapter 4. All
known drug information is given in Figure 87 and simulated EPT day 6 LC$_{50}$ curves are
shown for Panc-1, HAAE-1, MCF-7, and HT-29 cells in Figure 88.

(-)-(S)-{1-Chlormethyl-3-[(5-(2-(N,N-dimethylamino)ethoxy)-1H-indol-2-yl)-carbonyl]-1,2-dihydro-3H-benz[e]indol-5-yl}-ß-D-glucopyranuronat (KS108P)

Chemical Formula: C$_{32}$H$_{34}$ClN$_3$O$_9$
Exact Mass: 639,20
Molecular Weight: 640,09
m/z: 639.20 (100.0%), 640.20 (36.5%), 641.20 (34.2%), 642.20 (11.4%), 641.21 (6.1%), 643.20 (2.6%), 642.21 (1.3%)
Elemental Analysis: C, 60.05; H, 5.35; Cl, 5.54; N, 6.56; O, 22.50

a) KS108 1.1mg
b) Storage at -25 °C
c) Solubility: MeOH, DMSO
d) Compound is toxic. Take care.
e) Cytotoxicity (A549) IC$_{50}$: 6.8 nM   IC$_{50}$ in presence of ß-D-glucuronidase: 13 pM
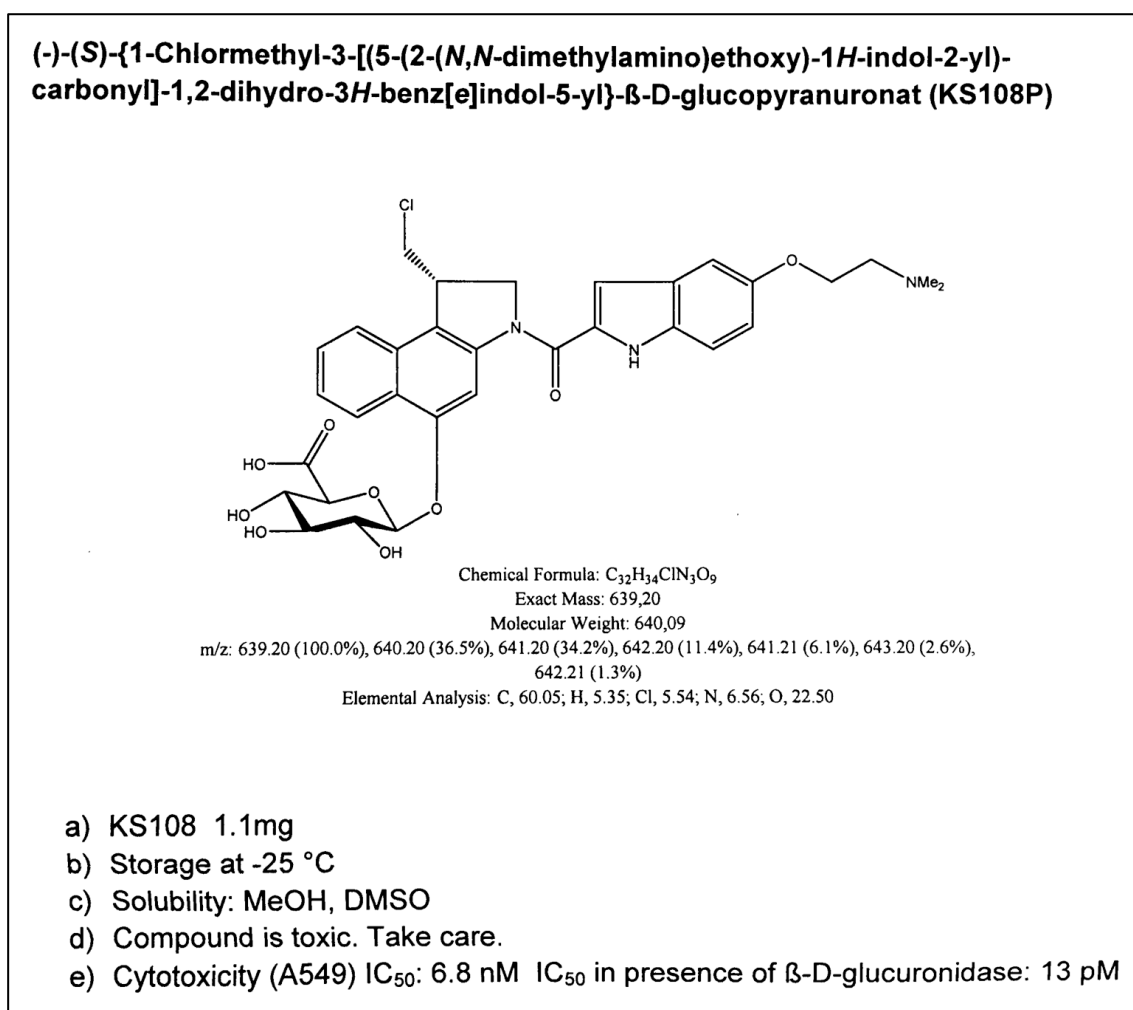
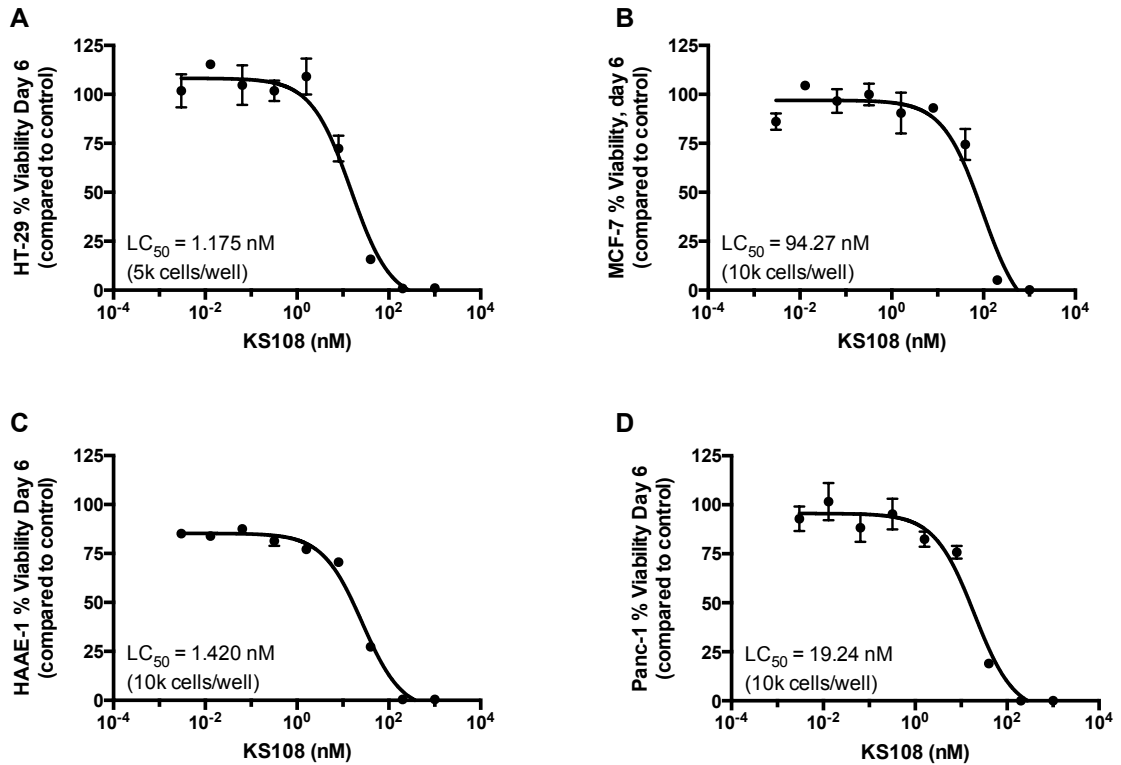**Figure 87: KS108 prodrug information**

Figure 88: KS108 simulated EPT LC$_{50}$ curves

Simulated EPT without any fusion proteins was executed as described in Appendix A.6.2 for (**A**) HT-29 cells, (**B**) MCF-7 cells, (**C**) HAAE-1 cells, and (**D**) Panc-1 cells. All data were normalized to a control matched for day 6 and fit with a three-parameter dose response curve (hill-slope = 1). Data presented as mean ± SE (n = 3).

Appendix I: Location of Cryo-Preserved Cell Stocks in Dewars

List of location of all cryopreserved stocks for cell lines acquired from ATTC for the projects in this dissertation and transfected cell lines created during these projects.

<u>**Older Dewar:**</u>

Rack #1:

PC-3 P4: Rack #1, Slot #1, and Position 16, 21-25 (3.15.12)

bxPC-3 P3: Rack #1, Slot #4, and Position 10-25 (5.22.12)

Panc-1 P4: Rack #1, Slot #3, and Position 4-6, 8-16, and 18-20 (3.3.12)

Capan-1 P4: Rack #1, Slot #5, and Position 14-25 and 8-10 (10.19.12)

Hek/Expi 293 P2: Rack #1, Slot #2, and Position 3, 4, 6, 7, 11, 13, 14

Rack #1, Slot #5, and Position 3, 19, 20, 21, 22

Rack #2:

Hek/Expi 293 (Original Stock): Rack #2, Slot #2, and Position 15 (7.23.13)

Cho Flp-In P1: Rack #2, Slot #2, and Position 6, 7, 11-14, 17, 18, 20, 22 (2.10.14)

Rack #2, Slot #5, and Position 4-11

Rack #3:

Cho Flp-In hA1$_{ns}$BG$_p$: Rack #6, Slot #1, and Position 4-12 (3.17.14)

Cho Flp-In hA1$_{ns}$BG: Rack #6, Slot #1, and Position 13-24 (3.17.14)

Cho Flp-In hA1$_s$BG: Rack #6, Slot #1, and Position 25 (3.20.14)

Rack #6, Slot #3, and Position 3 (3.20.14)

New Dewar (OCBC):

Rack #1:

Cho Flp-In hA1-16a3 Day 20, P1: Rack #1, Slot #1, and Position 1-5 (5.26.14)

Cho Flp-In hA1-16a3 Day 25, P2: Rack #1, Slot #1, and Position 6-22 (5.29.14)

Cho Flp-In hA5-16a3 Day 20, P1: Rack #1, Slot #2, and Position 1-5 (5.26.14)

Cho Flp-In hA5-16a3 Day 25, P2: Rack #1, Slot #2, and Position 6-22 (5.29.14)

Cho Flp-In hA1-16a3 SFM P7: Rack #1, Slot #3, and Position 18-20 (7.5.14)

Cho Flp-In mA1-16a3 P2: Rack #1, Slot #4, and Position 1-6 (7.5.14)

Cho Flp-In mA1-16a3 P3: Rack #1, Slot #4, and Position 7-17 (7.8.14)

Cho Flp-In mA5-16a3 P2: Rack #1, Slot #5, and Position 1-6 (7.5.14)

Cho Flp-In mA5-16a3 P3: Rack #1, Slot #5, and Position 7-22 (7.10.14)

Cho Flp-In hA1n$_s$BG$_p$ SFM P15: Rack #1, Slot #3, and Position 7-15 (6.24.14)

Rack #2:

HT-29 P3: Rack #2, Slot #5, and Position 9-25 (12.9.14)

Cho Flp-In hA5-16a3 SFM P8: Rack #2, Slot #3, and Position 1-6 (7.15.14)

Appendix J: List of Presentations

Guillen KP, Ruben EA, Harrison RG. Annexin Directed β-Glucuronidase for the

Targeted Treatment of Vascular Solid Tumors.

- 2nd place in graduate student division at the *Stephenson Cancer Center Symposium* (Oklahoma City, OK, 2015)

- 1st place poster in Engineering A at *Graduate Research and Performance Day (Norman, OK, 2015)*

Guillen/Passlack K, *et al.* Selective Targeting and Treatment of Pancreatic Cancer Via

Three Fusion Protein/Prodrug Systems.

- 1st place poster in Engineering A at *Graduate Research and Performance Day (Norman, OK, 2014)*

- 2nd place in graduate student division at the *Stephenson Cancer Center Symposium* (Oklahoma City, OK, 2014)

- Oral presentation at the *Biomedical Engineering Society Annual Meeting* (Seattle, WA, 2013).

Huggins E, *et al.* Vascular Targeted Single Walled Carbon Nanotubes for the Thermal

Ablation of Metastatic Breast Cancer via a Radiofrequency Field. *Biomedical Engineering Society Annual Meeting* (Seattle, WA, 2013).

Passlack K*, et al.* Targeted Enzyme Prodrug Therapy for Metastatic Prostate Cancer - A

Comparative Study of Three Fusion Proteins.

- 1st place poster in Engineering B at *Graduate Research and Performance Day (Norman, OK, 2013)*

- *Stephenson Cancer Center Symposium* (Oklahoma City, OK, 2013).

Restuccia A, *et al.* Selective Targeting and Treatment of Pancreatic Cancer Via Three

    Fusion Protein/Prodrug Complexes plus Docetaxel. *Stephenson Cancer Center*

    Annual Retreat (Oklahoma City, OK, 2013).

Passlack K*, et al.* Targeted Enzyme Prodrug Therapy for the Treatment of Metastatic

    Prostate Cancer. *Biomedical Engineering Society Annual Meeting* (Atlanta, GA,

    2012).